Méthodes et stratégies de contrôle optique pour la fabrication de filtres en couches minces par pulvérisation magnétron

Janis Zideluns

THÈSE DE DOCTORAT

Soutenue à Ecole Centrale de Marseille
le 28 septembre 2022 par

Janis ZIDELUNS

Optical monitoring methods and strategies for magnetron sputtered thin-film filters

Discipline
Physique et sciences de la matière

Spécialité
Optique, Photonique et Traitement d'Image

École doctorale
Physique et sciences de la matière (352)

Laboratoire/Partenaires de recherche
Institut Fresnel

Composition du jury

Dr. Volodymyr PERVAK	Rapporteur
Ludwig-Maximilians-University of Munich	
Dr. Laurent PINARD	Rapporteur
Laboratoire des Matériaux Avancés	
Dr. Eric LAVASTRE	Examinateur
CEA-CESTA	
Dr. Marie-Paule BESLAND	Examinateur
Institut des Matrériaux Jean Rouxel	
Karine MATHIEU	invité
CNES	
Dr. Marwan ABDOU AHMED	invité
IFSW (University of Stuttgart)	
Detlef ARHILGER	invité
Bühler Leybold Optics	
Dr. Julien LUMEAU	Directeur de thèse
Institut Fresnel	
Dr. Fabien LEMARCHAND	Co-directeur de thèse
Institut Fresnel	

Acknowledgements

This endeavour would not have been possible without my thesis supervisors Dr. Julien Lumeau and Dr. Fabien Lemarchand. I have benefitted a lot from their immense knowledge, never-ending support, encouragements, and guidance through these last three years. I'm very thankful for being accepted for the PhD position at RCMO team in Institut Fresnel.

I would like to thank to the thesis committee, to Dr. Volodymyr Pervak and Dr. Laurent Pinard for accepting the role of revivers, to Dr. Eric Lavastre and Dr. Marie-Paule Besland for accepting the roles of examiners. And to Karine Mathieu, Detlef Arhilger and Dr. Marwan Abdou Ahmed for being members of the committee.

I'm very grateful to be selected as one of the early-stage researchers of the GREAT project. It is great honour to be selected as one of the 15 researchers in this project.

I would like to thank our partners at Bühler Lebold Optics, especially to Detlef, Harro, Navas and Giulia for their support and help. This thesis would look much differently without the close collaboration between Institut Fresnel and Bühler.

Last but not the least, I would like to thank my family, my parents, my brothers for support and encouragement, especially to my girlfriend Laila for her endless support and being with me through these tough years.

Abstract

In this thesis, we describe the optical monitoring methods and strategies for magnetron sputtered thin-film optical filters. As with any technologies, the requirements for the performance of the thin-film filters increases, the number of layers in the designs grows and therefore the accurate monitoring of the deposited thicknesses becomes more and more crucial. Therefore, the methods of the thickness control have evolved as well, and, as of today, optical monitoring methods are the most precise ones. The quality of the filter, however, does not rely on the method that is used for the thickness monitoring, but rather on how the method is used. The *how* is what we call the monitoring strategy. To create a successful monitoring strategy, deep knowledge about the monitoring method and the thin film filter itself is required. In this thesis we investigate the three established optical thin film monitoring methods.

Turning point optical monitoring is arguably the first commercially available optical monitoring method. Although it is the least accurate optical monitoring method when it comes to thickness errors in monitored layers, it is still widely used, especially when it comes to bandpass filter deposition as it benefits from strong error self-compensation. The use of this method, however, is limited to so called quarter-wave designs and good results are usually obtained in limited wavelength range.

Monochromatic monitoring is probably the most popular monitoring method as of today, as it can be used to monitor almost any design with transparent layers. The difficulty of this method is the determination of the monitoring strategy, as the monitoring wavelength(s) has to selected for each design. The error self-compensation is less effective compared to the turning point monitoring, however good spectral match between experiment and theory is expected over wide wavelength range, if the strategy is chosen wisely.

Broadband optical monitoring is lately gaining popularity, similarly to monochromatic monitoring it can be used for various types of designs. Although this method is not associated with error self-compensation and the spectral resolution of the broadband systems is inferior to monochromatic systems, filters with very low thickness errors can be produced, what is crucial if indirect monitoring strategy is selected.

Each of these monitoring methods have their technical limits (for example spectral resolution and signal to noise ratio) that are either fixed or adjustable. The designs, that we want to deposit,

can have spectral regions that are not suited for optical monitoring (for example the transmittance can be too low for measurement) that can vary from layer to layer. To create the monitoring strategy, a good balance between the technical possibilities of the motoring system and the spectral behavior of the layer to be monitored must be found.

Résumé

Dans cette thèse, nous décrivons les méthodes et stratégies de contrôle optique pour les filtres en couches minces déposées par pulvérisation cathodique magnétron. Comme pour toutes les technologies, les exigences en matière de performance des filtres à couches minces augmentent, le nombre de couches dans les conceptions augmente et, par conséquent, le contrôle précis des épaisseurs déposées devient de plus en plus crucial. Les méthodes de contrôle de l'épaisseur ont donc également évolué et, à l'heure actuelle, les méthodes de contrôle optique sont les plus précises. La qualité du filtre ne dépend toutefois pas de la méthode utilisée pour le contrôle de l'épaisseur, mais plutôt de la manière dont cette méthode est utilisée. La manière est ce que nous appelons la stratégie de contrôle. Pour créer une stratégie de contrôle réussie, une connaissance approfondie de la méthode de contrôle et du filtre en couches minces lui-même est nécessaire. Dans cette thèse, nous étudions les trois méthodes classiques de contrôle optique des couches minces.

Le contrôle optique basé sur le principe de *turning point* est sans doute la première méthode de contrôle optique disponible dans le commerce. Bien qu'il s'agisse de la méthode de contrôle optique la moins précise en ce qui concerne les erreurs d'épaisseur dans les couches contrôlées, elle est encore largement utilisée, en particulier pour le dépôt de filtres passe-bande, car elle bénéficie d'une forte auto-compensation des erreurs. L'utilisation de cette méthode est toutefois limitée aux conceptions dites "quart d'onde" et de bons résultats sont généralement obtenus dans une gamme de longueurs d'onde limitée.

Le contrôle monochromatique basé sur le principe de *trigger point* est probablement la méthode de contrôle la plus populaire à l'heure actuelle, car elle peut être utilisée pour contrôler presque tous les empilements comportant des couches transparentes. La difficulté de cette méthode réside dans la détermination de la stratégie de contrôle, car la ou les longueurs d'onde de contrôle doivent être choisies pour chaque empilement. L'autocompensation des erreurs est moins efficace qu’avec un contrôle en *turning point*, mais on peut s'attendre à une bonne correspondance spectrale entre l'expérience et la théorie sur la gamme de longueurs d'onde, si la stratégie est choisie judicieusement.

Le contrôle optique large bande a gagné en popularité ces derniers temps. Comme le contrôle optique monochromatique, il peut être utilisée pour différents types d’empilements. Bien que

cette méthode ne soit pas associée à l'autocompensation des erreurs et que la résolution spectrale des systèmes à large bande soit inférieure à celle des systèmes monochromatiques, il est possible de produire des filtres avec des erreurs d'épaisseur très faibles, ce qui est crucial si une stratégie de contrôle indirect est choisie.

Chacune de ces méthodes de contrôle a ses limites techniques (par exemple la résolution spectrale et le rapport signal/bruit) qui sont soit fixes, soit ajustables. Les filtres que nous voulons déposer peuvent avoir des régions spectrales qui ne sont pas adaptées au contrôle optique (par exemple, la transmission peut être trop faible pour être mesurée) et qui peuvent varier d'une couche à l'autre. Pour créer la stratégie de contrôle optique, il faut trouver un bon équilibre entre les possibilités techniques du système de contrôle et le comportement spectral de la couche à surveiller.

Résumé étendu

Cette thèse est consacrée à l'étude de différentes méthodes de contrôle d'épaisseur de couches minces, des algorithmes et des paramètres qui vont influencer le contrôle optique monochromatique et large bande de filtres multicouches complexes. Ces techniques et leurs limites ne sont bien souvent pas universelles mais liées à des cas spécifiques qui vont dépendre de la conception des structures étudiées. A ce jour, il n'existe pas de solution universelle pour le contrôle de l'épaisseur des couches minces, donc en fonction de la conception et de l'application, on doit choisir comment contrôler les épaisseurs des couches. En d'autres termes, Il est important de déterminer une stratégie de contrôle avant de fabriquer le filtre. Dans cette thèse, nous discuterons en détail des méthodes et stratégies de contrôle utilisées pour le dépôt de filtres en couches minces.

Pour plus de clarté, nous avons décidé de limiter cette étude à 7 types de filtres différents tels que des miroirs quart d'onde, des séparateurs de faisceau, un filtre compensateur D65, un filtre coupe-bande, la conceptions de filtres à profil arbitraire et des filtres Fabry-Perot. En plus des designs décrits dans cette thèse, de nombreux autres dépôts ont été effectués et des filtres de complexité variable ont été livrés à d'autres chercheurs de l'Institut Fresnel et à des partenaires extérieurs à l'Institut pour les aider dans leur travail. Au cours de cette thèse ~20 mm de niobium ~25 mm de silice, et ~5 mm d'hafnium ont été déposés.

Chacun des filtres décrits dans cette thèse a des caractéristiques spécifiques et des difficultés de production qui seront utilisées pour illustrer le travail effectué. Pour des raisons de clarté toutes les formules de conception et les propriétés des matériaux peuvent être trouvées dans les annexes 1, 2 et 3, les informations détaillées sur les stratégies de contrôle de ces conceptions (méthodes, longueurs d'onde, etc.) sont données dans l'annexe 4.

Cette thèse s'inscrit dans le cadre du projet GREAT (Grating Reflectors Enabled laser Application and Training). Cette thèse a reçu un financement du programme de recherche et d'innovation Horizon 2020 de l'Union européenne, dans le cadre de la convention de subvention Marie Skłodowska-Curie n° 813159.

Plus de détails sur le projet GREAT, et le rôle des auteurs dans ce projet, sont disponibles dans l'annexe 5.

Le travail décrit dans cette thèse a été mené en étroite collaboration avec Bühler Leybold Optics. Deux séjours d'un mois au sein de la société à Alzenau ont été réalisés. Ces séjours ont permis de transférer une partie de ces résultats (stratégies de contrôle) décrits dans les chapitres vers des machines de dépôt du même type et de démontrer que ces résultats ne sont pas liés uniquement aux équipements disponibles à l'Institut Fresnel.

Cette thèse se compose de sept chapitres :

Dans le chapitre 1, nous présentons les traitements optiques de surface, en partant de l'histoirique des filtres à couches minces pour arriver aux revêtements multicouches qui sont largement utilisés aujourd'hui. Nous introduisons dans le premier chapitre les bases de la théorie des couches minces qui sont ensuite utilisées pour le calcul des propriétés (par exemple la transmittance en fonction de la longueur d'onde) des filtres en couches minces. De plus, nous décrivons l'équipement de dépôt par pulvérisation cathodique magnétron qui a été utilisé pendant cette thèse pour produire les filtres en couches minces.

Dans le chapitre 2, nous examinons d'abord la sensibilité des différents types de filtres optiques aux erreurs d'épaisseur et d'indice de réfraction. Cette analyse met en évidence la précision requise pour le contrôle de l'épaisseur. Nous décrivons en détail les méthodes de contrôle de l'épaisseur des films minces qui sont largement disponibles à l'heure actuelle. L'accent est mis ici sur le contrôle optique monochromatique (*turning and trigger point*) et large bande. Nous discutons des forces et des faiblesses de chacune de ces techniques de contrôle.

Dans le chapitre 3, nous décrivons le dépôt d'un type très particulier de revêtement optique - un filtre passe-bande étroit dans la gamme des longueurs d'onde UV. Nous étudions les modèles Fabry-Perot qui sont associés au techniques de *turning point*. En raison de la longueur d'onde qui nous intéresse, nous commençons par une étude de l'amélioration des propriétés matériaux des couches d'oxyde d'hafnium pour obtenir la transmittance nécessaire. Lorsqu'il s'agit de déposer le filtre, nous présentons des stratégies qui peuvent être utilisées pour surmonter les limites techniques de l'installation de contrôle, car la largeur totale à mi-hauteur de ce filtre ne permet pas de mettre en œuvre une stratégie de contrôle directe.

Dans le chapitre 4, nous discutons des forces et des faiblesses du contrôle optique monochromatique par *turning point*. Nous présentons les méthodes précédemment publiées pour la détermination de la stratégie de contrôle monochromatique. Nous proposons une méthode

entièrement automatisée pour la détermination de la stratégie de contrôle - ce que nous appelons le contrôle polychromatique. Nous démontrons notre approche en déposant plusieurs filtres de complexité croissante.

Dans le chapitre 5, nous discutons des forces et des faiblesses des méthodes de contrôle optique large bande. Nous mettrons en évidence les critères qui sont utilisés pour créer des stratégies de contrôle large bande. Nous comparons ensuite les résultats expérimentaux de filtres dont l'épaisseur est contrôlée par des méthodes à large bande et monochromatiques.

Dans le chapitre 6, nous abordons les stratégies de contrôle optique indirectes. Ce contrôle optique indirect ayant été à plusieurs reprises dans cette thèse, le chapitre 6 se concentre sur les nombreuses approches possibles pour déterminer le moment le plus opportun changer le verre témoin.

Dans le chapitre 7, nous soulignons les résultats les plus importants obtenus au cours de ce projet de thèse et nous présentons les perspectives futures.

Contrôle optique polychromatique

A titre d'exemple, examinons une petite section du chapitre 4. Dans le chapitre 4, nous présentons ce que nous appelons le contrôle optique polychromatique. Le contrôle optique polychromatique diffère du contrôle optique monochromatique par le nombre de longueurs d'onde de contrôle autorisées pour une conception donnée. Nous montrons qu'en sélectionnant les longueurs d'onde de contrôle d'une "manière intelligente" pour chacune des couches, nous pouvons définir des stratégies de contrôle optique robustes. Pour déterminer la stratégie de contrôle polychromatique, nous excluons d'abord l'utilisation des longueurs d'onde de contrôle qui pourraient augmenter les erreurs d'épaisseur des couches. Ensuite, parmi les longueurs d'onde restantes, nous sélectionnons la meilleure longueur d'onde pour chaque couche en trouvant la longueur d'onde qui sera la moins affectée par le bruit et les erreurs d'épaisseur. Tout ceci peut être fait sans avoir à regarder manuellement les courbes de contrôle et la stratégie est déterminée automatiquement. Il n'est pas possible de décrire le processus de détermination de la stratégie en quelques mots, le chapitre 4 s’intéresse donc à l’ensemble de ces paramètres.

Validation de la stratégie polychromatique sur une conception simple de composant en couches minces

Nous avons fabriqué une séparatrice 50/50 composée de 8 couches en utilisant 3 stratégies polychromatiques différentes dénommées MF2, MF3 et MF4 et déterminées avec l'approche citée ci-dessus. Pour comparer l'efficacité de ces stratégies, nous avons également déposé ce filtre avec une longueur d'onde sélectionnée manuellement pour contrôler toutes les couches (nous appelons cela une stratégie standard). À cette fin, la longueur d'onde de 595 nm a été choisie, car elle a montré la plus faible sensibilité au bruit dans les simulations. Les performances spectrales des quatre filtres déposés est présentée dans la figure 1.

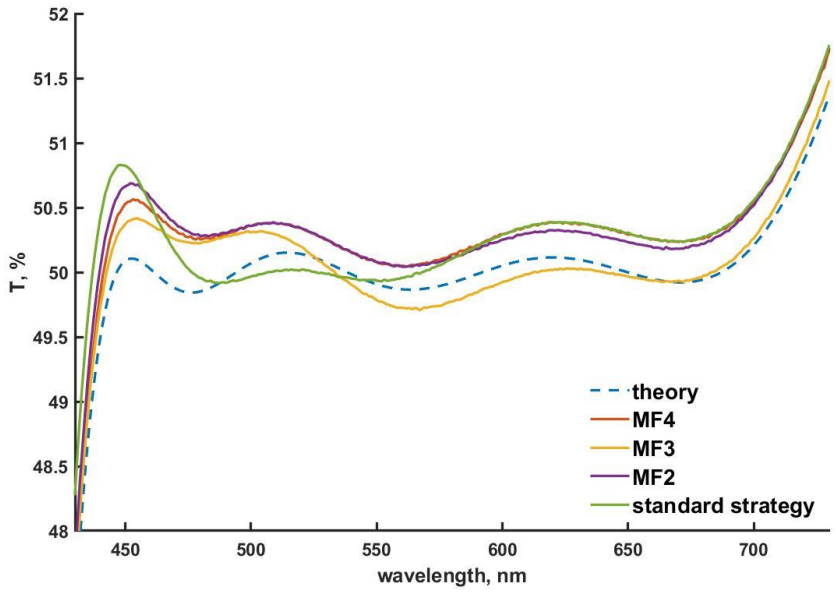

Figure 1 Transmittances mesurées des séparatrices déposées en utilisant 3 stratégies automatisées (MF2, MF3, MF4), et le contrôle d'une seule longueur d'onde (stratégie standard).

Pour tous les filtres fabriqués, une correspondance étroite entre l'expérience et la théorie peut être observée. Une observation intéressante est que, selon la stratégie, la déviation de la transmittance mesurée par rapport à la théorie est plus grande dans la région spectrale bleue ou rouge. Il s'agit d'une caractéristique systématique répétable qui montre que les erreurs d'épaisseur diffèrent en fonction de la longueur d'onde sélectionnée. Dans l'ensemble, il apparaît que la courbe mesurée obtenue par stratégie en utilisant les longueurs d'onde MF4 suit de plus près la théorie sur toute la gamme spectrale d'intérêt.

Sur la base de ce résultat, et afin d'éviter un trop grand nombre de tests, seule MF4 a été considérée pour la suite de cette étude.

Validation de la stratégie polychromatique sur des conceptions de filtres complexes en couches minces

L'étude du séparateur de faisceaux à 8 couches a confirmé, sur une conception simple mais sensible, que la stratégie polychromatique est une méthode valide pour le contrôle optique des filtres. Les simulations de cette conception décrites au chapitre 2 montre que les erreurs aléatoires d'épaisseur ne doivent pas dépasser 0,5% pour maintenir les fluctuations de transmission dans un corridor de ±1% centré autour de 50%. L'écart de transmission mesuré (±0,7%) démontre donc qu'une grande précision d'épaisseur des couches déposées a été atteinte pour les séparateurs de faisceaux fabriqués. Sur la base de ces résultats encourageants, nous avons étudié comment cette approche fonctionne avec des filtres plus complexes comportant plus de 30 couches. Pour les filtres multicouches (dépassant 20 couches), la recherche manuelle d'une stratégie devient fastidieuse et plusieurs stratégies peuvent être trouvées manuellement sans savoir laquelle est la meilleure avant de les tester. Pour cette raison, il est très intéressant de pouvoir générer automatiquement une stratégie de contrôle polychromatique pour les conceptions complexes de filtres en couches minces.

Filtre de compensation D65

Le premier filtre complexe que nous avons étudié est le filtre de compensation D65 [annexe 1.10]. L'illuminant standard D65 de la CIE décrit la dépendance spectrale de l'intensité de la lumière du jour à une température de couleur de 6500 K. Le filtre est alors conçu pour compenser la distribution de l'éclairement d'une source lumineuse potentielle présentant de telles caractéristiques. La distribution de l'éclairement et la conception du filtre correspondant sont illustrées à la figure 2 (a). L'étalon d'éclairement est défini avec un pas de 10 nm, de sorte que les spectres de distribution de puissance sont constitués de nombreuses caractéristiques nettes. Ceci ne peut pas être facilement reproduit par des structures en couches minces et nécessiterait un

nombre beaucoup plus important de couches pour que la conception corresponde aux arêtes vives.

C'est pourquoi nous avons conçu un empilement modèle composé de 37 couches qui compense une grande partie des fluctuations d'intensité. Le filtre est composé de couches dont l'épaisseur varie de 9 nm à 500 nm, comme le montre la figure 2 (d).

Une stratégie a également été déterminée à l'aide d'une approche manuelle standard, mais il n'a pas été possible de trouver une seule longueur d'onde permettant de controler les 37 couches du filtre. Pour surmonter ce problème, autant de couches que possible ont été controlées optiquement et les couches restantes ont été contrôlées au temps. La longueur d'onde de contrôle sélectionnée était de 400 nm. La première couche a fait l'objet d'un contrôle au temps, car il s'agit d'une couche de SiO_2 et le contraste d'indice de réfraction avec le substrat de silice fondue est trop faible pour un contrôle optique efficace. Les 19 couches suivantes ont été contrôlées optiquement et les couches restantes ont été contrôlées au temps en utilisant les vitesses de dépôt moyennes enregistrées pendant le contrôle optique de la $2^{ème}$ à la $20^{ème}$ couche. Les vitesses de dépôt des machines de pulvérisation magnétron étant connues pour être stables (la précision réalisable pour les épaisseurs de couche est au moins de l'ordre de 1%), ce type de stratégie est assez souvent utilisée comme solution de secours lorsqu'aucune stratégie de contrôle optique ne peut être trouvée.

Pour la stratégie de contrôle optique sélectionnée automatiquement, les couches numéro 1, 2, 3, 5 et 23 ont fait l'objet d'un contrôle au temps. Comme pour la stratégie manuelle, la première couche n'a pas pu être contrôlée optiquement en raison du faible contraste de l'indice de réfraction ; les autres sont des couches minces (< 20 nm) et aucune des longueurs d'onde n'a pu répondre aux critères décrits dans la section 2.2. Enfin, la plupart des longueurs d'onde de contrôle sélectionnées par le processus automatisé se situent entre 550 et 700 nm, ce qui correspond approximativement à la région où le rapport signal/bruit du système de surveillance est le plus élevé, et seules quelques longueurs d'onde sélectionnées sont inférieures à 500 nm [annexe 4.2].

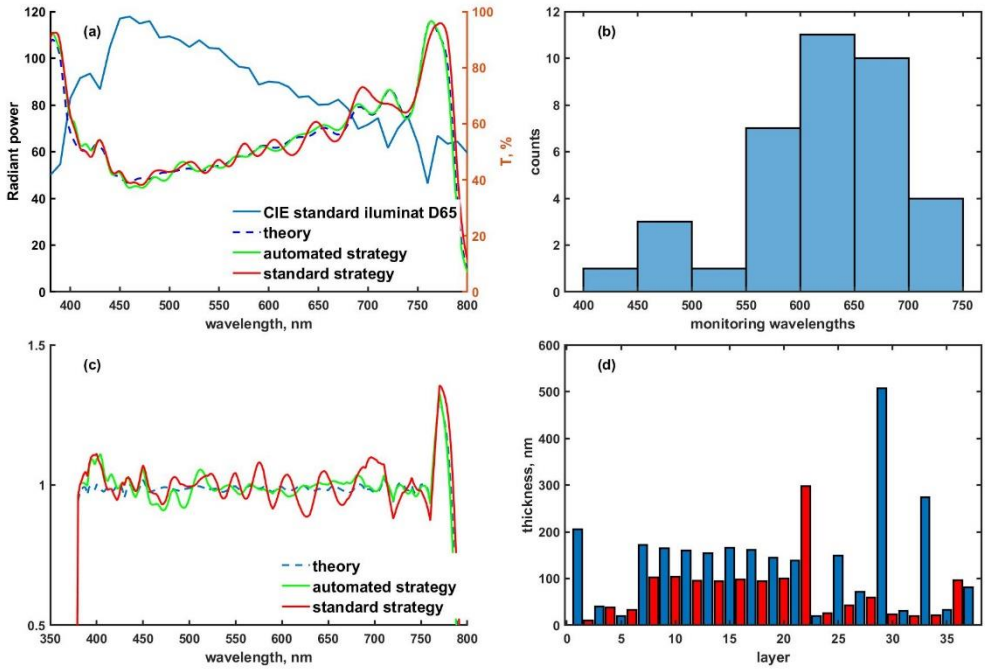

Figure 2 (a) - Distribution de puissance de l'illuminant standard et transmittance théorique du filtre de compensation et comparaison entre les réponses spectrales théoriques et expérimentales avec les stratégies automatisée et standard, (b) - distribution des longueurs d'onde de contrôle pour la stratégie automatisée, (c) - produit des réponses spectrales de l'illuminant D65 par celles des filtres déposés. (d) - épaisseurs du filtre de compensation D65, rouge - couches à haut indice, bleu - couches à bas indice.

Les filtres ont été fabriqués avec les stratégies manuelles et automatiques et les performances spectrales ont été mesurées et comparées à la théorie (Fig.2(a)). On constate que la stratégie manuelle donne d'assez bonnes performances, mais que la stratégie automatique est encore plus performante, surtout pour les grandes longueurs d'onde. Cette performance peut être analysée plus en détail en comparant la multiplication de la transmittance des filtres fabriqués avec la distribution de puissance D65 (Fig.2 (c)). Pour que le produit final soit " plat ", les oscillations de la transmittance mesurée doivent coïncider avec les franges de la distribution de puissance ; tout décalage le long de l'axe x peut entraîner de grandes déviations. Par rapport à la stratégie manuelle qui utilise une seule longueur d'onde de contrôle, ce résultat tend à suggérer que le fait d'avoir les longueurs d'onde réparties sur une plus large gamme de longueurs d'onde pour la

stratégie automatisée peut aider à obtenir de meilleures performances. L'ajout d'une ou plusieurs longueurs d'onde de contrôle à la stratégie standard pour couvrir une gamme spectrale plus large et éventuellement réduire le nombre de couches pour le contrôle au temps pourrait améliorer la performance finale du filtre D65 obtenue avec la stratégie standard. Cependant, l'amélioration des stratégies sélectionnées manuellement n'est pas l'objet de cette recherche car elle dépend de chaque individu.

Conclusions et perspectives

Dans cette thèse, nous avons étudié plusieurs des méthodes de contrôle optiques des filtres en couches minces disponibles (à ce jour), décrit leurs forces et faiblesses, et montré comment créer des stratégies de surveillance en utilisant les forces de chaque méthode. Nous résumons ci-dessous les résultats obtenus avec chacune des méthodes de contrôle optique décrites dans cette thèse et soulignons les actions futures possibles.

Les filtres Fabry-Perot et le contrôle en *turning point*

Nous avons montré qu'il est possible de réduire le coefficient d'extinction et d'améliorer la transmission des couches d'oxyde de hafnium dans la gamme de longueurs d'onde UV en augmentant la quantité d'oxyde de silicium co-pulvérisé.
Nous avons démontré une nouvelle approche pour le contrôle des filtres Fabry-Perot étroits. Nous avons montré qu'il est possible de surmonter les limites d’un système de contrôle optique (notamment la largeur de bande et la sensibilité) en choisissant une stratégie de contrôle intelligente. L'une des prochaines étapes serait de passer à des conceptions à 3 cavités (et plus).
La caractérisation des filtres passe-bande étroits reste un défi, car les spectrophotomètres disponibles dans le commerce présentent encore des limites. Par conséquent, pour un projet tel que celui décrit dans le chapitre 3 de cette thèse, une configuration de mesure personnalisée devrait être envisagée.

Stratégies de contrôle monochromatique et polychromatique

Les stratégies de contrôle optique polychromatique fonctionnent bien en combinaison avec la pulvérisation magnétron. Nous avons démontré avec succès, sur différents modèles, que nous pouvons créer automatiquement une stratégie de contrôle qui ne comporte aucune limite quant au nombre de longueurs d'onde utilisables et qui inclut, si nécessaire, des méthodes de contrôle non optiques. Les stratégies polychromatiques se sont avérées très robustes - nous n'avons pas besoin d'effectuer de simulations de dépôt avant l'expérience, et surtout, les cycles de dépôt ne sont pas interrompus prématurément lorsque des stratégies polychromatiques sont utilisées.

L'une des questions souvent posées est de savoir si ces stratégies fonctionnent avec d'autres types de technologies de dépôts. Nous n'avons pas de réponse claire à cette question car des tests supplémentaires sont encore nécessaires. Pour tester l'approche multi-longueurs d'onde, nous devons d'abord trouver les limites techniques de la combinaison d'une technologie de dépôt donnée et de son système de contrôle afin de définir les paramètres expérimentaux avant toute détermination d'une stratégie polychromatique automatisée. Il s'agit, bien entendu, d'une tâche très délicate et qui requiert beaucoup de temps et sera l'objet de développements futurs.

Stratégies de contrôle optique large bande

Nous avons démontré l'utilisation du système de contrôle large bande pour plusieurs conceptions de filtres. Comme la complexité des empilements augmente, des stratégies sont nécessaires pour le contrôle à large bande. Nous avons démontré que de bonnes performances spectrales peuvent être obtenues si le contrôle optique large bande est combiné à d'autres méthodes de contrôle.

Pour avoir une détermination de stratégie entièrement automatisée (similaire à l'algorithme polychromatique), plusieurs paramètres d'entrée, tels que la plage de longueur d'onde minimale et les niveaux de déclenchement des critères d'arrêts de dépôt, doivent être étudiés plus avant.

L'une des nombreuses caractéristiques intéressantes du contrôle optique large bande est la possibilité de déterminer l'erreur d'épaisseur pendant le dépôt du filtre multicouche. L'une des prochaines actions serait d'utiliser ces informations pour ré-optimiser l'empilement de couches en fonction des informations sur l'épaisseur précédemment déposées. Bien que cela semble être une tâche simple, il y a quelques considérations importantes. Par exemple, quand effectuer cette

ré-optimisation ? Voulons-nous le faire après chaque couche, ou après que plusieurs couches aient été déposées ? Une autre préoccupation est liée à la détermination de l'erreur elle-même. Pour l'instant, il semble que la détermination de l'épaisseur à partir de la mesure spectrale ne soit pas optimale, surtout lorsqu'une couche mince est suivie d'une couche épaisse. Cela signifie que, dans un premier temps, la détermination de l'épaisseur à partir de la mesure spectrale doit être encore améliorée, puis que l'emplacement optimal pour réaliser la ré-optimisation de l'empilement doit être déterminé.

Un autre domaine à explorer serait la compensation des erreurs avec à le contrôle optique large bande. Jusqu'à présent, nous utilisons les informations sur les erreurs dans les couches précédentes pour modifier les courbes cibles, ce qui permet de maintenir les erreurs à un faible niveau, mais, au final, la courbe de transmission cible diffère considérablement de la courbe théorique, et des spécifications initiales. Nous pourrions utiliser la gabarit spectral initial comme courbe cible pour la dernière, ou certaines des dernières couches, ou éventuellement utiliser une stratégie de contrôle mixte dans le but de bénéficier de compensations d'erreurs pour quelques couches.

Stratégies de contrôle indirectes

Dans cette thèse, nous avons utilisé avec succès des stratégies de contrôle optique indirecte. Nous devons souligner les bons résultats obtenus avec les filtres Fabry Perot et le design du concours OIC 2022. L'approche utilisée pour déterminer la stratégie indirecte pour le design du concours OIC est très prometteuse et doit être testée plus avant sur d'autres designs.

Cependant, outre les études sur la sensibilité d'une couche aux erreurs d'épaisseur, la géométrie de la machine de dépôt pose également des problèmes qui doivent être étudiés de manière plus approfondie. Nous savons déjà que l'uniformité à l'intérieur de la machine de dépôt n'est pas parfaite, il existe des différences d'une position à l'autre, ce qui signifie que l'épaisseur déposée sur le verre de contrôle n'est pas exactement la même que sur les autres positions. Il est donc nécessaire de déterminer s'il existe une différence aléatoire ou systématique dans l'épaisseur déposée en fonction de la position du verre à l'intérieur de la machine de dépôt.

Outline

Introduction

This thesis is devoted to the study of different thin-film thickness monitoring methods, algorithms and parameters that will influence monochromatic and broadband optical monitoring of complex multilayer filters. These techniques and their limits are quite often not universal but related to specific cases that will depend on the design of the studied structures. Up to this day, there is no universal solution for the thin film thickness control, therefore depending on the design and application, one must choose how to control the thicknesses of the layers. Or in other words, one must determine a monitoring strategy before fabricating the filter. In the following chapters of this thesis we will discuss in great detail the monitoring methods and strategies used for the thin film filter deposition.

For clarity, we have decided to restrict this study on 7 different types of filters such as quarter wave mirrors, beam splitters, D65 compensator filter, notch filter, shape-replicating designs, and Fabry-Perot filters. Besides the designs described in this thesis, many other deposition runs have been carried out and filters of various complexity have been delivered to other researcher of Institute Fresnel and partners outside the Institute to help with their work. To illustrate it, ~20 mm of niobium ~25 mm of silicon, and ~5 mm of hafnia have been deposited. The results from these deposition runs are supported by a wide range of experimental data (sputtering voltage, power, pressure etc.) that are not always presented in this thesis.

Each of the filters described in this thesis have specific features and production difficulties that will be used to illustrate the work that has been carried out. For clarity, we did not introduce in the following chapters the designs every time they are studied. However, all design formulae and materials properties can be found in Appendix 1, 2 and 3. The detailed information about monitoring strategies of these designs (methods, wavelengths, etc.) are given in appendix 4.

This thesis is a part of the GREAT (Grating Reflectors Enabled laser Application and Training) project. The thesis has received funding from the European Union's Horizon 2020 research and innovation program under the Marie Skłodowska-Curie grant agreement No 813159.

More details about the GREAT project and the author role in it can be found in appendix 5.

The work described in this thesis has been conducted in close collaboration with Bühler Leybold Optics. The author has twice conducted experiments at the facilities of the company in Alzenau.

Therefore, the results (monitoring strategies) described in following chapters of this thesis were at least partially transferred to deposition machines of the same type and are not linked only to the equipment available in Institute Fresnel.

This thesis consists of seven chapters:

In chapter 1 we introduce the optical coatings. Starting from the history of thin film filters, we move on towards multilayer coatings that are widely used today. We introduce in the first chapter the fundamentals of thin-film theory that is later used for calculation of the properties (for example transmittance as function of wavelength) of the thin-film filters. Additionally, we describe the coating equipment that is used by the author to produce the thin-film filters.

In chapter 2 we at first look how sensitive are various types of optical filters towards thickness and refractive index errors. This analysis highlights the required accuracy for the thickness monitoring. We describe in detail the thin-film thickness control methods that are widely available as of today. The main focus here is on monochromatic (turning point and level cut) and broadband optical monitoring. We discuss the strengths and weaknesses for each of these monitoring techniques.

In chapter 3 we describe the deposition of a very special type of optical coating – narrow bandpass filter in the UV wavelength range. We investigate the Fabry-Perot designs that are associated with the turning point monitoring. Because of the wavelength of interest, we start by fine-tuning the material properties of hafnia oxide layers to achieve necessary transmittance. When it comes to deposition of the filter, we introduce strategies that can be used to overcome technical limits of the monitoring setup, as the full width at half maximum of this filter does not allow to implement direct monitoring strategy.

In chapter 4 we discuss the strengths and weaknesses of monochromatic (level cut) monitoring. We introduce the previously published methods for monochromatic monitoring strategy determination. We propose a fully automated method for monitoring strategy determination - what we call polychromatic monitoring. We demonstrate our approach by depositing several designs with increasing complexity.

In chapter 5 we discuss the strengths and weaknesses of the broadband monitoring methods. We will highlight the criteria that are used to create broadband monitoring strategies. We compare

experimental results of filters which thicknesses are controlled by broadband and monochromatic methods.

In chapter 6 we discuss the indirect monitoring strategies. We use indirect monitoring many times in this thesis, and in chapter 6 we show one of the many possible approaches how to determine when to change the witness glass.

In chapter 7 we highlight the most important results achieved during this thesis project and introduce the future perspectives.

Chapter 1 - Optical coatings and deposition methods

In this chapter we will introduce the thin film optical coatings. We will look at some of the notable achievements in the past, discuss the thin film designs and applications, introduce the main properties of a thin film coatings, and introduce the basic equations that are used for the thin film calculations. We will present the coating technologies that are available to deliver the multilayer coatings at Institute Fresnel.

1.1 Thin film optical coatings

1.1.1 History of thin film coatings

Thin film coatings are known to mankind for thousands of years and can be dated back to ancient Egypt where thin gold films were used to cover the statues of gods and emperors[1]. However, the most important period of time for optical coatings is the 20^{th} century. Indeed, during last 100 years, the progress has been immense with several important breakthroughs in thin film field especially starting from 1930s. With the advances in vacuum pumps, power supplies and computers, the complexity of the fabricated thin film filters have noticeably increased[2][3]. Different deposition methods have been developed and moved from laboratories to industry. Nowadays it is unthinkable to use optical instruments without coated components. Arguably, one of the most produced coatings up until now are the antireflective coatings. The exact history of the antireflective coating is not clear, with some authors suggesting Joseph Fraunhofer to be the first to witness and report improvement of transmittance as a result of manipulation with glass surface in mid-19^{th} century[4]. These works have been translated and partially published in several books, such as *Thin film optical filters* by A. Macleod[5]. Almost 100 years later, the development of fluoride antireflective coating[6] started the thin film field as we know it today. Single layer MgF_2 can reduce the reflectivity in visible range from 8% to 1.3% if coating on both sides of glass is applied. During the second world war, more advanced multi-layer antireflective coatings were developed as the deposition methods allowed to use wider range of materials. Because the war time developments were kept secret, the exact timeline might never be revealed to us, but very notable design – lets call it the *optimized 4-layer stack* was developed in 1940s

and is still used today[7]. The comparison of the two AR coatings can be seen in Fig.1-1(a). It was also found that mirrors constructed of dielectric layers are superior in terms of reflectivity and the laser damage threshold is higher compared to mirrors consisting of metallic layers[8] paving the way to laser systems constructed entirely of dielectric optical elements. The reflectivity comparison of silver mirror with a dielectric multilayer mirror is plotted in Fig.1 (b). As the power of computers continued to increase, the calculation for the thin film designs changed as well. Designs started to drift away from quarter wave stacks to designs consisting of layers of different thicknesses, as the thin films stack optimization algorithms started to appear[9]. Besides the advances in designs and deposition techniques, the developments in thin film thickness control are as important. During the last century, the control of thin film deposition has gone from the determination of thickness by observing the color change with eyes[10] as the layer is deposited to invention of turning point monitoring[11] to lately popular broad band optical monitoring[12][13][14][15]. Arguably, the turning point monitoring is the most important development as it unveiled the error self-compensation[16] mechanism that is still a *hot topic* in the thin film community. Indeed, many studies have been done and are still in progress about the error compensation mechanisms linked to various thin film monitoring methods.

1.1.2 Thin film coating examples and applications

Different spectral performances then require different thin film designs. In Fig.1-1 (a) we have plotted the performances of single layer-based MgF_2 antireflective (AR) coating compared to multilayer AR [appendix 1.1 and 1.2]. The multilayer coating consists of 4 layers, two are Nb_2O_5 and two are SiO_2. As can be seen, the reflectance is significantly lower for the 4-layer design over the visible wavelength range. The same can be seen for mirrors in Fig.1-1(b). The reflectance of a 17-layer quarter wave dielectric multilayer mirror (Nb_2O_5/SiO_2) is higher than for single layer silver mirror [appendix 1.3 and 1.4]. The advantage for the silver mirror is of course the wide wavelength range it can be used in. However, for many applications maximizing the reflectance at a single wavelength is the key parameter. Besides the reflectance, the dielectric mirrors have lower absorption losses, what is important for high-power applications such as laser systems. As more and more lasers generate high power densities, the heating of the coating

linked to absorption is becoming a limiting parameters that needs to be controlled[17] and for which dielectric mirrors represent an efficient alternative. Another example of classical thin-film filters are 50-50 beam splitters Fig.1-1(c) [appendix 1.5]. This filter, as the name suggests, splits the incidence beam power in two – it reflects half and transmits the other half.

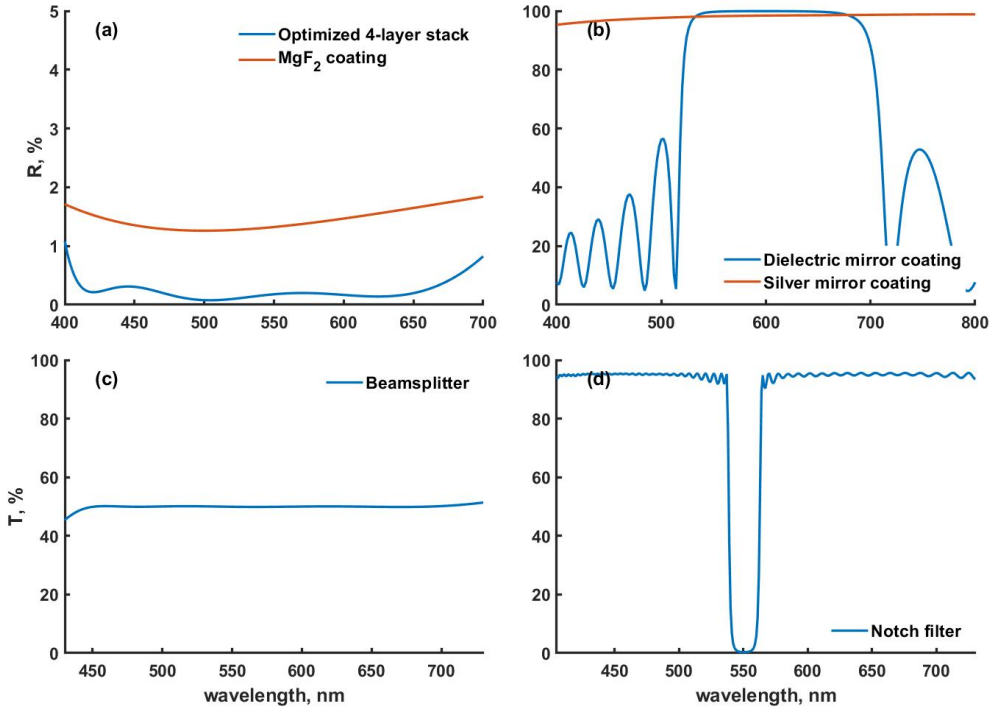

Figure 1-1 Examples of thin film designs: (a) and (b) compares peformance of conventional single layer with multilayer AR and mirror coating. (c) and (d) example of beamsplitter and notch filter design.

As we will demonstrate in following chapters, with the correct deposition and monitoring methods, more complex filters can be fabricated. A typical example is notch filter Fig.1-1(d) [appendix 1.6]. The notch filter is designed to reflect a narrow spectral range and transmits the remaining one. This type of filter is generally quite complex as it includes several tens or hundreds of layers with various thicknesses, but it has many applications in telecommunication, image processing, it can be used in Raman and fluorescence spectroscopy and can be used as protective coating if known radiation source is present (for example laser).[18][19][20]

Besides scientific applications, optical coatings are part of our day-to-day life. AR coating are applied to eyeglasses, TV and computer monitor screens, solar cells[21] and many more devices

we interact with. Heat control coatings[22] are gaining popularty in architectural glazing and automotive industries. Several optical color-filters[23] are used for camera lenses of smatphones and several coatings are applied to construct OLED screens[24].

Various other types of coatings are used not only for optical purposes: so called hard coatings[25] are present on most drills and saws, corrosion resistant coating are used for marine applications[26]. The non-optical types of coatings will not be considered in this work.

In order to obtain high performance optical thin-film filters, various areas of expertise have to be combined: thin film design, optical/mechanical/thermal property determination, deposition methods, thickness monitoring. The aim of this thesis is to further investigate this last field of research.

1.2 Thin film theory

To further look at the optical thin film monitoring, it is necessary to remind the basics of thin film physics. A detailed explanation of thin film calculations and properties have been described by several authors including Angus Macleod[5]. Here we will take a look at the most important parameters and equations that are required to better understand the following work in this thesis.

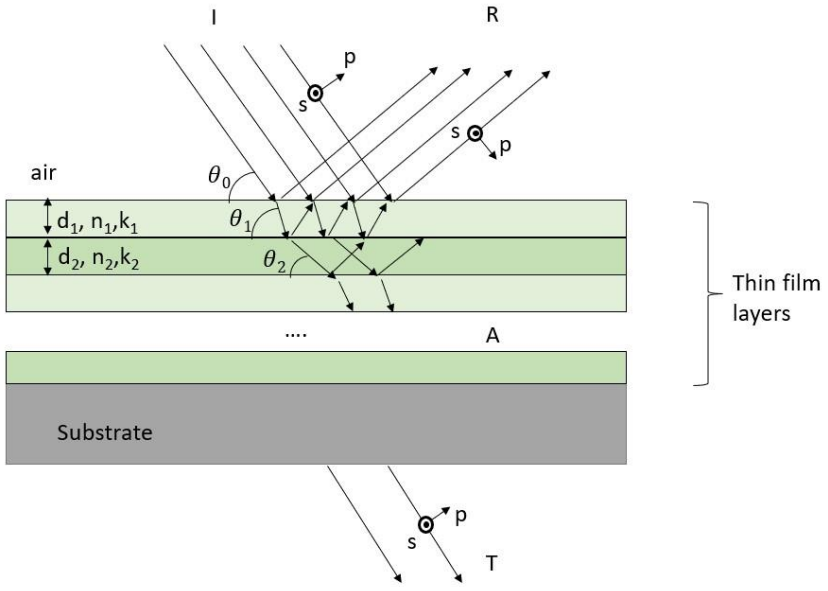

Figure 1-2. Shematics of thin film layers on substrate and light propagation, where I is incidend light, R is reflected, T transmitted, and A is the absorbed light.

When considering a thin film stack, each layer will be characterized by several properties: material related properties such as the refractive index n of the layer, the extinction coefficient k and physical properties as layers physical thickness d. Both refractive index and extinction coefficient are wavelength (λ) dependent but are usually noted as n and k rather than n(λ) and k(λ). Due to interferences within the layers, it is possible to control the spectral properties of the thin film stack, namely the transmittance T, the reflectance R, the absorption A and scattering S. The principle of energy conservation applies to thin films.

$$R + T + A + S = 1 \tag{1.1}$$

Usually, when considering completely transparent materials such as dielectrics, absorption and scattering can be neglected. In this case, the transmittance and the reflectance of the thin film structure are directly related.

A useful method to calculate the thin film stack properties is the matrix method. The important thin film parameters can be combined into individual matrices for each layer which are referred to as *characteristic matrix*. The properties of the full layer stack then can be obtained from multiplying the characteristic matrices in the correct order. It allows relatively easy to calculate the reflectance and transmittance dependence on wavelength and on thickness at the same time.

$$\begin{bmatrix} B \\ C \end{bmatrix} = \left\{ \prod_{j=1}^{q} \begin{bmatrix} \cos\delta_j & \frac{i\sin\delta_j}{y_j} \\ iy_j\sin\delta_j & \cos\delta_j \end{bmatrix} \right\} \begin{bmatrix} 1 \\ y_{sub} \end{bmatrix} \tag{1.2}$$

Where B and C are normalized total tangential electric and magnetic fields at the surface between incidence medium and top layer, $\delta_j = \frac{2\pi\,(n_j - ik_j)d_j\,cos\theta_j}{\lambda}$ is the phase thickness of the j-th layer, $n_j - ik_j$ is the complex refractive index of the layer j, d_j is the thickness, y_j and y_{sub} are the characteristic admittances of the layer and substrate, q is the number of the layers. The characteristic admittance y_j depends on the polarization when the thin-film stack is illuminated under angle of incidence (θ_0) Fig.1-2.

$$y_j = \begin{cases} (n_j - ik_j)cos\theta_j & for\ s-\ polarization \\ (n_j - ik_j)/cos\theta_j & for\ p-polarization \end{cases} \tag{1.3}$$

Where θj is the angle of incidence of the light in the jth layer, and it is depending on the refractive index of the layer according to Snell's law. It is important to note that layers are ordered so that the first layer is facing incident medium, and q is the closest to the substrate. This

contrasts with how we usually denote layers, starting from the substrate. From C and B, we can calculate the admittance Y at the interface of two adjacent layers as

$$Y = \frac{C}{B} \tag{1.4}$$

From this admittance value, we can calculate the reflectance using Eq 1.5 and 1.6. and by considering the entering irradiance and emerging irradiance ratio, we can obtain the transmittance of the filter Eq. 1.7 and 1.8.

$$\rho = \frac{y_0 - Y}{y_0 + Y} = \frac{y_0 B - C}{y_0 B + C} \tag{1.5}$$

$$R = \rho\rho^* = \frac{y_0 B - C \;\; y_0 B - C^*}{y_0 B + C \;\; y_0 B + C^*} \tag{1.6}$$

$$\frac{I_{entering}}{I_{emerging}} = \frac{Re\; 1 \cdot y_{sub}^*}{Re\; BC^*} = \frac{Re\; y_{sub}}{Re\; BC^*} = \frac{T}{1 - R} \tag{1.7}$$

$$T = 1 - R \cdot \frac{Re\; y_{sub}}{Re\; BC^*} = \frac{4 y_0 Re\; y_{sub}}{y_0 B + C \;\; y_0 B + C^*} \tag{1.8}$$

Where ρ is the amplitude reflection coefficient and y_0 is the admittance of incidence medium. These equations correspond to transmittance and reflectance of a thin-film stack deposited on an infinite substrate and therefore do not consider possible multiple reflections at substrate backside.

In this thesis, we only considered spectral measurement at or close to normal incidence. Hence, angular dependence of coatings was neglected. Then, in the case of real substrate with a backside reflection and no absorption the reflectance and transmittance can be calculated using:

$$R = \frac{R_f + R_b - 2R_f R_b}{1 - R_f R_b} \tag{1.9}$$

$$T = \frac{T_f T_b}{1 - R_f R_b} \tag{1.10}$$

Where R_f, R_b, T_f, T_b, are the reflectance and the transmittance respectively at the front and back surfaces. The reflection and transmittance at the back surface of the substrate can be calculated from the Fresnel equations.

The matrix approach is very useful and straightforward method for calculations. For example, let's consider a single layer deposited on a glass substrate. Once the materials have been selected, the only variable input parameters for the characteristic matrices Eq. 1.2 are the

wavelength and the layer thickness. We can then vary the wavelength at a fixed thickness and calculate the spectral dependence of reflection/transmission for a given design or vary the thickness for one wavelength and calculate the evolution of the transmittance/reflectance as function of thickness. We can perform this calculation for a wavelength range, and we can consider our layer to consist of several very thin layers of the same material as shown in Fig. 1-3. In this case we see spectral performance over given spectral range, and we can look at the transmittance evolution as the layers thickness is increased until its final thickness.

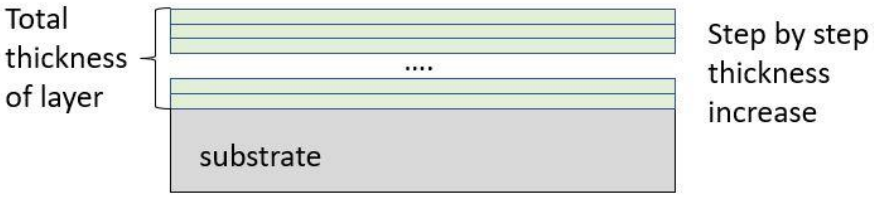

Figure 1-3. Schematic representation of dividing the layer into smaller sub layers of the same material.

The steps for increasing thickness of layer can be adjusted to match the deposition rates of the deposition system. That way, we can calculate exactly what the monitoring system should detect. Usually, we look at the thickness evolution curve with one wavelength, but it can be also beneficial to see how spectra changes in wide spectral region.

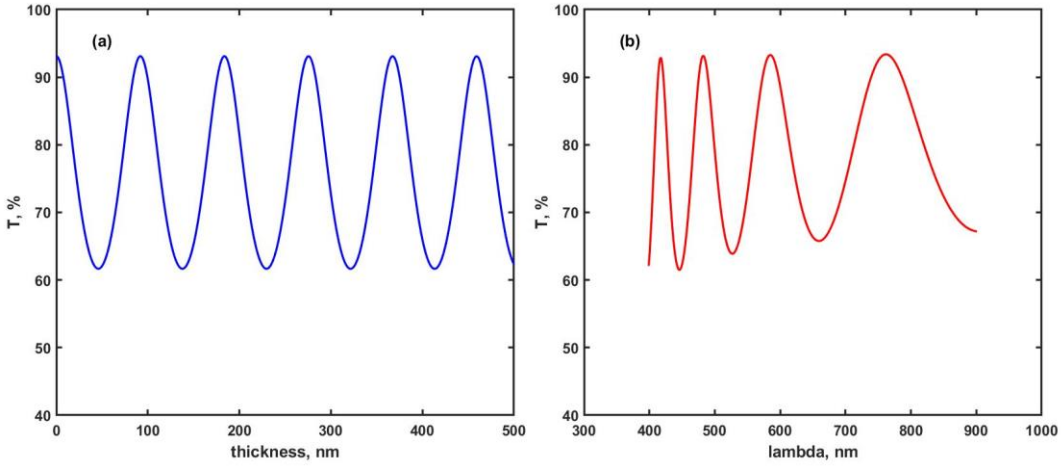

Figure 1-4. (a) - Transmittance evolution depending on the layers thickness, (b) - tranmitance spectra of 500 nm thick Nb_2O_5 layer.

In Fig.1-4 (b) we see the spectral performance of single 500 nm thick Nb_2O_5 layer on top of fused silica substrate. Fig.1-4 (a) shows the same layer if we look at how the transmittance would change with increasing thickness. In this case, we look at wavelength of 450 nm. This curve in Fig.1-4 (a) is often called monitoring curve and the wavelength with what the curve is calculated is called monitoring wavelength.

As can be seen from Fig.1-4(a), at some specific thicknesses, transmittance is maximum - at the level of the bare substrate. In this case the layers optical thickness is $n \cdot d = q\,\frac{\lambda}{2}$, where q is an integer, this is called *half-wave* layer. For half-wave layers the phase thickness δ becomes a multiple of π, meaning that cos δ =±1 and sin δ =0. In this case the *characteristic matrix* of this layer becomes unity matrix and has no effect on the transmittance of the thin film assembly at this wavelength. Therefore, the half-wave thick layers are sometimes called *absentee* layers.
In case when the transmittance is at minimum, the optical thickness becomes $n \cdot d = q\,\frac{\lambda}{4}$ – this is called *quarter-wave* layer. For quarter wave layer the phase thickness δ becomes a multiple of π/2, meaning that cos δ =0 and sin δ =±1. This again is a special case, where the admittance (Y) of the assembly of a quarter wave layer with admittance y_f and substrate becomes $\frac{y_f^2}{y_{sub}}$. This illustrates how, in case of high index material on low index substrate, the minimum achievable transmittance is related to the contrast between the admittances (or refractive indices) of the substrate and the thin film.
We will use the notation H and L to represent a layer which is one quarter wave thick (high or low refractive index respectively). Quarter wave layers are important as various designs are based on quarter wave thicknesses and the *turning point monitoring* is a monitoring technique designed to monitor the quarter wave (optical) thickness.

1.3 Thin film deposition

1.3.1 Deposition methods

There are several methods to obtain thin film layers. On the basis of the growth mechanism of the layers, we can divide these methods in two main groups – physical or chemical deposition

methods. The main difference between the two is the origin of the material that will serve as the basis for the thin film. In case of physical deposition, the thin film is produced by removing atoms from the source (which we will call the target) and then allowing them to move in the vapor phase until they land on the substrate and form a thin film layer[27]. The material can be evaporated by heating the target (thermal/boat evaporation or electron beam evaporation) or it can be sputtered by different methods such as magnetron sputtering, pulsed laser deposition, ion beam sputtering, etc. In both cases, the atoms are removed from the bulk material by physical means, and then they can form a thin film layer. The atoms, when they land on the substrate, can be involved in chemical reactions, such as oxidation. In order for the atoms to move from the target to the substrate, they should not experience additional collisions with other particles in their path. To ensure this the deposition is performed in vacuum chambers.

In chemical deposition, as the name suggests, a new material that will form the thin film layer is obtained by means of a chemical reaction. There are many methods for thin film formation through chemical processes such as *sol-gel*, spin coating, dip coating etc. Two of the most popular chemical thin film production methods are *sol-gel* and chemical vapor deposition (CVD). Both are widely used by the semiconductor industry. The *sol-gel* process involves the formation of a colloidal suspension – *sol*, and then the conversion of *sol* into *gel* – creating viscous gels or solids on the substrate surface. Usually, this process involves a chemical reaction between metallic salt and alcohol. In CVD, the evaporated material forms a layer on the substrate surface by undergoing a chemical reaction. CVD is used not only for the growth of thin film but if certain precursors are used, two dimensional structures such as nanowires and nanoroads can be deposited[28][29]. In contrast to PVD, for some applications, CVD can be carried out at atmospheric pressure, which makes it somewhat easier to realize[30]. Many methods therefore can be used to create thin film layers, each with its strengths and weaknesses. Therefore, the method usually is selected based on the application of the thin film layers.

1.3.2 Physical vapor deposition at Institut Fresnel

Two physical vapor deposition methods are widely used at Institut Fresnel: – plasma-ion-assisted deposition (PIAD) and plasma-assisted reactive magnetron sputtering (PARMS). These two methods differ greatly in their principle of operation and the materials that can be used for the

deposition of thin films. Because of this the field of application, the types of filters associated with each of the methods are different.

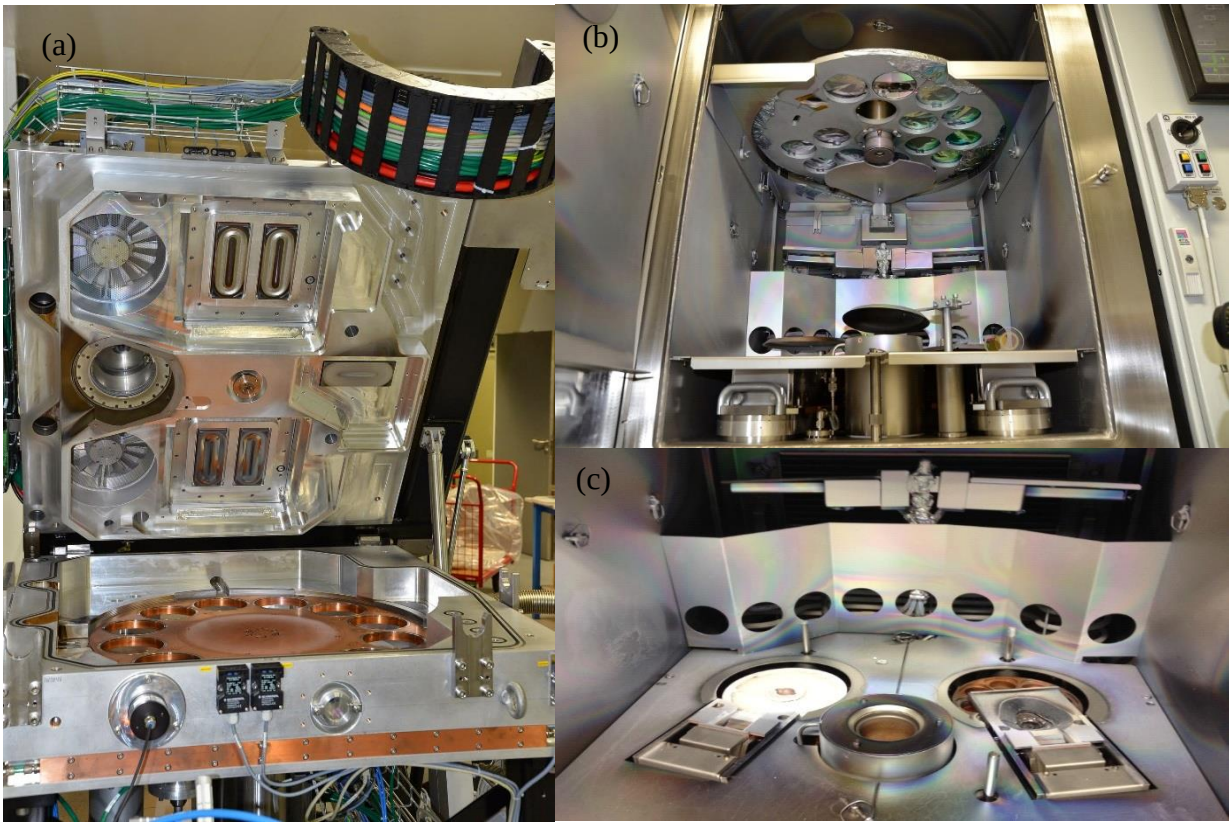

Figure 1-5 (a) HELIOS coater without shutter, targets are on the top and the sample holder rotates beneath them, (b) SYRUSpro coater, the sample holder is on the top, partially covered by the uniformity mask, (c) SYRUSpro coater, targets and ion source (in middle).

At Institut Fresnel, plasma-assisted reactive magnetrons sputtering (PARMS) is performed with the *HELIOS 400* coater and plasma ion assisted deposition (PIAD) with a *SYRUSpro 710* machine, both developed by *Bühler Leybold Optics.* In both coaters, high and low index materials can be deposited in the same deposition run. As both are physical vapor deposition methods, there are similarities between the two coaters, but their differences make one more suitable than the other for the optical filters we will discuss in this thesis.

1.3.2.1 Plasma ion assisted deposition

One of the well-known methods of physical vapor deposition is evaporation. By heating material to sufficiently high temperatures, it is possible to reach a point where a solid material melts and, if it is heated even further, the material starts to evaporate. These evaporated atoms can land on other surfaces, cool down and form a thin film layer. There are several ways to heat the target. Some form of resistivity heating can be implemented; however, it would be inefficient because the melting point is very high for several materials. To increase the efficiency, it is possible to heat small spots of a target surface with a highly energetic particle beam.

One such method is electron beam evaporation or *E-Beam.* To evaporate material from target, the chamber must be evacuated to levels of 10^{-5} mbar or less. To achieve this high vacuum, Meissner traps and turbomolecular vacuum pumps are typically used for these types of coaters. The high vacuum is necessary to minimize contamination of the coating and to avoid collisions of the deposited atoms before they condense on the substrate surface. The electron gun can be used as source of energy for the evaporation. The electron beam from the electron gun is accelerated towards the target surface where it increases the temperature high enough to start the evaporation process. The evaporated material can then deposit on the substrate surface and form a thin film. The deposition rate can be controlled by the power applied to the electron gun.

To improve the layers density and stoichiometry of the layer, a plasma ion source can be added to the vacuum chamber [31]. The ion bombardment adds energy onto the forming layer, allowing the atoms to ‘move’ and re-structure the layer compared to its original state, resulting in a denser coating compared to standard evaporation techniques[32]. A reactive gas such as oxygen can be added to the process either via a plasma source or through a designated inlet, to create oxide layers. This process, when the plasma source is used to assist the evaporation, is called plasma ion assisted deposition – PIAD. Simplified schematics of the PIAD process are presented in Fig.1-6.

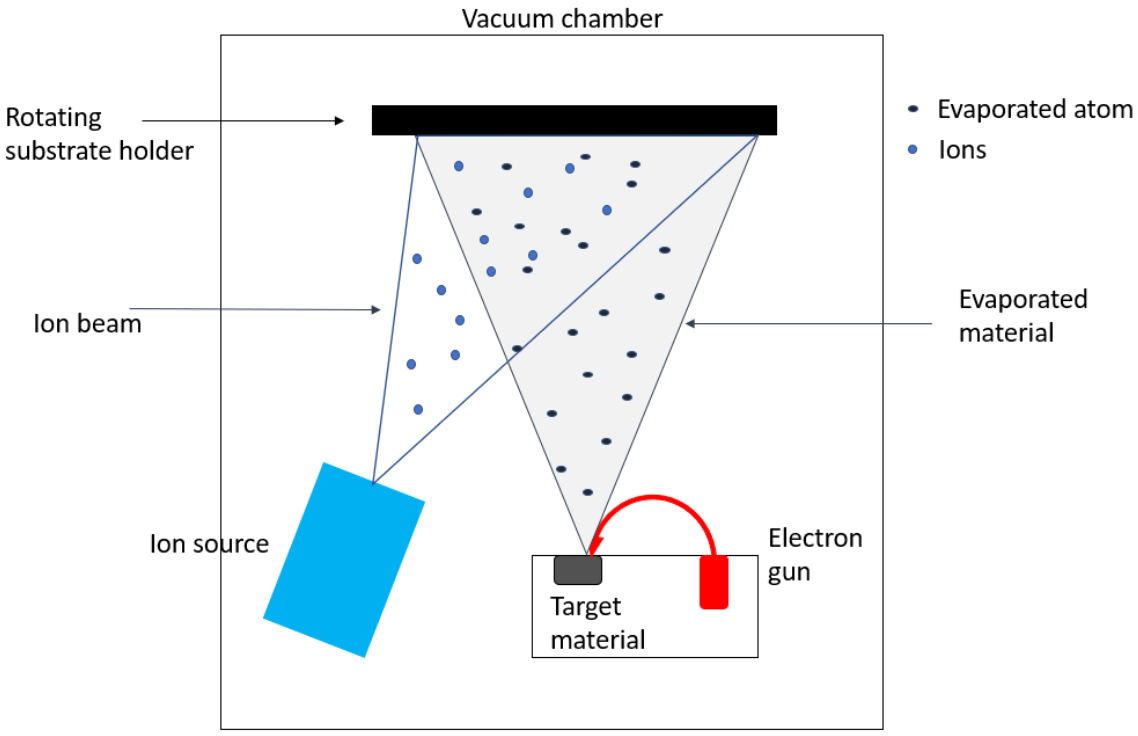

Figure 1-6 Schematics of PIAD coater.

The evaporated material from the target forms a balloon like shape and the sample holder is sometimes bent to fit the shape of evaporated flux (calotte). The uniformity mask is used to control the material distribution and achieve more uniform layers. Various types of materials can be used with this deposition method, the targets can be metallic, ceramic, alloy, composite, etc. The target can be fixed on a copper cooling plate, or it can be in granular form and placed inside a crucible. This deposition method is popular, as coatings with low contamination can be produced, but the deposition rates are lower than those of magnetron sputtering.

The SYRUSpro coater is a typical *box coater*, the chamber has to be vented each time there is a need for sample change. Samples are placed on a rotating sample holder table, and as the table rotates, a thin layer is applied in each revolution. There are two shutters to cover the two targets. The shutters are opened during deposition and closed to terminate the deposition of given layer. Additional substrate heating is possible with SYRUSpro coater. Heating is often required to achieve the needed stoichiometry of the layers. Layers thickness can be controlled by an optical monitoring or a quartz crystal microbalance.

1.3.2.2 Plasma assisted magnetron sputtering

Sputtering is a process where energetic particles bombard the target material, causing atoms to leave the target, which can then condense on the substrate or other surfaces.

In case of magnetron sputtering, the energetic particles (usually argon ions) are generated in a plasma that is captured by the magnetic field created by permanent magnets placed behind the target. As shown in Fig.1-7, when negative voltage is applied to the target, positively charged ions are accelerated towards the target surface and can eject atoms off the surface. These atoms can then land on the surface of the substrate and form a thin film layer[27]. Noble gases such as argon, krypton or xenon are usually used for deposition and are referred to as working gas.

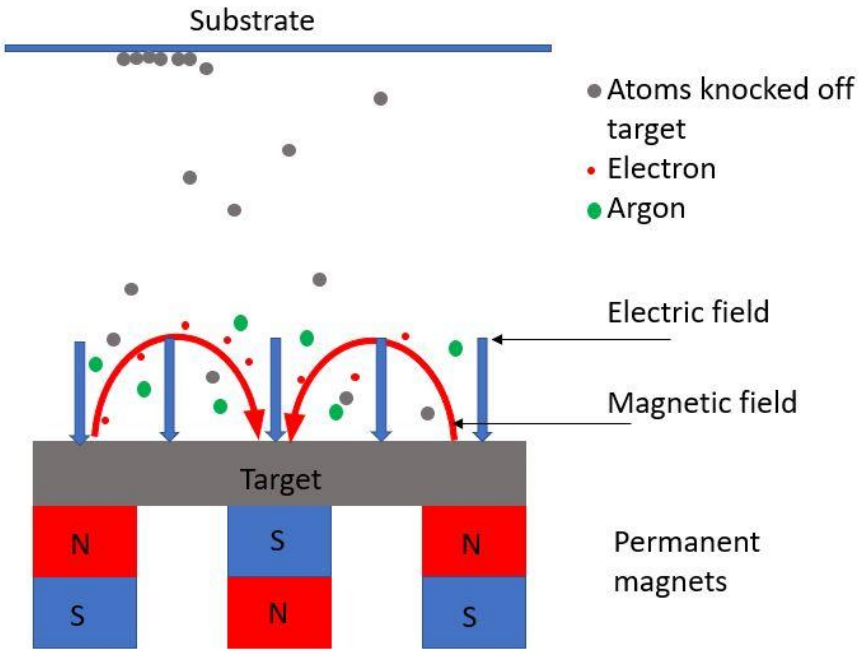

Figure 1-7 Simple schematics of magnetron sputtering deposition process.

Magnetron sputtering is performed under a relatively high vacuum to ensure the necessary main free path for atoms to reach the substrate surface. The vacuum is usually maintained by two level pumping with root pumps for pre-vacuum and turbomolecular pumps for high vacuum. Meissner traps are also sometimes used to provide high vacuum levels. Although most vacuum chambers can reach 10^{-7} mbar, the deposition is usually performed at 10^{-4} mbar levels.

The deposition process can be further improved by adding a reactive gas to the deposition zone. Indeed, the atoms landing on the surface of the substrate can take part in chemical reactions and

form not a purely metallic thin film but rather a compound. This type of deposition is called reactive magnetron sputtering. For optical applications, the most popular thin films are oxides, however nitride and sulfide thin films are also deposited for some applications. Besides adding reactive gases, it is also possible to co-sputter from targets containing different materials to create composite thin film[33].

A wide range of target materials can be used for magnetron sputtering. Depending on the type of power supply used, the targets can be metallic or ceramic (partially oxidized). As for the substrates, unless they are made of materials evaporating in vacuum, they can be coated if the adhesion between the layer and the substrate is good. For optical applications, the most popular thin film materials are SiO_2 as the low refractive index material and Nb_2O_5, TiO_2, Ta_2O_5 and HfO_2 as high index materials, all of which can all be deposited from corresponding metallic or ceramic targets.

When the deposited atoms arrive at the substrate during deposition, their energy can be low and these atoms will stick and form the growing layer where they landed. This can result in a situation where the films have a high surface roughness and the thin film has a self-shadowing effect. This can lead to a porous thin film. Additional energy must then be added to the growing thin film to improve its quality (porosity, surface roughness). One option is to heat the substrate if the deposition system configuration allows it. However, heating cannot be done when considering plastic substrates. Another option is to introduce additional bombardment of the growing layers by energetic particles such as ions[27].

Indeed, by implementing additional ion bombardment on the surface of the growing layer, higher density thin films can be produced. In addition, to improve surface and bulk properties, if oxygen plasma is used, it can also be used as a reactive gas for reactive deposition. This can reduce the amount of oxygen distributed near the cathodes, which is beneficial for deposition rates and reduce arcing of the targets[27][34].

This process, in which an oxygen ion source is used to oxidize and transfer energy to the magnetron sputtered layers, is called plasma assisted reactive magnetron sputtering (PARMS). This type of deposition is implemented in Bühler *HELIOS* coaters.

The HELIOS coater consists of a deposition chamber and a substrate handling chamber separated by a load lock. This allows the substrates to be changed without braking vacuum in the

deposition chamber. The deposition chamber consists of a rotating table where the samples are placed. As the table rotates, the samples pass under a mid-frequency dual magnetron where a sub oxide or metallic layer is deposited. This layer then can be completely oxidized as it passes under a radio frequency plasma source that uses oxygen as the working gas. The rotation speeds are in 200 rpm range. With such high rotation speeds, an atomic thickness layer can be deposited with each revolution. During each rotation, an intermittent transmittance measurement also can be performed. For most applications, a halogen lamp is used as a light source because it emits from ultraviolet to infrared range. The light that has passed through the measuring window is then collected in an optical fiber, and a monochromatic or broadband monitoring unit can be used for thickness control.

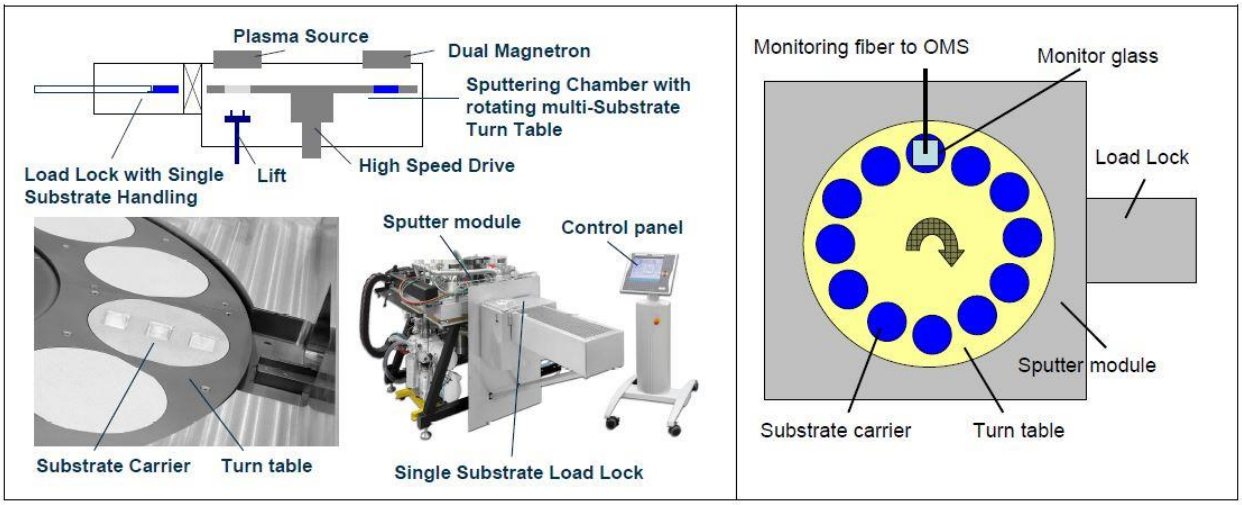

Figure 1-8 Schematics of HELIOS coater [34].

There is also a shutter between the targets and the rotating table that can separate the two. The shutter is necessary, not only to terminate the deposition of a layer, but also to allow the targets to reach operational power before starting the deposition on the substrates. HELIOS is also equipped with a heater to maintain a more or less constant temperature during deposition. Three different targets can be placed in HELIOS at the same time. Two dual magnetron positions are used for high and low index oxide layers and one single magnetron position is reserved for the deposition of metallic layers [34].

1.3.2.3 Comparison of the PVD methods

HELIOS and SYRUS are different thin film coaters, not only the basic operational principle is different, but also the geometry of the two machines. The targets are further away, and the deposition is performed upwards and under in higher vacuum for SYRUS compared to HELIOS. As a result, the thin film coating associated with this method are less contaminated by particle defects. However, the deposition rates are higher for magnetron sputtering - ~0.5 nm/s compared to ~0.25 nm/s for PIAD and more importantly, the rate is more stable for magnetron sputtering. The rotational speed of the sample holder is around 200 rpm for the HELIOS coater, while it is only 33 rpm for the SYRUS coater. A higher rotational speed of the table ensures a higher precision of the thickness monitoring. With the HELIOS coater, we can adjust the rotation speed so that a 0.1 nm layer is deposited each time substrate the passes under the target. We cannot always measure the layer *in-situ* with such precision, as we will show in following chapters, but this level of control is necessary for the complexity of optical components required today. The stable deposition rate associated with magnetron sputtering and the level of thickness control that can be achieved in the HELIOS coater is the one of the reasons why we are using this machine for the thin film optical filters we will describe in this thesis.

1.3.3 Materials associated with the two deposition methods

Different materials can be used with both deposition methods. Magnetron sputtering is more limited in the materials that can be deposited because targets must be fabricated for each material. Some of the materials that can be deposited in Institut Fresnel with both deposition machines and their properties are listed in Tab.1-1.

Deposited material	HELIOS		SYRUSpro	
	n	k	n	k
Nb_2O_5	2.395	$1 \cdot 10^{-6}$	2.311	$1 \cdot 10^{-6}$
HfO_2	2.072	$2.3 \cdot 10^{-5}$	2.026	$7.5 \cdot 10^{-5}$
SiO_2	1.488	-	1.496	-
Ta_2O_5	2.188	$3.1 \cdot 10^{-5}$	2.187	$4.6 \cdot 10^{-5}$
Sb_2S_3	-	-	3.456	0.587
Sb_2Te_3	-	-	3.477	2.136
As_2S_3	-	-	2.656	0.011

Table 1-1 Comparison of material deposited by both PVD methods, refractive index n and extinction coefficient k given at 500 nm wavelength.

As we can see, the SYRUS coater is associated with a wider range of materials, as it is not limited to oxide layers. If we compare the materials we can deposit on the two coaters, we see that the refractive indices and dispersion data for the same materials are different. In fact, if we look at Nb_2O_5 and SiO_2 – two very popular materials for optical thin film filters – we find that the refractive index contrast defined as $n(Nb_2O_5)$ /$n(SiO_2)$ is 4% higher for the layers obtained with HELIOS coater. Since high index contrast is desirable for many optical coating designs, this is another reason why the depositions for this thesis were carried out with HELIOS coater.

Chapter 2 - Monitoring techniques of optical coatings

In this chapter we will discuss the needed precision for the control of thin film thickness for optical filters using several examples. We will discuss the thin film thickness monitoring methods available to date. We will also illustrate the strengths and weaknesses associated with the different monitoring techniques.

2.1 Design sensitivity to errors

The spectral performances of thin-film filters are given by the optical properties and thicknesses of individual layers. Changing the properties of one or more layers will therefore influence the final spectral performances of the filters and this sensitivity is design and layer dependent. In order to secure final performance close to the theoretical one, it is important to minimize these errors. There are many known methods to control the thickness of the deposited layers. Thickness determination can be performed inside the coater, during the coating run, or after the coating is completed. The thin film thickness can be determined from optical measurements or from physical measurements. Each of the methods used has some tolerances and limits of application.

Besides the measurements, coating methods and coater geometries can influence the achievable accuracy of the thickness monitoring. In the end the combination of coating method and the measurement method will set the limits for achievable accuracy. In this section, we will analyze the error sensitivity for different types of designs and parameters

2.1.1 Random thickness errors in optical coatings

Before we look into details at the various thin film thickness control methods, we can look at how filter designs are affected by thickness errors. We can make a simple calculation where we compare the theoretical design to a slightly modified design where a random thickness error is added. There are several ways in which we can add a random thickness error. We will consider here two options: we can assume an absolute error with a fixed thickness value or a relative error

that can be defined as a specific percentage of each of the layers' thickness. In the first case, we can assume that the thickness error is ±1 or ±2 nm for each of the layers, and in second case we can assume that the error is ±0.5% or ±1% of the layers thickness. These errors were applied to different types of filters and the final spectral performances were recalculated.

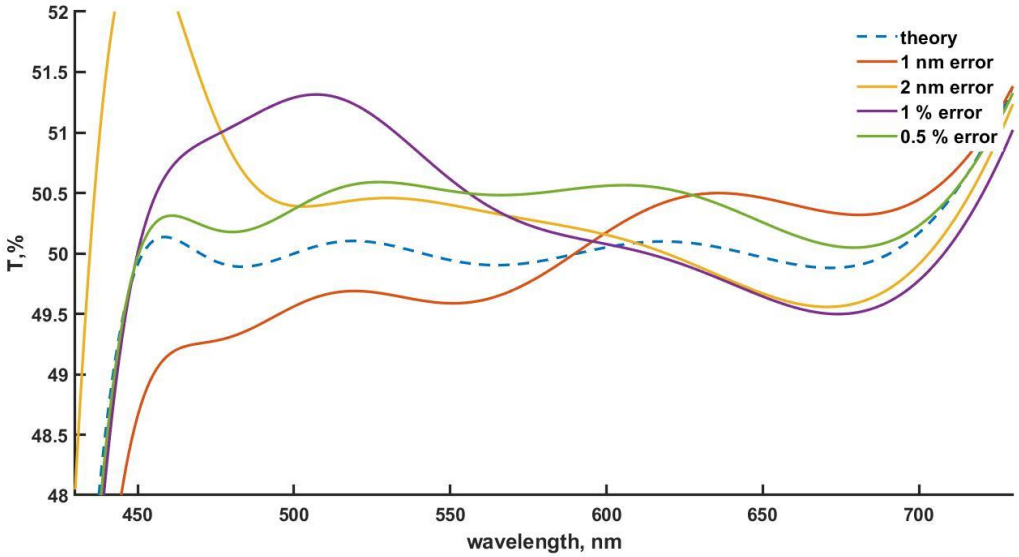

Figure 2-1 Different random error influence on the spectral performance of a 50% /50% beamsplitter design.

In Fig.2-1 we plotted the typical effect of these random errors on a 8-layer beam splitter design [appendix 1.5]. The thinnest layer in this design is 20 nm thick and the thickest is 135 nm. As can be seen, a random thickness error of 2 nm for each of the layers in the design has a very significant impact on performance, changing the spectral response by several percent. Except for the 0.5% error, in all cases, the errors highly distort the filter's spectral performances and do not allow to stay in the 50% ± 1% transmittance corridor. In addition, different spectral regions may be affected. Ideally, one must run multiple simulations to test how various pairs of errors affect performance, as it is sometimes possible that even random errors in later layers compensate for errors in previous layers. As a conclusion, keeping the transmittance within a 50% ±1 % corridor would require a deposition setup that can deliver coatings with a thickness accuracy around 0.5%. However, there are not many deposition and monitoring setups that can easily deliver coating with such narrow thickness error tolerance.

Another interesting example is the antireflective coating which consists of 4 layers with thicknesses ranging from 12 to 120 nm [appendix 1.1]. If similar random errors are applied to each layer thickness, and the transmittance is recalculated (Fig.2-2(a)), we see this time that the spectral performances are hardly affected by the errors. This means that this simple 4-layer design is not sensitive to thickness errors, and that we do not need as accurate deposition/monitoring setups as for the beam splitter.

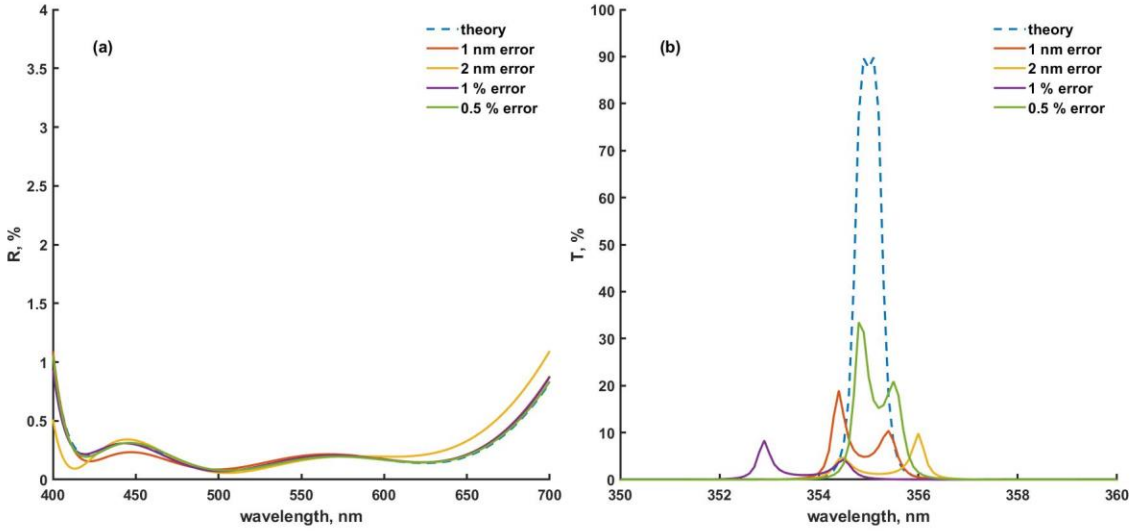

Figure 2-2 Random thickness error influence on antireflective coating and multi cavity Fabry-Perot filter.

Finally, in terms of sensitivity to random thickness errors, one of the most sensitive designs is the multi-cavity Fabry-Perot filter. If random errors are incorporated into a two-cavity Fabry-Perot filter [appendix 1.7] and the transmittance is recalculated (Fig.2(b)), any random thickness errors would completely destroy the performance of the filters, reducing the transmittance at resonance from 90% to <10% (note that in Fig.2-2(b) we are now looking at the full 100% scale compared to the 4% scale we used to illustrate the error effect on previous designs). The key word for this example is 'random' as it can be shown that these designs can actually tolerate quite large thickness errors if they are followed by compensating layers of varying thickness[35]. This result shows that very specific and adapted optical monitoring methods must be used for the deposition of these filters in order to obtain high performance filters. Therefore, monitoring techniques

associated with error self-compensation such as *turning point monitoring* are well known for bandpass filter monitoring and will be discussed later on.

2.1.2 Refractive index errors in optical coatings

In addition to thickness errors, the refractive index may also differ from the nominal value used in the design phase. There can be several reasons for instabilities of refractive index, mainly associated with the deposition method used. The error can therefore be systematic or random. Systematic error can be related to changes in optical properties as samples move from vacuum to air (especially for porous or non-oxide layers), changes in deposition parameters/conditions over time (which usually means that the index determination must be repeated), or simply to an ex-situ spectral measurement biased by the non-linearity of a detector. Random refractive index errors are generally associated with deposition methods, such as PIAD, where deposition conditions (temperature, crucible and target material quality) can change and will affect the refractive index during deposition. We implemented an approach similar to that in section 2.1.1, to evaluate the effect of random refractive index errors from 0.2% to 2% for each of the previously studied designs.

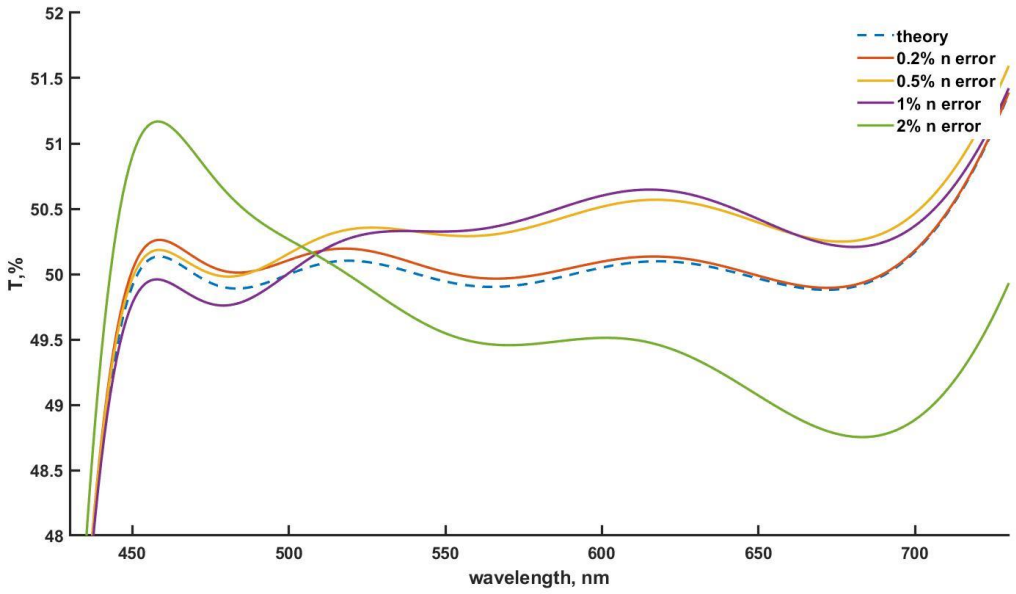

Figure 2-3 Random refractive index error influence on beamsplitter design.

We have plotted in Fig.2-3 the spectral response of the beamsplitter design with different random refractive index errors. As can be seen, as the error increases, the deviation from the nominal spectral performance becomes more and more noticeable. In case of systematic errors, we would see that the spectrum is either above or below the target, however, since we consider here random error, we see that the spectra is tilted.

If we introduce the same errors to the antireflection coating (Fig.2-4(a)) we also don't see large deviations from the original spectrum. These types of coating can indeed tolerate relatively large errors, not only in thickness but also in refractive index.

An interesting situation is that of Fabry-Perot filters. If one considers random refractive index errors while maintaining the expected physical thickness, the effects are very similar to that of random thickness errors. The filters shape would be destroyed for the same reasons as before, the important parameter being the optical thickness (product of the refractive index and physical thickness) of each layer. However, if we consider random refractive index error and re-calculate the physical thickness for each layer to maintain the expected optical thickness of each layer, there is virtually no effect on filters performance. This is of course the result of the so-called *quarter-wave* design, and the self-error compensation mechanism[36]. As already mentioned, Fabry-Perot filters are generally optically monitored by *turning point monitoring*, a method designed to control directly the optical thickness of the layers by adjusting physical thickness in case of an index variation.

In the case of very narrowband filters, however, there is an aspect of refractive index errors that sometimes influence the Fabry-Perot filters performances. On some occasions it can be seen, that although the production run is completed as expected, when the filter is measured outside the coater, the centering wavelength has been shifted. This can be the result of the fact that the layers, when deposited in the vacuum chamber, have different properties to those determined *ex-situ*.

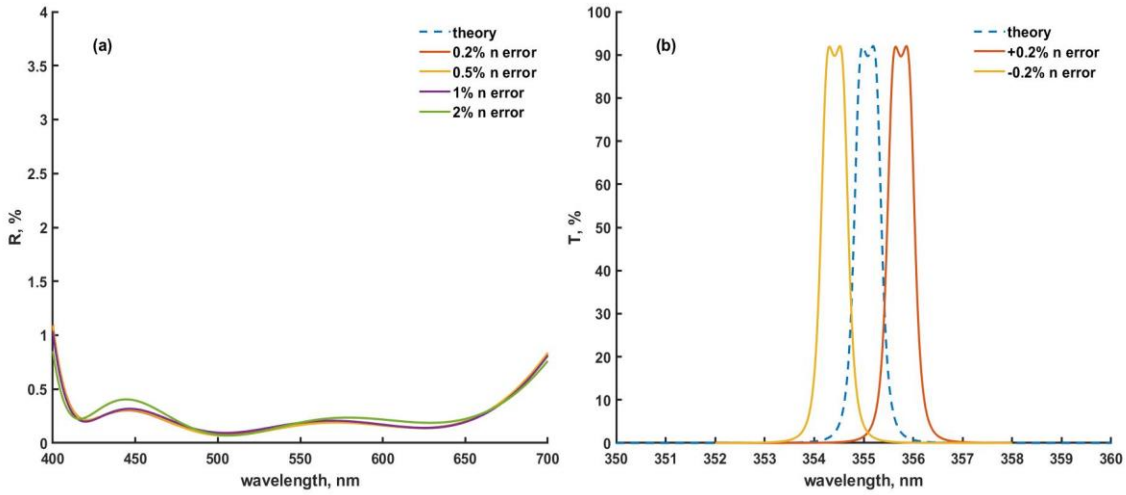

Figure 2-4 Random refractive index error influence on antireflective coating and multi cavity Fabry-Perot design.

In Fig.2-4(b), we have calculated the spectral performances of a filter if all layers have a systematic refractive index error for each layer of ± 0.2%. We can see how the filter centering is shifted in the same direction as the refractive index. The refractive index changes with temperature[37] and the temperature in the deposition chambers is usually well above 100 degrees Celsius, therefore we sometimes see this effect. For Fabry-Perot filters, various other parameters can influence the centering, such as substrate expansion with increasing temperature[38][39], and while refractive index errors can play a role, this will not always be the dominant effect. We will discuss Fabry-Perot filters in detail in chapter 3.

As we have seen in these three examples, different designs have different errors sensitivities. Because errors sensitivity differs, different coating technologies and thickness monitoring strategies are needed for different designs. Since a simple four-layer antireflective coating has low error sensitivity, it can be deposited by various technologies, including large scale *in-line* coaters and thickness monitoring can be performed *ex-situ*. In contrast, for more complex thin film filter such as beamsplitters or Fabry-Perot filters, much more precise coating tools, such as HELIOS or SYRUSpro (both discussed in previous chapter), must be used in combination with advanced *in-situ* thickness monitoring systems.

2.2 Thin film monitoring techniques

Regardless of the design and the fabrication technology of a coating, some type of layer thickness control is necessary. There are many methods of thin-film monitoring: the monitoring can be performed inside the coating machine (*in-situ*) or outside of it (*ex-situ*); the measurement itself can be physical or optical. The measurement can be used online to control the deposition or it can be performed off-line to characterize the filter performance after deposition. Currently, the most accurate technique is based on an *in-situ* optical measurement of the thin film properties with several options for performing it.

The most important monitoring methods can be summarized in the flowchart in Fig.2-5. A similar chart was proposed by Tikhonravov *et al*.[35], but here we have added the two broadband strategies currently available at Institut Fresnel and also the polychromatic monitoring, that we will discuss in great details in chapter 4. All of these measurement methods shown in Fig. 2-5 are used to control the thickness of the thin film.

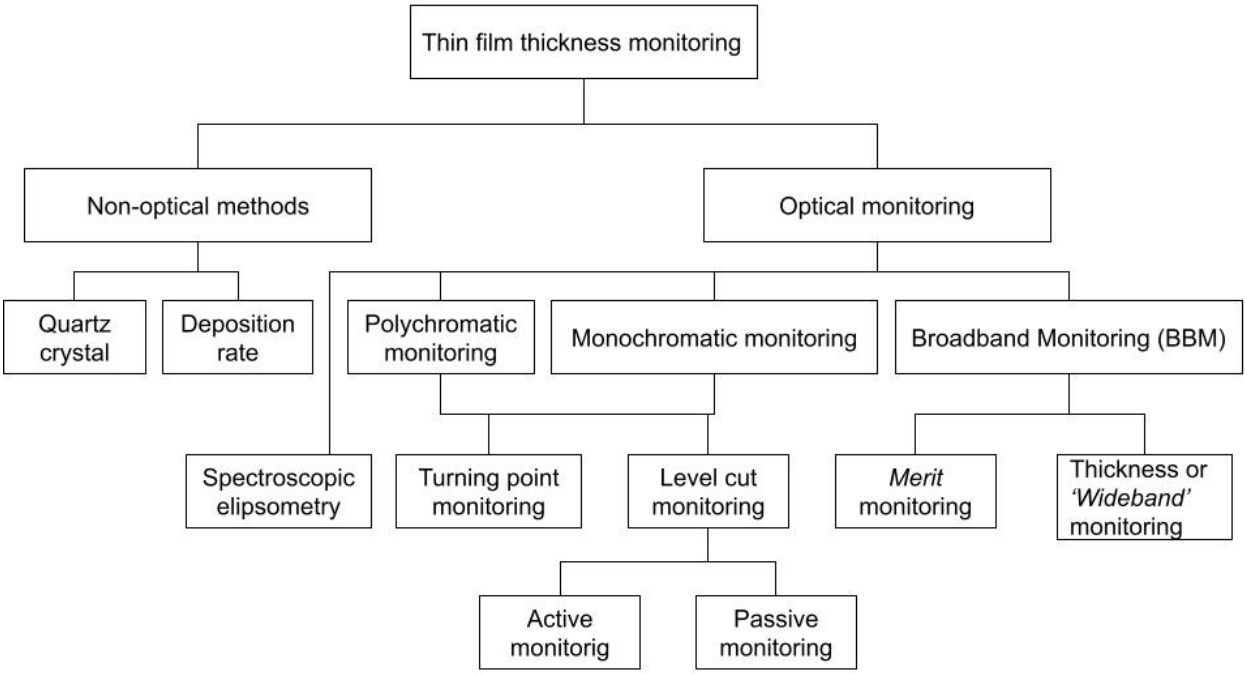

Figure 2-5 Schematic overview of the monitoring methods.

We have divided thin film monitoring methods into two main groups – optical and non-optical monitoring. Both have their strengths and weaknesses and a precise knowledge about all methods is necessary when selecting a monitoring strategy because there is no single method that is suitable for all thin film designs and applications. As we will show later, selecting a monitoring strategy involving multiple monitoring methods can be very desirable.

Regarding optical methods, the difference between monochromatic and polychromatic monitoring is the restriction of the number of usable wavelengths. Generally, one tries to minimize the number of wavelengths used for monitoring, but we will show that good results can be achieved even if the number of monitoring wavelength changes is equal to the number of layers. This last method is called polychromatic monitoring. We have excluded the direct/indirect monitoring division because it applies to all optical methods. To understand the strengths and weaknesses of these methods, we investigate hereafter each of them. However, we have mainly focused on the methods available and frequently used in Institut Fresnel.

2.2.1 Non optical monitoring methods

2.2.1.1 Quartz Crystal monitoring

One of the most popular non-optical thin film measurement methods is quartz crystal microbalance monitoring (QCM). An oscillating quartz crystal can be placed in the deposition chamber, and when the deposited material lands on it, the resonant frequency of the crystal decreases. The mass that landed on the crystal is proportional to the thickness that is deposited on the substrate. The frequency shift will be different for different materials that can be deposited. The oscillation frequency is usually 5 or 6 MHz which should provide atomic scale control accuracy, however the accuracy of the measurement depends on several factors related not only to the crystal but also to the mechanical setup[40]. Since this is an indirect method, the placement of the crystal and substrate inside the chamber is not exactly the same and the amount of material reaching the two will be different. An additional calibration for this offset must then be performed.

The achievable precision is ~2% of the thin film thickness[41] which is not sufficient for complex multilayer optical filters as we demonstrated at the beginning of this chapter. The

resonance frequency change with increasing thickness is quite linear until layers with several micron total thickness are deposited. Beyond this thickness, the relationship between the resonant frequency change and the deposited mass is no longer linear and makes it more difficult to use it to complete an accurate deposition process[5].

To ensure precise control over larger thicknesses, several QCMs' can be placed inside the coater and changed when they become unreliable. The accuracy is then highly dependent on the crystals themselves as the calibration factor of one QCM will be used for the rest of the batch. As it is a non-optical monitoring method, it can be used for metallic and oxide layers.

QCM is a popular control tool for evaporation technologies. For sputtering, the deposition rate is generally stable enough to achieve a similar level of accuracy through time monitoring.

2.2.1.2 Time (rate) monitoring

Another non-optical method for thin film monitoring is time or deposition rate monitoring. The idea of this method is to record the deposition rate in nm/second and use this rate to determine the deposition time for each of the layers. The rate can be obtained by additional calibration runs when thin films are deposited for a certain time and then the thicknesses are determined by *ex-situ* measurement, both physical and optical. If an *in-situ* optical monitoring is available, the rates can be recorded for the first deposited layers, and then used for the last layers of the filter. Similarly to QCM, rate monitoring can be used for both transparent and opaque thin films. One concern with this approach is that the deposition rate might change with target erosion and is not constant over long periods of time.

For designs that are not too sensitive to thickness errors, non-optical monitoring is sufficient. For example, antireflective coatings as we have shown, are not too demanding in terms of thickness monitoring accuracy. Bragg mirrors, consisting of tens of layers, can be successfully deposited by calibrating the rate on the first few layers, and then depositing the majority of the layers by rate monitoring, as small errors will slightly shift the centering wavelength without losing the mirror properties[42]. With non-optical monitoring methods, only the physical thickness of the layers can be controlled. However, for designs such as Fabry-Perot filters, the optical thickness must be controlled and, for such designs, optical monitoring is mandatory.

2.2.2 Optical monitoring methods

To achieve greater accuracy in thin film control, optical monitoring is widely used. There are several ways to implement it in a vacuum coater, but the main principle remains the same: to monitor online the evolution of transmitted or reflected intensities as thin films are deposited on a substrate, and then to terminate the deposition when the measured intensity corresponding to the required layer thickness is reached. The setup is generally quite basic. It usually consists of a light source and a detector, with a monochromaticity obtained either by the source or by the detector. Apart from the quality of the optical systems which is not the subject of this thesis, most of the performance depends on how the signal is processed and analyzed. Below, we will review the various monitoring techniques available today.

2.2.2.1 Spectroscopic ellipsometry

One of the optical monitoring methods that can be used for thin film layer monitoring is *in-situ spectroscopic ellipsometry*. Ellipsometry is a measurement method for determining the thickness and optical properties of thin films and substrates, generally working with a reflection configuration. With this method, the change in polarization upon reflection is measured under a fixed oblique incidence. The polarization change can be used to model the thin film properties such as thickness and refractive index. For reflected light, the polarization change ρ can be described by two values - Ψ and Δ representing respectively, the ratio of the reflected amplitudes, and the phase difference upon reflection.

$$\rho = \tan(\Psi)\, e^{-i\Delta} = \frac{r_p}{r_s} \tag{2.1}$$

Eq.2.1 is the fundamental equation of ellipsometry, where r_s and r_p are the reflection coefficients of polarized light. Spectroscopic ellipsometry is sensitive to thin film thickness and optical constants, but it is not a direct measurement. In general, ellipsometric characterization of a thin film is an inverse problem – the measurement can be predicted (simulated) from the sample description, but the properties of the thin film cannot be calculated directly from the measurement. The accuracy of the method then depends heavily on the precision of the refractive index dispersion models used for the simulations[43][44].

Although this technique is commonly used for single layers characterization (especially for metallic thin layers) and has already been implemented in coatings machines[45], it remains marginal compared to other techniques – such as spectrophotometric measurements of *in-situ* optical monitoring. Moreover, as such a technique is not available at Institut Fresnel, therefore we will not go into the details of this method.

2.2.2.2 Spectrophotometric optical monitoring

Several very popular and widely used methods for the fabrication of thin film filters are based on the measurement of light intensity. To implement these methods, the modulation of the light intensity during the deposition of the layer are measured. The intensity of the light passing through the sample to be coated (I_{sample}) is compared to the incident intensity ($I_{reference}$) measured by the same detector and the dark signal (I_{dark}, i.e. when incident light if off). Transmittance (or reflectance) can be easily calculated using the following normalization formula.

$$T = \frac{I_{sample} - I_{dark}}{I_{referenece} - I_{dark}} \cdot 100 \qquad (2.2)$$

Depending on the type of detector, two types of optical monitoring techniques can be implemented:

Monochromatic optical monitoring is performed if a monochromator and a detector are used to collect the transmitted intensity. As the name suggests, in this case, only one wavelength is considered for the measurement. The measured signal is the transmittance, dependent of the thickness, (T(d)), and this information can be used to terminate the deposition of a given layer. By pre-calculating the T(d) curve before the deposition and comparing it to the measured data in real time, one can determine the trigger points – instances when the deposition should be stopped. Of course, nowadays, this is done automatically, and the end of deposition is triggered by a designated computer. We will discuss all parameters and functionalities of such a monitoring system with examples in the following sections.

Broadband optical monitoring is possible if an imaging CCD/CMOS/PDA spectrometer (generally grating-based) is used for collecting the transmitted intensity. In this case, the transmittance is measured simultaneously over a wide spectral region, providing much more data

for processing. The idea of broadband measurement for thin film monitoring is almost as old as monochromatic measurement, but it is only recently that the computational power and advances in detector matrices have allowed this type of systems to be used with confidence. As with monochromatic monitoring, broadband spectral measurement can be used to stop layer deposition. The principle of data acquisition is very similar, the same process as in Eq.2.2 is performed, this time over the full spectral range. The broadband measurement provides more information compared to the monochromatic measurement: from the spectral data, it is possible to calculate the physical thickness of the deposited layers, assuming that the refractive index dispersion of all materials is well-known. The thicknesses information can also be used to re-optimize the remaining layer thicknesses, re-calculate the target curves, or give an indication that the witness glass should be changed. There are several ways to use the broad band signal for thin film monitoring, which will be discussed later on.

2.3 Monochromatic optical monitoring at Institut Fresnel

Monochromatic optical monitoring has proven to be a very effective method for thin film control. It has been demonstrated on various types of deposition machines[34][42][46][47]. This means that it is now one of the most used methods for the control of various types of optical filters. This is why all the thin film coaters in Institut Fresnel are equipped with this type of thin film optical monitoring systems.

2.3.1 Bühler HELIOS 400 coater and OMS5100

The HELIOS 400 coater used in this work is equipped with the OMS (optical monitoring system) 5100 also developed by Bühler Leybold Optics. The monitoring setup consists of a light source, collimating lenses, an optical fiber cable and the detector. The complete arrangement of the detector layout is confidential, but the most important parameters are known: several detectors can be used (Si, InGaAs, PTM, Pb), the wavelength is selected by diffraction gratings and mechanical slits are placed in the light path. The width of the slits is adjustable; only one detector can be used at a time. Schematics of the setup are presented in Fig.2-6.

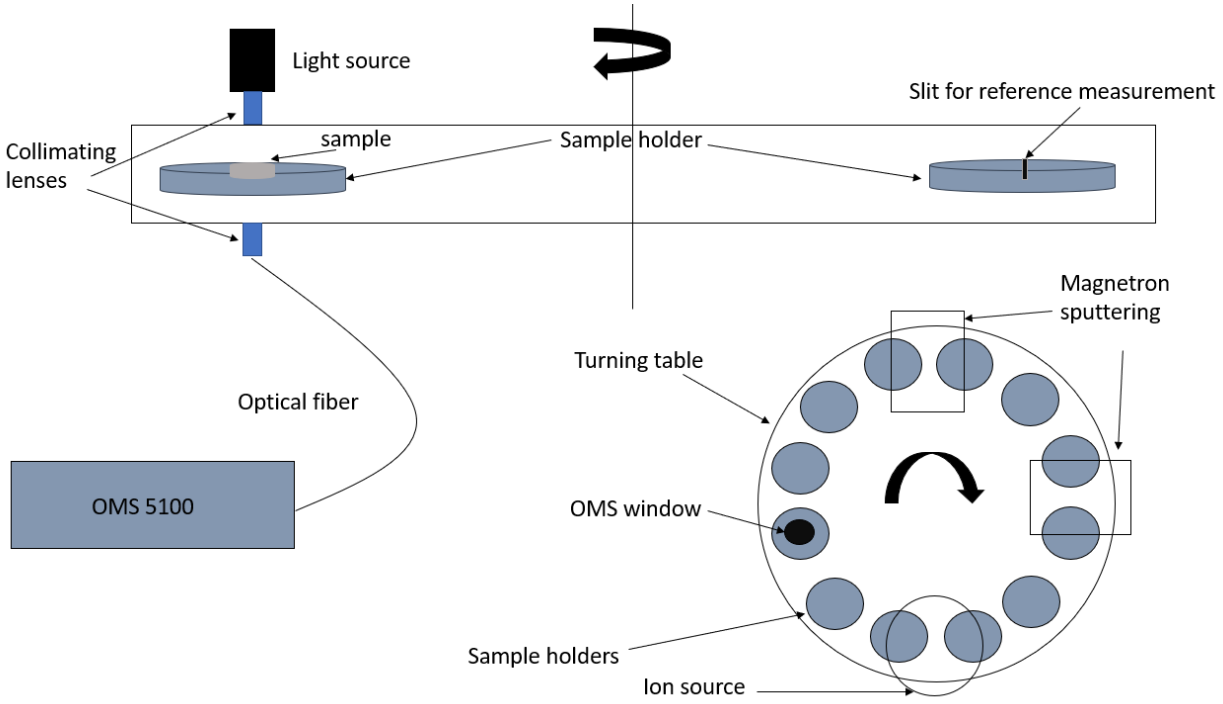

Figure 2-6 Simplified overview of HELIOS coater equipped with OMS5100 optical monitoring system.

During each revolution, the sample passes through the sputtering station (magnetron), ion bombardment (PBS) and the OMS window. Only the designated measurement sample and the sample holder for reference measurements (which has a slit to measure the 100% transmitted intensity) are measured. At every revolution of the table, the transmittance is then calculated according to Eq.2.2 [47]. The OMS5100 controls the deposition, and the system stops the layers deposition based on the optical measurement or when the thickness is reached based on the estimated deposition rate. The deposition rate can be recorded during a current run, or values from previous coating runs can be used. It is possible to combine several monitoring algorithms (turning point monitoring, level-cut monitoring or time monitoring) in one coating sequence. These different algorithms are based on different criteria for stopping the deposition of a layer, described below.

2.3.2 Turning point monitoring

Turning point monitoring was the first optical monitoring technique to be implemented because it does not require as stable monitoring signals as other techniques like level-cut monitoring. Its name comes from the fact that deposition is terminated when the monitoring curve reaches a minimum or a maximum in the monitoring curve, also called the turning point. These extrema in the T(d) curve are significant not only for thin film monitoring but also for thin film design. Layers with a thickness equal to that of the turning point are often called quarter wave layers, because their optical thickness is equal to one quarter of the reference wavelength.

$$q\frac{\lambda}{4} = nd \tag{2.3}$$

Where q is an integer. Mirrors, and bandpass filters can be designed in a way that all layers are quarter wave or multiple of a quarter wave thick. Thus, turning point monitoring is an attractive monitoring method for these designs. Since the deposition is terminated when a quarter wave thickness is deposited, this method does not track the physical thickness but rather the optical thickness of the layer. If there is a difference in refractive index, the layer will always be terminated at a turning point, and the physical thickness will change to satisfy the Eq.2.3 with the actual refractive index during deposition. Thus, this is an active or dynamic monitoring method where the condition for layers' termination changes based on real time measurements.

We can look at an example of first 7 layers of a mirror coating in Fig.2-7. The mirror coating consists of alternating quarter wave layers of high and low index materials, represented respectively by blue and green segments in the plotted monitoring curve. The monitoring wavelength and the wavelength for the optical thickness calculation are 500 nm. This means that the optical thickness is quarter wave for all the layers.

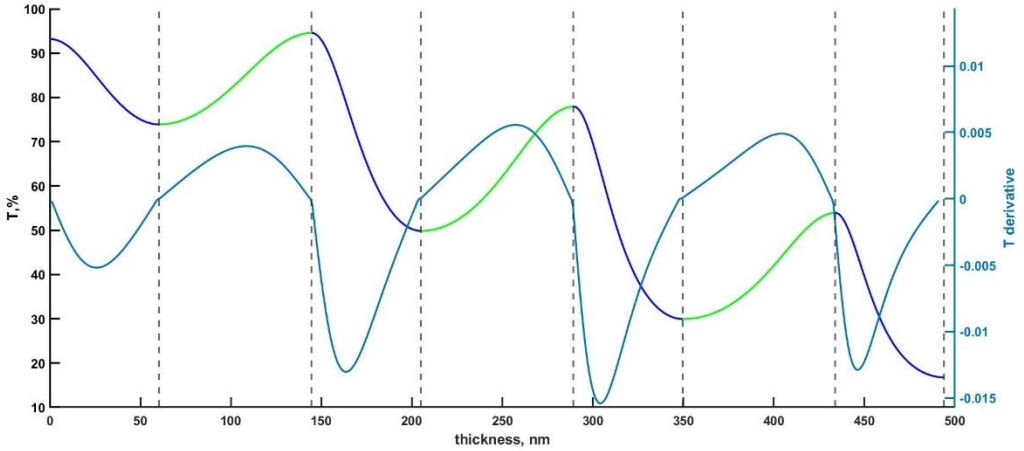

Figure 2-7. Blue and green line represent the transmittance evolution with time (or increasing thickness) for high and low index materials, the light blue line is the corresponding derivative, the dashed vertical lines correspond to quarter-wave thickness 1.

Although this method is very attractive, its accuracy depends on the precision of the detection of the minima or maxima of the measured signal which correspond to the region of lowest sensitivity of the transmittance to the deposited thickness. To increase the sensitivity of the method, the monitoring is generally performed by analyzing the derivative of the transmittance. Its value changes sign at the turning points and generally has an almost linear behavior when it passes through 0 [48]. The derivative for the 7 layers is plotted in right axis of Fig.2-7. Turning point monitoring is very sensitive to the measurement noise of the signal. To overcome this issue, it is usually not the raw signal that is used, but an averaged of the data from several consecutive measurements, which may however result in a systematic thickness error (delay in the measurement) that must be taken into account.

It is also well-known that turning point monitoring benefits from strong error compensation at the monitoring wavelength. For some designs such as Fabry Perot filters, if the deposited layer is slightly thicker or thinner, the error can be compensated by the deposition of the next layer that will be thinner or thicker respectively, such that the spectral performance of the filter is almost not affected at all at the monitoring wavelength (but might be affected over a wide spectral range). The influence of errors and compensations for Fabry Perot filters has been studied by several authors in the last decades[11][16]. Early on, it was clear that without the self-compensation effect, it would be impossible to produce narrow bandpass filters[48]. Despite the

success of deposition results with TPM since the seventies, the fabrication of Fabry Perot filters with a narrow bandpass (below 1 nm) remains a challenging task.

2.3.3 Level cut monitoring

Another method of optical monitoring is level cut monitoring, often also called trigger point monitoring. In this case, the monitoring curve is pre-calculated for the selected wavelengths before the deposition, and when the theoretical transmittance level is reached, deposition is stopped. This can be done passively – without adjusting the trigger point levels - or there can be algorithms that change the trigger point as the transmittance curve evolves (*monitoring by swing values*). The latter type of monitoring can be called *active* monitoring. The level cut monitoring has a greater degree of freedom than the turning point monitoring because there are no limits for the monitoring wavelength. However, choosing the monitoring wavelength is not a straightforward task, and a method for automatically selecting the wavelength based on various criteria is presented later in this thesis.

If we consider the passive level cut strategy, the technique relies on pre calculating the monitoring curve for all layers and then stopping the deposition when the required level of transmittance is reached. This means that, unlike the turning point monitoring, this method does not take into account changes in layers' properties that may occur during deposition (e.g., refractive index deviations, thickness errors in previous layers).

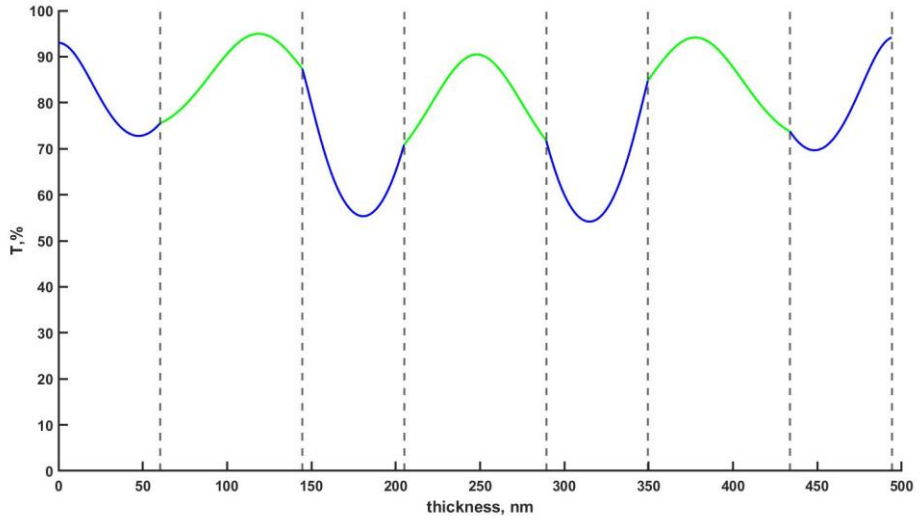

Figure 2-8. Blue and green line represent the transmittance evolution with time (or increasing thickness) for high and low index material, the dashed vertical lines show where the layers end.

To illustrate this method, we calculated the monitoring signal of the same 7-layer mirror we discussed in previous section (Fig.2-8). All layers have the same optical thickness (they are quarter wave at 500 nm), but the monitoring wavelength has been reduced to 400 nm. This means that the number of quarter waves at the monitoring wavelength is now greater than unity, and the layer deposition must be stopped after crossing a turning point, when reaching the desired calculated transmittance. This criterion is then applied to all layers and this technique keeps the amplitude of the monitoring curve in the ~60-90% region. In contrast, the turning point monitoring of a mirror results in a continuous decrease in transmittance (Fig.2-7) and with an increasing number of layers the measured transmittance converges to zero. For highly reflective mirrors, turning point monitoring becomes then unusable.

In the case of trigger point monitoring, the derivative of the transmittance signal is no longer useful for stopping the layers but is used to detect intermediate turning points. Tracking of turning points in necessary because the layers are stopped when the pre-calculated transmittance value is reached, after a given number of extrema. The level cut is widely used because many designs are not based on quarter wave thickness, especially when obtained with numeric design software such as Optilayer[49].

2.3.4 Error correction algorithms associated with level cut monitoring

Most of the time, level cut monitoring is not used passively but rather in an 'active' way. The idea here is to liken it to turning point monitoring – where the actual trigger point is not a pre-calculated value, but changes dynamically.

Active monitoring methods can avoid or, more realistically, slow down the accumulation of errors as the number of layers increases. One of the well described active level cut methods is the percentage of optical extrema monitoring (POEM)[50] or what is sometimes referred to *monitoring by swing values*[35]. The idea here is that the deposition is not stopped on previously pre-calculated transmittance values, but rather on a ratio between the distance from the last turning point and the trigger point, and the total amplitude between consecutive turning points (see Eq.2-4). In this case, if the turning point is shifted relative to transmittance axis, the trigger point is also shifted to maintain the pre-calculated *swing*. This approach has been shown to make the monitoring less sensitive to calibration errors, previous thickness errors and even refractive index errors[35][50].

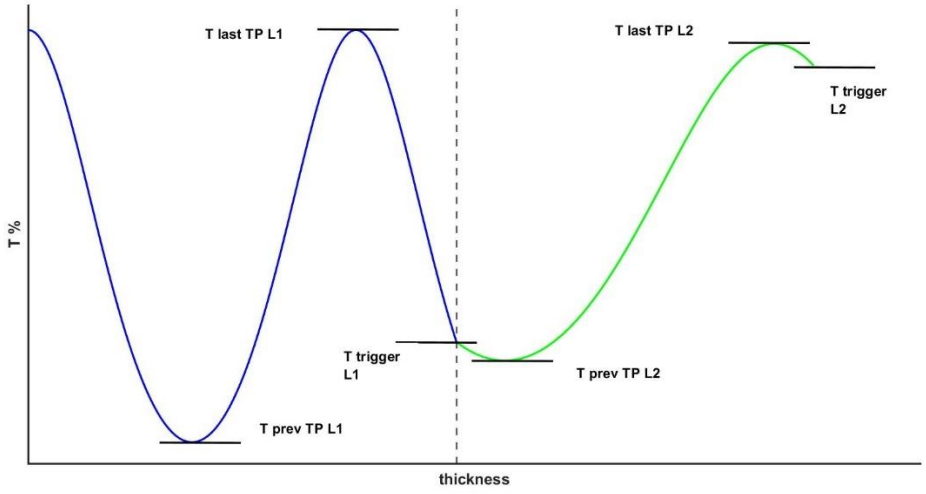

Figure 2-9 Example of monitoring curve of high (blue) and low (green) index layers.

$$\text{Swing} = \frac{T_{\text{trigger}} - T_{last\ TP}}{T_{\text{last TP}} - T_{prev\ TP}} = const \qquad (2.4)$$

To illustrate this method, we have plotted in Fig.2-9, the monitoring signal of a bilayer (Nb_2O_5/SiO_2) of 135 nm and 120 nm thickness respectively, optically monitored at 500 nm. For each layer, the previous and last turning points ($T_{last\ TP}$ and $T_{prev\ TP}$) can be defined. The deposition is not stopped when the pre-calculated trigger value is reached, but when the pre calculated *swing* is reached with respect to the positions of the turning points measured online. With this active monitoring strategy, and similarly to turning point monitoring, we take the refractive index into account and we monitor the optical thickness of the layer. The error compensation effect is the main advantage of active monitoring strategies[51].

The turning point for the swing calculation does not have to be in the same layer, the turning point of the previous layer can be used to adjust the trigger point if the same wavelength is used for both layers. We will discuss the monitoring curve in more detail when we discuss the monitoring wavelength selection process.

2.3.5 Technical limitations of monochromatic monitoring

Although optical monitoring is very powerful, there are several conditions under which it is known to be ill-suited to terminate the deposition of a layer. The limitations may be technical, meaning that they may come from one or more components of the monitoring system, or they can be a design feature that needs to be monitored. For example, a highly reflective mirror cannot be monitored in the reflection region because the transmittance may reach a level where almost no signal can be detected. In this case, one can choose to monitor in a region where the transmittance is higher (as in example in Fig.2-8) and the monitoring limitations can sometimes be avoided. Although there are many other limitations, the following two are not often taken into account.

2.3.5.1 Spectral bandwidth

One limitation related to the spectrophotometer and thin film design is the spectral bandwidth. The bandwidth of a monochromatic monitoring system is fixed at a certain value, which depends on the linear dispersion of the grating ant the slit width of the monochromator. Thin film coating (especially when the total optical thickness of the stack becomes very large) may exhibit high frequency spectral characteristics that can only be measured with a very high spectral resolution, which is generally not possible for *in-situ* spectrometers. As an example, let us analyze the spectral transmittance after the deposition of the 28^{th} layer of 2^{nd} witness glass from a '*Bonne Mère*' design [appendix1.8] which we will study in detail in chapter 4. In Fig.2-10 (c), we first plotted the spectral transmittance at the end of the 28^{th} layer. The spectral transmittance shows many sharp peaks in the 400-600 nm spectral region. These sharp peaks close together can impact the monitoring signal if we select a monitoring wavelength in this range and the spectral resolution of the monochromator is not high enough. To illustrate, we plotted the monitoring curve for a single λ wavelength (420 nm or 659 nm) and an average of $\lambda+\Delta\lambda$, where $\Delta\lambda$ is equal to 3 nm and represents the resolution of the monitoring system (Fig.2-10 (a) and (b)). One can see that not only will the spectral resolution influence the measurement at the very end of the layer, but also that the maximum and minimum values at the turning points can be affected. Hence, we see that it is beneficial to select the monitoring wavelength only if the spectral resolution does not affect the monitoring process, and the spectral resolution requirements of the monitoring system should be dictated by the component to be manufactured.

This conclusion is true for a wide range of filters, and in particular for narrow bandpass filters that are generally monitored within the bandpass region using a turning point monitoring. As a general rule, we consider that for successful monitoring, the desired spectral resolution should be at least one fifth of FWHM (full width at half maximum). If this is not the case, the optical monitoring signal will start to be affected after the first cavity, to the point where the layers cannot be terminated on true turning points.

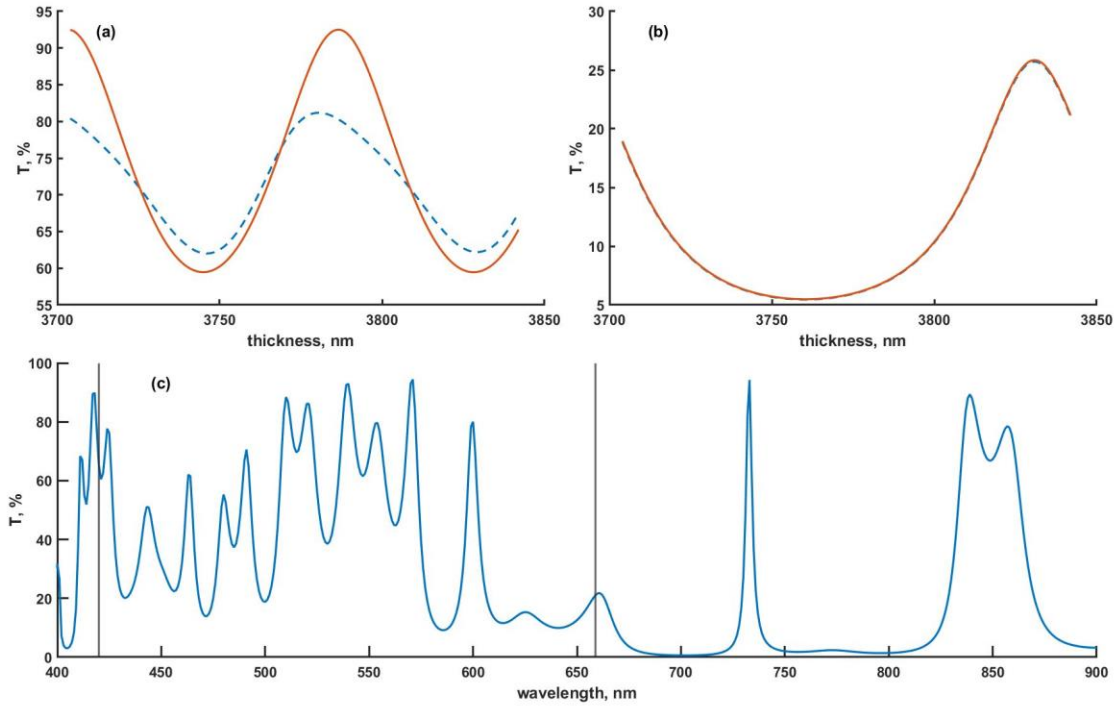

Figure 2-10 Monitoring curves of different wavelengths, solid line represents theoretical monitoring curve, dashed line represents theoretical monitoring curve if bandwidth is 3 nm. (a) - the monitoring wavelength is 420 nm, (b) - 659 nm, (c) - spectral performance at the end of the layer, vertical lines are plotted at 420 and 659 nm.

Furthermore, even though broadband monitoring systems have become more attractive in recent decades (see section 2.4), the bandwidth of these systems is not tunable and is generally larger than for monochromatic monitoring setups[15], i.e. on the order of a few nanometers. This makes bandwidth an even more important consideration even for the determination of broadband strategies.

Finally, it seems rather perilous to try to take into account the spectral resolution in the theoretical calculation of turning points. It would be necessary to know perfectly, wavelength by wavelength, the resolution of the system according to the setting of the slits. This would possibly deserve additional investigations.

2.3.5.2 Noise and measured signal sensitivity

As mentioned earlier, the spectral resolution of the monochromatic monitoring setup can be controlled by the slit width of the monochromator. We can improve the spectral resolution by closing the slits. However, by doing so, the amount of light reaching the detector also decreases. This generally results in a decrease in the signal to noise ratio (SNR). A compromise between spectral resolution and SNR is generally required.

Finding this balance is not easy, as different thin film designs have different requirements. Additionally, the spectral sensitivity of the detector and the spectral power density of the light source must also be considered. For example, for a silicon-type detector, it is well-known that at the limit of the sensitivity range (around 400 nm or 1100 nm), the responsivity drops by one order of magnitude from the maximum sensitivity range. This means that the slit configuration that works for one wavelength range might not be suitable to other wavelength range. Therefore, a trade-off must be made by taking into account the light source/sensor wavelength dependence. To illustrate this point, we have plotted in Figure 11 the noise profile of the OMS5100 with a halogen light source and Si detector obtained from a 100% measurement with 0.5 mm slits (corresponding to a nominal resolution of ~1.75 nm). The noise is minimal around 600 nm with an amplitude of less than 0.01% while it increases by almost an order of magnitude around 400 nm.

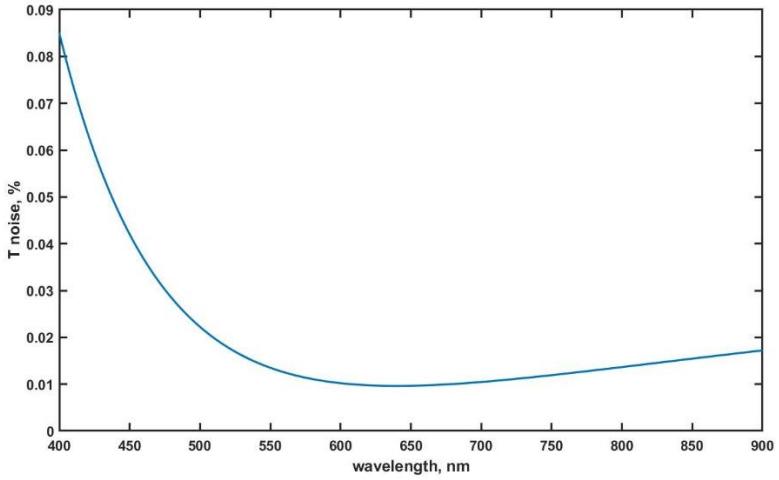

Figure 2-11 Noise profile of the OMS5100 with a halogen light source and Si detector.

Another factor to consider is the sensitivity of the optical monitoring setup. In general, the measurement noise is composed of two main contributions: a multiplicative one that dominates at high transmittance values and an additive one that contributes to low transmittance measurements. From experience, it is known that measurements below 5% transmittance are not very reliable. The other key parameter is the minimum change in transmittance that can be reliably measured during deposition of a layer. A typical example to illustrate the decrease of the measured signal and transmittance amplitude is a mirror monitored with the turning point monitoring technique (Fig.2-7). The optical monitoring becomes unreliable when the number of layers approaches 10. Indeed, with the OMS5100 that we have at Institut Fresnel, we have found that the transmittance amplitude must be least a 4% for reliable measurement. The empirical reason we selected at least 4% change in transmittance amplitude is related to the noise level as well as the magnetron sputtering technology. At the very beginning of the deposition, the deposition rate is not stable. When the shutter that normally closes the target is opened, the cathode is suddenly exposed to the whole volume of the coater. This change of volume modifies the partial gas pressures and influences the deposition for a few seconds. The instability of the deposition rate can cause sudden changes in the measured transmittance and lead to large thickness errors.

In this thesis, we did not delve into instabilities related to the deposition technology, but rather used the fact that for reliable measurements, the transmittance amplitude for monitoring wavelength should be at least 4%. The signal integration time can be increased to limit the influence of measurement noise. However, due to a longer averaging time, this procedure may result in delays and loss of layer termination accuracy.

2.4 Broadband optical monitoring at Institut Fresnel

In addition to monochromatic optical monitoring, broadband optical monitoring is also available with the HELIOS coater. Both monitoring systems are interchangeable, the light source, collimating lenses and even the optical fiber are the same for both systems. For broadband measurement, the rotation speed of the turning table must be reduced from 240 to 180 rpm to allow sufficient time for signal processing.

2.4.1 WB-OMS

The broadband monitoring system used at Institut Fresnel is called WB-OMS and was developed by *Buhler Leybold Optics*. The WB OMS consists of WBM1000 spectrometer and the control software -TOMS (Thin film optical monitoring software). The WB-OMS can also be used as a monochromatic monitoring system and can terminate the deposition based on the measured deposition rate. This gives a large degree of freedom with respect to monitoring strategies, as it is possible to mix different monitoring methods, which can lead to the fabrication of high performances filters[15][52].

This system provides a measurement of the transmitted spectrum at each turntable rotation with the same procedure used by the OMS5100. The spectrum is measured in the spectral range 350-1200 nm with a nominal spectral resolution equal to 3.5 nm. The associated software (TOMS) can then process the measured spectra to define different criteria to terminate the deposition.

- One option is to use the broadband signal to determine, by comparison with the theoretical transmittance, the thickness increase with each revolution of the turning table [12]. This method will be referred to as *broad band thickness* monitoring or *wideband* monitoring.
- Another option is to compare the measured spectra after each measurement instance with the theoretical spectrum of the given layer, calculate a figure of merit defined as the root mean square difference between the two spectra, and stop the deposition when the minimum is reached[53]. This monitoring method will be called *Merit* from now on.
- Another option is to use broadband measurement to calculate admittance loci in real time [54] and use it for layer termination[55]. This method is expected to have error compensation comparable to that of turning point monitoring. A similar method for monochromatic monitoring is proposed by the same authors[56], but it is not known if these methods are implemented in commercially available systems.

Another very attractive feature of broadband monitoring is that a lot of information can be obtained from the spectral measurement. For example, after the layer deposition is complete, an additional spectral measurement can be performed independently for the reverse engineering of the deposited thickness and thickness errors are calculated online. This then allows the remaining

film stack to be re-optimized by taking into account the errors already made[57][58]. Of course, this also brings some uncertainty as the number of layers increases and, from a mathematical point of view, several thickness solutions are possible for a given spectrum. Moreover, if no re-optimization of the design is performed, these errors can still be taken into account when calculating the theoretical target curves for the following layers.

2.4.1.1 Broad band *thickness* monitoring

Broadband spectra are recorded after each revolution of the turning table – that is, after each pass under the magnetron of the monitoring sample. These spectra can be compared to the theoretically calculated spectra based on the expected deposition rate. Then, the thickness can be determined by iterative comparison of the transmittance measurement with the thin film theory. The thickness that gives the best match is then considered as the one that has been deposited. After some sequential measurements, the average deposition rate can be refined and used to predict when the required thickness will be deposited. In Fig.2-12 we illustrated an example of broadband thickness monitoring of a 22.8 nm thick Nb_2O_5 layer deposited on a fused silica substrate. Four different data sets are provided: the online fitted thickness and design thickness, measured and expected deposition rates, all as a function of deposition time. The online fitted curve is almost linear, showing that the thickness increase is almost stable over time. This can also be seen in the measured deposition rate; the rate is very close to the expected level, and after the first 10 seconds of deposition, it does not change much although small oscillations remain.

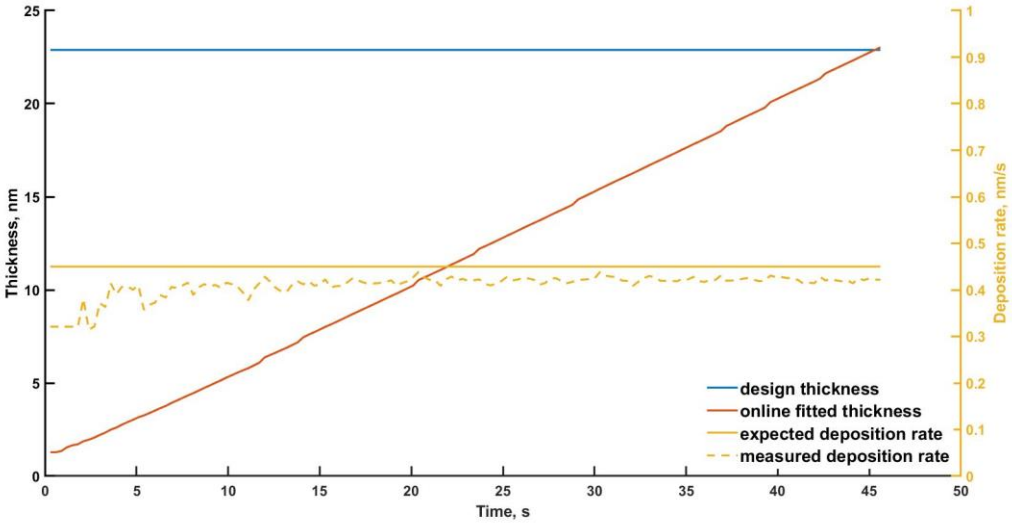

Figure 2-12 Broadband thickness monitoring.

The time remaining for deposition is re-calculated as often as the new deposition rate is recorded, and the layer deposition is terminated based on the remaining deposition time, not on the actual measured thickness, even though the two are close. As can be seen, the final value of the fitted thickness curve is greater than the target thickness, showing that a small error is present for this layer.

Of course, measurement noise can influence the accuracy of the thickness control of the deposited layers. The accuracy of the termination of the deposition also depends on the optical signature of the layer, i.e. whether the layer formed over a partial stack has a noticeable change in transmission over the spectral range must be considered. This last point must be taken into account when choosing the broadband monitoring strategy and will be discussed in detail in the following chapters.

2.4.1.2 Broadband *merit* monitoring

Another method is to terminate the deposition after each layer when a merit value (M_i is the merit for i-th layer) between the measured spectra and the theoretical spectra at the end of the layer reaches the minimum or is equal 0 in the ideal case. It is defined as:

$$M_i = \frac{1}{N}\sqrt{\sum_{j=1}^{N}[T(\lambda_i, d_i)_{th} - T(\lambda_i, d_i)_{measured}]^2} \tag{2.5}$$

where, N is the number of wavelengths used, $T(\lambda_i, d_i)_{th}$ is the theoretical spectral transmittance for the i-th layer and $T(\lambda_i, d_i)_{measured}$ is the measured spectrum during deposition of the i-th layer. Since the spectra are collected with increasing layer thickness, the evolution of M_i is recorded and the deposition is stopped when the merit with respect to the target spectrum is minimum[15]. To illustrate the principle, we have plotted in Fig.2-13 an example of broadband *Merit* monitoring as implemented in the WB-OMS of a 22.8 nm thick Nb_2O_5 layer. This time, we examine three different variables: measured and expected deposition rates and the merit value as a function of deposition time. Firstly, we find that the deposition is not terminated when the merit value is at its minimum, but just after passing this minimum and its starts to increase again. Ideally the control software predicts the time when the minimum will be reached and stops the deposition when this predicted time is reached, but in the case of thin layers, the deposition is often stopped after the minimum has been detected. As a result, the layer is slightly thicker than expected. However, this error is small and represents only 2 additional data points, so the expected absolute thickness error in this case is ~0.2 nm.

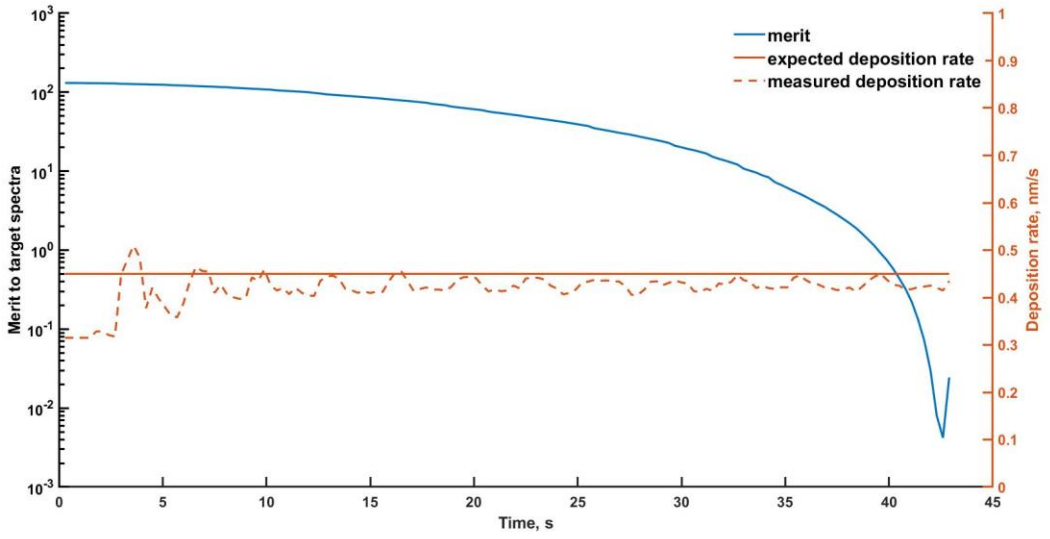

Figure 2-13 Broadband monitoring by Merit.

We again find that the measured deposition rate fluctuates at the beginning of the deposition. These fluctuations in the deposition rate make it difficult to accurately monitor layers with thicknesses between 5 and-10 nm, regardless of the thickness control method.

2.4.2 Technical limitations of broadband monitoring

The technical limitations of broadband monitoring are similar to those of monochromatic monitoring. These limitations are related to the spectral resolution of the monitoring setup and the accuracy of the signal processing itself. For broadband monitoring, we need to define the range of wavelengths that will be used. As with monochromatic monitoring, the wavelength range is limited by the light source and the detector. The spectral range for the detector is 350-1200 nm, but the sensitivity of the system drops significantly when going down into the UV or too high in the near-IR. We therefore found that we could use the system in the 400-1000 nm range. As with the monochromatic monitoring, there is more noise at both ends of the spectrum, because the light source has a lower power output in the blue range and the detector has lower sensitivity.

2.4.2.1 Broadband monitoring and spectral resolution

Somewhat similar to the choice of monitoring wavelength for monochromatic monitoring, for broadband, different wavelength ranges can be defined for each layer. There are several reasons for changing the wavelength range. The first is related to the bandwidth of the monitoring system. For broadband monitoring, the spectrometer bandwidth is fixed at 3.5 nm and, unlike monochromatic monitoring, it cannot be adjusted by the slits. However, as discussed with monochromatic monitoring, one wants to avoid wavelengths regions where the measured transmittance could potentially be influenced by the spectral resolution of the instrument. The same approach can be implemented with broadband monitoring, i.e. calculating transmittance with a fixed spectral resolution, but, in this case, the changes in transmittance must be calculated as a function of wavelength for an increasing thickness. Based on these results, it is possible to determine the wavelength ranges that are more likely to be successfully controlled. We will discuss this topic in detail Chapter 5 when we discuss broadband strategies. To illustrate this

approach, we have plotted in Fig.2-14 the theoretical transmittance spectra with finite (4 nm) and infinite spectral resolution of the filter obtained after depositing the 31st layer of the OIC2022 thin film filter manufacturing contest design [appendix1.9].

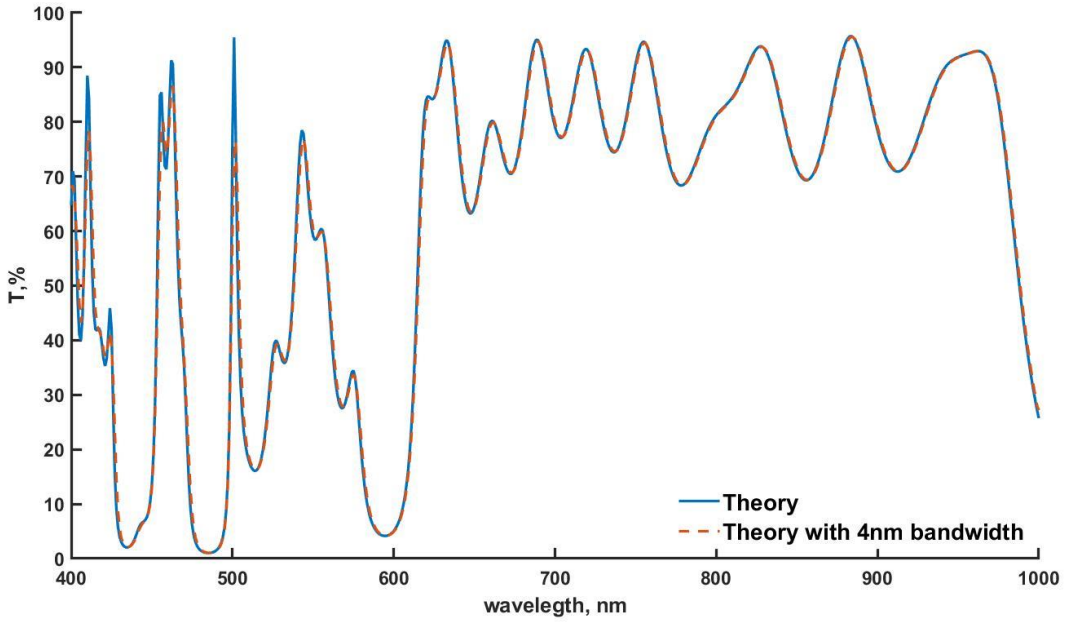

Figure 2-14 Example of the influence of the spectral resolution on a wideband domain.

As can be seen, there are many narrow peaks in the 400 – 530 nm spectral range where the two calculated spectra do not overlap perfectly. However, for longer wavelengths, the spectral resolution of the WB-OMS does not affect the measured spectra. It is therefore in our interest to avoid spectral ranges where the spectral resolution of the measurement may be problematic, and, consequently, spectral regions below 530 nm should be excluded from the signal analysis. To properly find the usable wavelength range, the same analysis should be implemented while increasing the thickness of a given layer step by step, as the spectrum can change significantly during the deposition of the layer. The step increase in thickness should ideally be the same as the deposited thickness each time the substrate passes under the target. However, most of the time, this simple spectral evaluation at the end of each layer is sufficient.

2.4.2.2 Noise and measured signal sensitivity

Due to the spectral sensitivities of the light source and detector, the highest signal to noise ratio for broadband measurement is in the 500-700 nm range. Noise for broadband monitoring poses the same problems as for monochromatic monitoring: any sudden jump in the measured data can introduce large thickness errors. There is an advantage for the new broadband system that we use, as we can adjust the measured signal integration time for individual layers compared to the monochromatic system where it is a global parameter for the material. However, this is not a parameter associated with the broadband technique, but rather that shows that the newer control system provides better control of the deposition process.

Another consideration is the absolute value of transmittance as the layer grows. This is again similar to monochromatic monitoring: only transmittance above a certain level can be detected with high accuracy. For example, if we consider the monitoring of a multilayer quarter wave mirror, as soon as the reflectivity of the mirror becomes higher than 95%, the accurate measurement of the transmittance in this spectral region becomes unreliable. Therefore, in the case of monochromatic monitoring, the monitoring wavelengths are usually switched to one of the sides of the mirror where the transmittance during deposition is high enough to allow reliable measurements. The same approach can be applied to broadband monitoring: spectral regions where the transmittance is below a certain value should be eliminated from the signal analysis.

The amplitude of the measured transmittance when depositing a layer is another very important factor for broadband monitoring as spectra are used for online fitting of the thicknesses. If the transmittance amplitude is small with the thickness change, it makes the monitoring insensitive and leads to large thickness errors. This is for example very often the case when the first layers of a given design are very thin. In this case, not only are the changes in transmittance small, but the curves are smooth without any spectral oscillations. To illustrate this point, we have plotted in Fig.2-15 the theoretical spectra after each of the first 5 layers from a D65 compensator filter [appendix1.10]. Indeed, we see that these thin layers do not change the spectrum too much.

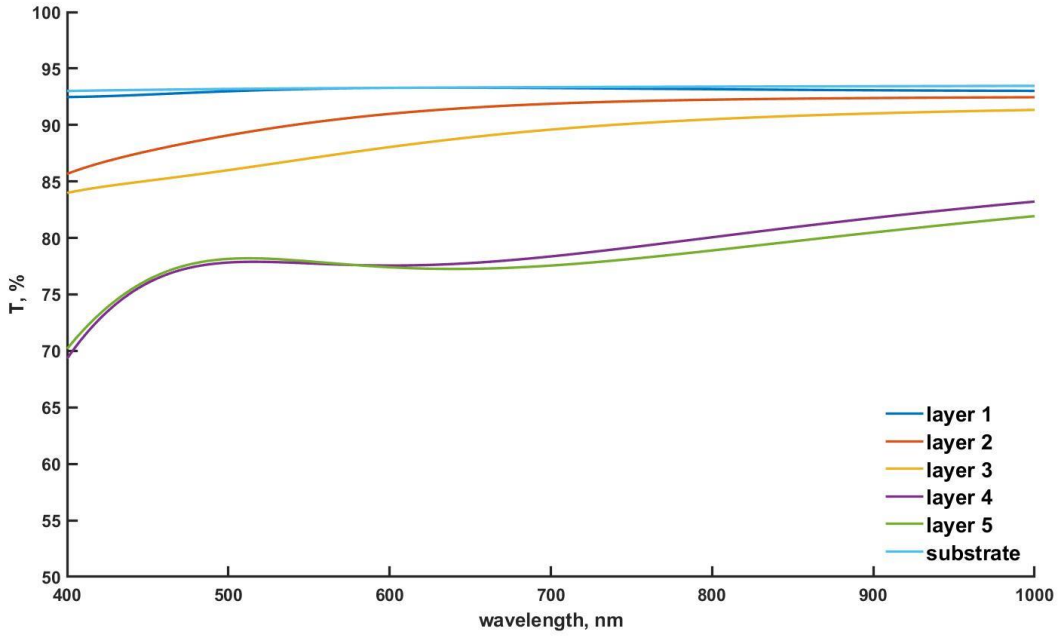

Figure 2-15 Spectra of first five layers of D65 compensator filter design

In table 2-1, the thicknesses of these layers are given. The first layer is made of SiO_2 and the substrate is fused silica. Both having very close refractive indices [appendix.2], the change in amplitude is very small (less than 1%). For the layers 2 and 3, we see that the spectral changes are significant in the shorter wavelength range. Then, there is significant change in the whole spectrum after the deposition of layer 4, followed by an almost negligible change after layer 5. After the fifth layer, we can show that more pronounced oscillations in the spectra appear because the thicknesses of the following layers (not displayed in the table) are significantly higher.

Layer	Material	Thickness, nm
1	SiO_2	205.4
2	Nb_2O_5	9.9
3	SiO_2	39.6
4	Nb_2O_5	38.0
5	SiO_2	20.0

Table 2-1 Thicknesses of the first 5 layers of the D65 compensator design.

These first 5 layers are crucial to the final performance of the filter, after depositing all the 37 layers of the D65 compensator, but to date, it is hardly possible to find an optical monitoring system that will be sensitive enough to accurately monitor the 1st and 5th layers. Although the transmittance changes for the 2nd, 3rd, and 4th layer are pronounced, optical monitoring of these layers, especially with broadband methods, is not an easy task, as we will demonstrate in Chapter 5. For monochromatic monitoring, we know that a difference of at least 4% in amplitude is required to perform optical monitoring. For broadband monitoring, we can find wavelength regions in the shorter wavelength range to fulfill similar criteria, but how the width of the spectral region being analyzed affects the accuracy of the achievable thickness needs to be investigated.

These preliminary analyses of broadband monitoring techniques show that in many cases, either different monitoring methods must be considered or other parameters, such as wavelength range, must be adjusted. In other words, broadband monitoring systems are not plug-and-play systems and adapted strategies are needed to meet the spectral requirements of complex filters.

2.5 Indirect monitoring

The most reliable way to monitor thin film optical filters is to control all layers on the same piece of glass in order to benefit from possible error compensations. However, this is very rarely possible.

Indeed, many thin-film filter applications require complex designs consisting of hundreds of layers. For these filters, it is often impossible to monitor all the layers on the same glass. As the number of layers increases, thickness errors begin to accumulate. At some point, the thickness errors in the previous layers can influence the measured transmittance to such an extent that optical monitoring can no longer be performed. To illustrate the effect of error accumulation, we have plotted in Fig.2-16. the monitoring curves for layers 43 to 50 of the Bonne Mère design. Two curves were generated: the blue and green curves represent the theoretical signal for the high and low refractive index materials respectively, while the red and yellow curves are the same monitoring curves when a 1% random thickness error is applied for each layer. For the second to last layer in this example, the difference in turning point transmittance is greater than 5%.

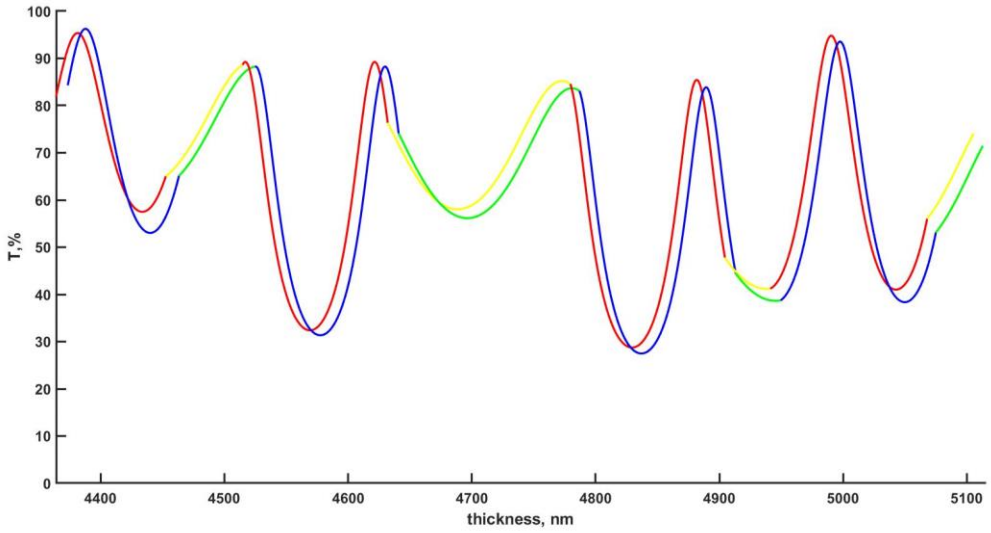

Figure 2-16 Monitoring curve of layers 43-50 of the Bonne Mère design, blue and green curves are the theoretical High and low index monitoring curves, red and yellow are the same monitoring curves when the random thickness errors are added.

As we can see, not only are the trigger points changed, but the amplitude between the turning points is also affected. This shift of course means that the final performance will be strongly degraded. To overcome the problem of signal divergence and at the same time limit the accumulation of errors, an indirect monitoring can be implemented.

In the HELIOS coater, 12 substrates holders are available but only one test glass is used for optical monitoring. Therefore, we can change the monitoring glass after certain number of layers is deposited, while the glasses in remaining positions are coated with all of the layers in the design. This method is called indirect monitoring – the monitoring glass is not the same as the one used for final application.

Using this approach, thickness monitoring can be performed on multiple witness glasses. As we will show later, we did not monitor more than 34 layers for this design on one monitoring glass.

Another occasion when indirect monitoring is necessary is when the first layer to be deposited has a very small refractive index difference with the substrate (as it is the case for D65 filter). This means that the transmittance measurement (broadband or monochromatic) is not sensitive enough to be used for control. In this case, the substrate used for monitoring can be pre-coated

with one layer of high refractive index material compared to the substrate. This pre-coated glass is then used for the monitoring purpose only.

The drawback of indirect monitoring is the discontinuity in the monitoring curve when the witness glass is changed. This means, of course, that any error compensation is only possible on individual glasses used for monitoring, but that there is no overall correction for the entire filter.

2.6 Deposition simulation software

In addition to the deposition equipment, computer simulations of a deposition are widely used today. The software that simulates the deposition run can be used to test and improve the selected monitoring strategy[59] or to draw conclusions about the monitoring method itself, as hundreds of simulations can be run to gather statistics[60].

The deposition simulation software is designed to reproduce the transmittance (or reflectance) signal that the optical monitoring system would record as the layers thickness increases. The layer thickness is increased sequentially, with a given deposition rate and rotation speed. This simulated signal is then analyzed by the same type of software that controls the HELIOS and SYRUSpro (or similar) coaters[61][62].

To make the simulation realistic, several sources of errors can be introduced into the simulation software:

Additive and multiplicative noise: the noise of the measurement system can be an important source of errors and should therefore be taken into account in the simulations. As shown in section 2.3.5.2, the noise of the light source/detector pair is wavelength dependent and therefore the values in the simulation software must be set according to the slit configuration and wavelength.

Packing density: in the simulation we can set the packing density to be less than 100%, which means that the layer is not as dense as it should be. With this setting, we can simulate a non-perfect deposition (small vacuum leakage, unwanted impurities in the targets or in the gas supply).

Noise of deposition rate: the actual deposition rate is not a constant value (as can be seen in Fig.2-13) and can have influence on the accuracy of the termination of a layer. Therefore, a deposition rate error should be also introduced into the simulation.

Shutter delay, it is known that the shutter that covers the target when the deposition is completed has a delay time – it does not move in front of the target instantaneously. Although the delay time is short and the associated thickness error is very small (within 0.1 nm range), if the number of layers in a design is large, these small errors will accumulate.

There are other sources of error that can be introduced into the simulation software; however, we will only use the simulation software to demonstrate the effect of noise on different monitoring strategies in chapter 4 and we will not use the simulation to draw conclusions about the monitoring strategies themselves. Therefore, we did not investigate the capabilities of the deposition simulation software further.

Chapter 3 - Fabry-Perot filters and turning point monitoring

In this chapter we will discuss Fabry-Perot filters and turning point monitoring. We will explore the material properties necessary to manufacture highly transmissive filters in the UV range, and we will look at the monitoring challenges associated with this wavelength range and the requirements needed to monitor narrow bandpass filters. We will discuss the monitoring strategies that can be used to overcome technical limits of the monitoring setups to monitor the narrow multi-cavity Fabry-Perot filters.

3.1 Narrow band-pass filters

Numerous applications require band-pass filters, i.e. filters that only transmits a narrow bandpass and reflect the other spectral components. Among them, LIDAR (light detection and ranging) used for atmospheric studies[63], require bandpass filters with very narrow bandpass. During this thesis, a study for specific narrow band-pass filter for LIDAR application was requested by the French space agency (CNES). The very tight specifications of the desired filter are listed below:

- The spectral range of interest is from 290 nm to 420 nm.
- Centering wavelength λ: 354.8 nm.
- Inner limits 354.8 ± 0.05 nm.
- Outer limits: 354.8 ± 0.5 nm.
- Between the limits the transmittance must be greater than 85% and the fluctuations of maximum transmittance must not exceed 2%.
- Outside the transmittance band, the transmittance shall not exceed 0.001%.

The specifications of the band pass spectral region are visualized in Fig.3-1. We did not plot all the wavelength range of interest, as in that case, the band pass region cannot be distinguished. The designed and later the manufactured filter must lay between the inner and outer limit curves. For filter with such narrow band pass region, we studied several Fabry-Perot filter designs, the formulae and additional information are given in appendix 3.

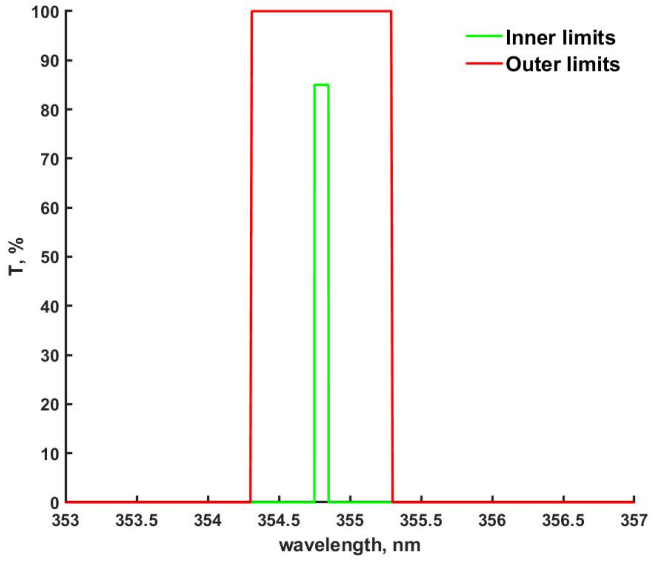

Figure 3-1 Specified transmittance corridor for the for the Fabry Perot filter.

A Fabry-Perot filters consists of a cavity layer, which optical thickness is equal to an integer number of half of the reference wavelength (half wave layer). The cavity is surrounded on both sides by highly reflecting mirrors. These conditions ensure that the incident light of reference wavelength undergoes constructive interference upon many reflections between the mirrors and therefore is transmitted through the filter. Incident light of wavelengths other than the reference wavelength undergoes destructive interference, and the transmittance of these wavelengths therefore is reduced towards zero[5][64]. To ensure high transmittance at the reference wavelength, mirrors are dielectric rather than metallic, because the maximum transmittance is limited by absorption in the mirrors. The downside of dielectric mirrors is the limited wavelength range where they are reflecting. For this particular application, the high transmittance in the band-pass region required using dielectric mirrors. To ensure wide blocking region, additional dielectric mirrors, blocking the needed spectral ranges, have to be added.

Given the spectral range of this application, to ensure the necessary transmittance, not all dielectric oxide materials could be used, as some start to absorb in the UV wavelength range. Therefore, the starting point for this study is the material properties. From the available high index materials, HfO_2 was chosen, as its extinction coefficient (k) is lower in the UV range [appendix.2]. The low index material remained SiO_2 as it is in general considered to be absorption free for wavelengths above 320 nm.

We will use the notations for quarter wave thicknesses (H and L) introduced in chapter 1. In addition, we will denote dielectric mirrors consisting of q quarter wave layers as Mq (for example M6 is mirror consisting of HLHLHL layers). When counting the mirrors of a Fabry-Perot filter, we start in order of deposition, meaning that the first mirror is closest to the substrate, and last closest to air.

3.2 Properties of HfO_2 layers

From previous experience, it was clear that some transmittance losses will be linked to HfO_2 layers. However, how high is the k value and can it be decreased remained an open question. In order to evaluate the starting properties, it was decided to deposit the first cavity of Eq.A3.2 [appendix.3] - M11 10L M11. For the first test, mixed strategy of optical monitoring and rate monitoring was used and the centering wavelength was set to 355 nm. With the mixed monitoring strategy, the first 7 layers were monitored by turning point monitoring, and the deposition rates were recorded while these layers were deposited. These recorded deposition rates were used to monitor the remaining layers of the filter. We could not use turning point monitoring for all of the layers because of reasons already highlighted in chapter 2: the transmittance amplitude decreases as the mirror is deposited to levels where reliable measurement is no longer possible. The measured and theoretical transmittance of the fabricated filter are plotted in Fig.3-2. At the beginning of this project a k value $1 \cdot 10^{-4}$ for HfO_2 was estimated and considered. As the maximum transmittance at resonance was lower than expected, the extinction coefficient of HfO_2 had to be increased when calculating the theoretical transmittance curve to match the measured transmittance at the peak.

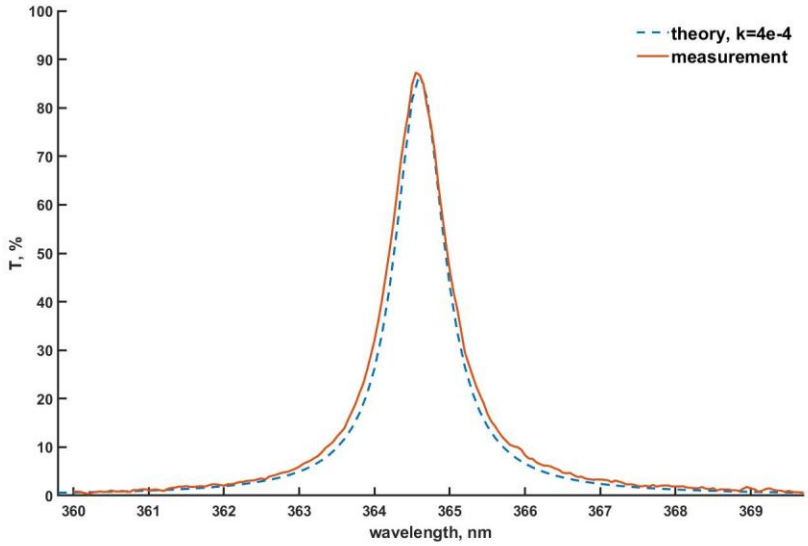

Figure 3-2 Transmittance of the M11 10L M11 filter compared to theory with increased k value

The maximum transmittance of the deposited Fabry Perot filter is 87.2% and the same transmittance can be obtained with a value of $k = 4 \cdot 10^{-4}$. This is a 4-time increase compared to our first estimation of the k value of HfO_2. With such k value, it can be shown that the transmittance would be well below 50% when several cavities are combined, and therefore, it would not be possible to achieve the maximum transmittance required by the project. The fabricated filter is centered at ~365 nm, i.e. it is shifted almost by 10 nm compared to starting monitoring wavelength, showing that the monitoring strategy of turning point and rate monitoring is not accurate enough. Therefore, in parallel to the study of HfO_2 properties, we also search for ways to increase the precision of optical monitoring. We investigated the use of a more powerful light source with our monitoring setup to increase the signal to noise ratio and reach accurate low transmittance measurement (down to 5% range).

However, as a first step, we investigated ways to reduce the residual absorption of HfO_2 layers. With HELIOS coaters, it is possible to turn on both targets at the same time and deposit mixed layers. By default, HfO_2 is co-sputtered with silicon in order to limit crystallization in HfO_2 layers and reduce mechanical stress of the coatings[65]. This means that we can influence the stoichiometry of the formed layers by playing on the power ratio between the 2 targets. A series of runs were performed in order to find out whether or not it is possible to decrease k value by increasing the amount of silica in the HfO_2 layer. For each run, the power on the Hf cathode was

kept constant and the power at Si cathode was increased from 400 to 800 W by 100 W steps. Each time, the optical thickness was monitored and 6 H (or 6 quarter-wave thick) layers at 355 nm were deposited. The spectral transmittance of these single layers measured ex-situ with a Perkin Elmer Lambda 1050 are plotted in Fig.3-3. As can be seen, the curves do not overly completely but the minima and maxima are very close, meaning that the refractive index has not changed too much. And most importantly, in Fig.3-3(b), we see that the so called 'cut off' in UV range has shifted towards shorter wavelengths with increased power for Si cathode. This shift indicates a possible decrease of absorption in the HfO_2 layers. However, precise determination of the new dispersion parameters is quite complex with such low k-values.

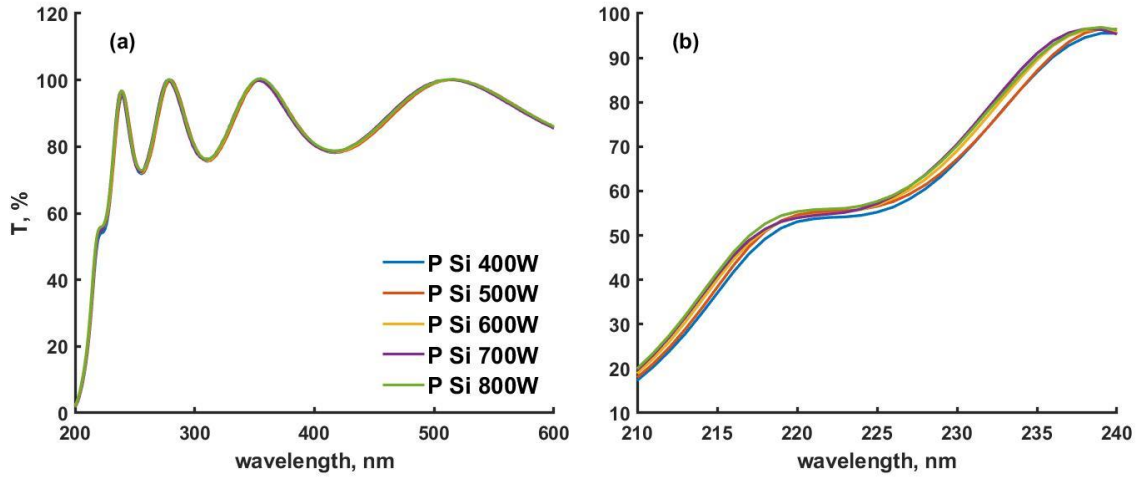

Figure 3-3 Transmittance measurements of 6H thick HfO_2 layers with different power for Si co-sputtering.

To verify that the extinction coefficient is indeed decreased, we deposited a Fabry-Perot filter with high index cavity made of HfO_2 with P Si set to 800 W. By placing the high index layer in between the two mirrors, where the electric field reaches its maximum, any small absorption will decrease the transmitted light significantly at the centering wavelength. The selected design was M6 2H M6 with the centering wavelength once again set to 355 nm. Since the number of layers in the mirrors has been decreased, the bandpass of the filter is wider than with the previous design. In addition, the monitoring signal of cavity layer during deposition is also higher (minimum transmittance is 15%), meaning that we could perform optical monitoring for all the layers. The spectral performance of the deposited filter is plotted in Fig.3-4. For the *ex-situ*

measurement of the filter, uncoated fused silica substrate was used for 100% calibration of the spectrometer, meaning that the measurement of lossless filter should reach 100% transmittance. From calculation without considering the backside reflection, we can show that maximum transmittance of 99.65% for this design means the k is $\sim 1 \cdot 10^{-4}$. As can be seen in Fig.3-4. the maximum measured transmittance is very near 100%, in peek it reaches 99.8% confirming that with the optimized deposition parameters the HfO_2 layers have very low losses at 355 nm. However, as can be seen in Fig.3-4(b), even for this filter that has a wider bandwidth, the measurement at the peak is noisy. This represents an important issue for both *ex-situ* and *in-situ* measurements of narrower Fabry Perot filters.

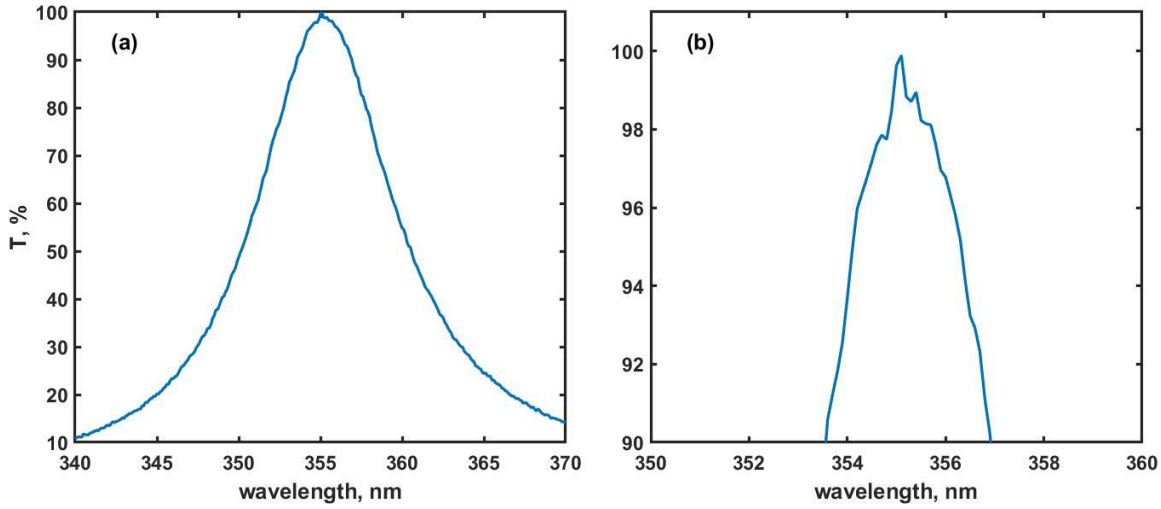

Figure 3-4 Transmittance of M6 2L M6 design when spectrometer is calibrated with uncoated substrate.

In conclusion, we have improved (reduced k) the optical properties of HfO_2 layers by increasing the amount of co-deposited silica. With the new material properties, we are able to theoretically meet the requirements of the project, and thus can move on to the challenges of optical monitoring of narrow bandpass filters.

3.3 Optical monitoring of Fabry Perot filters

Although Fabry Perot filters are known for decades and the turning point monitoring has been proven to be a reliable monitoring method for this class of filters as it benefits from the error

compensation[11][16], several challenges remain when the filters FWHM is few nanometers or below. Measurement of narrow filters is difficult even for *ex-situ* spectrophotometers as we have shown in previous section. *In-situ* measurement in the deposition systems is even more difficult as the spectral resolution cannot match the *ex-situ* standards and the time frame of the measurement is in milliseconds. This is, for example, very well-known monitoring challenge for WDM filter (wavelength division multiplexing filter) where a very narrow bandpass (below 1 nm) around 1550 nm is required[66]. However, in this spectral region, tunable lasers with ultra-narrow bandwidth are available and can be used in optical monitoring systems to overcome bandwidth and power issues.

To illustrate the difficulties of in-situ optical monitoring, we plotted in Fig.3-5 (blue and green) the theoretical monitoring curve for the M11 10L M11 design. As layers are deposited, the transmittance decreases with every high index layer, and, after several high and low index layer pairs, the transmittance is well below 10%. Additionally, the total amplitude of the transmittance for each of the layers decreases. This means that the measurement becomes more and more sensitive to noise. For this particular design, the minimum transmittance during the deposition of the cavity layer is 3.6% and maximum 7.9%.

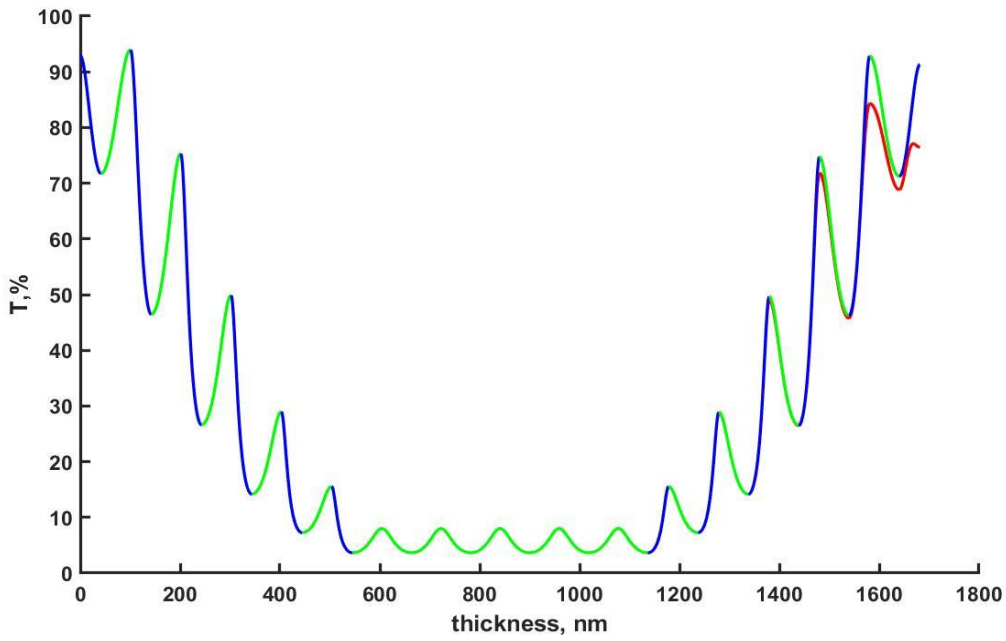

Figure 3-5 Monitoring curve of M11 10L M11 filter, high index layers in blue and low index layers in green, red represents the monitoring curve respecting 0.6 nm bandwidth.

If we suppose that we have successfully deposited the cavity layer, the next challenge arises when the second mirror is deposited and filter starts to take its shape. At this stage, spectral resolution of the monitoring system becomes a decisive factor for the quality of filter. To illustrate it, we plotted in Fig.3-5, together with theoretical monitoring curve, the same monitoring curve that is calculated with a 0.6 nm spectral resolution (red curve). As can be seen, the monitoring signal of the last layers is highly disturbed by the spectral resolution limit. The last layers are usually terminated too soon when the filter is deposited. Therefore, the spectrometer bandwidth must be improved or a different monitoring technique for the last layers should be used.

To increase the measurement accuracy, we used a more powerful light source than the classic halogen or deuterium lamp. A more powerful lamp, in addition to improving the SNR, would also allow to close the slits to improve spectral resolution.

Therefore, the standard lamp was replaced with laser driven light source (LDLS), where a laser is used to generate plasma between electrodes in xenon filled bulb, produced by *Hamamatsu*[67]. The LDLS light source although powerful is very sensitive to mechanical vibrations, making it difficult to use near all the pumps needed for vacuum systems. Mechanical vibration of the light source causes sharp fluctuations in the emitted light. On various occasions, the noise of the measurement signal was the reason to stop experimental run as deviations from theory became too large and the safety algorithms of the optical monitoring system stopped the process. In Fig.3-6, we have plotted the actual monitoring curve of one of the deposition runs where HfO_2 layer is followed by SiO_2 layer on fused silica substrate.

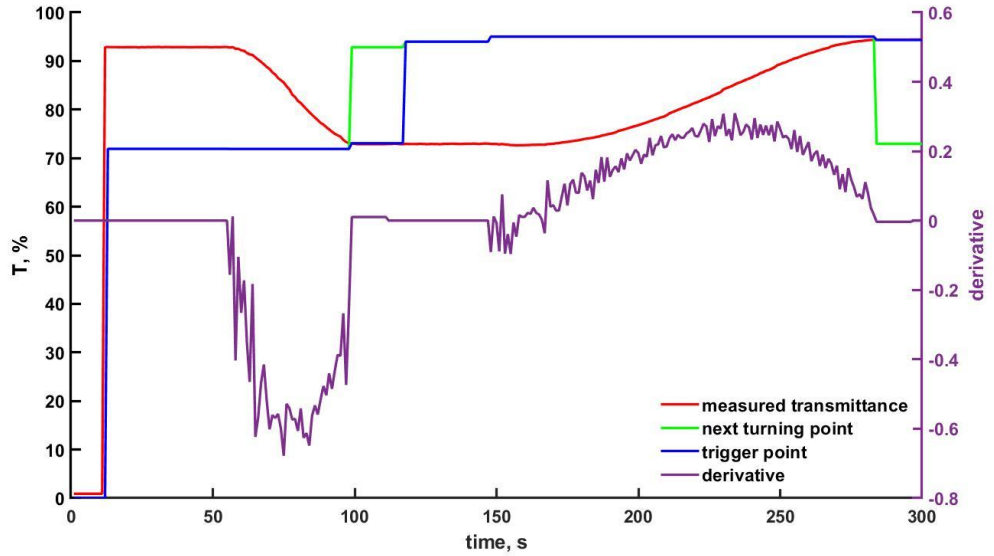

Figure 3-6 Monitoring curve of H and L layer on silica substrate.

The transmittance is plotted in red, the derivative in purple, the transmittance of the expected trigger point in blue, and the expected transmittance of next turning point in green. In case of turning point monitoring of quarter wave layers, trigger point is equal to the next turning point.

The fluctuations in derivative of the measured transmittance signal can reach one third of its full amplitude, and, as can be seen in this example, can cause the termination of layer in wrong place. First layer is stopped well before the actual turning point is reached. To avoid issues linked to noise of monitoring signal, the settling time can be increased. The settling time for this kind of measurement means how many measurements are taken for averaging. For example, if we consider that the rotation speed is 180 rpm, if settling time is set to 2 seconds, it means that an average of 6 measured values will be used to determine the trigger point. Increasing settling time decreases the effect of noise but can create systematic errors as layers will be triggered too late. However, that is not as problematic as layers being terminated randomly. As we showed in the chapter 2, uncompensated random errors completely destroy the multi cavity Fabry-Perot filter. The systematic error, for example if every layer is terminated to late, will shift the centering of the filter towards longer wavelength, but the shape of the filter will be preserved. To limit the effect of noise, besides increasing signal settling time, we also placed the light source on an independent optical breadboard to limit the mechanical vibrations.

Finally, even with the more powerful light source, we were unable to improve the bandwidth of the setup below 0.6 nm by closing the slits further, as the maximum transmittance signal was already low (too much noise for the cavity layer).

Nevertheless, we managed to deposit one filter of the M11 10L M11 design centered at 355 nm with all layers monitored optically by turning point monitoring. Plotted in Fig.3-7 is the experimental and theoretical transmittance of the studied filter. Although the match between experiment and theory is good, statistical fluctuations do not allow easily reproducing these performances.

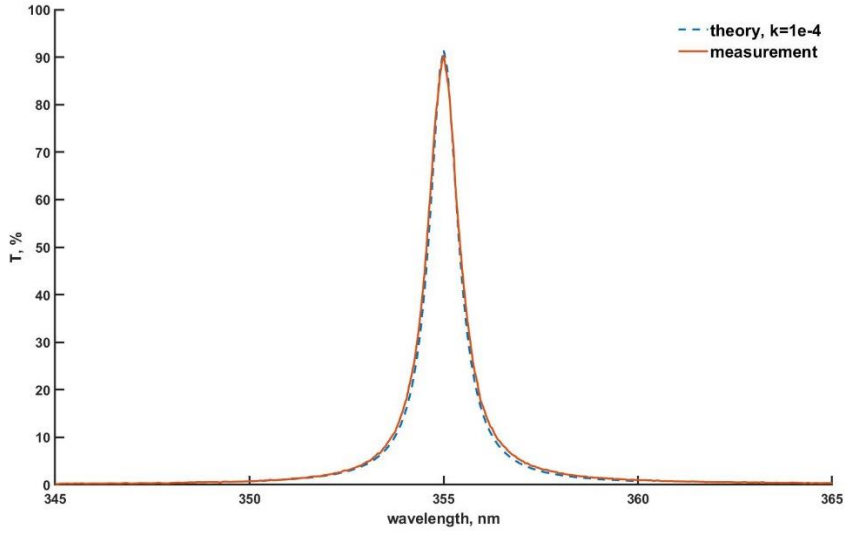

Figure 3-7 Transmittance of the M11 10L M11 filter with increased power for Si co-sputtering compared to theory.

HfO_2 layers were deposited with the optimized parameters described in previous section, this result confirms once again that we now can deposit filters with required level of transmittance in the UV range.

3.4 Two cavity filters

Since the result plotted in Fig.3-7 is not easily repeatable it was clear that we would not be able to optically monitor ultra-narrow bandpass UV-filters with more than one cavity using purely

turning point monitoring. In order to obtain multi cavity Fabry-Perot filters, the cavities must be perfectly centered. To be able to control the centering of the cavities we therefore needed to increase the signal to noise ratio when monitoring the cavity layer and improve the spectral resolution of the monitoring system. Since we could not improve the monitoring setup any further, we therefore looked at monitoring strategies that can be used to work around the limits of the spectrometer.

3.4.1 Multiple witness glass strategy

Because the first deposited filter (Fig.3-2) with rate monitored layers had quite large error in spectral centering of the bandpass, and in order to have good centering for both cavities,we used multiple witness glasses and optical monitoring for all layers, rather than rate monitoring for the last mirror layers. At first, we looked at a strategy that would allow us to widen the bandwidth of the filter when it is monitored and ease the spectral resolution requirements of the spectrometer. If we look again in Fig.3-5, we see that the monitoring curve taking into account the spectrometer resolution (red curve) deviates from the theoretical monitoring curve (blue/green) only for the last four layers of the second mirror. Therefore, we could create an indirect monitoring strategy where the monitoring glass is changed before the last layers of the second mirror, i.e. when measurement is unreliable. It is known that for Fabry-Perot filter, error compensation is very important, and therefore turning point monitoring for all of the layers is crucial. However, not all layers are sensitive towards thickness errors. To illustrate this statement, the relative error sensitivity for the two-cavity (M11 10L M11 L M11 10L M11) design, calculated with commercially available thin film software, is plotted in Fig.3-8. The relative sensitivity highlights the layers which have the largest effect on the filter if its thickness is changed (if there is an error). It is calculated by adding small thickness change to one layer at a time and comparing the new spectral performance to the original (error free) one. The most sensitive layers of a multicavity Fabry Perot filter are the cavity layers and few mirror layers close to cavities. Therefore, to obtain a filter with optimal spectral performances, any errors in these layers must be compensated. The last mirror layers in this design are more than 10 times less sensitive than the cavity layers, meaning that uncompensated errors in these layers should not affect too much the filter’s performances.

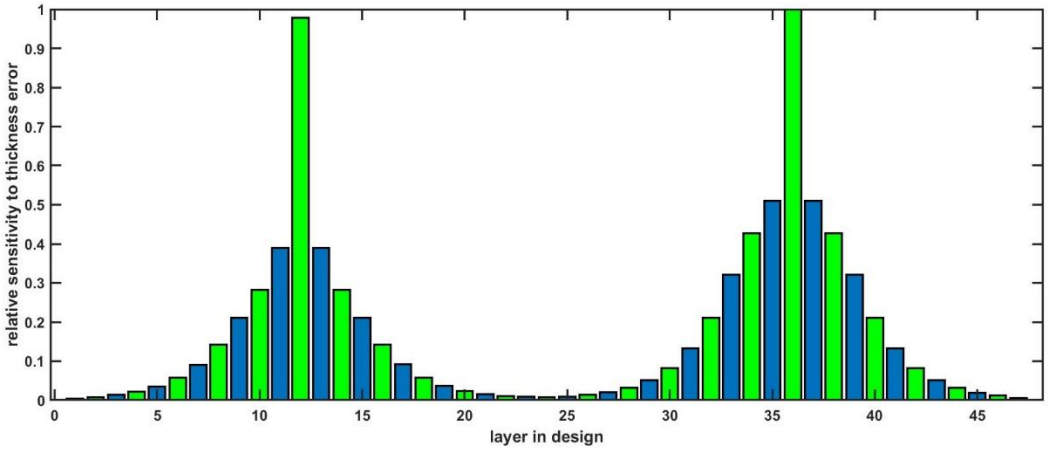

Figure 3-8 Layer sensitivity to thickness errors for M11 10L M11 L M11 10L M11 design. Blue are high index and green are low index layers.

Since the layers away from the cavities are not as error sensitive, we could consider a strategy that includes 4 witness glasses for two a cavity filter as shown in table 3-1. The witness glasses 1 and 3 that contain the cavity layers have the same un-symmetrical sub-design so that monitoring is stopped before the spectral resolution starts to influence the monitoring curve (Fig.3-5) and remaining of the mirror layers are optically monitored on additional glasses. The equal sub-design around the cavity layers also allowed us to compare the two monitoring glasses and observe if the centering for both monitored cavities is the identical or not.

Witness glass	Partial design
1	M11 10L M8
2	M4
3	M11 10L M8
4	M3

Table 3-1 Fabry-Perot filter divided into sub-designs to be monitored on individual witness glasses.

As can be seen in Fig.3-9, spectral response measured on witness glass 1 and 3 are not exactly the same. However, the centering of the filters is nearly identical for both witnesses. The mismatch is a result of error compensations which are crucial for the final filter's performances as soon as several cavities are combined.

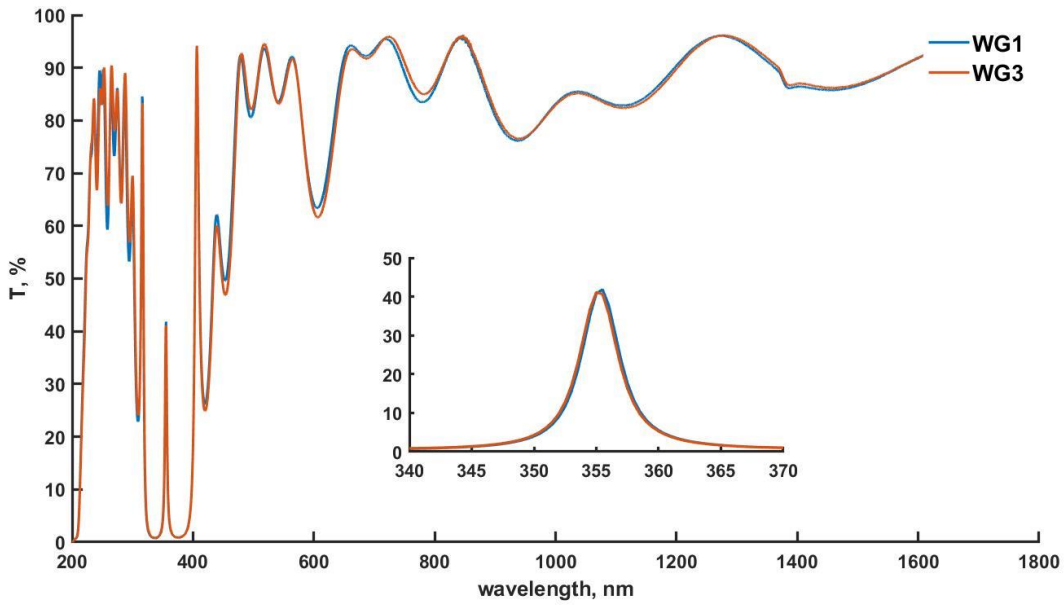

Figure 3-9 Transmittance of witness glasses (WG) 1 and 3.

The transmittance of the two-cavity filter monitored by this strategy is plotted in Fig.3-10. The centering is only slightly shifted, and the maximum transmittance is close to the theoretical target. This result confirms that the two witness glasses with the cavity layers are indeed centered on the same wavelength, as any misalignment of the centering of cavity layers results in decrease of maximum transmittance. Additionally, if cavities are misaligned, the filter width is usually very noticeably wider than the theoretical one.

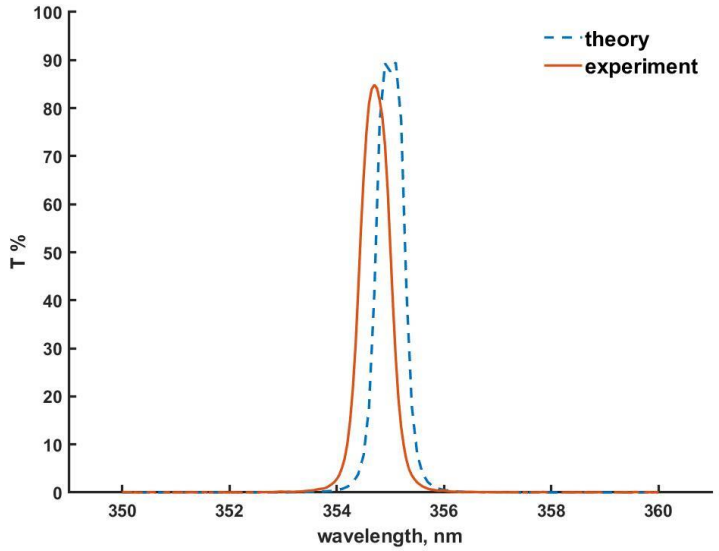

Figure 3-10 Transmittance of the two-cavity filter produced with multiple witness glass strategy compared to theory.

Additional concern for the multi witness glass strategy is the uniformity inside the vacuum coater. In the HELIOS coater we can place multiple sample holders for indirect monitoring. And in case of 25 mm diameter samples, several glasses can be placed into one holder. The elevation of the samples surface then can differ from one position to another as the holders most likely are not perfect. In addition, it has been observed that the uniformity measured on larger samples differs if measured in the direction of central axes of the turntable or perpendicular to it. Ideally this would only result in a shift of centering wavelength and this shift would be constant for a given position. However, in practice, we noticed that there is a random nature of these fluctuations that were not further investigated. In fig.3-11 we plotted the transmittance of two-cavity Fabry-Perot filters that were altogether coated on different glass substrates but that were placed in different positions inside the coater. Marked as Px-y, where x represents the position of the sample holder, and y the position of the glass in this holder. No two filters have the same centering wavelength and for some filters the cavities are not matched. The unmatched cavities cause the filter to be wider and with lower transmittance at the peak.

Another important factor to take into account is the temperature of the filter when it is deposited. These narrow filters are sensitive towards substrate temperature[38] and if the temperature of the witness glasses used for monitoring are not the same as for the glasses that are coated with all the

layers of the filter (especially if thermal stabilization is not achieved when changing witness glass), the deposited thicknesses can also differ.

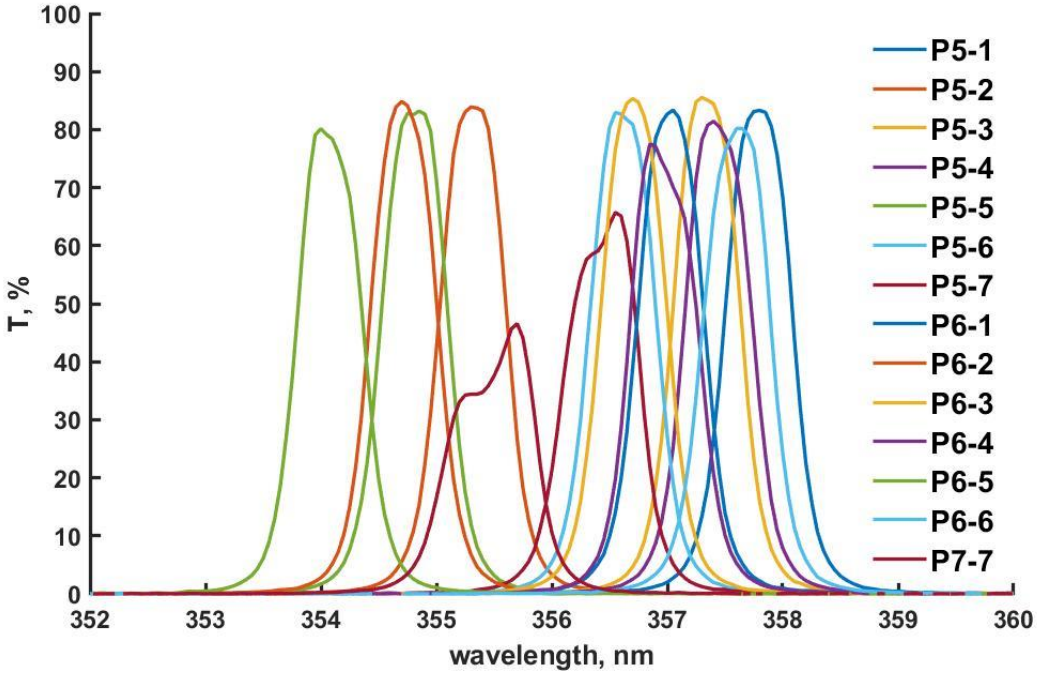

Figure 3-11 Two-cavity Fabry Perot filters from different position inside the coater.

One of the possibilities to achieve correct centering with indirect monitoring then would be to repeat multiple runs to find a position for the sample holder where the shift of centering is negligible or constant. In case of constant shift, the monitoring wavelength could be adjusted to match the wavelength from project specification. Additionally, the final filter can be angularly tuned if the central wavelength is centered at longer wavelength. Hence, we kept focusing on the monitoring strategies.

3.4.2 Returning witness glass strategy

With the previous strategy, we have improved the monitoring strategy by eliminating the potential spectral resolution limitation. However, from the monitoring point of view, difficulties remained because the transmittance of the cavity layer is very low. Therefore, another strategy to increase the transmittance level of the cavity for monitoring was created. Once again, we used the indirect monitoring approach, this time we used a different monitoring glass also for the first

layers of the first mirror. By doing so, we can reduce the reflectivity of the mirrors surrounding the cavity layer. We aimed for the transmittance for monitoring of the cavity to be higher than 10%. Additionally, if less layers are in mirrors surrounding cavity, the bandpass of the filter is wider, meaning that the required spectral resolution of monitoring setup is sufficient.

Instead of disregarding the first witness glass after the first mirror layers, we kept it and used it once again when monitoring the last mirror layers. To illustrate this approach, let's look at M11 2L M11 design. We ca re-write the formula as M6 - M5 2L M5 - M6. The two M6 mirrors are monitored on the same witness glass. With this strategy, we monitor the M6 mirror on the first witness glass, M5 2L M5 on second witness, and then use the first witness glass to monitor the remaining 6 mirror layers. In this case the 6^{th} (last layer of first M6) and 7^{th} (1^{st} layer on second M6) layer on the first witness glass are low index layers that form another cavity layer, forming a second Fabry-Perot filter, identical to the filter monitored on 2^{nd} witness glass. We have plotted this monitoring curve in Fig.3-12. The blue curve represents the high index layers and the green one the low index layers.

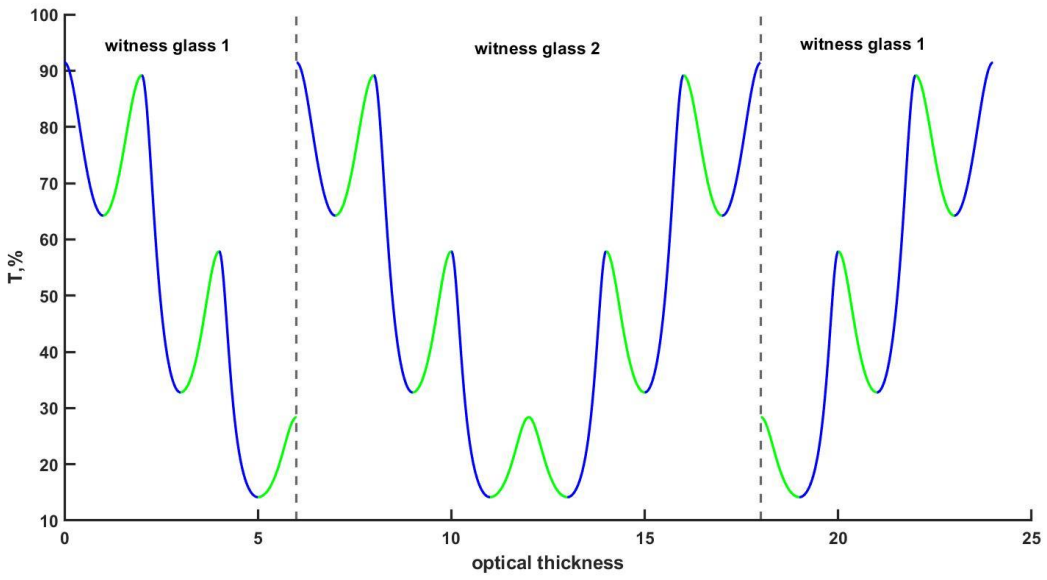

Figure 3-12 Monitoring curve of Fabry Perot filter with returning witness glass.

As we see in Fig.3-12, from monitoring point of view, both of the witness glasses have indeed the same design - M5 2L M5. We can assume that some form of error compensation can be retained when the first witness glass is coated a second time.

To test this idea, we needed make sure that the monitoring setup allows to use the same test glass twice. This means that all information about the first 6 layers deposited on first witness glass and calibration of the glass itself should not be deleted when the second test glass is coated. Additionally, it would be preferable that the monitoring glasses are kept in vacuum while they wait to be re-entered for deposition.

Thanks to our partner *Bühler Leybold Optics*, we were able to test this strategy using the HELIOS 800 coater equipped with automatic test glass changer in Alzenau, Germany. The M11 2L M11 L M11 2L M11 design was selected and divided into sub-designs as shown in table 3-2. The materials were Nb_2O_5 and SiO_2 as high and low index respectively and the reference wavelength was changed to 500 nm to avoid potential issues with Nb_2O_5 absorption. A 1 mm thick D263 glass was used as substrate. All layers, except the coupling layer between the two filters, were optically monitored. Rate monitoring was used for the coupling layer.

Witness glass	Partial design
1	M6
2	M5 2L M5
1 (returns)	M6 L
3	M6
4	M5 2L M5
3 (returns)	M6

Table 3-2 Coating sequence for two-cavity filter with returning witness glasses.

The spectral response of each individual witness glasses is plotted in Fig.16. As we can see, the centering is identical for filters on all witness glasses. The spectrum for witness glass 1 differs from the others because it also contains the coupling layer.

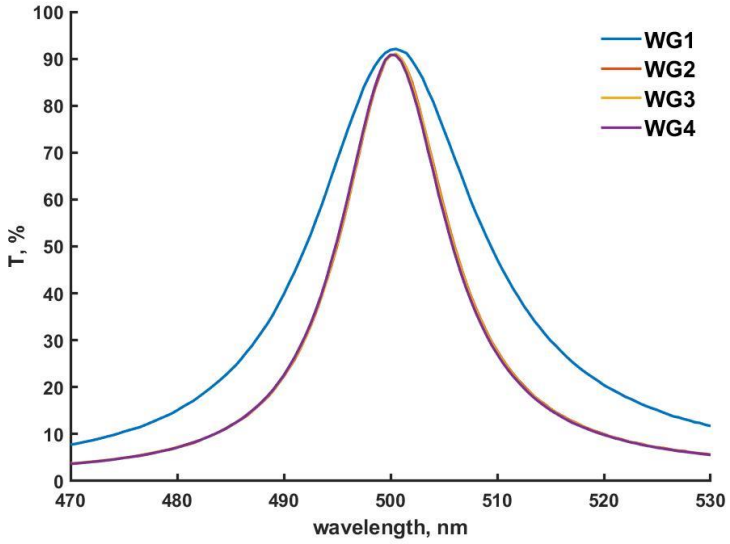

Figure 3-13 Transmittance of the 4 witness glasses of a two-cavity Fabry-Perot filter centered at 500 nm.

Witness glasses containing all the layers of the filter were again placed in several positions inside the coater. From previous experiments with this deposition setup, it was known that the position close to the monitoring position (position 1) gives the best results in terms of reproducibility. Positions 2, 3, 11, 12 were chosen for the glasses that will have the full design (note that there are 12 positions inside this coater). The measured transmittance is plotted in Fig.3-14. Each filter has a different centering wavelength, shorter for positions 2 and 3 and longer for 11 and 12 compared to monitoring wavelength. In fig3-14(a) the measurement step was set at 0.05 nm. In Fig.3-14(b) we measured the uniformity of filter from position 2. Transmittance was re-measured in 4 positions on this sample with a 0.01 nm step, which is the smallest step possible with the PerkinElmer Lambda 1050 spectrophotometer.

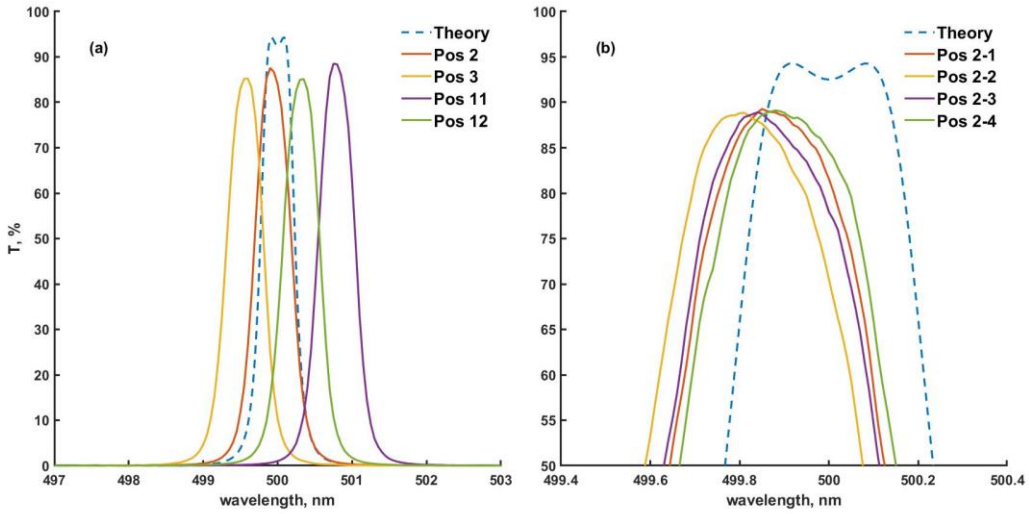

Figure 3-14 (a) - Transmittance of filters from different position inside the coater. (b) - Measurement of glass in position 2 in multiple places.

Maximum transmittance does not vary by more than 2% from one sample to another. Also, as can be seen form Fig.3-14(b), the centering of the filter is not the same across the sample, showing that the uniformity can also influence measurement if filter is very narrow. Most likely, these filters are on the edge of what is possible to achieve with multiple witness glass strategy, as some mismatch between the two cavities is expected and the filter's structure is very sensitive to any kind of error or instability.

Since the measurement of narrow filters are so difficult, we believe that clever strategies for monitoring narrow Fabry Perot filters are important as the *in-situ* measurement during the deposition is not as accurate and lacks the control of parameters compared to *ex-situ* measurement.

Additionally, to achieve these well-matched filters with the returning witness glass strategy, heating time before starting the deposition was significantly increased compared to standard processes. The usual practice is to heat the substrate to 150°C and hold this temperature for 5 minutes. For these filters the temperature was held for 15 minutes.. Deposition run with the standard 5 min heating did not produce filters with matched centering wavelength. Therefore, we believe that this additional heating time ensured that coating conditions were the same for all witness glasses

3.5 Thoughts about turning point monitoring of narrow Fabry Perot filters

As we have showed, the narrow Fabry-Perot filters are very challenging designs from a monitoring point of view. Either a dedicated monitoring system containing laser light source should be created for narrow Fabry Perot filter monitoring, or indirect monitoring strategies should be used. It is possible to overcome the technical limits of the standard monitoring systems by the indirect monitoring strategies, however by doing so, we limit the error compensation associated with the turning point monitoring as the compensations can work only on local witness glass level. Because of this, one must be sure that the deposition conditions are equal throughout the whole deposition time, as these filters are very sensitive towards changes of the substrate temperature, height of the substrates and even the precision of the sample holder manufacturing.

Therefore, although the Fabry-Perot designs are known for many years, the manufacturing is still a very challenging task. The indirect monitoring strategies presented in this chapter appear to be promising solution for overcoming the technical limits of the monitoring setups.

Chapter 4 - Polychromatic optical monitoring

In this chapter, we will discuss the process of developing monitoring strategies for non-quarter wave thin film designs. We will begin by reviewing the conventional methods for determining monitoring strategies. We will discuss the manual wavelength selection process and two algorithms designed to automate the wavelength selection processes. After exploring previously established methods for monitoring strategy determination, we will propose alternative approaches for fully automated monitoring strategy determination, referred as polychromatic monitoring, which differs from standard monitoring practices in the large number of wavelengths used for filter monitoring on a single witness glass.

4.1 Classical methods for optical monitoring strategy determination

The selection of monochromatic monitoring wavelengths is a key point for accurate thickness control during thin film filter deposition process, especially if we are talking about non-quarter wave designs. The usual process involves the operator visually evaluating the theoretical monitoring curves and based on experience, selecting the most promising wavelengths. Simulation software can be used to validate the strategy, and if it works, the operator proceeds to experiment. Although simulation software is useful, it is difficult to define all possible sources of errors and their impact on the deposition run. Thus, even if the simulation is satisfactory, the actual experiment may be disappointing, and new strategies must be designed. This process can be time and resource consuming, especially if the number of layers in the design is high. When operators try to find the monitoring strategy, they usually focus on finding one or very few monitoring wavelengths. Often, it is not possible to find a monitoring wavelength that is satisfactory for all layers in a filter. One solution is to use optical monitoring for as many layers as possible, and then use rate monitoring for the remaining layers. The disadvantage is that with rate monitoring, the use of error compensation algorithms that accompanies monochromatic monitoring is no longer possible. One of the reasons operators try to find a single monitoring wavelength is that it allows the use of error compensation algorithms because they rely on information given at the turning points. And if the turning points are not in the same layer, using

a single monitoring wavelength collects enough information to correct the trigger points, even in the case of thin layers.

4.1.1 Empirical or 'manual' monitoring strategy

The empirical or 'manual' determination of the monitoring strategy is to visually evaluate the monitoring curves and based on experience, select the most promising wavelengths. But what would be the perfect monitoring curve? In addition to the fact that there should be at least one or better two turning points in each layer for corrections, one also wants the trigger points to be not too close to these turning points. The reason for this is that the transmittance signal evolves slowly around them, which decreases the accuracy of the trigger point determination because the effect of noise is more pronounced when the signal evolves slowly. In general, if one cannot find a wavelength where the trigger point is far enough away from the turning point, it is better to select a wavelength where the trigger point is shortly after the turning point. If the trigger point is close before to the turning point, it is possible that errors in the preceding layers will change the transmittance in a way that the turning point occurs before the transmittance level for trigger point is reached, and, as a consequence, the signal will never reach the trigger level. In this situation, the deposition must be stopped by time-based safety mechanisms. These are some of the questions that an operator tries to answer when designing a monitoring strategy.
To better illustrate these situations, we can look at some possible monitoring curves for the 8-layer beam splitter design [appendix 1.5]. The monitoring curves show the evolution of transmittance at a single wavelength as layer thickness increases. Visual evaluation is a powerful method, if the number of layers is small, because experienced operators can quickly see if the monitoring process may be problematic on any of the layers.

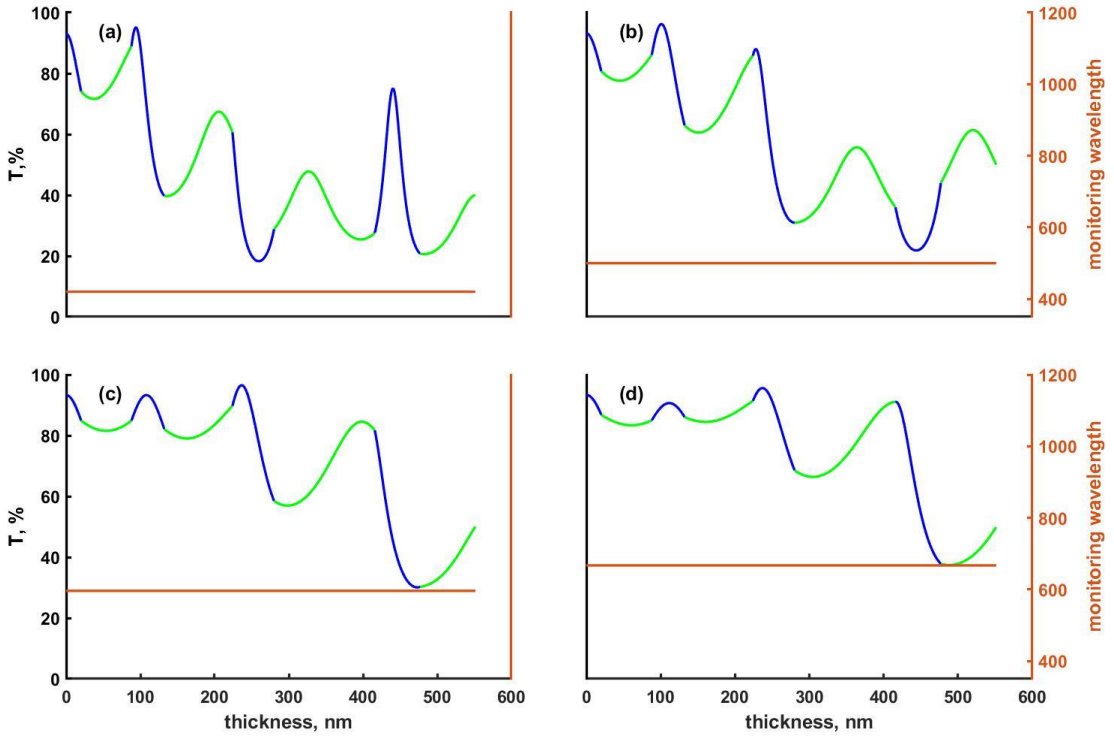

Figure 4-1 Potential monitoring curves for beam splitter design, blue curves represent high index layers and low index layers are plotted in green. In (a) the monitoring wavelength is 420 nm, (b) – 500 nm, (c) – 595 nm and (d) – 666 nm.

In Fig.4-1 we have plotted monitoring curves for different wavelengths. In the first case, Fig.4-1(a) where the monitoring wavelength is set at 420 nm, the problematic layers are layers 3, 7 and 8, because they are terminated not far from the turning points. For better evaluation of the monitoring curve, we usually calculate the remaining distance to the next turning point, but at this scale it is not always easily understandable, so we decided not to represent it on the graph.

The second wavelength selected is 500 nm, Fig.4-1(b). Increasing the monitoring wavelength moved the trigger point away from the turning point for 3rd layer but moved it closer to the turning point for 5th layer. Also, the first turning point for this layer is very close to the beginning of this layer, meaning that there will not be too many measured data points, which could lead to inaccuracies in detecting this turning point.

Next, we look at the monitoring curve if we increase the monitoring wavelength further to 595 nm, Fig.4-1(c). We no longer have a turning point in the 8th layer, which is undesirable for

the use of correction algorithms, and the 7^{th} layer ends very shortly after the turning point. However, the rest of the layers are terminated on a 'good' slope, where the transmittance changes noticeably with increasing thickness.

If we continue to increase the monitoring wavelength, as in Fig.4-1(d) at 666 nm, we significantly decrease the signal amplitude for the first 4 layers. Also, in this case, layers 6 and 7 end shortly before the turning points.

Hence, we can see that determining an optimal optical monitoring strategy is not easy because the entire monitoring curve changes by modifying the monitoring wavelength. Of course, when determining a strategy, all wavelengths between these four must also be evaluated. Therefore, strategy selection can be very time-consuming.

To see how these 4 strategies potentially differ, we can use a coating simulation software. For this example, we used only transmittance noise as the source of errors. We set the additive and multiplicative noise to 0.05%, assumed equal deposition rates of 0.5 nm/s for both materials, and the rotation speed of the turning table was set to 240 rpm. These parameters are close to the reality with our HELIOS coater. In this case, the simulation is performed without using correction algorithms in order to highlight the influence of noise of the monitoring setups. A single representative simulated curve is plotted in Fig.4-2, but a large number of simulations have been performed for statistical purpose.

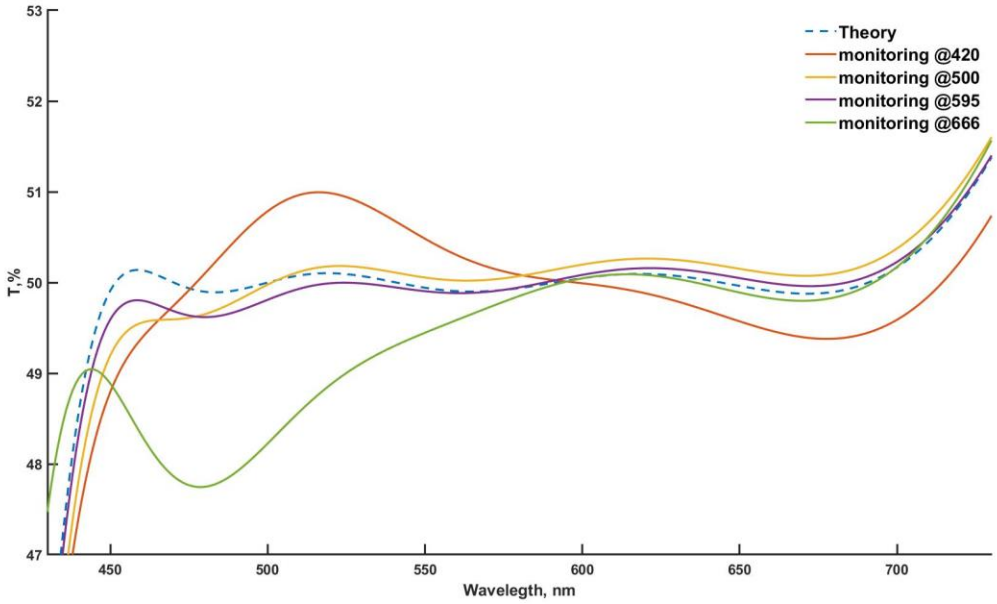

Figure 4-2 Simulated transmittance of a beamsplitter design with different monitoring wavelengths.

As can be seen in Fig.4-2, using different monitoring wavelengths results in very different transmittance spectra. The 500 nm and 595 nm strategies have similar performance, with the 595 nm strategy being slightly closer to the target spectrum. The 420 and 666 nm strategies are not only quite far from the target, but the spectral performance is different, showing that the errors are indeed different for various monitoring wavelengths. Since these are simulated results, we can also extract the thickness errors for each layer (Fig.4-3). We see that in terms of errors, the strategies at 420 and 666 nm perform the worst, while the strategy at 595 nm is the most promising because it is less affected by measurement noise.

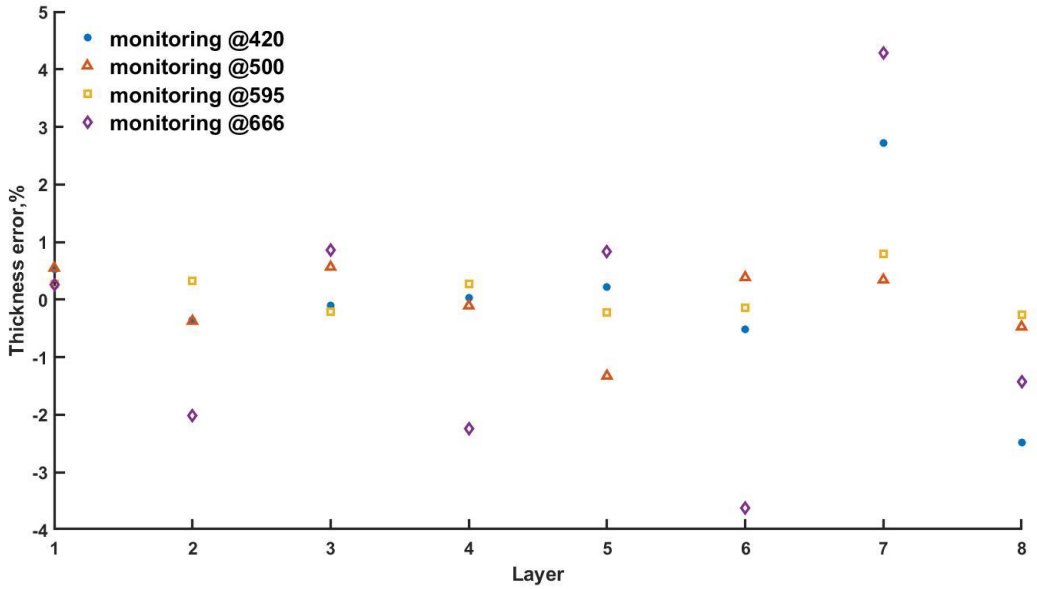

Figure 4-3 Simulated relative thickness errors for the beam splitter design at different monitoring wavelengths.

In practice, other effects than noise can of course influence the monitoring process. Refractive index errors are often quantitatively associated with the deposition process, the error can be systematic or random, there can be a small systematic error every time the deposition is terminated and the shutter is moved between the target and the sample. For this simulation, we did not use a correction algorithm, however all potential causes of errors can also influence the online re-calculation of the trigger point. For example, if the turning point is incorrectly detected, the POEM algorithm can become a cause of thickness error and not compensate for anything.

If the strategy is tested by simulation software, the input parameters of potential errors should be studied to match the real situation as closely as possible, and several simulations should be performed to estimate the stability of the strategy.

The visual evaluation of the monitoring curves in combination with the deposition simulation, the so-called classical approach, to select the monitoring strategy will be used as a reference for the following study of optical monitoring strategies. However, since it is performed manually, it is time consuming and of course very interesting to automate the strategy development process.

4.1.2 Algorithms for automatic determination of the monitoring strategy

For an eight-layer design, the monitoring strategy can be found relatively quickly by an experienced scientist working in the optical thin-film field. For thin film designs consisting of hundreds of layers, the process of manually selecting the strategy can be time consuming or even impossible. To solve this problem, Trubetskov *et al*. published a paper that addresses the issues of the monitoring strategy selection process and provided a solution to make the process automatic[68]. The goal is to automatically find no more than 5 wavelengths for monitoring a thin-film stack. The reason for limiting the number of allowed wavelengths is the desire to benefit as much as possible from the possible correction algorithms.

In order to achieve this goal, the authors specified some definitions of the monitoring curve that can also help in the manual wavelength selection process. First, they defined the amplitude A of the monitoring signal (V) as the difference between the maximum V_{max} and minimum V_{min}.

$$A = V_{max} - V_{min} \tag{4.1}$$

For the signal amplitude, they considered the distance between the extrema of the monitoring curve - the turning points. In case of thin layers, the virtual increase in thickness is used to locate the missing turning points.

Next the *initial* and *final swings* are defined as follows:

$$S_{in} = \begin{cases} \frac{V_{max} - V_{in}}{A} 100\% \; if \; the \; first \; extremum \; is \; maximum \\ \frac{V_{in} - V_{min}}{A} 100\% \; othervise \end{cases}$$

$$S_{fin} = \begin{cases} \frac{V_{max} - V_{fin}}{A} 100\% \; if \; the \; first \; extremum \; is \; maximum \\ \frac{V_{fin} - V_{min}}{A} 100\% \; othervise \end{cases} \tag{4.2}$$

Where V_{in} is the signal level at the start of deposition for a given layer, and V_{fin} is the transmittance level for the trigger point. The first extremum is the first turning point starting the count from the side of substrate. If there is no turning point in layer, as it is typically the case for thin layers, the theoretical increase in thickness is calculated to find the extremum values. Swing values that are close to 0 or 100% indicate that the monitoring signal (either at the beginning or end of a layer) is close to an extremum. Of course, the S_{in} for first layer will be 0%.

Another parameter of the monitoring curve that was considered is the distance (Δ) between the trigger point (V_{fin}) and the next extremum E_{next}.

$$\Delta = \left|V_{fin} - E_{next}\right| \tag{4.3}$$

Again, a theoretical increase in thickness is required to find this parameter. With these definitions, it is then possible to add boundaries to the factors considered and search for the best wavelength for automatic monitoring by finding the minimum of the F_M monitoring function:

$$\begin{aligned} F_M = {} & w_{in}[q(a_1 - S_{in}) + (S_{in} - a_2)] \\ & + w_{fin}\left[q\left(b_1 - S_{fin}\right) + \left(S_{fin} - b_2\right)\right] \\ & + w_A q(\varepsilon - A) + w_\Delta q(\delta - \Delta) \end{aligned} \tag{4.4}$$

Where a_1 and a_2 are boundaries for the swing at the beginning of the layer, the b_1 and b_2 limit the swing at the end of the layer, ε is the minimum amplitude allowed, and Δ specifies the distance between the trigger point and the next extremum. In this formula, $q(x)=x^2$ if $x \geq 0$ and $q(x)=0$ if $x<0$; w_{in}, w_{fin}, w_A and w_Δ are weight factors for the equation. The selection of the wavelength then depends on the definitions of the boundaries and weight factors. The usable wavelengths range and step is also an input parameter, the F_M is calculated for the given wavelength range and the wavelength that matches the minimum F_M is selected for monitoring. To use this method successfully, a significant amount of experimental work is required to find the correct values for the many variables of Eq.4.4.

Another approach to select the monitoring wavelength semi-automatically has been presented by Vignaux *et al.*[69]. Again, the focus is on the use of correction algorithms, in particular POEM. This method also implements deposition simulations to select the strategy. The wavelength selection process is done in two parts: at first, the so-called *trinary mapping* is performed to define the usable wavelengths for optical monitoring. A wavelength is considered usable if it can be used by the POEM algorithm to control the trigger point. Basically, 3 criteria are tested for each of the allowed wavelengths:

- Is there a turning point during the deposition of the layer? If yes, this wavelength can be used for POEM, otherwise the wavelength cannot be used for monitoring.
- If there is a turning point, what is the distance between the turning point and the trigger point? To avoid problems with noise and the influence of thickness errors in the previous

layers, the authors state that the absolute transmittance difference should be at least 2%. In such case, the wavelength is marked as good for monitoring.

- Layers that have at least two turning points and meet the second criterion are considered good layers for a possible wavelength change. The authors state that if it is necessary to change the monitoring wavelength, it is best to do this with a layer that has two turning points. After two turning points are recorded, there should be no more corrections to the trigger point by the POEM algorithm.

In general, this process finds several possible wavelengths and wavelengths pairs that can be used for optical monitoring. In order to select the best strategy, simulation software is used. The coating simulation is performed 100 times with each of the possible wavelength pairs in order to collect enough data for statistical analysis. This task is of course very time-consuming. Then, it is necessary to find a mechanism to determine the best wavelength. One possibility is to calculate the merit between the theoretical transmittance of the target and the simulated transmittance. However, this requires the simulation to be in the full spectral range. Therefore, another criterion is used to evaluate the quality of strategy.

The authors call this method *PhaseEval Method.* With this approach, the root mean square deviation (φ_{RMSD}) of the reflected phase after the last layer of the design and the cumulative phase error ($\Sigma\phi_{RMSD}$) - as the number of layers increases- is used to evaluate the considered strategies. The advantage for the phase is that it can be calculated only for one wavelength, which reduces the computation time.

$$\varphi_{RMSD} = \sqrt{\frac{\sum_{i=1}^{Npr}(\varphi(i) - \varphi_{th})^2}{Npr}} \tag{4.5}$$

And the cumulative phase error after each of the N deposited layers can also be used for strategy evaluation:

$$\sum \varphi_{RMSD}(N) = \sum_{i=0}^{N} \varphi_{RMSD}(i) \tag{4.6}$$

Where φ_{th} is the theoretical reflection phase after each layer in the given filter, $\varphi(i)$ is the phase obtained by simulation for the i^{th} layer, Npr is the number of predictions. The wavelength or wavelength pairs where the difference between the simulated and theoretical phase is the smallest is then selected as the best monitoring strategy.

Since this method requires simulations of the signals obtained during deposition, the accuracy will depend heavily on the ability of the simulation software to reproduce the actual deposition.

The first method described is implemented in the *Optilayer*[49] software which is often used for thin film design. We tried this method without changing the proposed weight factors or the default input parameters as defined in the publication, in order to search for one wavelength for monitoring the beamsplitter. The wavelength that the calculation suggests is 504 nm. This is very close to one of the wavelengths we selected manually.

The second method is a bit more complicated, because we do not know exactly the error parameters used by the simulation software. Nevertheless, the one-wavelength strategy suggested by this method is 527 nm.

The corresponding monitoring curve are plotted in Fig.4-4.

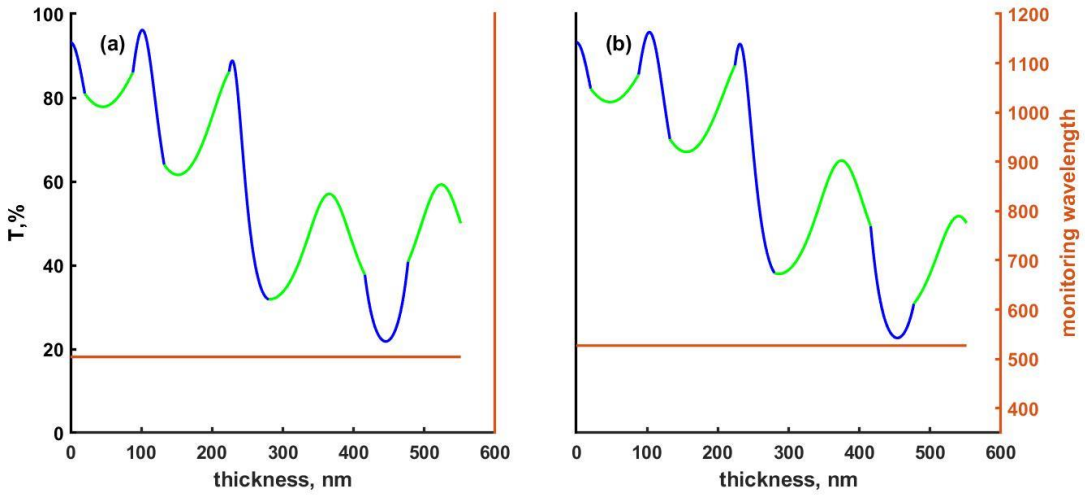

Figure 4-4 Monitoring curves selected by automatization algorithms, (a) monitoring wavelength is 504 nm, (b) monitoring wavelength is 527 nm.

For both of these monitoring strategies, the 5th layer is where monitoring difficulties can be expected, as the layer must end very close before a turning point, especially for the 504 nm strategy where the trigger point is almost equal to the turning point. In addition to the noise sensitivity noise for this trigger point, any error that results in a positive or negative offset of the signal could completely destroy the monitoring sequence. Such y-axis shift is sometimes observed for the actual deposition, and can come from a refractive index error or a small

substrate calibration error. We again ran the simulation software with the same conditions as for the manually selected monitoring curves, and representative transmittance spectra from a simulation run are plotted in Fig.4-5. As can be seen, the strategy with a wavelength of 527 nm seems to work quite well. However, even though this strategy works well, one should always be careful with trigger points so close to a turning point (specifically just before). Ideally, the simulation should be run several times to gather statistics on the stability of the strategy. The simulated spectra from the 504 nm strategy deviates significantly from the target, and it is interesting to note that the difference is larger than for the 500 nm strategy we choose as example in Fig.1-2.

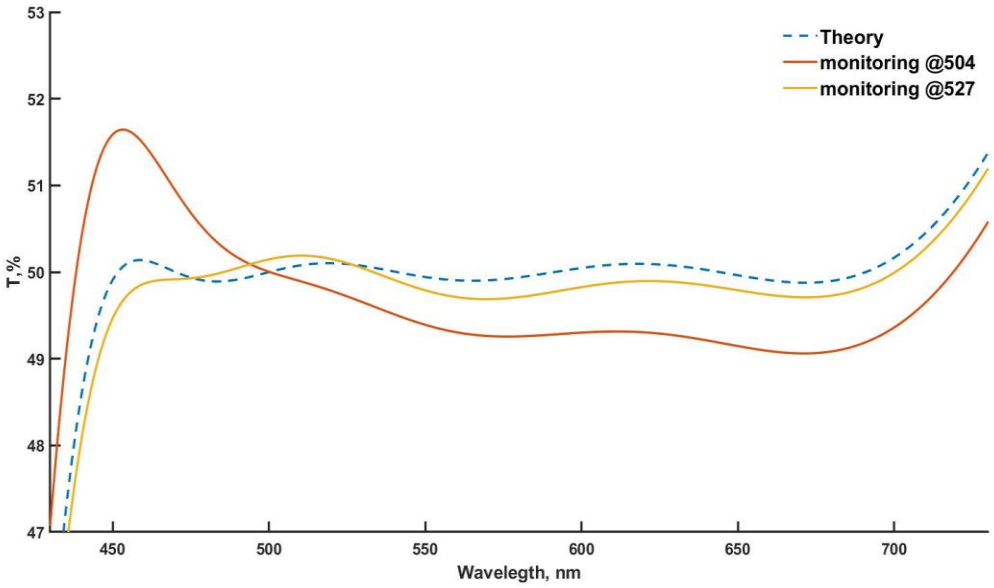

Figure 4-5 Simulated transmittance spectra of the beam splitter obtained when (a) monitoring wavelength is 504 nm, (b) monitoring wavelength is 527 nm.

Although the simulation is promising, it should be kept in mind that we are using only measurement noise as the source of errors. Since this is a simulated deposition process, we can extract the thickness errors for these two runs. We have plotted the errors in Fig.4-6. As expected from the monitoring curve analysis, we see a large error on layer thickness number 5 for the 504 nm strategy. This can be easily associated with the trigger point being closer to the next turning point than for the 527 nm strategy. Due to the low dynamic range of the signal, even a

small noise error can lead to large thickness errors. These examples illustrate why we do not want the trigger points to be close to the turning points.

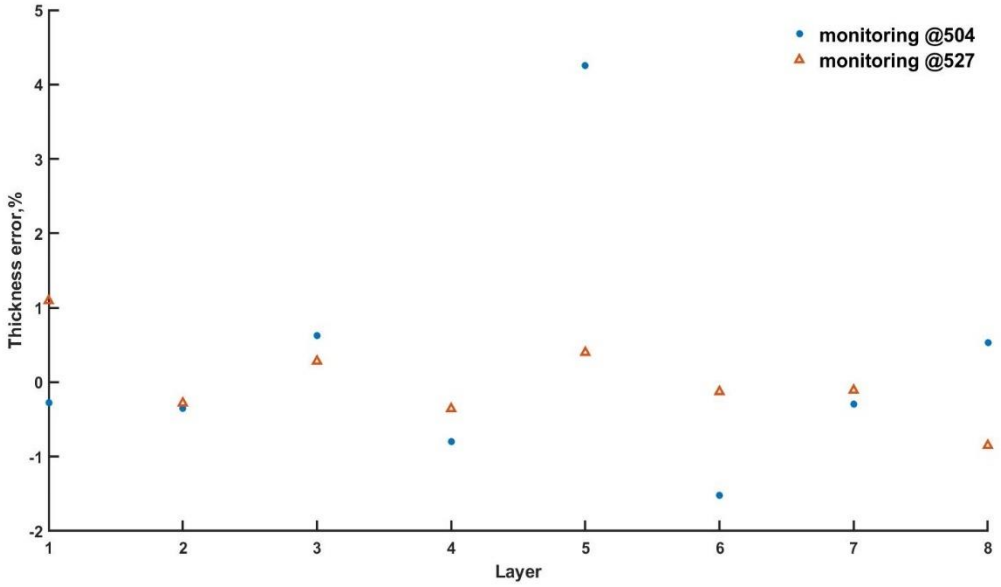

Figure 4-6 Simulated relative thickness errors of the two monitoring strategies.

Finally, of all the strategies we have presented here, the manually selected strategy – monitoring all layers with a wavelength of 595nm - performs best and was therefore used for the actual deposition run.

As we have shown, the selection of the monitoring wavelength/strategy is a very delicate task because many parameters have to be taken into account and a very large number of solutions can be found. Simulation software represents an interesting and efficient technique to test the selected strategies.

However, this software must be very well configured to reproduce all possible sources of error that may be present in the deposition chamber. Previously published algorithms for wavelength selection can be useful, but they still require a thorough knowledge of the deposition equipment to properly define each value of the input parameters.

By combining all the important factors that impact thin film monitoring that have been already published, and introducing new ones, we have developed an alternative automated method for determining the monitoring strategy for thin film filters, that we will now discuss.

4.2 Polychromatic monitoring strategies

The automated strategy selection described above are designed to use the error compensation algorithms for their full potential. This significantly limits the number of wavelengths used in the strategy, and the goal is also to use optical monitoring for all layers. These constrains raise the question: is it always the best thing to do? When we look for a single wavelength to monitor a given filter, it is not necessarily the best for each of the layers, but rather a compromise that could work for all layers. The idea then is to look for the best monitoring wavelength for each of the layers, even if it means changing the monitoring wavelength for each layer. By doing this, we lose some of the potential of the correction algorithms, but we gain accuracy for the deposition at the individual level – the thickness errors in general should be smaller. This idea can be extended to the inclusion of non-optical monitoring methods: if optical monitoring could lead to a larger thickness error compared to rate monitoring, it should not be used. Therefore, we developed a method that not only uses versatile monitoring wavelengths for each layer (we called this approach polychromatic optical monitoring) but also switches to rate monitoring whenever optical monitoring performs worse.

4.2.1 Key input parameters affecting optical monitoring signal

To increase the chances of successful thin film deposition, it is important to avoid wavelengths that can have a destructive impact on the thin film monitoring process. There are several conditions that must be considered, otherwise a poorly chosen monitoring wavelength can become the cause of significant thickness errors. And, in fact, there can be situations where it is impossible to find a suitable monitoring wavelength. In this case, it is advantageous to use other monitoring methods such as quartz crystal microbalance or time monitoring. Below we review some of the main parameters to consider when choosing monitoring wavelengths:

First, one must consider the possible wavelength range to be used. The usable wavelength range is defined by the light source and detector pair. Secondly, from our experience, we know that it is advantageous to use the monitoring wavelength(s) in the same wavelength range as for the application of the filter, if it is possible. Third, if the layer to be monitored is thin, in the 20 nm range or less, there may not be an appropriate wavelength that has a turning point (and no

correction algorithm can be implemented). In this case, rate or quartz crystal microbalance monitoring may be used if it produces a smaller error than optical monitoring. The possibility of large thickness errors increases with the number of layers deposited and the total thickness before the thin layer is monitored. Due to the accumulation of thickness errors in previous layers, the error in the transmittance level at the beginning of the layer can become comparable to the total transmittance amplitude expected during measurement of this layer. If the corrections related to the turning points are not performed, the thickness errors can reach tens of percent for these thin layers.

If non-optical monitoring is not possible, the monitoring wavelength of these layers can be identical to the one of previous layer. In this case, corrections related to the turning point can be made. At this point, however, we do not consider layer pairs for monitoring strategies.

To use the algorithms that may be available with the monitoring setup, e.g. POEM or monitoring *by swing*, at least one turning point must be present in the monitoring signal of the layer to be controlled. However, situations where the correction algorithm itself can become a cause of an error should be avoided. This is because both of the correction methods described above make adjustments with respect to measured turning points, so errors in the detection of turning points can lead to errors in the trigger points. Therefore, we need to examine the transmittance levels at the beginning of the monitoring curve with respect to the first turning point of the layer. We will call this the *start amplitude*.

To illustrate it, we have plotted in Fig.4-7 the evolution of transmittance as a function of thickness where the monitoring curve was plotted for a bilayer (Nb_2O_5/SiO_2) with a respective thickness of 30 nm and 100 nm. The *start amplitude* is a similar factor to *swing in* (Eq.4.2) that has been used by other authors[68][35]. If the initial transmittance for the selected monitoring wavelength is too close to a turning point, this may lead to false detection of this turning point. As mentioned earlier, a falsely detected turning point will result in an erroneous trigger point correction, if the correction algorithms are used. The reason for this false detection may be the instabilities in the deposition rate that cause a noisy measurement at the very beginning of the deposition. This is usually not a problem with thick layers that have multiple turning points, but if we look at designs like the beamsplitter where most layers have only one turning point, this factor becomes of primary importance. From various experiments, we concluded that for a

monochromatic optical monitoring setup (OMS5100), a *start amplitude* of at least 4% is needed. The measurement noise will also be influenced by the light source and detector and even by the slit configuration. For this reason, we cannot adapt the *swing in* but rather use the *start amplitude* to determine whether or not we can use a given wavelength for monitoring. It is possible to reduce the minimum *start amplitude* by increasing the signal processing times and our experience shows, especially with the new broadband monitoring system, that the detector performance plays a crucial role in reducing signal noise.

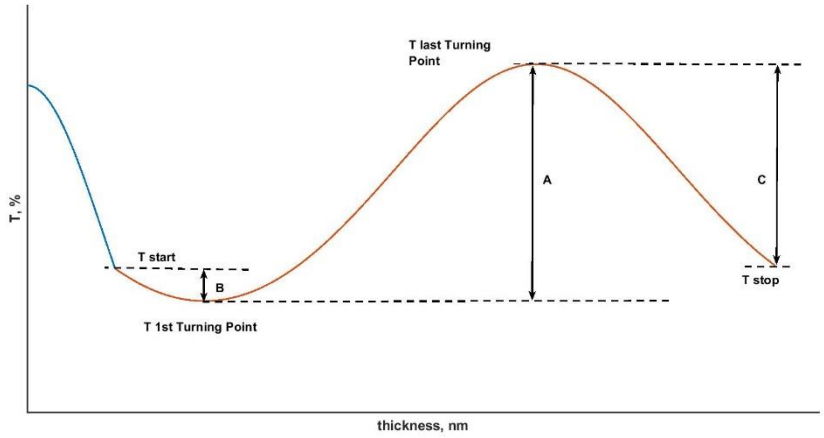

Figure 4-7 Transmittance evolution versus thickness or 'monitoring curve'. A – total amplitude – difference between turning points (or maximum and minimum of monitoring signal); B - start amplitude – difference between start transmittance and first turning point; C – final amplitude – difference between last turning point and trigger point.

Our next consideration is the *swing out* value. This parameter is the same as used by Trubetskov *et.al* (Eq.4.2). We will simplify it here and use the abbreviations from our monitor curve example in fig.4-7.

$$\text{Swing out} = \frac{\left|T_{\text{last TP}} - T_{stop}\right|}{A} \tag{4.7}$$

Where T_{TP} is the transmittance at the last turning point, T_{start} and T_{stop} are the transmittance at the beginning and the end of the layer, A is the amplitude between the turning points. If there is no or only one turning points in a layer, the theoretical thickness increase is calculated to find the two extrema. *Swing out* is then the ratio between the final amplitude and the full amplitude

between the turning points. With this parameter, we can quantify the slope of the curve at the trigger point and determine a wavelength with a high sensitivity of transmittance to thickness. As we saw with the beamsplitter, the trigger point in the range 15-85% of the full amplitude between turning points appears to be the most efficient region. And this range is consistent with that reported by other authors[51][68]. This constrain prohibits the trigger point from being close to a turning point. However, we added an exception when the trigger point is an actual turning point. The idea of monitoring at turning point for non-quarter wave stacks was discussed few decades ago[70]. Therefore, the combination of turning point monitoring and level cut monitoring in the same monitoring sequence should be considered because both monitoring methods are readily available with the OMS5100.

A final important factor to consider when selecting the wavelength is the spectral resolution of the monitoring system. As shown with the example in 2nd chapter, it is mandatory to select monitoring wavelengths that are not perturbed by the spectral resolution of the measurement system. This means that regions with sharp peaks in the spectra for the layer to be monitored should be avoided. Whether or not the spectral resolution is an issue depends on the design, as some designs do not have sharp peaks in the spectral region of interest, even if the number of layers is high. Spectral resolution, similarly to thin layer monitoring, is usually an issue when tens of layers have already been deposited. This means that it becomes increasingly difficult to find good monitoring wavelengths as the number of layers increases.

4.2.2 Use of *merit* functions to select the monitoring wavelength

There is another powerful method for selecting the monitoring wavelength that is not directly related to the monitoring system itself but to the design of the filter. It is based on the sensitivity of transmittance to change in thickness as a function of wavelength. If we look at how the transmittance changes when a small change in thickness is introduced, we can observe that it is wavelength dependent. There may be spectral regions where the change in thickness may introduce barely measurable changes in transmittance, and regions where the change is prominent. For the layer we want to monitor, we want to make the measurement in a spectral range where the smallest change in thickness results in the largest change in transmittance. On the other hand, if we have a design with d_n layers (d_1,..,d_i,..,d_n) and we imagine that there is an

error in the d_j layer where j<i, we would prefer to start monitoring the i-th layer with a wavelength λ_i for which the error in j-th layer has the smallest effect on transmittance.

The previous two considerations depend only on the design itself, but here we add a parameter for the monitoring system. To avoid errors, due to the non-constant signal to noise ratio (SNR) as a function of wavelength in optical monitoring system, it is preferable to perform monitoring in the spectral region where SNR is the highest.

In summary, in this paragraph, there are three important input parameters to consider when selecting the monitoring wavelength:

1. **The final value of transmittance at the end of the layer.** We want the trigger point to be on the maximum slope where the transmittance changes most rapidly with increasing thickness of the monitored layer.
2. **The impact of errors in previous layers.** We want to select monitoring wavelengths in spectral regions where potential thickness errors in previous layers have the least effect on the transmittance, allowing the monitor curve to be as close to theory as possible.
3. **SNR versus wavelength range.** Ideally, we would use the wavelengths that have least amount of noise to achieve the greatest accuracy in the thickness control.

The first and second points may contradict each other, so we must find a compromise between them. To find the wavelength, all the criteria presented above can be summarized in the merit function (MF) shown in Eq.4.8.

$$MF_i(\lambda) = \frac{1}{\left|\frac{\partial T}{\partial d_i}(\lambda)\right|} * \left[\alpha * \sum_{1 \le j \le i-1} \left|\frac{\partial T}{\partial d_j}(\lambda)\right| + \beta * \Delta T_{NOISE}(\lambda)\right] \tag{4.8}$$

Where T is the transmittance after the deposition of i layers, d_i is the thickness of the i-th layer, MF_i is the merit function after the deposition of i layers, $\left|\frac{\partial T}{\partial d_i}\right|$ is the derivative of the transmittance with respect to the thickness d_i, ΔT_{NOISE} is the spectral noise of the monitoring system (fig.2-11), α, β –are some weighting coefficients, and λ- the considered wavelength.

To find the ideal monitoring wavelength, we search for the minimum of the merit function for each of the layers in a given design.

Theoretical study for this type of approach for wavelength selection was done by Tikhonravov *et al*.[71] where the authors present an idea for selecting the monitoring wavelength based on the sensitivity of the wavelength to thickness errors. Here, we have added the weighting factors and the noise of the monitoring system. The consideration of noise is also somewhat controversial as, at least for our monitoring system, it suggests using wavelengths at the longer end of the visible spectrum. However, this means that there will be fewer turning points in the monitoring curve compared to the 400 nm region, which reduces the possibilities of the trigger point correction algorithms, as they generally make adjustments based on turning point measurements.

For the initial tests, 4 merit functions were considered with different weighting factors, modifying the influence of transmittance derivative and system noise.

Merit function	α	β
MF1	1	0
MF2	0	1
MF3	0.5	0.5
MF4	0.5*	0.5

Table 4-1 Weighting coefficients for MFs

In the case of MF4, we replace the sum of the transmittance derivatives of the previous layers with the average value of the derivatives, as shown in Eq.4.9.

$$\alpha * \left[\frac{\sum_{1 \le j \le i-1} \left| \frac{\partial T}{\partial d_j}(\lambda) \right|}{i} \right] \tag{4.9}$$

The wavelength range that is considered for each of the layer is defined by the technical limitations described earlier.

4.2.3 Summary of the wavelength selection process for polychromatic strategy

To conclude this section, we described the process of selecting a monitoring wavelength. First, we define the criteria that the wavelength should match, then we select the best wavelength for each layer by finding the wavelength that will be least affected by noise and thickness errors. All of this can be done without having to manually look at the monitoring curves. The entire wavelength selection process can be summarized in the following flowchart (Fig.4-8).

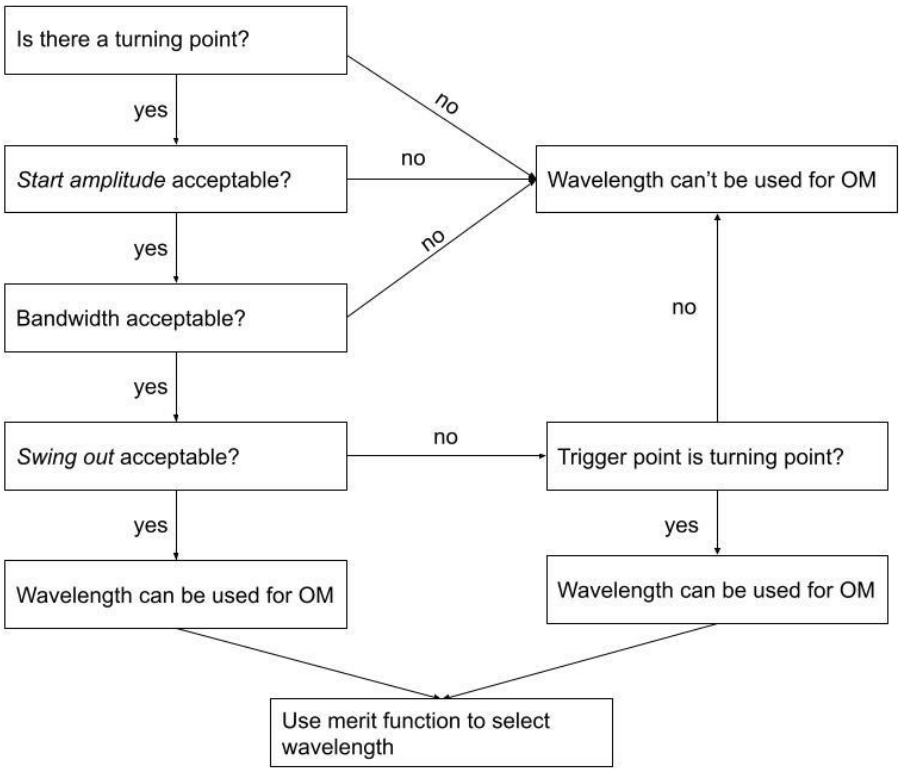

Figure 4-8 Flowchart of the Polychromatic wavelength selection process.

Since it is possible to perform this selection process automatically, it is a promising tool for generating monitoring strategies. One concern is that the input parameters are most likely dependent on the optical monitoring system and the coater, and thus would need to be adapted and optimized for other coaters.

4.2.4 Experimental demonstration of the polychromatic monitoring

Initially, we tested only the use of wavelengths selected by merit function minimization. No other constrains were added. In fact, the procedure can be simplified by directly calculating the merit function for designs with up to ten layers if the individual thicknesses are on the order of 100 nm. The 8-layer beamsplitter design was first considered. The usable spectral range for finding the monitoring wavelength was set between 400 and 900 nm. The 4 different merit functions in Table 4-1 were implemented, and the calculated monitoring wavelengths are summarized in table 4-2.

Layer	MF1 (nm)	MF2 (nm)	MF3 (nm)	MF4 (nm)
1	400	603	603	603
2	429	571	552	561
3	575	567	575	575
4	697	569	562	566
5	745	626	745	694
6	840	555	792	550
7	900	484	487	485
8	707	628	677	628

Table 4-2 Monitoring wavelengths resulting from merit function optimization for the beam splitter design.

MF1 selected 400 nm for the 1st layer and 900 nm for the 7th, which means that we did not reach the absolute minima and that the strategy is not optimal. For this reason, the experiment with MF1 wavelengths was not conducted. The rest of the MFs converged to a minimum in the given wavelength range. As a first step, we plotted in Fig.4-9, the monitoring curves for each strategy and analyzed them visually. Again, the high index layers are plotted in blue, and the low index layers in green. On the right axis, we plotted the reference (or monitoring) wavelengths.

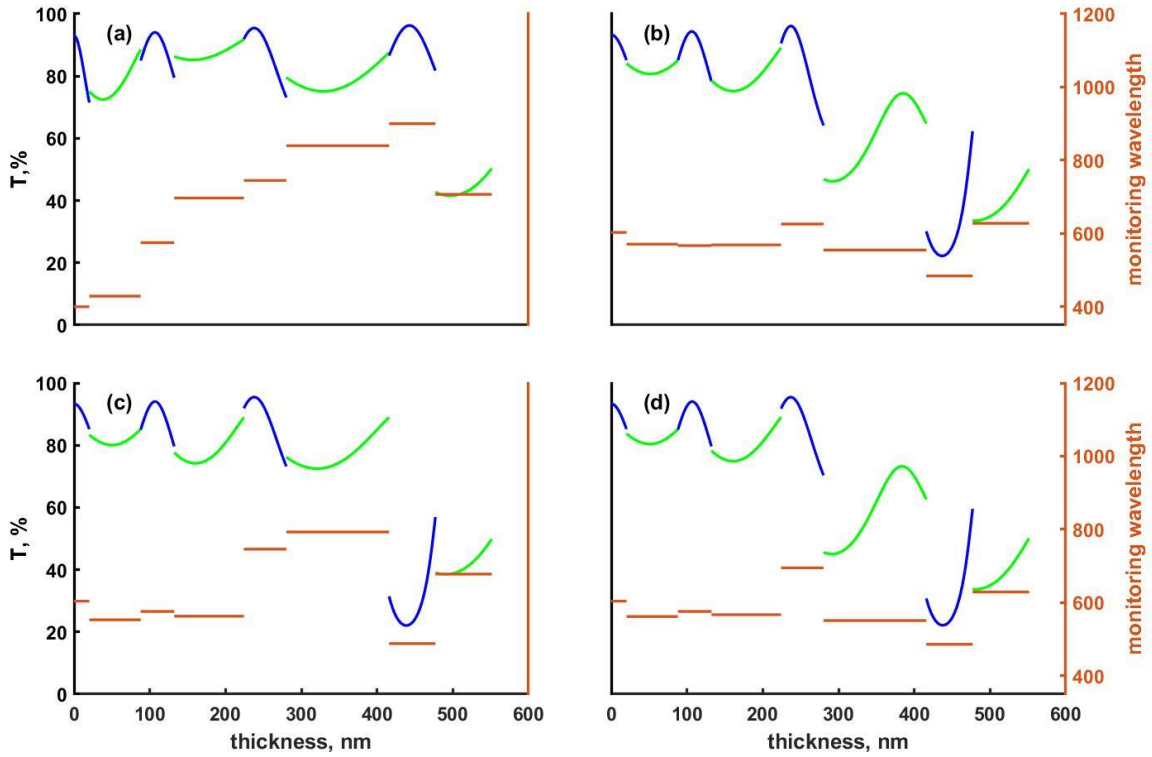

Figure 4-9 Automatically generated monitoring curves for the beamsplitter design, (a) - MF1, (b) – MF2, (c) – MF3, (d) – MF4. Blue curves are for high index layer, and green for low index layer.

Let us note that MF2 and MF4 result in quite similar strategies and monitoring curves, whereas MF1 and MF3 are very different. For all these strategies, the visual evaluation confirms that they all meet the criteria discussed previously. Because these strategies allow as many monitoring wavelengths as needed, the monitoring curve is discontinued from layer to layer due to the change in wavelength. With these strategies, none of the monitoring curves for an individual layer end near a turning point. In a few cases, the starting transmittance is close to the turning point, but as mentioned earlier, for a small number of layers, these technical limitations are not as critical. Since the layers are mostly thinner than 100 nm for this design, only the 6^{th} layer has two turning points for MF2 and MF4 strategies.

We then fabricated the beamsplitter using strategies from MF2, MF3 and MF4. To compare the effectiveness of these strategies, we also deposited this filter with a manually selected wavelength to monitor all layers (we call this a standard strategy). For this purpose, the

wavelength of 595 nm was chosen, as it showed the lowest noise sensitivity in the simulation. The spectral performance of the four deposited filters is shown in Fig.4-10.

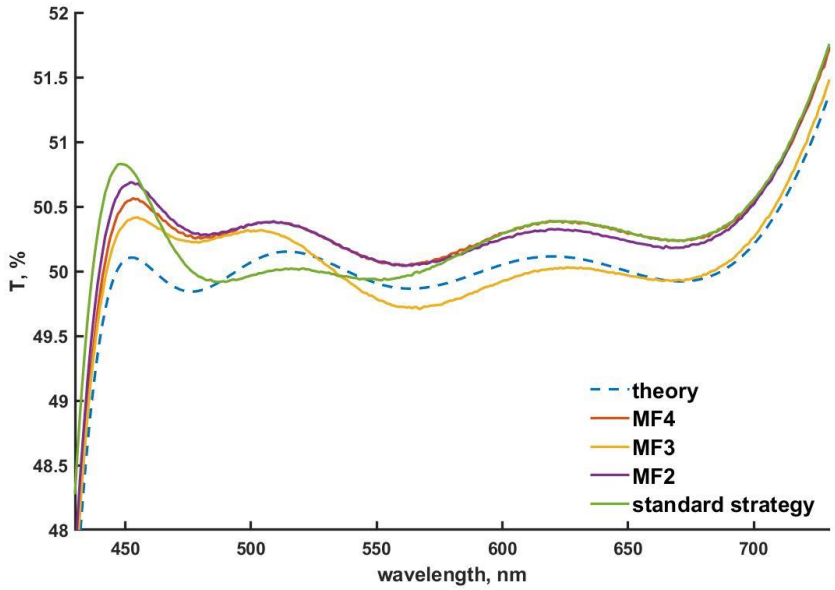

Figure 4-10 Measured Transmittances of deposited beam splitters using 3 automated strategies (MF2, MF3, MF4), and single wavelength monitoring (standard strategy).

For all the fabricated filters, a close match between experiment and theory can be observed. An interesting observation is that, depending on the strategy, the deviation of the measured transmittance from the theory is greater in the blue or red spectral region. This is a repeatable systematic feature that shows that the thickness errors do differ depending on the selected wavelength. Overall, it appears that the measured curve obtained by strategy using MF4 wavelengths more closely follows the theory across the spectral range of interest.

Based on this result, and in order to avoid too many coating runs, only MF4 was considered for the rest of this study.

4.3 Validation of the polychromatic strategy on complex thin film filter designs

The study of the 8-layer beamsplitter has confirmed, on a simple but sensitive design, that the polychromatic strategy is a valid method for optical monitoring of filters. The simulation of this design described in chapter 2 shows that the random thickness errors should not exceed 0.5% to

keep the transmission fluctuations within a corridor of ±1% centered around 50%. The measured transmission deviation (±0.7%) thus demonstrates that a high thickness accuracy of the deposited layers has been achieved for the fabricated beamsplitters. Based on these inspiring results, we investigated how this approach works with more complex filters with more than 30 layers. For multilayer filters (exceeding 20 layers), manually searching for a strategy becomes tedious and several strategies can be found manually without knowing which one is the best before testing them. For this reason, it is very interesting to be able to automatically generate a polychromatic monitoring strategy for complex thin film designs.

4.3.1 D65 compensation filter

The first complex filter design we studied was the D65 compensation filter [appendix1.10]. The CIE standard illuminant D65 describes the spectral dependence of daylight intensity at a 6500 K color temperature[72]. The filter is then designed to compensate for the illuminance distribution of a potential light source with such characteristics. The power distribution and corresponding filter design can be seen in the Fig.4-11. (a). The illuminant standard is defined with steps of 10 nm so the power distribution spectra consist of many sharp features. This cannot be easily reproduced by thin film structures and would require a much larger number of layers for the design to match the sharp edges.

For this reason, a design consisting of 37 layers that compensates for much of the intensity fluctuations was designed. The filter is composed of layers ranging in thicknesses from 9 nm to 500 nm, as shown in Fig.4-11 (d). From this design, the monitoring strategy was determined by following the flowchart in Fig.4-8 and using MF4 criterion.

A strategy was also determined using a standard manual approach, but it was not possible to find a single wavelength that would monitor all 37 layers of the filter. To overcome this issue, as many layers as possible were monitored optically and the remaining layers were monitored by rate monitoring. The selected monitoring wavelength was 400 nm. The first layer was rate monitored, because it is a SiO_2 layer and the refractive index contrast with the fused silica substrate is too low for a usable optical monitoring. The next 19 layers were optically monitored and the remaining layers were monitored using the average deposition rates recorded during the optical monitoring from the 2^{nd} to the 20^{th} layer. Since the deposition rates of magnetron

sputtering machines are known to be stable (the achievable accuracy for layer thicknesses is at least in the order of 1%), this type of strategy is quite often used as a backup when no optical monitoring strategy can be found.

For the automatically selected monitoring strategy, optical monitoring was not possible for 5 of the layers: layers number 1,2,3,5,23 that were rate monitored. Similarly to the manual strategy, the first layer could not be optically monitored due to the poor refractive index contrast; the others are thin layers (<20 nm) and none of the wavelengths could meet the criteria described in section 2.2. Finally, most of the monitoring wavelengths selected by the automated process are between 550 and 700 nm, which is approximately the region where the signal to noise ratio of the monitoring system is highest, and only a few of the selected wavelengths are below 500 nm [appendix 4.2].

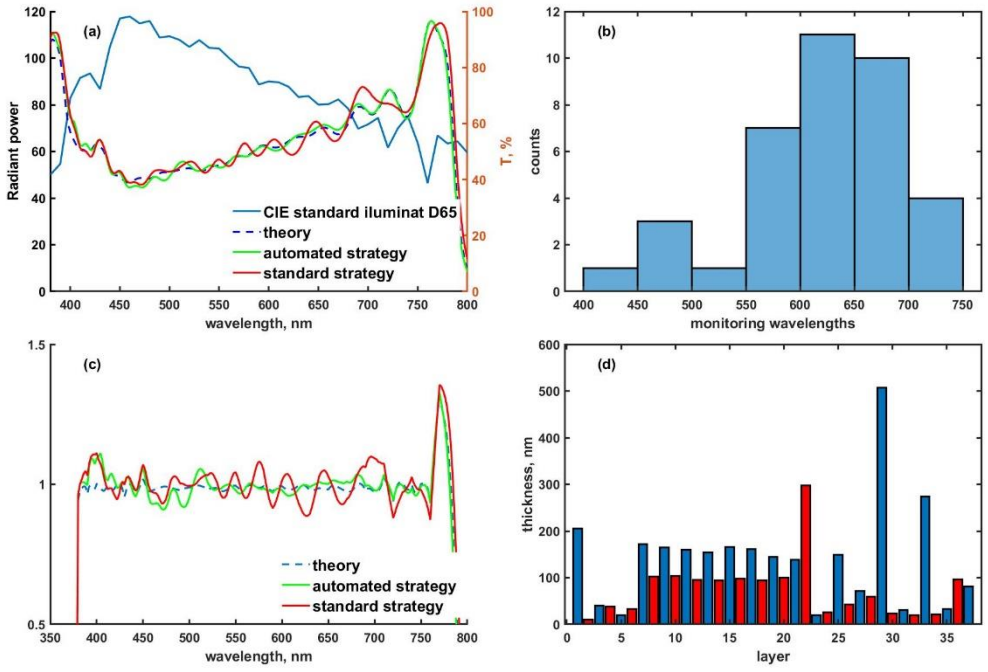

Figure 4-11 (a) - Power distribution of the standard illuminant and theoretical transmittance of the compensating filter and comparison between theoretical and experimental spectral responses with the automated and standard strategies, (b) – distribution of monitoring wavelengths for automated strategy, (c) – product of the spectral responses of the D65 illuminant by those of the deposited filters. (d) - thicknesses of D65 compensation filter, red - high index layers, blue - low index layers.

Filters were fabricated with both the manual and automatic strategies and the spectral performance was measured and compared to the theory (Fig.4-11(a)). It can be seen that the manual strategy gives quite good performance, but the automatic strategy performs even better, especially at longer wavelengths. This performance can be further analyzed by comparing the multiplication of transmittance of the fabricated filters with the D65 power distribution (Fig.4-11 (c)). For the final product to be 'flat', the oscillations in the measured transmittance must coincide with the fringes of the power distribution; any shift along the x axis may result in large deviations. Compared to the manual strategy that uses a single monitoring wavelength, this result tends to suggest that having the wavelengths distributed over a wider range of wavelengths for the automated strategy may help to achieve better performance. Adding one or more monitoring wavelengths to the standard strategy to cover a wider spectral range and possibly reduce the number of layers for rate monitoring might improve the final performance of the D65 filter obtained with the standard strategy. However, improving the manually selected strategies is not the focus of this research as it is individual dependent.

4.3.2 Notch filter

Another example of a complex design that we have studied is a notch filter composed of 98 layers [appendix 1.6]. In this design, the difficulty in monitoring is related to the many thin SiO_2 layers. Similar to the D65 filter, it is difficult to find a monitoring wavelength that would have large enough transmittance signal amplitude for these layers. SiO_2 layers are mostly thinner than 30 nm, and in many cases even thinner than 10 nm. In contrast to SiO_2, Nb_2O_5 layers are mostly a few hundred nanometers thick, which means that the total thickness is significant. For this reason, it was clear that a single witness glass could not be sufficient, and we must choose an indirect monitoring strategy with multiple witness glasses. Determining when to change the test glass is an important job in itself. Therefore, at this stage, we did not investigate where to change the witness glasses and opted for a conventional approach consisting of dividing the sequence of layers into 5 more or less equal parts (around 20 layers) with the constraint that the partial design of each of the witness glasses would start with high index layer. The witness glasses were changed after layers 24, 44, 64 and 84.

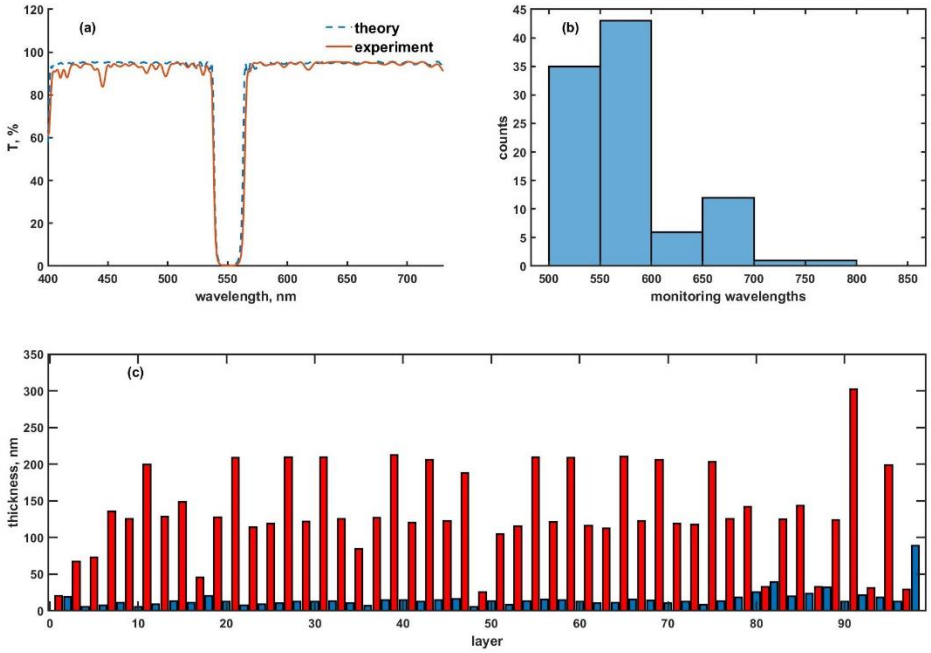

Figure 4-12 (a) – Transmittance spectra of notch filter, (b)- distribution of the monitoring wavelengths (c) - thicknesses of layers, red bars – high index layers, blue – low index layers.

The monitoring wavelengths selected by the automated method are mostly between 500 and 600 nm (Figure 4-12-b) [appendix 4.3]. Such a narrow wavelength range can be explained by the fact that the wavelengths are represented equally for thin layers, even though they were consistently controlled by rate monitoring. In addition, the partial designs on each of the witnesses are similar, with a thin SiO_2 layer following a thick layer of Nb_2O_5, meaning that the selected monitoring wavelengths sequences are also similar.

Due to the complexity of the design, no manual monitoring strategy was determined for this design. The transmittance of the deposited filter is compared with that of the theory in Fig.4-12(a). A fairly good agreement can be observed despite some larger deviations from theory in the shorter wavelength range. The reflectance in the rejection region is >98% as expected, and the FWHM is 21 nm instead of 20 nm. These performances are comparable to that reported previously[46] , where, for the same design, a manually selected monitoring strategy was applied. It is important to note that the results in Fig.4-12 (a) were obtained from a single deposition run without any optimization. Further optimization of the strategy, especially with respect to the placement of the witness glasses, could yield better results.

4.3.3 The Marseille challenge

There is an interesting approach in the thin film community to demonstrate the latest achievements and developments in optical filter design and manufacturing. For several decades, researchers replicated various shapes using thin film filter design and also demonstrated the latest achievements of deposition techniques by coating some of these filters[73][74]. We decided to follow this tradition by replicating the shape of *la Bonne Mère*, the famous 19th century cathedral overlooking Marseille (Figure 4-13 (a)).

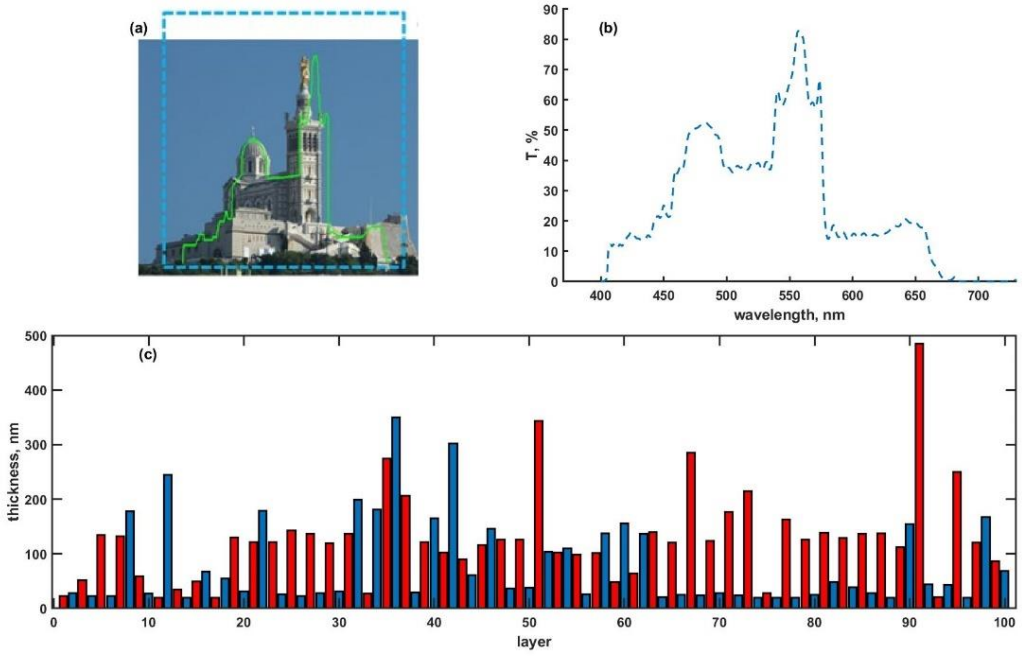

Figure 4-13 (a) - la Bonne Mère (b) - transmittance profile from a photograph of la Bonne Mère, (c) - thicknesses of the filter, red bars – high index layers, blue – low index layers

The design consists of 100 layers alternating Nb_2O_5 and SiO_2 (Figure 4-13-c) [appendix 1.8]. The thicknesses of the layers vary from 20 to 500 nm. Since even more layers would be needed to reproduce all the features of the cathedral profile, it was decided to stop at a 100-layer solution. From experience, we know that too small details in the design will be lost anyway due to manufacturing errors for such complex filters. As for the notch filter, it was decided to go with the indirect, multi-witness glass strategy. First, it was decided to divide the filter into 3 parts, so that the first two glasses consist of 34 layers and the last one of 32. The automated wavelength

selection process with MF4 was used again to determine the monitoring wavelengths for each of the witness glasses.

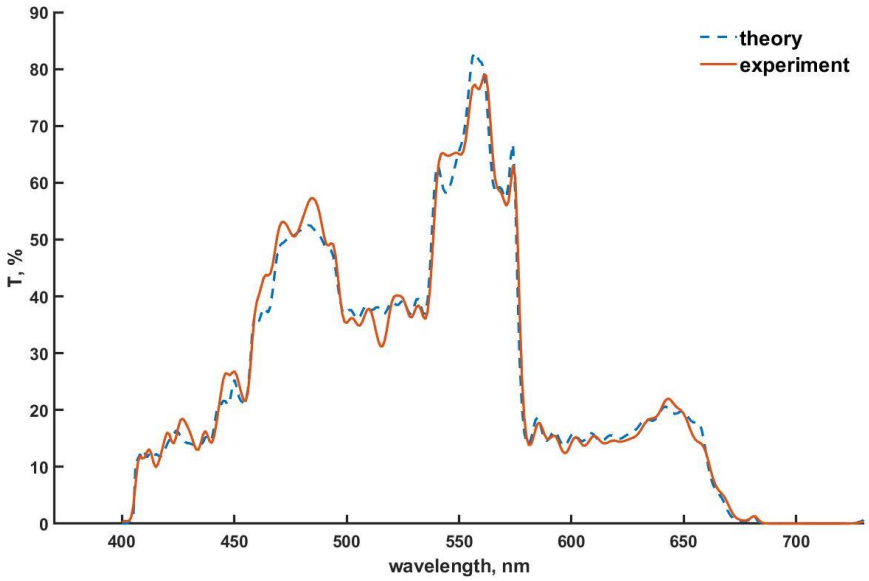

Figure 4-14 Measured transmittance of the Bonne Mère filter compared to theoretical spectra.

The measured transmittance of the fabricated filter is shown in Fig.4-14. The transmittance spectrum follows the theoretical one very closely, with an average target deviation equal to 2%. Very close agreement is observed in the 550 – 700 nm region, in contrast to the shorter wavelengths where the match is not as good. A similar observation could be made for the D65 and the notch filter. To further investigate these results, we analyzed the spectral performance of the individual witnesses that were used for monitoring and compare measurements of the partial designs to theory (Fig.4-15). It can be seen that the 1st and 3rd witness glasses show very good agreement between theory and measurement. However, the 2nd one shows notable deviations, especially in the 400-600 nm range. Naturally, this suggest the need to improve the strategy of the second test glass, or to study how the layers should be distributed differently. Although the number of layers is the same for all three test glasses, the total thickness to be deposited is considerably higher for the 2nd witness glass compared to the first and third witness glass.

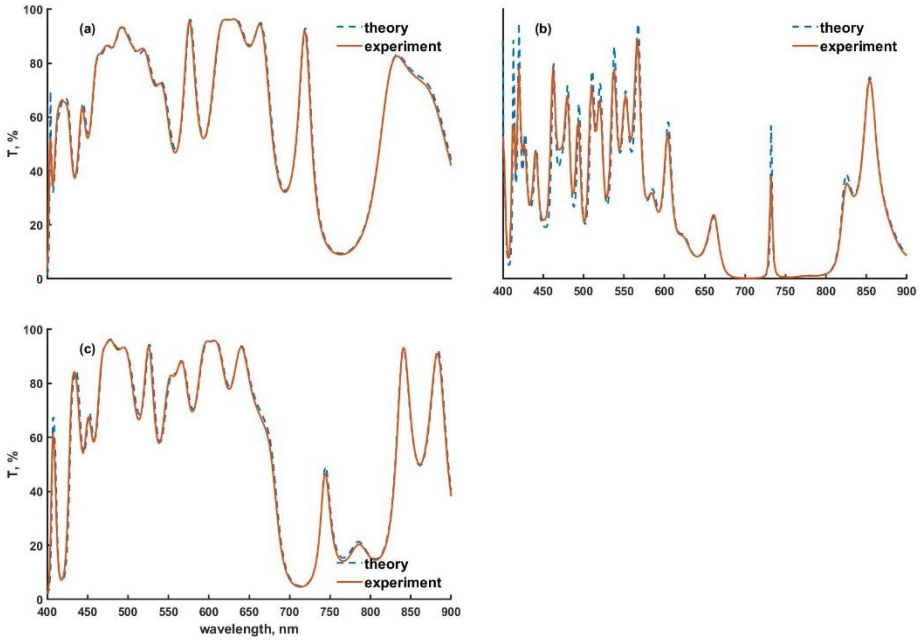

Figure 4-15 Measured transmittance of each witness glass compared to theory, (a) -witness glass 1, (b) – 2, (c)-3.

To obtain an even better experimental result, another method of layer distribution was proposed, this time based on the uniform distribution of optical thicknesses between the test glasses, and not on the number of layers. As the spectra of the layers deposited on the first witness glass showed a good agreement between theory and experiment, it was decided to take the optical thickness of this test glass as a reference and to redistribute the remaining layers on 3 different witness glasses with the same optical thickness. This resulted into 4 witness glass strategies, and they were changed after layer 34, 52 and 80. For each of these, polychromatic strategies were determined, and the wavelength spread for the 3 and 4 witness glass strategies is shown in Fig.4-16 (a) and (b) [appendix 4.4]. It is interesting to note that the wavelength spread is wider for the 4^{th} witness glass strategy, and more layers are monitored in the 500-700 nm region.

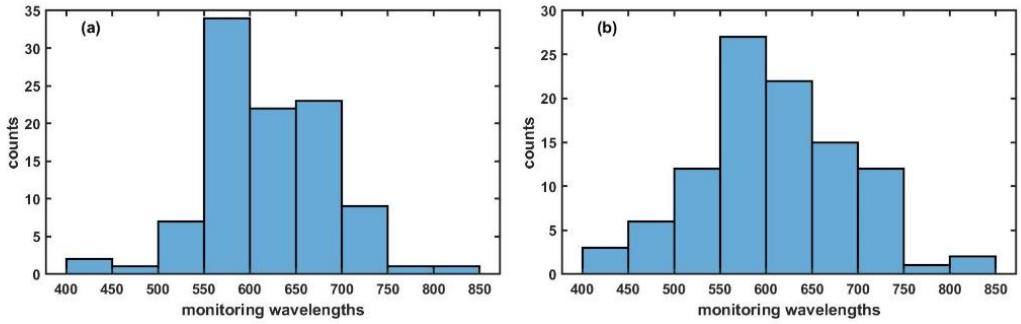

Figure 4-16 Wavelength distribution for Bonne Mère design (a) – for 3 witness glasses, (b) – for 4 witness glasses.

After fabrication, the performance of each individual witness glasses was measured and is shown in Fig.4-17. Splitting the stack from 3 to 4 witness glasses improved the spectral performance obtained on each individual witness glass. The measured spectra agree very well with the theory and the deviation from the target is no more than a few percent.

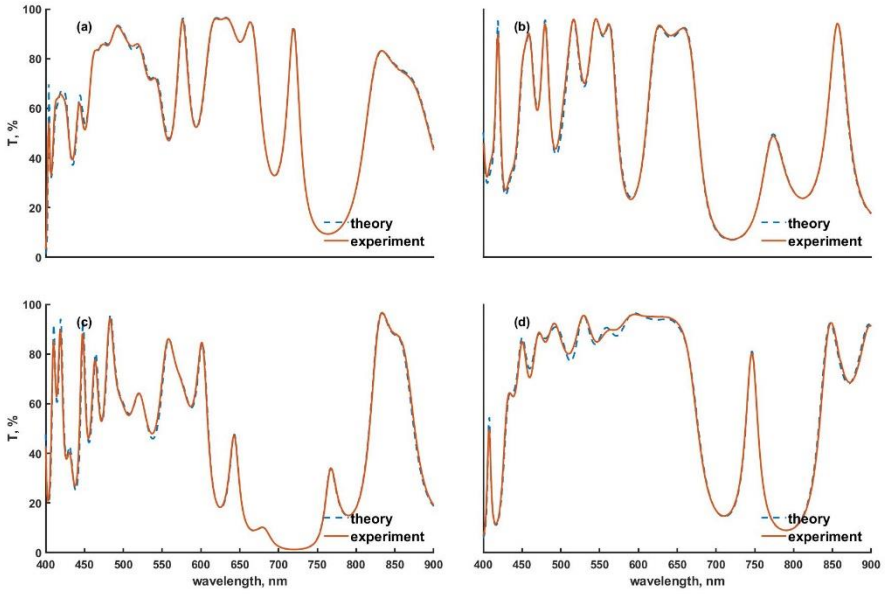

Figure 4-17 Measured transmittance of each witness glass compared to theory, (a) -witness glass 1, (b) – 2, (c) – 3,(d) – 4

Finally, the performance of the full stack was measured on a coated glass containing all 100 layers and is shown in Fig.4-18. The spectral performances obtained are overall worse than with

the 3-witness glass strategy. And, in particular, in the 550-700 nm range, the agreement between theory and measurement does not fit very well.

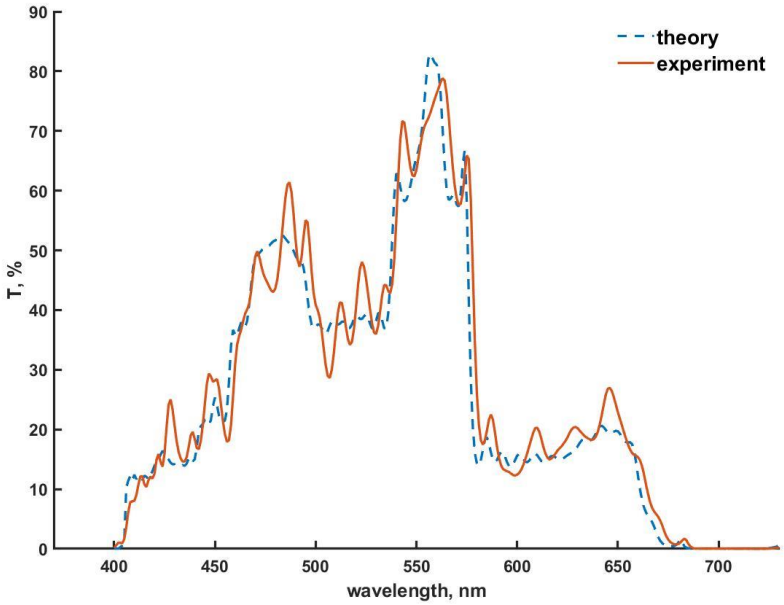

Figure 4-18 Spectral performance of la Bonne Mère using 4 witness glasses.

The reasoning behind dividing the design into 4 parts was based on the idea that the thickness error accumulation is more related to the total optical thickness of the stack, and not on the number of layers. Since the agreement between experiment and theory is better with the 4-witness glass division, there might be some truth behind this reasoning.

However, for indirect monitoring strategies, the spectral agreement between experiment and theory on individual witness glasses is not the most important thing. One should focus more on the accuracy of individual deposited thicknesses. It is possible that the good spectral agreement on the witness glasses is at least partially related to the error compensation algorithms. The information on previous errors is of course lost when the witness glass is changed. There is therefore no error compensation possible at the level of the complete filter. This means that error compensation at the level of each individual witness glass level can produce large scale error on the complete filter.

Another factor that can lead to errors in indirect monitoring is the geometry of the sample holders. If there is a difference in height between the glass used for monitoring and that of the final filter, there will be a systematic error in thickness.

We will analyze this design in more detail in chapter 6, and we will see that this design is very sensitive to uncompensated (random) thickness errors.

4.4 Thoughts about polychromatic monitoring strategies

Here, we have described a method for automatically creating a robust monitoring strategy. Indeed, the algorithm described in this chapter has been used successfully for various designs. With polychromatic strategies, we decrease the benefit of error compensation algorithms, but we believe we also decrease the thickness errors themselves. Most likely, the need for error compensation also depends on the design- very important for quarter wave designs such as Fabry Perot filters, less important for designs such as D65 filter. Compensation algorithms typically significantly improve the spectral performance of the deposited filter around the monitoring wavelength, not for a wide spectral range. The designs we have analyzed in this chapter cover most, if not all, of the visible spectral range. To produce filters with good agreement between theory and experiment over a wide spectral range, the thickness errors must be small regardless of the layer deposited.

Indirect monitoring strategies will need to be studied in more detail because, so far, it is unclear how to select locations for the witness glass changes.

Chapter 5 - Broadband optical monitoring

In this chapter we will review broadband optical monitoring. We will present results from several deposition runs and discuss the strengths and weaknesses of broadband monitoring methods. We will give our insights on determining the possible broadband monitoring strategies. We will discuss the input parameters for broadband monitoring and their relationship to the technical limitations of the monitoring setup and the thin film filter itself.

5.1 Important input parameters for Broadband optical monitoring

While broadband monitoring seems to be a quite simple and straightforward technique, the use of strategies become necessary as the complexity of designs increases, and special attention must be given to very thin layers. Before moving on to monitoring complex designs using broadband methods, we review here the control parameters associated with broadband monitoring, as we have used these parameters in developing monitoring strategies.

- ***Wideband* or *Merit?***

  As a first step, one needs to decide which of the broadband monitoring methods to use: *Wideband*, which tracks thickness growth and stops layer deposition based on real-time deposition rate measurement; or *Merit*, which tracks the difference between measured and theoretical transmittance spectra, then stops deposition when the difference (merit), is minimal.

  Wideband is a more robust method than *Merit* broadband monitoring. The reason is that if the spectral measurement is problematic, for example if the measured spectrum does not indicate an increase in deposited thickness although the deposition is in progress, this measurement is automatically replaced by a simulated measurement[12]. This is often necessary at the beginning of the layer deposition when the layer thickness is small. If the measurement is not reliable throughout the deposition, *Wideband* monitoring, in theory, works as a pure rate monitoring.

Merit monitoring appears to be a more accurate monitoring method (thickness errors are smaller), as will be illustrated later, but not as reliable as *Wideband.*

- **Spectral range selection**

  One of the input parameters for both broadband monitoring methods is the spectral range used for the measurement. This parameter can be adjusted for each layer, but in general it is held constant. However, it would be advantageous to adjust the spectral range so that the highest signal to noise ratio is used for the measurement and spectral regions where spectral resolution might be an issue are excluded. Changing the wavelength range to avoid bandwidth problems is a more or less straightforward task. A procedure very similar to that of monochromatic monitoring can be performed (see section 4.2.1).

  The overall signal to noise ratio can be optimized by adjusting the measurement wavelength range to maximize the transmittance amplitude change as the layers thickness increases. In many cases, especially for a thin layer, the transmittance signal may change rapidly in one spectral region and barely in another. Therefore, it is advantageous to select the spectral region with the highest transmittance amplitude change to increase the accuracy of the measurement.

  Some preliminary tests suggest that a wavelength range as small as 50 nm may be sufficient for standard configurations. However, many more experiments must be conducted to verify the minimum wavelength range.

- **Rate monitoring using broadband**

  There is a clear advantage for broadband monitoring over monochromatic monitoring if we use rate monitoring. With monochromatic monitoring, the deposition rate is not sensitive to thickness errors because it is calculated by dividing the theoretical thickness by the actual deposition time of the layer. If the deposited thickness differs from the theoretical thickness, the calculated deposition rate is wrong. With broadband optical monitoring, the final deposited layer thickness is calculated from the measured spectra. This means that the deposition rate is calculated using the actual thickness and the actual deposition time of a layer. Therefore, the broadband monitoring setup can be used to

control the deposition rate of thin layers with more confidence than the monochromatic monitoring setup.

- **Monochromatic monitoring with broadband system**

  The WB-OMS includes all the same algorithms as those provided by the OMS5100. In other words, by selecting a single wavelength, the broadband monitoring system can be used as a monochromatic optical monitoring system. However, in this case, one must keep in mind that the spectral resolution and measured spectral range are more limited than those of the standard monochromatic system. Despite these limitations, mixed monitoring strategies – using broadband and monochromatic monitoring in the same run - have already proven to be effective[15]. The question is, therefore, what criteria should be considered when choosing one or the other method.

- **Settling time for *Merit* monitoring**

  In addition to the wavelength range, other parameters may be important when using *Merit* monitoring. The settling time, or signal integration time, can play an important role in minimizing the effect of noise. By averaging a few measurements instead of using each measured spectrum, we can obtain 'smoothed' curves for thickness fitting or merit calculation. Increasing the settling time has the disadvantage of delaying the information, but, as we have shown in this thesis, noise caused by random errors is much more damaging to the deposition of a filter than a slight overshoot during termination of the layer. The settling time can be controlled individually for each layer with the broadband system, which means that we can sacrifice accuracy for only some of the layers, because for many designs not all layers are equally sensitive to noise.

- **Release level for *Merit* monitoring**

  Another important parameter associated with *Merit* broadband monitoring is the merit release level. This parameter is used to avoid false minimum detections, by setting a threshold merit value (merit release level). If the measured merit is higher than this value,

the deposition is not terminated even if a minimum of merit is detected. This parameter can be used as a safety mechanism for thick layers - by setting this value, we can avoid terminating layers on local minima of the merit curve. In addition, the merit release level can be used to increase the accuracy of thin layer deposition. However, one must be careful when setting this value. As the number of layers increases, the accumulation of errors can lead to an increase in the minimum achievable merit that can exceed this value, meaning that if this value is set too low, the measured merit does not fall below this threshold and the deposition cannot be terminated.

- **Re-optimized target curves**

  Broadband monitoring is often associated with the idea that the layer stack can be re-optimized based on the thickness errors of previous layers. However, this is time-consuming and an unstable process if the thickness errors have not been determined with sufficient accuracy. There is another interesting way to use the error information from previous layers. Instead of re-optimizing the thickness of following layers, it is also possible to use the actual thicknesses to calculate new target curves, starting with the 2nd layer. This means, of course, that the target curve for the last layer will be slightly different from the one originally set by the design. And this approach does not compensate for errors. The advantage is that the thickness errors always remain small, which is more important for many applications than the ability to compensate the errors in previous layers. Especially if several witness glasses are used for monitoring. The question of whether or not to use this approach for all of layers remains open. For example, it is questionable whether it would not be advantageous to use the pure theoretical target curve for the very last layer, or maybe for the few last layers, in order to get closer to the final specifications.

As we have seen, there are several variables to consider when designing a broadband optical monitoring strategy. To better understand the impact of these parameters on the monitoring sequence, we studied several different thin-film filters.

5.1.1 Broadband optical monitoring of simple thin-film designs

To evaluate the performances of broadband optical monitoring methods and compare them to monochromatic monitoring, we fabricated some of the filters already studied in the previous chapter. We started with simple designs and progressed to more challenging layer stacks.

5.1.2 Broadband optical monitoring of an 8-layer beamsplitter

As a first step, we tested broadband optical monitoring on the 8-layer beam splitter design. We fabricated an 8-layer beam splitter using the two broadband monitoring methods (broadband thickness monitoring - *Wideband*, and monitoring by *Merit*), and compared it to the polychromatic strategy described in the previous chapter. Since the 8-layer design remains a structure with moderate complexity, we were able to use the broadband system without adjusting the input parameters associated with the monitoring methods. We have plotted in Fig.5-1 the transmittance curves for each of the fabricated filters. We note that the two filters monitored by broadband methods have comparable performance to the filter previously obtained with the polychromatic monitoring strategy (marked as MF4 in the figure). Although the transmittance curves have different shapes, they all fall within a corridor of ±1%.

Between the two broadband methods, the filter controlled by *Merit* monitoring appears to be closer to the theoretical target, however the difference is very small and thus several repeated runs would be required to confidently state that one of these monitoring methods is better than the other at this point. It is interesting to note that the largest deviation from theory for both broadband monitoring methods are in the 500-600 nm range, which could indicate a possible systematic error of this monitoring setup.

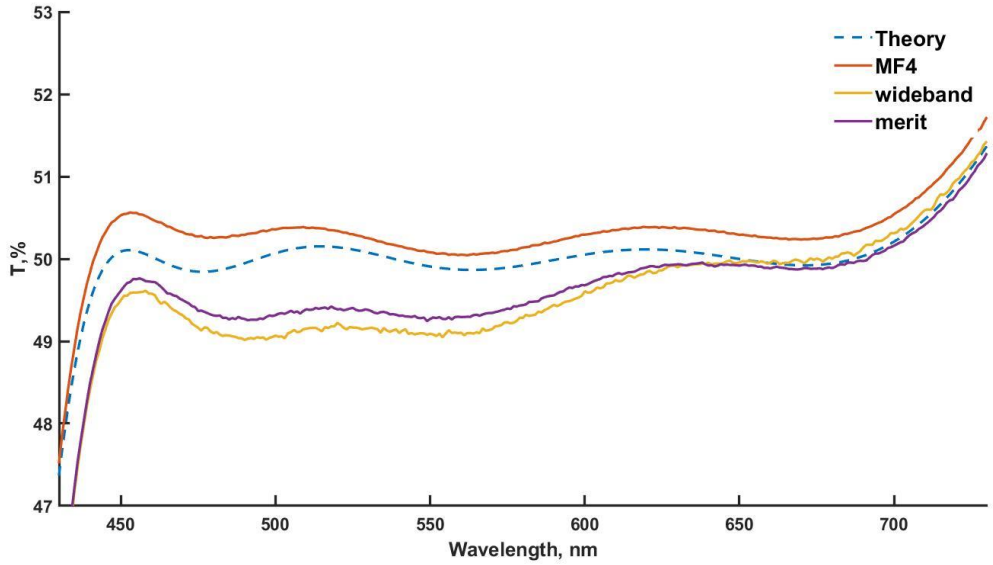

Figure 5-1 Transmittance of an 8-layer beamsplitter controlled by broadband methods versus the polychromatic strategy (MF4).

In conclusion, the overall performance of the filters controlled by broadband methods is good, the thickness errors in both runs are small, mostly less than 0.5% with the largest error in the first layer reaching 1%.

Since broadband monitoring is generally not associated with error compensation, the good spectral performance is the result of low thickness errors.

This first example clearly illustrates one of the advantages of broadband monitoring: no monitoring strategy is required to achieve near-theoretical performance, at least for simple filters.

5.1.3 Broadband optical monitoring of dielectric mirrors

Monochromatic monitoring strategies for quarter wave mirrors are already well-established. Therefore, we wanted to see if we could propose an effective broadband monitoring strategy for a classical mirror design. For the broadband strategy, we chose the A5D5 design from the GREAT project [appendix 5]. The mirror in this example is a quarter wave stack consisting of 28 layers centered at 1030 nm. As with monochromatic monitoring, it is not possible to monitor layers in the rejection band of the mirror, and the monitoring wavelength(s) must be selected from one side of the rejection band. This means that for this design, we can use the broadband

setup in the visible range. With monochromatic monitoring, the aim is to find a wavelength on the shorter wavelength side but as close to the rejection band as possible. With broadband optical monitoring, it is not always possible to use the wavelengths close to the rejection band, because the peaks in the transmittance curve near the rejection band are narrow and have strong fluctuations that may be too narrow for the spectral resolution of the broadband monitoring system. The spectral resolution of the broadband system also becomes the limiting factor for shorter wavelength range as the number of layers increases. Therefore, by performing the calculation as described in chapter 2 (section 2.4.2.1), we limited the usable wavelength range for broadband monitoring from 530 nm to 820 nm as shown in Fig.5-2.

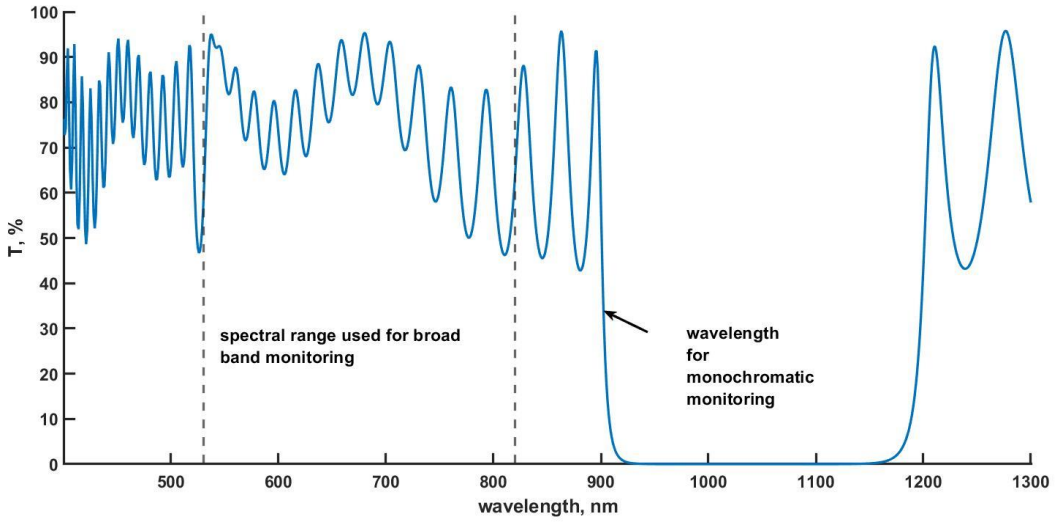

Figure 5-2 Wide range transmittance spectra of an infrared mirror. The dashed interval is the region of visible spectra used for broadband monitoring.

This wavelength limit does not necessarily have to be used for the first few layers and the spectral range used can be changed as the number of layers increases. For the first few layers, the usable spectral range can be 400-1000 nm (the maximum range for the broadband system) because there are no sharp oscillations in the spectra. As layers are added, the wavelength range used must be reduced because oscillations in the transmittance spectra become more frequent at both ends of the maximum usable wavelength range. Since all layers of this mirror are 'thick', only spectral resolution is an important factor for monitoring. The broadband monitoring strategy implemented was *Merit* monitoring for all layers with a reduced wavelength range as the number of layers increases [appendix 5].

The final transmittance measured at the end of the filter is shown in Fig.5-3(b). For comparison, we have plotted in Fig.5-3(a) the transmittance of a mirror of similar design – A3D1 [Design and strategy is provided in appendix 5], also consisting of 28 layers, which was controlled by monochromatic monitoring. As can be seen, the performance is indeed similar over the entire measured spectral range. These results confirm that broadband monitoring is reliable, and that with processes such as magnetron sputtering where the refractive index is stable, optical monitoring can be performed quite far from the spectral region of interest (monitoring at about half of the maximum measured wavelength range) if the refractive index dispersion has been accurately characterized.

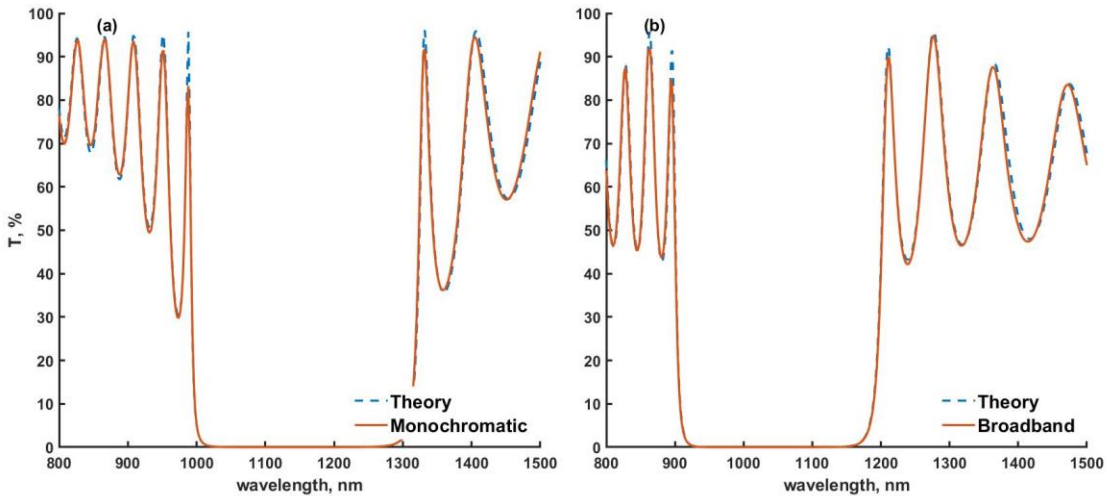

Figure 5-3 Experimental transmittance spectra of two mirrors compared to theory, (a) – deposition controlled by monochromatic monitoring, (b) – deposition controlled by broadband monitoring.

The relative thickness errors measured for the broadband strategy are shown in Fig.5-4. The errors are mostly less than 0.5% and slowly increase with the number of layers, reaching ~1% at the end of the filter. Since this is a classical quarter wave mirror, the layers of the same material have the same thickness, and we don't expect any problems of re-fitting thicknesses from spectral measurement Re-fitting the thickness to estimate thickness errors is sometimes problematic, as we will illustrate on following designs. After a layer is deposited, the thickness is calculated from the newly obtained spectra. However, the software is allowed to re-fit the thickness of the last 5 deposited layers, up to date it is unclear whether this is the best approach.

An important question here is whether the increase in error at the end of the mirror is caused by the number of layers deposited or related to total thickness? The answer to this question would be important for indirect monitoring strategies. However, at this point, the answer is not yet very clear, and in any case, being able to deposit layers with thickness errors less than 0.5% using broadband optical monitoring for at least 20 layers is an encouraging result.

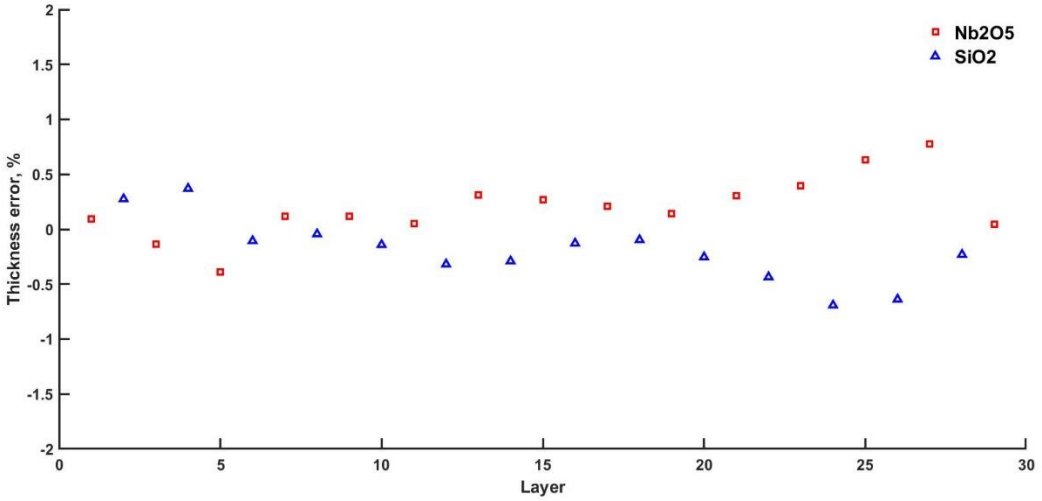

Figure 5-4 Relative thickness errors of the mirror deposited by broadband strategy

For mirrors in the infrared range, we can of course find a monitoring strategy for monochromatic optical monitoring quite easily. However, it is not as easy for mirrors in the UV range, because we usually cannot use monitoring systems at wavelengths even shorter than the reflecting region and have to find a monitoring strategy on the side of the long wavelength rejection band. In this case, it can be shown that it is more difficult to find a monochromatic strategy because the turning points can no longer be present for all monitored layers. Therefore, broadband monitoring strategies could be an efficient alternative for mirrors in the UV range.

5.2 Broadband optical monitoring of complex thin film designs

Based on the results obtained with the 8-layer beam splitter and the classical mirror, it is interesting to see how broadband optical monitoring can be implemented for more complex designs. Increasing the complexity of the designs requires better tailoring of the input parameters and eventually combining various monitoring methods to create the monitoring strategy.

5.2.1 Broadband monitoring of a D65 compensator filter

The D65 compensator filter was first studied to evaluate the broadband system, as it is a complex design that can be monitored on a single witness glass. Based on the results presented in chapter 4, a direct comparison can be made with the monochromatic monitoring system. As in the case of the filter made using a polychromatic strategy, not all layers could be optically monitored with the broadband system. In addition, preliminary tests showed that the broadband monitoring could not be implemented without optimizing it for most thin layers, in particular, for the first several layers that are thinner than 50 nm. For these reasons, we initially chose a mixed monitoring strategy, using rate and monochromatic monitoring for the first few layers. It is important to note that for this filter, spectral resolution is not an issue because the spectral response of the filter is 'flat' throughout the fabrication process.

For the other layers, we tested both broadband monitoring methods – *Wideband* and *Merit*. The strategies associated with the two broadband monitoring methods are described in the table 5-1. For the layers monitored by the monochromatic method, the wavelengths were selected by the automated method described in Chapter 4.

Layer \ Strategy	Mixed Wideband	Mixed Merit
1	Rate	Rate
2	Monochromatic	Monochromatic
3	Monochromatic	Monochromatic
4	Monochromatic	Monochromatic
5	Rate	Rate
6	Wideband	Merit
7	Wideband	Merit
…	Wideband	Merit
37	Wideband	Merit

Table 5-1 Mixed broadband monitoring strategies for D65 design. Exact strategies are provided in appendix 4.2.

For both strategies, the broadband monitoring wavelength range was set to 400-900 nm starting from layer 6. The settling time and the release level for *Merit* monitoring were not used.

The transmittance for the three tested strategies as well as for the theoretical strategy are shown in Figure 5-5(a). Since this design is made to compensate for the CIE standard illumination profile, we compared the final performance of the filters by multiplying the filters spectral responses with the illuminant standard (Fig.5-5(b)).

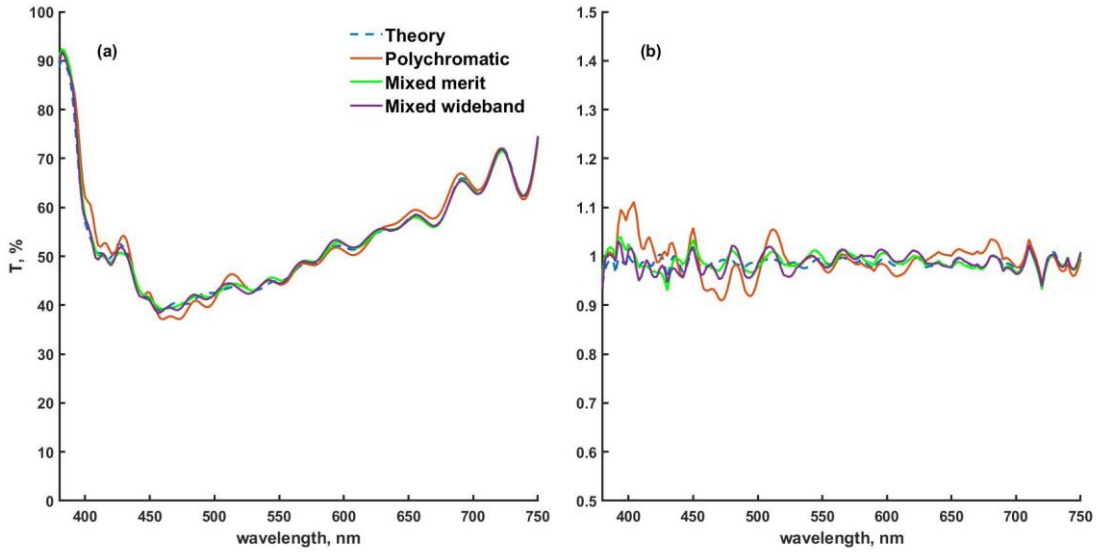

Figure 5-5 (a) Transmittance of D65 compensating filters controlled by different monitoring methods, (b) – spectra multiplied by the power distribution of the illuminant.

We clearly see that the filters obtained by the broadband strategies outperform the filter previously achieved with the polychromatic monitoring strategy. With the broadband strategies, the performance of the filters is similar in all spectral region compared to polychromatic strategy where we observe larger oscillations for shorter wavelengths.

In addition to the spectral performance, we can look at the thickness errors for both broadband strategies (Fig.5-6). It is interesting to note that the errors for the first 5 layers that were controlled by rate and monochromatic monitoring differ from experiment to experiment. The errors for layer 6 also differ between the methods, with *Merit* having a smaller error than *Wideband*. Two possible explanations come to mind: the first is that the error compensation with the monochromatic monitoring may be different because the previous layers have different errors, the second is related to the fact that layer 6 has a thickness of less than 50 nm, and that the *Wideband* broadband monitoring method does not perform as well as *Merit* with layers in this thickness range. The same conclusion can be made for layer 23, which has a thickness of 20 nm,

as the error associated with the *Merit* monitoring strategy is lower compared to *Wideband*. Despite these two layers, the overall thickness errors are kept well below 0.5%, explaining the good spectral agreement between experiment and theory. However, for thin layers, broadband monitoring without adjusting some of the control parameters does not work as well as other monitoring methods.

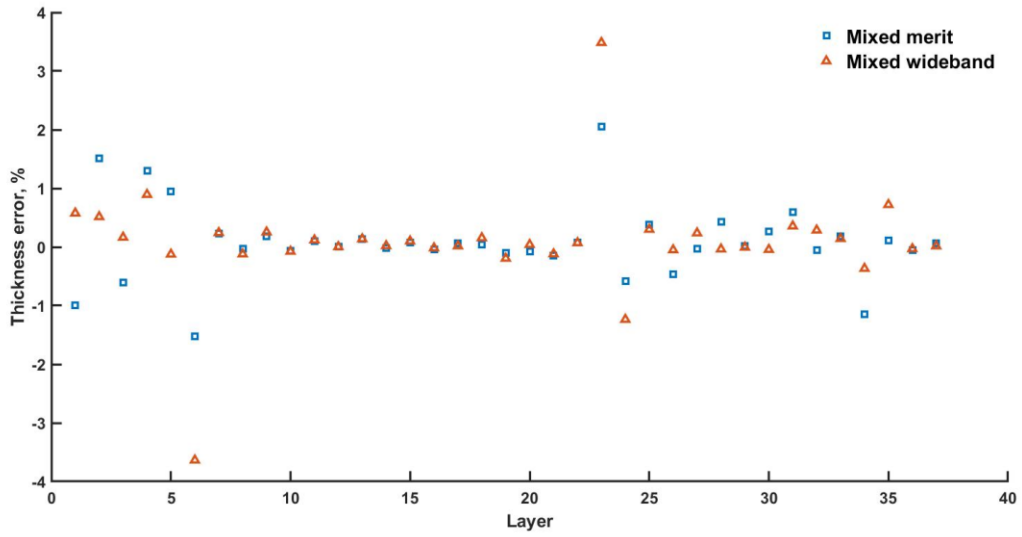

Figure 5-6 Thickness errors recorded while depositing the D65 compensation filter by broadband monitoring strategies.

The problem with thin layers for broadband monitoring is not really related to the thickness itself, but rather to the spectral measurement and its evolution with thickness. Indeed, it can be shown that even thick layers can be problematic for broadband monitoring if the changes in transmittance with increasing thickness are negligible. And this is in fact the situation for several layers of this particular design, because in this case, the layer-to-layer changes are not as pronounced as for other designs.

For both monitoring methods, we cannot use the broadband system ‘as is’ for the first 5 layers of this design because layers 2-4 are terminated too early. Therefore, to create monitoring strategies without monochromatic monitoring, we need to adjust the input parameters of both broadband methods.

In the case of *Wideband* monitoring, filter performance comparable to that obtained with the mixed monitoring strategy was produced when the wavelength range of the first 5 layers was

reduced to 400-700 nm. Excluding the longer wavelengths increased the accuracy of the online thickness fitting. The measured transmittance of the filters is shown in Fig.5-7.

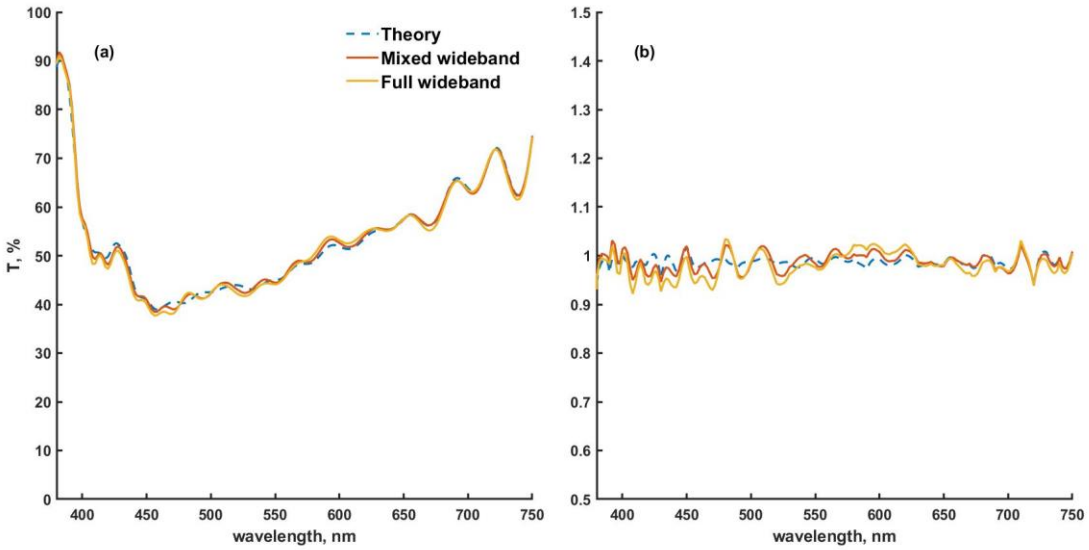

Figure 5-7 (a) - Transmittance of D65 compensator filters controlled by mixed Wideband and full Wideband monitoring strategies, (b) – spectra multiplied by illuminant power distribution.

The transmittance measurements of the filters produced with the mixed *Wideband* (Wideband, monochromatic, and rate monitoring) and full *Wideband* (wideband and rate) monitoring strategies are similar. Details about the strategies can be found in appendix 4.2.

Implementing the same approach for *Merit* is more difficult; in addition to the reduced wavelength range, we also need to set a really low release level of the minimum merit detection. The exact value of the minimum can be found by analyzing previous runs, as we made this filter with several other monitoring strategies. Therefore, we know that we want the layers deposition to be terminated if the merit calculated as shown in Eq.2.5 is below 0.05. The merit curves for the first layers are plotted in Fig.5-8. Layers 1 and 5 were rate monitored and therefore excluded from this example.

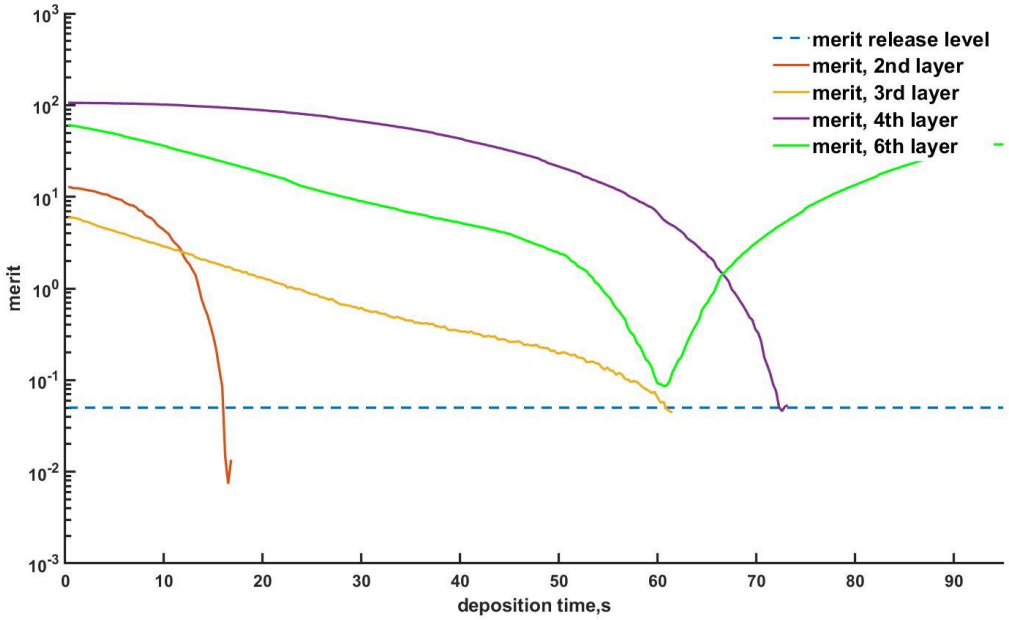

Figure 5-8 Example of merit release level not reached from deposition run for D65 compensator design.

Although this approach worked for layers 2-4, overall, it backfired because the merit release level was not reached for the 6th layer. In fig.5-8, we can see that the 2nd layer is terminated well below the merit release level, the 3rd and 4th layer are terminated as soon as the release level is achieved – we would have a larger thickness error without setting this release level, however the minimum for the 6th layer is above the release level, and this layer is not terminated at all. The reason we use a very low release level for these thin layers can be seen if we look at the merit curves for the layers 3 and 6. The layers have a similar thickness, but the merit curves differ significantly. The curve is almost linear for the 3rd layer, and the merit value at the beginning of the deposition is an order of magnitude lower. It seems that in this case any of the small oscillations on the merit curve can trigger the end of the layer deposition. It might be possible to increase the chance to find real minimum for such example by increasing the signal integration time, however that remains to be validated. Therefore, for now we can conclude that for high accuracy of layers' termination with *Merit*, we would need a merit curve that is similar to that of layer 1 - almost parallel to the y axis as we approach the trigger point.

Since the strategy backfired and we need the information about the merit release level from previous (or possibly calibration) runs, this does not seem to be a reliable monitoring strategy for these layers.

5.2.2 OIC 2022 thin-film manufacturing contest

Based on the work done during this thesis, we have decided to participate in the OIC (optical interference coatings) thin-film manufacturing contest that takes place every 3 years. The design problem for the year 2022 is complicated, as usual, because the target is a transmittance curve with a staircase shape including target values changing abruptly by two orders of magnitude as shown in Fig.5-9. For the contest, no limits were set for the design or deposition methods, the only requirement is that toxic materials such as ZnSe or ThF_4 cannot be used[75]. For the substrate, a 1.0 mm thick Schott N-BK7 glass with 50.0 mm diameter had to be used by all applicants.

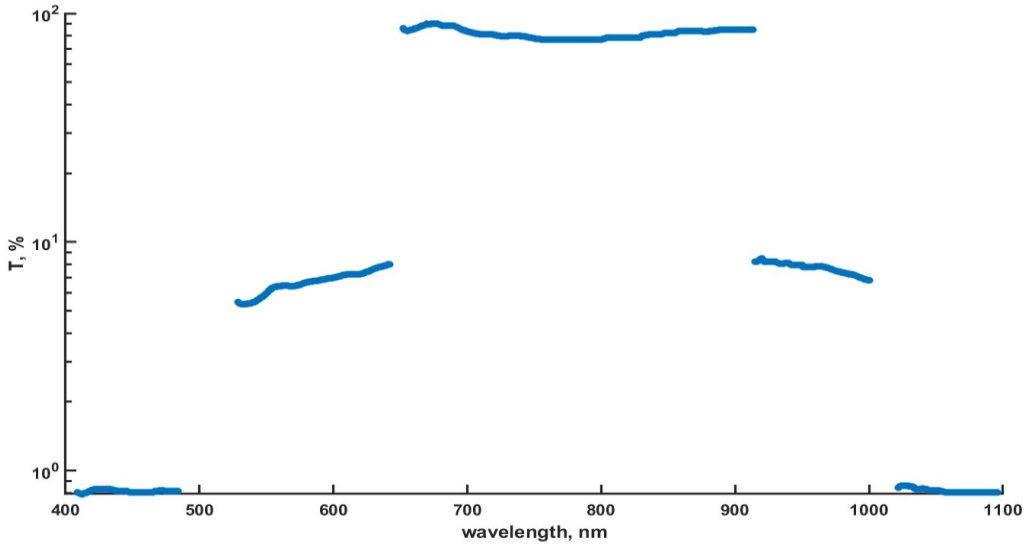

Figure 5-9 Target transmittance for OIC 2022 manufacturing problem contest.

Magnetron sputtering was chosen as the deposition method for our application to the contest. As for the coating materials, Nb_2O_5 and SiO_2 were selected for the high and low index layers. The design was calculated with *Optilayer* software; one of the restrictions set for the design phase

was that the minimal thickness of layers was set to 20 nm in order to avoid the difficulties of monitoring very thin layers. The design consists of a total of 68 layers, ranging in thickness from 20 to 500 nm [appendix 1.9].

Regarding the monitoring, based on the results we have already described, several strategies were possible. We opted for splitting the deposition into two witness glasses controlled with a strategy mixing broadband *Merit* and rate monitoring. Rate monitoring was used for 10 layers, the complete strategy and the design are given in appendix 4.5. Not all 20 nm thick layers were rate monitored (e.g., layers 8, 11 or 37), because the signal variation with increasing thickness was sufficient.

A few layers thicker than 20 nm (e.g., layers 46, 48 or 60) were rate monitored because the change in transmittance spectra with increasing layers thickness was not sufficient [appendix 4.5]. The spectral range was changed as the number of layers on each of the monitoring glasses increased, starting with a range of 400 to 900 nm and reducing to a range of 600 to 900 nm for the last layers. By using this spectral region for the last layers, we benefit from a significant transmittance amplitude and avoid the spectral resolution problem in the short wavelength range. The settling time was set to 2 seconds for all layers, the merit release level was set to 3. For this design, the merit release level was used to avoid detection of false minima for thick layers, not to decrease accuracy for thin layer monitoring. The theoretical and measured experimental transmittance of the filter are shown in Fig.5-10.

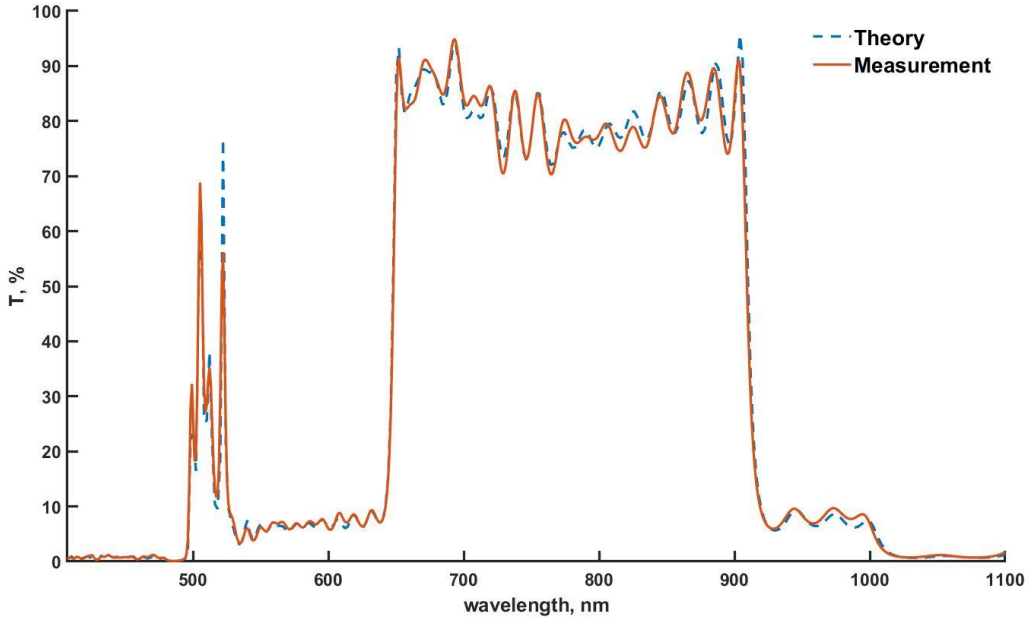

Figure 5-10 Transmittance spectrum of the deposited filter compared to theoretical spectrum.

A very close match between theory and experiment is observed. The measured transmittance is about 2% higher than expected in the 930 – 1000 nm range, which could be the result of a small problem in the knowledge of the refractive index in this particular region. In the middle part of the spectrum, where the transmittance is highest, we see that the oscillations in the spectrum are mostly overlapping, with a very slight shift to smaller wavelengths in the 800-900 nm region.

The measured thickness errors are shown in Fig.5-11. The errors are generally less than 0.5% with a few exceptions of 10% and more for very thin layers. This result tends to show that the re-fitting of the spectra to calculate the deposited thickness is sometimes not accurate when thin layer is followed by a thick layer. Therefore, the 10% errors are considered as calculation errors and do not represent the real situation.

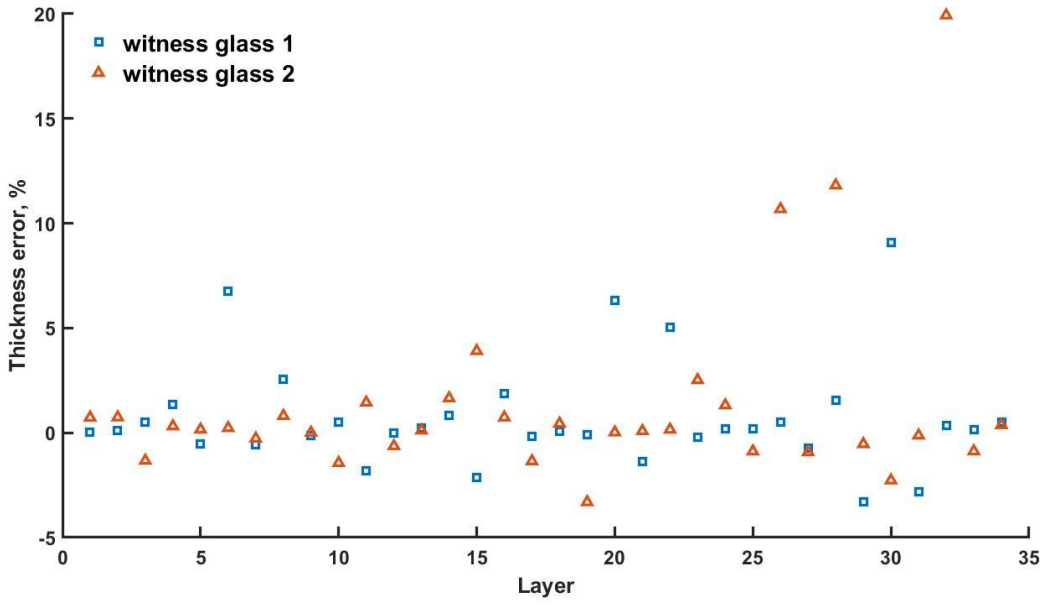

Figure 5-11 Relative thickness errors of the filter manufactured for the OIC contest.

It is important to keep the thickness errors low as we chose a two-witness glass strategy for this design.

As this work was done within the OIC manufacturing problem contest, it is important to see how the filter first fits into the expected spectral profile. In fig.5-12 we have plotted together the target of the OIC contest and the spectral measurement of the delivered component. We can see that in logarithmic scale, the blocking band at short wavelengths is not as 'flat' as at long wavelengths. A rather large deviation from the target is observed around 900 nm; in this region, the target curves are not separated when the order of magnitude changes, and it is not possible to design such an abrupt change in transmittance without significantly increasing the optical thickness and the number of layers of the design.

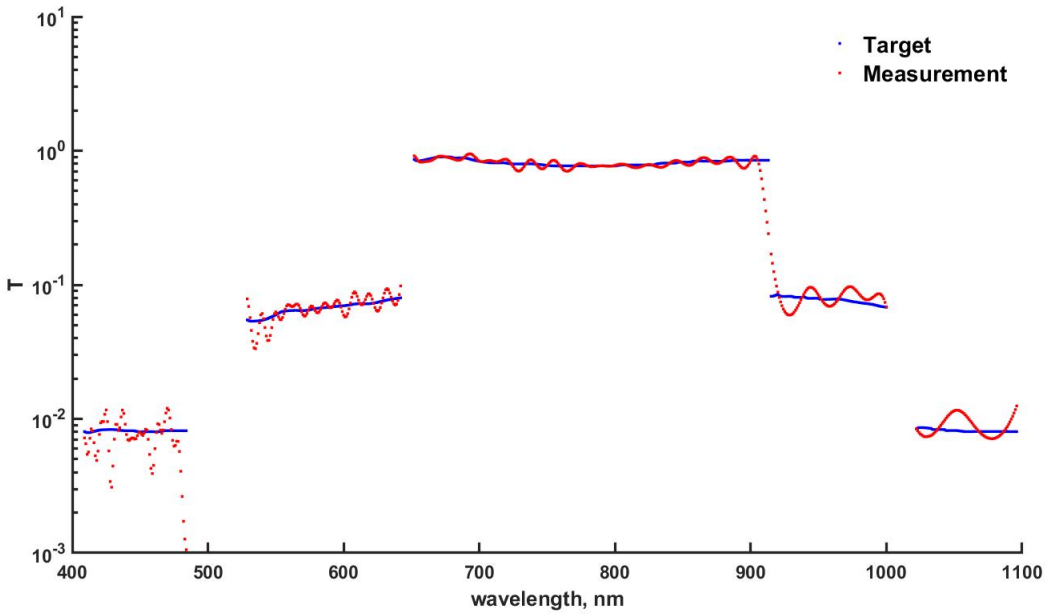

Figure 5-12 Transmittance spectra of the deposited filter compared to the OIC contest target plotted in logarithmic scale

The organizers of the OIC contest have defined the merit function to evaluate the submitted filters for the participants as shown in Eq.5.1.

$$MF = \left\{ \frac{1}{N_0 + N_1 + N_2} \left[\sum_{i=1}^{N_0} \left(\frac{T_{0,i} - T_{0,i}^D}{\Delta T_{0,i}} \right)^2 + \sum_{i=1}^{N_1} \left(\frac{T_{1,i} - T_{1,i}^D}{\Delta T_{1,i}} \right)^2 + \sum_{i=1}^{N_2} \left(\frac{T_{2,i} - T_{2,i}^D}{\Delta T_{2,i}} \right)^2 \right] \right\}^{1/2} \quad (5.1)$$

Where $T_{0,i}$ $T_{0,i}^D$ are the measured and target transmittance with logT≈0, while $T_{1,i}$ $T_{1,i}^D$ are the measured and target transmittance where logT ≈-1 and the $T_{2,i}$ $T_{2,i}^D$ are the target and measured transmittance where the logT≈-2 at the specified wavelength λ_i. N is the total number of datapoints and ΔT are the given transmittance tolerances for corresponding wavelength ranges[75]. Our submitted sample results in MF=6.8.

For this design, indirect monitoring as well as the *Merit* broadband monitoring strategy worked very well. Additional information on the location of the witness glass change is provided in chapter 6.

If we compare this design with the D65 compensator, from a monitoring point of view, the OIC contest design was easier as the layer thicknesses at the beginning of both witness glasses are larger, resulting in more oscillations in the spectra.

The sharp spectral features can cause problems related to the spectral resolution of the spectrometer, however, since we can change the wavelength range used for the measurement, it seems that the limited spectral resolution is not a major drawback for broadband monitoring. The disadvantage of broadband monitoring compared to monochromatic monitoring is the stability of the measurement, as it seems that this method struggles if the change in transmittance - as the layer is deposited- is small, as illustrated with the D65 filter.

5.3 Thoughts on broadband monitoring strategies

At the time of writing this thesis, some of the parameters for broadband monitoring are still under investigation, and therefore, we do not yet have a similar automated solution for strategy determination as we have for polychromatic monitoring. However, it is very likely that at some point, an automated process for broadband strategy will be provided. We have already identified several criteria that must be considered when creating the strategy for broadband optical monitoring of a thin film filter. Also, as with monochromatic monitoring, it is recommended that rate monitoring be used for a given layer if optical methods do not appear to be reliable.

In addition to rate monitoring, it appears that the use of monochromatic monitoring will be necessary in some situations, as in the D65 compensator filter example. But the criteria have yet to be defined.

The question of whether to use *Wideband* broadband thickness monitoring or *Merit* monitoring remains open. Thickness errors appear to be smaller when using the *Merit* monitoring method, but the *Wideband* method is more robust. To increase confidence in *Merit* monitoring, additional input parameters such as signal settling time and release level must be adjusted. Good results were obtained when using a 2 second settling time for the OIC contest design, with the release level for merit detection set to 3. It is tempting to use very low merit release levels, but this may result in a failed deposition run.

The wavelength range used for broadband monitoring is probably the most important control parameter, as it varies from design to design and layer to layer. We observed that the wavelength

range must be adjusted to avoid potential problems with the spectral resolution of the imaging spectrometer. In addition, the wavelength range also influences the sensitivity of the measured transmittance when the thickness is increased. The uncertainty that remains at this time is the minimum wavelength range that can be used for monitoring and then determining the deposited thickness at the end of the layer.

In all the examples of deposited filters in this chapter, the errors of the previous layers were taken into account in the calculation of the target curves of the following layers, in order to keep the thickness errors low. This approach is important if indirect monitoring, with multiple witness glasses, is used, because correction information cannot be transferred from one witness glass to another, and the success of the deposition will depend on the thickness errors.

Chapter 6 - Indirect monitoring strategies

In this thesis we have used indirect monitoring strategies (multiple witness glasses) for most of the examples studied. And while these strategies were mostly successful, in general, the placement of the witness glass change was determined by the 'educated guess' method. In this chapter, we will examine one possible approach, based on the calculation of thickness errors, that can be used to determine the best places for the witness glass change.

6.1 Sensitivity of layer to thickness errors

In chapter 3, we introduced the concept of relative error sensitivity and used it to create a monitoring strategy for Fabry Perot filters. The same approach can be used for the non-quarter wave designs.

To find the layers that are the most sensitive to errors, we can use the *merit to target spectrum (m)* to evaluate how close a spectrum calculated with an error in one of the layers is to a theoretical spectrum with no error.

$$m_j = \sqrt{\frac{\sum_{i=1}^{N}(T_{iErr} - T_{iTh})^2}{N}} \tag{6.1}$$

Where m_j is the merit to target spectrum for jth layer, N is the number of measured datapoints – wavelength range used, $T_{iErr(j)}, T_{iTh}$ are the simulated spectrum with the thickness error in layer j and the theoretical spectrum. If the design consists of n layers, the theoretical transmittance is $T_{Th}(\lambda; d_1, .. d_j, .. d_n)$; we can assume that there is small thickness error e in one of the layers and calculate the transmittance with the thickness error as $T_{Err\,(j)}(\lambda; d_1, .. d_j + e, .. d_n)$. After calculating m_j for each layer j of the design, we find that the one with the highest value is the most sensitive to thickness errors. The error sensitivity is usually considered in relative values (percentage).

While this is an easy concept, there are few considerations to keep in mind. The first is the wavelength range: the results (the most sensitive layers) may change if this calculation is performed with different wavelength ranges. The second is the type of error – it can be in nanometers or as a percentage of the thickness. Finally, we will consider two ways of calculating

the merit (m): first we will assume that the thickness errors is only in one of the layers at the time – to find the most sensitive layer towards thickness errors; and secondly we will perform this calculation by adding random errors, layer by layer, until all layers in the design are calculated with a random thickness error – to see the effect of error accumulation.

6.2 Influence of layers thicknesses and wavelength range on sensitivity calculations for Bonne Mère design

To begin the process of evaluating the sensitive layers, we can examine the expected thickness errors relative to the thickness that needs to be monitored. As mentioned earlier, one of the advantages of broadband optical monitoring is the ability to calculate the thickness of deposited layers from the spectral measurement. This means that we can gather statistics on the magnitude of thickness errors to be expected depending on the layer thickness. Fig.6-1 shows the average errors measured by the broadband system as a function of thickness. A 50 nm step is considered for the thickness range. The data are collected from all available designs and monitoring methods (broadband, monochromatic, rate). As we have shown in chapter 5 with the OIC 2022 design, some doubts remain about the accuracy of the thin layers thickness determination from the broadband spectra. Nevertheless, we consider this to be a good starting point for the calculations. We see that the thickness errors are greater than 2.5% for layers in 1-50 nm range and the errors decrease significantly as the layers thickness increase. The data come from several depositions runs with a total of 140 deposited layers, which is not sufficient for a good statistical evaluation, but can nevertheless be used as illustration that the errors depend on the layers' thickness and this dependence can be taken into account when searching for error sensitive layers.

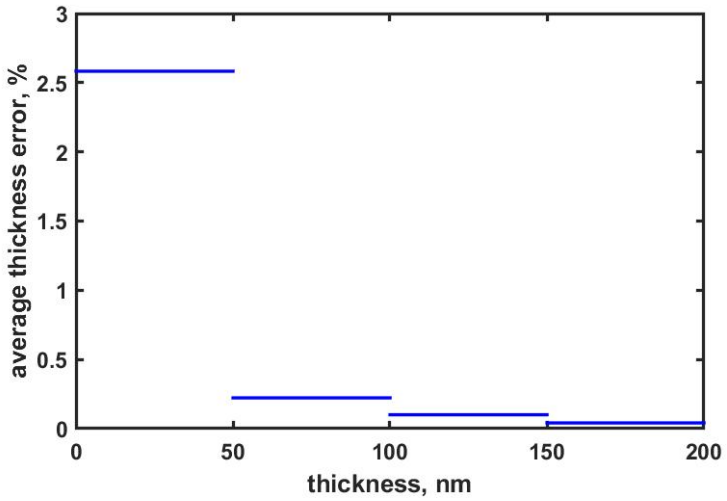

Figure 6-1 Average thickness error measured with the Broadband monitoring setup.

We will use these errors to calculate the sensitivity of the layers, because for most of the designs we studied in this thesis, the thickness varies from a few tens of nanometers to a few hundred nanometers. If we use a constant error for all layers in designs such as Bone Mère or OIC, the thickest layers are marked as the most sensitive ones.

Next, we can examine the wavelength range. We calculated the relative sensitivity to thickness errors for the Bonne Mère design that we analyzed in chapter 4. First, we examined the 400-900 nm range, as we used this range when searching for the monitoring strategy. The results are plotted in Fig.6-2.

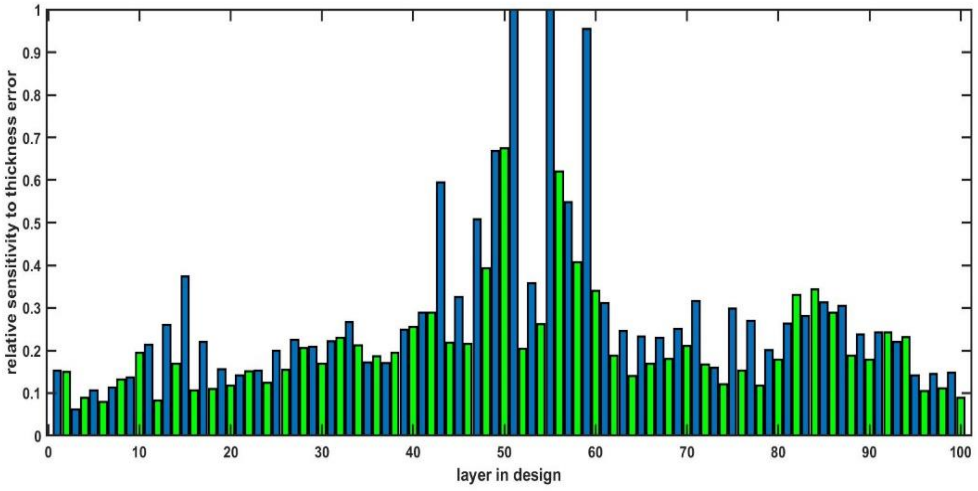

Figure 6-2 Relative sensitivity of the "Bonne Mère" filter layers for a target in the 400-900 nm wavelength range.

We note that layers 51, 55, and 59 stand out for their high sensitivity to thickness errors. The sensitivity of these layers is almost 10 times higher than most layers in this design. This suggests that the monitoring strategy should be designed so that the errors in these layers are as small as possible. However, this design is for a much narrower range of wavelengths. Indeed, if we look again at the measurements of this filter in chapter 4, we see that we are only considering the 400-700 nm range. Therefore, we recalculated the sensitivity of the layers in the restricted 400-700 nm range. The result is shown in Fig.6-3. As we can see, in this wavelength range, the most sensitive layers are 55 and 59, and the difference between the most sensitive layer and the majority of the layers has decreased.

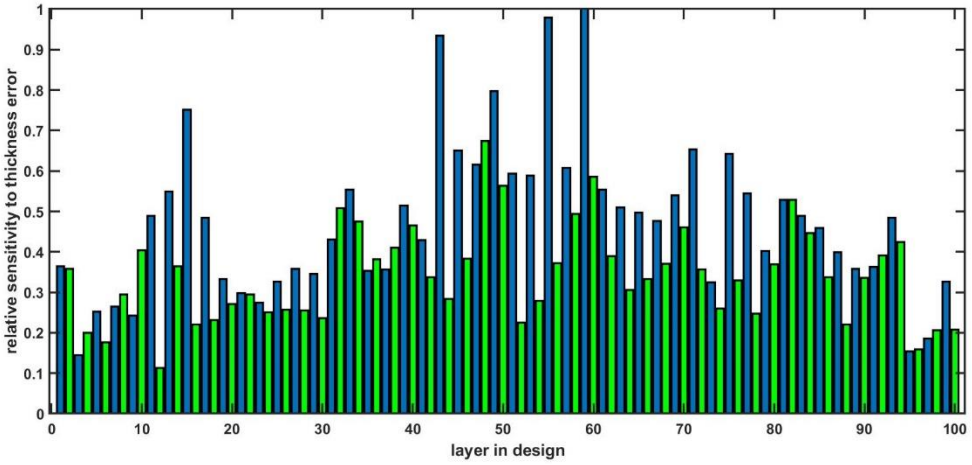

Figure 6-3 Relative sensitivity of the Bonne Mère filter layers for a target restricted to the 400-700 nm wavelength range.

The reason why the difference between the most sensitive layers and the rest of the filter decreased is related to the maximum merit values for the different wavelength ranges. The maximum merit (m_{max}) in the 400-900 nm range is m_{max} =1.46 what is 1.65 times higher than for the 400-700 nm range (m_{max} =0.88).

The reason why the spectral range plays such an important role for this design can be understood if we plot the spectral response for the entire filter in the 400-900 nm range (Fig.6-4) and plot the spectra together with the error in the layer 51. The spectra behave similarly to a narrow bandpass filter in the 732-734 nm range and the layer 51 apparently plays a similar role to a cavity layer in a Fabry Perot design. This means that the error here affects the centering. This of course makes a big difference when the merit is calculated.

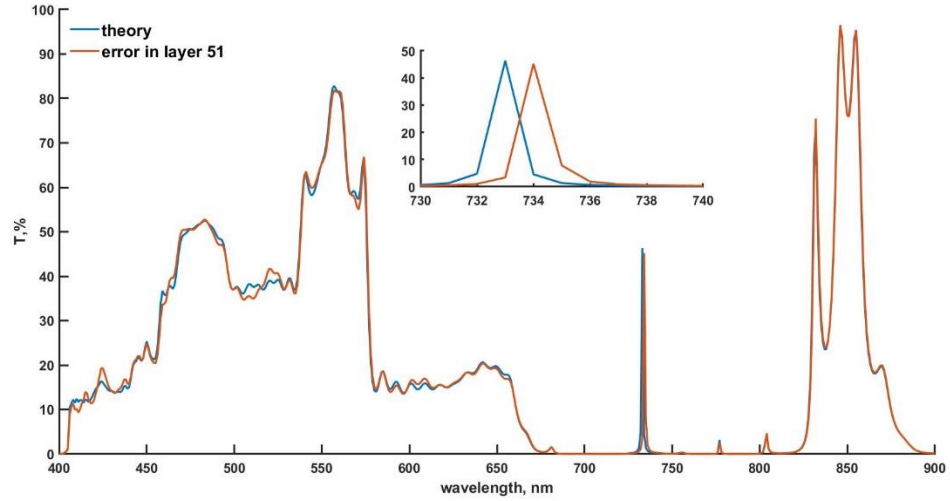

Figure 6-4 Theoretical transmittance spectra of the Bonne Mère design and calculated spectra with error in layer 51. Zoom around 730 nm on the mismatch.

It should be noted here that in addition to the shift in the centering of the bandpass element around 730 nm, this error adds noticeable ripple at shorter wavelengths. Since layer 51 is no longer the most sensitive to thickness errors, this illustrates the sensitivity of this design is to uncompensated errors.

We can further highlight the sensitivity of this design if we compare it to another design. We calculated the relative sensitivity to thickness errors also for the notch filter, analyzed in chapter 4 and plotted it in Fig.6-5. Only this time, we normalized the data to the maximum merit of the Bonne Mère design. As for the wavelength range, we chose 400-750 nm. In general, any type of bandpass filter can be expected to be very sensitive to uncompensated errors, because the edges between the blocking and passing regions are steep, and any edge shift along the x axis caused by a thickness error will result in a large value of m, as also shown in the Fig.6-4.

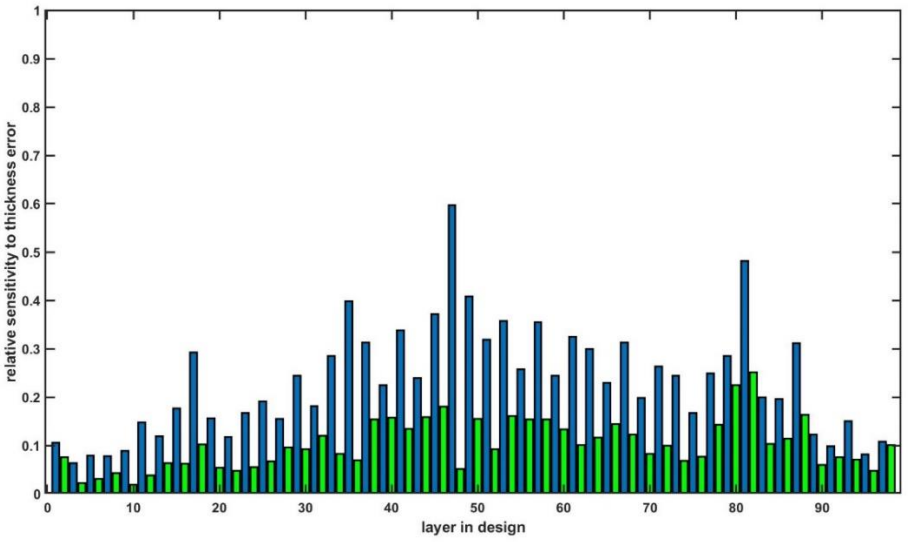

Figure 6-5 Relative sensitivity of the notch filter layers for a target in the 400-700 nm wavelength range. Values are normalized to those of the Bonne Mère design.

As shown in Fig.6-5 the most sensitive layer of the notch design is ~60% of the sensitivity of the most sensitive layer of the Bonne Mère design. In addition, the difference between the most and least sensitive layers is larger (~10 times) compared to Bonne Mère design (~3 times). Therefore, we can say that the Bonne Mère design is indeed very sensitive to uncompensated thickness errors.

6.2 Random error simulation for the Bonne Mère design

Another interesting method that evaluates the sensitivity of designs to random thickness errors is to calculate the merit value between an error-free spectrum and a spectrum with errors, but this time we added random errors, layer by layer (keeping the error of the previous layer). For example, when calculating the merit value after the 3rd layer, we keep the errors of the previous 2 layers - $T_{Err\,(3)}(\lambda; d_1 \pm e, d_2 \pm e, d_3 \pm e, d_4, .. d_n)$. The remaining layers are considered error-free. The thickness error is taken from Fig.6-1, the sign (±) of the error is chosen randomly. In Fig.6-6, we have plotted the results of this calculation for the Bonne Mère design. We performed this calculation 10 times, with errors randomly assigned. The wavelength range for this calculation was set to 400-700nm.

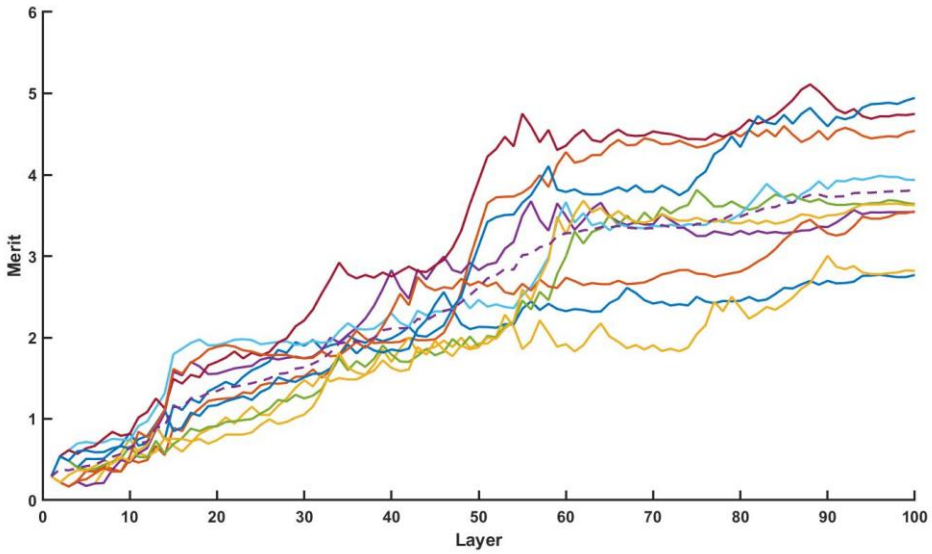

Figure 6-6 Simulated merit curves with random thickness errors function of the layer number, for the Bonne Mère design. The Dashed line represents the average merit value.

From 10 random errors simulations, we found that in the end, the merit gap is between 2 and 5. This means that several scenarios are possible with random errors. A few curves seem to show a steady increase in merit, without pronounced 'jumps'. For a few curves, we observe a 'jump' in the merit values at layer 15 and for most curves, between layers 30 and 60. This roughly corresponds to the most sensitive layers in the design (Fig.6-3). The average merit increases almost linearly until layer ~60th. After layer 60, almost all simulated merit curves remain parallel to the x axis. This means that the random errors at the beginning and middle of this filter will determine the quality of the agreement between experiment ant theory.

The question is whether we can develop an indirect monitoring strategy from this information. It seems that the layers to be monitored on individual glasses should be evenly distributed, as the last layers have less effect on the achievable merit value. Since the average merit value increases linearly for the first 60 layers, and from the experiments described in the previous chapter, we know that with broadband monitoring we can achieve small thickness errors (~0.5%) for 20 layers, a strategy where the witness glass is changed after layers 20,40 and 60 and the thicknesses are monitored with broadband strategies could be tested. In addition, a design of this

complexity could be an excellent candidate for a monitoring strategy with layer optimization based on previous errors during witness glasses change.

6.3 Indirect monitoring strategy for the OIC 2022 contest design

We have shown that the Bonne Mère design is very sensitive to random thickness errors, and from the random error simulation, we cannot see clearly where to change the test glass. Nevertheless, we think that this approach can be useful, and we are trying it on other designs as well. The design for the OIC 2022 manufacturing contest has 68 layers, and from our previous experiences, we know that we could not successfully monitor that many layers on a single witness glass. Therefore, we repeated the same process as for the Bonne Mère design to see if we could find a solution for indirect monitoring strategy in this way.

As a first step, we calculated the relative sensitivity of the layers to thickness errors and plotted it in Fig.6-7. We note that a few layers are more sensitive to errors than the rest of the filter. We normalized the results to the most sensitive layer of the OIC2022 design. Comparing the absolute values, the most sensitive layer in the OIC2022 design is slightly more sensitive than the most sensitive layer in the Bonne Mère design (m_{max} = 0.91 in OIC2022 and m_{max} =0.88 in Bonne Mère). The wavelength range for this design is set to 400-1100 nm.

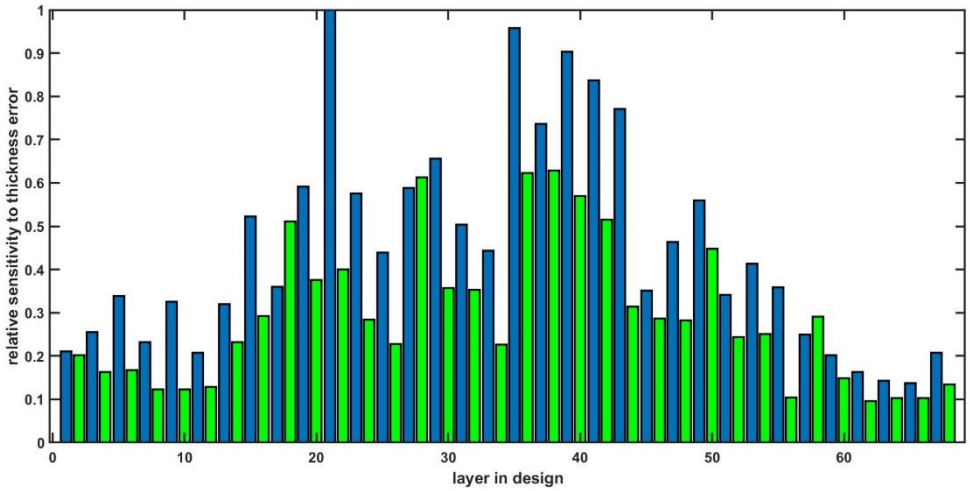

Figure 6-7 Relative sensitivity of the OIC2022 design for a target in the 400-1100 nm wavelength range. Values are normalized to those of the Bonne Mère design.

This design again seems sensitive to thickness errors. There are several sensitive layers starting at layer 35, while the last layers of the design are less sensitive than the middle ones. Based on this, we could say that the best position for the witness glass change is in the middle of the filter, because we would then start the sensitive layers on a new monitoring glass, and we know that the errors are smaller for the first new layers to be monitored.

Again, we also can simulate cumulative random error effect for this design. The results of 10 simulations are shown in Fig.6-8.

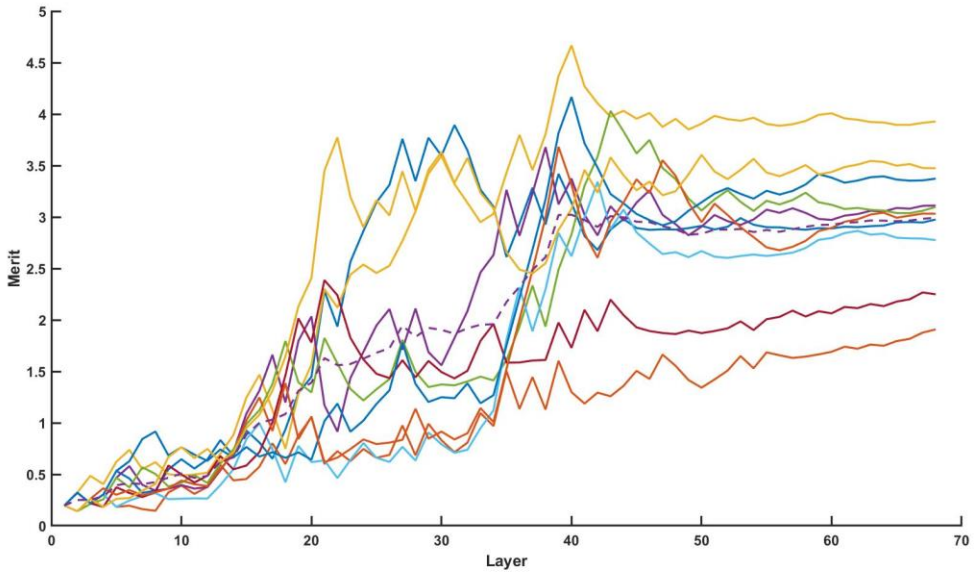

Figure 6-8 Simulated merit curves with random thickness errors function of the layer number, for the OIC 2022 design. The Dashed line represents the average merit value.

For the OIC2022 design, we observe different situations compared to the Bonne Mère design. For this design, the errors in the first 15 layers have a very small effect, and all simulated curves are close to each other. After layer 15, several scenarios are possible. For the majority of the simulated curves, the merit value increases strongly around the middle of the filter. And the errors in the last layers have little impact on the merit value.

This contrasts with the Bonne Mère design where the merit increased linearly. Therefore, we can conclude that the witness glass for this design should be changed after layer 34, just before the random errors have strongly increased the average merit by 50%. The very good results of the deposition of the OIC2022 contest design with this indirect strategy were presented in Chapter 5. Of course, we do not have the comparison with other indirect strategies to confirm that splitting

this design at other places would lead to a decrease in performance of this filter. Nevertheless, this approach is interesting and can be used to select the placement of witness glass changes.

Chapter 7 - Conclusions and perspectives

In this thesis, we have studied several of the available (to date) thin film monitoring methods, described their strengths and weaknesses, and shown how to create monitoring strategies using the strengths of each method. Below we summarize the results obtained with each of the optical monitoring methods described in this thesis and highlight possible future actions.

7.1 Fabry-Perot filters and turning point monitoring

We have shown that it is possible to reduce the extinction coefficient and improve the transmittance of hafnium oxide layers in the UV wavelength range by increasing the amount of co-sputtered silicon oxide.

We have demonstrated a new approach for the monitoring of narrow Fabry-Perot filters. We have shown that it is possible to overcome the limitations of the monitoring setup (including bandwidth and sensitivity) by choosing a smart monitoring strategy. One of the next steps would be to move to 3 cavity (and larger) designs.

Characterization of narrow bandpass filters remains a challenge, as commercially available spectrophotometers still have limitations. Therefore, for a project such as the one described in chapter 3 of this thesis, a custom measurement setup should be considered.

7.2 Monochromatic and polychromatic monitoring strategies

Polychromatic optical monitoring strategies work well in combination with magnetron sputtering. We have successfully demonstrated on various designs that we can automatically create a monitoring strategy that has no limit on the number of usable wavelengths and including, if necessary, non-optical monitoring methods. The polychromatic strategies have proven to be very robust – we do not need to perform deposition simulation prior to the experiment, and most importantly, deposition runs are not terminated prematurely when polychromatic strategies are used.

One of the questions often asked is whether these strategies work with other types of coaters. We do not have a clear answer to this question because additional testing is still needed. To test the multi-wavelengths approach, we first need to find the technical limits of the combination of a given coater and its monitoring system in order to set the experimental parameters before any determination of an automated polychromatic strategy. This is, of course, a very delicate and time-consuming task.

7.3 Broadband monitoring strategies

We have demonstrated the use of the broadband monitoring system for several filter designs. As the complexity of the designs increases, strategies are needed for broadband monitoring. We have demonstrated that good spectral performance can be achieved if broadband monitoring is combined with other monitoring methods.

To have a fully automated strategy determination (similar to the polychromatic algorithm) several input parameters such as the minimum wavelength range and release levels for *Merit* detection need further investigation.

One of the many interesting features of broadband optical monitoring is the ability to determine thickness error during the deposition of the multilayer filter. One of the next actions would be to use this information to re-optimize the layer stack based on the previously deposited thickness information. While this seems like a simple task, there are some important considerations. For example, when to perform this re-optimization, do we want to do it after each layer, or after multiple layers have been deposited. Another concern is related to determining the error itself. At the moment, it seems that determining the thickness from the spectral measurement is not optimal, especially when a thin layer is followed by a thick layer. This means that, initially, we need to be confident in the thickness determination from the broadband measurement, and then we can try to find what would be the best place for a given design for re-optimization.

Another area to explore would be error compensation with broadband monitoring. So far, we use the error information in the previous layers to modify the target curves, which keeps the errors low, but, in the end, the target transmittance curve differs significantly from the theoretical one, and from the initial specifications. We could use the design as the target curve for the last, or

some of the last layers, or possibly use a mixed monitoring strategy with the goal of benefiting from error compensations for a few layers.

7.4 Indirect monitoring strategies

In this thesis, we have successfully used indirect monitoring strategies. We should highlight the good results obtained with the Fabry Perot filters and the OIC 2022 contest design. The approach used to determine the indirect strategy for the OIC contest design is very promising and needs to be further tested on other designs.

However, in addition to studies on the sensitivity of a layer to thickness errors, there are also issues with the geometry of the coater that need to be further investigated. We already know that the uniformity inside the coater is not perfect, there are differences from one position to another, which means that the thickness deposited on the monitoring glass is not exactly the same as on other positions. Therefore, it is necessary to determine whether there is a random or systematic difference in the deposited thickness depending on the position of the glass inside the coater.

References

[1] E. Darque-Ceretti, E. Felder, and M. Aucouturier, “Foil and leaf gilding on cultural artifacts; forming and adhesion,” *Rev. Mater.*, vol. 16, no. 1, pp. 540–559, 2011, doi: 10.1590/S1517-70762011000100002.

[2] D. M. Mattox and M. Plus, “History Corner A Short History : Magnetron Sputter Deposition,” *Soc. Vac. Coaters*, 2015.

[3] J. E. Greene, “Review Article: Tracing the recorded history of thin-film sputter deposition: From the 1800s to 2017,” *J. Vac. Sci. Technol. A Vacuum, Surfaces, Film.*, vol. 35, no. 5, p. 05C204, 2017, doi: 10.1116/1.4998940.

[4] J. von Fraunhofer, “Versuche über die Ursachen des Anlaufens und Mattwerdens des Glases und die Mittel, denselben zuvorzukommen, in Joseph von Fraunhofer’s Gesammelte Schriften,” *München Verlag der K. Bayer. Akad. der Wissenschaften*, 1887.

[5] A. Macleod, *Thin film optical coatings*, 4th ed. CRC /Taylor & Francis Group, 2010. doi: 10.1007/978-3-642-19409-2_6.

[6] J. Strong, “On a Method of Decreasing the Reflection from Nonmetallic Substances,” *J. Opt. Soc. Am.*, vol. 26, 1936.

[7] A. Thelen, “The pioneering contributions of W Geffcken, in Thin Films on Glass,” *Springer-Verlag*, 1997.

[8] B. Wang and L. Gallais, “A theoretical investigation of the laser damage threshold of metal multi-dielectric mirrors for high power ultrashort applications,” *Opt. Express*, vol. 21, no. 12, p. 14698, 2013, doi: 10.1364/oe.21.014698.

[9] B. T. S. and J. A. Dobrowolski, “Implementation of a numerical needle method for thin-film design,” *Appl. Opt.*, vol. 35, pp. 5484–5492, 1996.

[10] M. BANNING, “Practical methods of making and using multilayer filters,” *J. Opt. Soc. Am.*, vol. 37, no. 10, pp. 792–797, 1947, doi: 10.1364/JOSA.37.000792.

[11] H. A. Macleod, “Turning Value Monitoring of Narrow-band All-dielectric Thin-film Optical Filters,” *Opt. ACTA.*, vol. 19, no. 1, pp. 1–28, 1972, doi: 10.1080/713818494.

[12] M. Lappschies, T. Gross, H. Ehlers, and D. Ristau, “Broadband optical monitoring for the deposition of complex coating designs,” *Adv. Opt. Thin Film.*, vol. 5250, p. 637, 2004, doi: 10.1117/12.514800.

[13] A. Zöller, D. Arhilger, M. Boos, and H. Hagedorn, “Advanced optical monitoring system

using a newly developed low noise wideband spectrometer system," *Opt. Syst. Des. 2015 Adv. Opt. Thin Film. V*, vol. 9627, pp. 1–5, 2015, doi: 10.1117/12.2191269.

[14] L. Li and Y. Yen, "Wideband monitoring and measuring system for optical coatings," *Appl. Opt.*, vol. 28, no. 14, pp. 2889–2894, 1989.

[15] O. Lyngnes *et al.*, "Optical monitoring of high throughput ion beam sputtering deposition," *Opt. Syst. Des. 2015 Adv. Opt. Thin Film. V*, vol. 9627, no. September 2017, p. 962715, 2015, doi: 10.1117/12.2194090.

[16] P. Bousquet, A. Fornier, E. Pelletier, and P. Roche, "Optical filters: Monitoring process allowing the auto-correction of thickness errors," *Thin Solid Films*, vol. 13, pp. 285–290, 1972.

[17] C. Petite *et al.*, "Multipass lock-in thermography for the study of optical coating absorption," *Appl. Opt.*, vol. 61, no. 4, p. 978, 2022, doi: 10.1364/ao.445045.

[18] M. Salehpoor, H. Vahid, A. H. Fard, H. Fallah, and M. Hajimahmoodzadeh, "Designing and manufacturing of interference notch filter with a single reflection band," *Optik (Stuttg).*, vol. 249, no. November, p. 168202, 2022, doi: 10.1016/j.ijleo.2021.168202.

[19] V. Janicki *et al.*, "Comparison of gradient index and classical designs of a narrow band notch filter," *Adv. Opt. Thin Film. II*, vol. 5963, no. 2005, p. 59631O, 2005, doi: 10.1117/12.624640.

[20] G. L. M. R.W. Sprague, B. Shnapir, "Rugate notch filters find use in laser-based applications," *Laser Focus world*, vol. 40, no. 9, pp. 107–111, 2004.

[21] M. Afzaal and P. O'Brien, "Recent developments in II–VI and III–VI semiconductors and their applications in solar cells," *J. Mater. Chem.*, vol. 16, no. 17, pp. 1597–1602, 2006, doi: 10.1039/B512182E.

[22] C. Schaefer, G. Bräuer, and J. Szczyrbowski, "Low emissivity coatings on architectural glass," *Surf. Coatings Technol.*, vol. 93, no. 1, pp. 37–45, 1997, doi: https://doi.org/10.1016/S0257-8972(97)00034-0.

[23] J. Lee, J. Kim, and M. Lee, "High-purity reflective color filters based on thin film cavities embedded with an ultrathin Ge2Sb2Te5 absorption layer," *Nanoscale Adv.*, vol. 2, no. 10, pp. 4930–4937, 2020, doi: 10.1039/D0NA00626B.

[24] S. Choi *et al.*, "Thin-film transistor-driven vertically stacked full-color organic light-emitting diodes for high-resolution active-matrix displays," *Nat. Commun.*, vol. 11, no. 1,

p. 2732, 2020, doi: 10.1038/s41467-020-16551-8.

[25] A. Ul-Hamid, “Microstructure, properties and applications of Zr-carbide, Zr-nitride and Zr-carbonitride coatings: a review,” *Mater. Adv.*, vol. 1, no. 5, pp. 1012–1037, 2020, doi: 10.1039/D0MA00233J.

[26] X. Guan, Y. Wang, G. Zhang, J. Xin, L. Wang, and Q. Xue, “A novel duplex PDMS/CrN coating with superior corrosion resistance for marine applications,” *RSC Adv.*, vol. 6, no. 90, pp. 87003–87012, 2016, doi: 10.1039/C6RA19729A.

[27] D. Depla, S. Mahieu, and J. E. Greene, “Sputter Deposition Processes,” in *Handbook of Deposition Technologies for Films and Coatings*, Third Edit., Elsevier Ltd., 2010, pp. 253–296. doi: 10.1016/B978-0-8155-2031-3.00005-3.

[28] M. Cumbul Altay and S. Eroglu, “Chemical vapor deposition of Ge nanowires from readily available GeO2 and CH4 precursors,” *J. Cryst. Growth*, vol. 551, p. 125886, 2020, doi: https://doi.org/10.1016/j.jcrysgro.2020.125886.

[29] B. Polyakov *et al.*, “A comparative study of heterostructured CuO/CuWO4 nanowires and thin films,” *J. Cryst. Growth*, vol. 480, pp. 78–84, 2017, doi: 10.1016/j.jcrysgro.2017.10.011.

[30] A. Jilani, M. S. Abdel-wahab, and A. H. Hammad, “Advance Deposition Techniques for Thin Film and Coating,” *Mod. Technol. Creat. Thin-film Syst. Coatings*, 2017, doi: 10.5772/65702.

[31] Z. Wang and Z. Zhang, “Electron Beam Evaporation Deposition,” in *Advanced Nano Deposition Methods*, 2016, pp. 33–58. doi: 10.1002/9783527696406.ch2.

[32] S. Pongratz and A. Zöller, “Plasma ion-assisted deposition: A promising technique for optical coatings,” *J. Vac. Sci. Technol. A Vacuum, Surfaces, Film.*, vol. 10, no. 4, pp. 1897–1904, 1992, doi: 10.1116/1.578112.

[33] J. Musil, P. Baroch, J. Vlček, K. H. Nam, and J. G. Han, “Reactive magnetron sputtering of thin films: present status and trends,” *Thin Solid Films*, vol. 475, no. 1, pp. 208–218, 2005, doi: https://doi.org/10.1016/j.tsf.2004.07.041.

[34] M. Scherer, “Magnetron sputter-deposition on atom layer scale,” *Vak. Forsch. und Prax.*, vol. 21, no. 4, pp. 24–30, 2009, doi: 10.1002/vipr.200900391.

[35] A. V. Tikhonravov, M. K. Trubetskov, and T. V. Amotchkina, *Optical monitoring strategies for optical coating manufacturing*. Elsevier LTD., 2018. doi: 10.1016/B978-0-

08-102073-9.00003-5.

[36] H. A. Macleod and E. Pelletier, “Error Compensation Mechanisms in Some Thin-film Monitoring Systems,” *Opt. Acta Int. J. Opt.*, vol. 24, no. 9, pp. 907–930, Sep. 1977, doi: 10.1080/713819668.

[37] B. J. Frey, D. B. Leviton, and T. J. Madison, “Temperature-DependentReflactiveIndexOfSiliconAndGermanium.pdf,” *Optomech. Technol. Astron. Pts 1 2*, vol. 6273, pp. J2732–J2732, 2006, [Online]. Available: https://core.ac.uk/download/pdf/44119759.pdf

[38] H. Takahashi, “Temperature stability of thin-film narrow bandpass filters produced by ion-assisted deposition,” in *Proc.SPIE*, Nov. 1994, vol. 2253. doi: 10.1117/12.192086.

[39] S. Michel, F. Lemarquis, and M. Lequime, “Determination of thermal and elastic coefficients of optical thin-film materials,” *Adv. Opt. Thin Film. III*, vol. 7101, p. 71010S, 2008, doi: 10.1117/12.797707.

[40] H. K. Pulker, “Thickness Measurement, Rate Control And Automation In Thin Film Coating Technology,” 1983, pp. 100–108.

[41] A. Wajid, “On the accuracy of the quartz-crystal microbalance (QCM) in thin-film depositions,” *Sensors Actuators A Phys.*, vol. 63, no. 1, pp. 41–46, 1997, doi: https://doi.org/10.1016/S0924-4247(97)80427-X.

[42] T. Begou *et al.*, “High performance thin-film optical filters with stress compensation,” *J. Opt. Soc. Am. A Opt. Image Sci. Vision, Opt. Soc. Am. C121. hal-02350443*, 2019.

[43] M. Sakurai, *Spectroscopic ellipsometry*, vol. 57, no. 7. 2012.

[44] J. N. Hilfiker, “In situ spectroscopic ellipsometry (SE) for characterization of thin film growth,” *Situ Charact. Thin Film Growth*, pp. 99–151, 2011, doi: 10.1533/9780857094957.2.99.

[45] “https://www.horiba.com/int/scientific/products/detail/action/show/Product/spectroscopic-ellipsometer-in-line-1848/.”

[46] A. Zöller, M. Boos, R. Goetzelmann, H. Hagedorn, B. Romanov, and M. Viet, “Accuracy and error compensation with direct monochromatic monitoring,” *Opt. InfoBase Conf. Pap.*, pp. 1–3, 2013, doi: 10.1364/oic.2013.wb.5.

[47] A. Zoeller, M. Boos, R. Goetzelmann, H. Hagedorn, and W. Klug, “Substantial progress in optical monitoring by intermittent measurement technique,” *Adv. Opt. Thin Film. II*,

vol. 5963, p. 59630D, 2005, doi: 10.1117/12.624865.

[48] H. A. Macleod, “Monitoring of optical coatings,” *Appl. Opt.*, vol. 20, no. 1, p. 82, 1981, doi: 10.1364/ao.20.000082.

[49] “www.optilayer.com,” 1377.

[50] R. R. Willey, “Simulation comparisons of optical monitoring strategies in narrow bandpass filters,” *Opt. InfoBase Conf. Pap.*, vol. 53, no. 4, pp. 27–34, 2013, doi: 10.1364/oic.2013.wb.8.

[51] R. R. Willey, “Preserving Error Compensation Benefits While Changing Monitoring Wavelengths with Each Layer,” pp. 3–9, 2016, doi: 10.14332/svc16.proc.0014.

[52] J. Zideluns, F. Lemarchand, D. Arhilger, H. Hagedorn, and J. Lumeau, “Automated optical monitoring wavelength selection for thin-film filters,” *Opt. Express*, vol. 29, no. 21, p. 33398, 2021, doi: 10.1364/oe.439033.

[53] L.-Y. C. Yun-Fei Wu, Qing-Yuan Cal, Yu-Xiang Zheng, Rong-Jun Zhang, “Application of a High-Resolution Spectrometr in a Broadband Optical MOnitor for Film Coating,” *J. Korean Phys. Soc.*, vol. 53, no. 4, pp. 2307–2311, 2008.

[54] A. Macleod, “Admittance and Circle Diagrams,” 2008.

[55] K. Wu, C.-C. Lee, and T.-L. Ni, “Advanced broadband monitoring for thin film deposition through equivalent optical admittance loci observation,” *Opt. Express*, vol. 20, no. 4, p. 3883, 2012, doi: 10.1364/oe.20.003883.

[56] C.-C. Lee, K. Wu, S.-H. Chen, and S.-J. Ma, “Optical monitoring and real time admittance loci calculation through polarization interferometer,” *Opt. Express*, vol. 15, no. 26, pp. 17536–17541, 2007, doi: 10.1364/OE.15.017536.

[57] K. Starke, T. Grosz, M. Lappschies, and D. Ristau, “Rapid prototyping of optical thin film filters,” *Opt. Infrared Thin Film.*, vol. 4094, p. 83, 2000, doi: 10.1117/12.404754.

[58] A. V. Tikhonravov and M. K. Trubetskov, “Online characterization and reoptimization of optical coatings,” *Adv. Opt. Thin Film.*, vol. 5250, no. 095, p. 406, 2004, doi: 10.1117/12.513379.

[59] T. V Amotchkina, S. Schlichting, H. Ehlers, M. K. Trubetskov, A. V Tikhonravov, and D. Ristau, “Computational manufacturing as a key element in the design – production chain for modern multilayer coatings,” 2012.

[60] A. Tikhonravov, I. Kochikov, I. Matvienko, T. Isaev, and A. Yagola, “Strategies of

broadband monitoring aimed at minimizing deposition errors," *Coatings*, vol. 9, no. 12, 2019, doi: 10.3390/coatings9120809.

[61] A. Zöller, M. Boos, H. Hagedorn, and B. Romanov, "Computer simulation of coating processes with monochromatic monitoring," no. September, 2008, doi: 10.1117/12.797612.

[62] A. V Tikhonravov and M. K. Trubetskov, "Computational manufacturing as a bridge between design and production," *Appl. Opt.*, vol. 44, no. 32, pp. 6877–6884, 2005.

[63] A. Behrendt and J. Reichardt, "Atmospheric temperature profiling in the presence of clouds with a pure rotational Raman lidar by use of an interference-filter-based polychromator," *Appl. Opt.*, vol. 39, no. 9, p. 1372, 2000, doi: 10.1364/ao.39.001372.

[64] D. Li, Ed., "Fabry-Perot Optical Filter," in *Encyclopedia of Microfluidics and Nanofluidics*, Boston, MA: Springer US, 2008, pp. 662–663. doi: 10.1007/978-0-387-48998-8_522.

[65] L. Khomenkova, X. Portier, P. Marie, and F. Gourbilleau, "Hafnium Silicate dielectrics fabricated by RF magnetron sputtering.," *J. Non-Crystalline Solids, Elsevier*, vol. 357, no. 8–9, p. 1860, 2011, doi: 10.1016/j.jnoncrysol.2010.12.048ff. ffhal-00737872f.

[66] R. Faber, K. Zhang, and A. Zoeller, "Design and manufacturing of WDM narrow-band interference filters," in *Proc.SPIE*, Oct. 2000, vol. 4094. doi: 10.1117/12.404748.

[67] "https://www.hamamatsu.com/eu/en.html."

[68] M. Trubetskov, T. Amotchkina, and A. Tikhonravov, "Automated construction of monochromatic monitoring strategies," *Appl. Opt.*, vol. 54, no. 8, p. 1900, 2015, doi: 10.1364/ao.54.001900.

[69] M. Vignaux, F. Lemarchand, T. Begou, C. Grezes-Besset, and J. Lumeau, "Semi-automated method for the determination of the all-optical monitoring strategy of complex thin-film filters," *Opt. Express*, vol. 27, no. 9, p. 12373, 2019, doi: 10.1364/oe.27.012373.

[70] B. Bobbs and J. E. Rudisill, "Optical monitoring of nonquarterwave film thicknesses using a turning point method," *Appl. Opt.*, vol. 26, no. 15, 1987, doi: 10.1364/AO.26.003136.

[71] A. V. Tikhonravov, M. K. Trubetskov, and T. V. Amotchkina, "Statistical approach to choosing a strategy of monochromatic monitoring of optical coating production," *Appl. Opt.*, vol. 45, no. 30, pp. 7863–7870, 2006, doi: 10.1364/AO.45.007863.

[72] N. Ohta and A. R. Robertson, *CIE Standard Colorimetric System*. 2006. doi:

10.1002/0470094745.ch3.

[73] D. Poitras, L. Li, M. Jacobson, and C. Cooksey, “2019 Topical Meeting on Optical Interference Coatings: Manufacturing Problem Contest [invited],” *Appl. Opt.*, vol. 59, pp. A31–A39, Dec. 2019, doi: 10.1364/AO.59.000A31.

[74] B. T. Sullivan and J. A. Dobrowolski, “Deposition error compensation for optical multilayer coatings II Experimental results—sputtering system,” *Appl. Opt.*, vol. 32, no. 13, p. 2351, 1993, doi: 10.1364/ao.32.002351.

[75] D. Poitras and P. Ma, “OIC 2022 manufacturing problem contest,” *OIC Conf. Pap.*, vol. 1, 2021;https://www.optica.org/en-us/events/topical_meetings/optical_interference_coatings/program_topics/contests/.

Appendix 1 – Details about the designs

In this appendix, the additional data about the designs discussed in this thesis are gathered. Since most of the designs are mentioned several times, the designs are in order as they are introduced in the thesis. The _B marked indexes are from experiments conducted at Bühler in Alzenau.

1.1 Optimized 4-layer antireflective coating

Layer	Index	Material	Optical thickness	Physical thickness	Reference wavelength
1	H	Nb_2O_5	0.243	12.677	500
2	L	SiO_2	0.391	32.869	500
3	H	Nb_2O_5	2.116	110.462	500
4	L	SiO_2	1.015	85.244	500

1.2 Single layer antireflective coating

Layer	Index	Material	Optical thickness	Physical thickness	Reference wavelength
1	M	MgF2	1	90.58	500

1.3 Dielectric mirror

Layer	Index	Material	Optical thickness	Physical thickness	Reference wavelength
1	H	Nb_2O_5	1	64.3	600
2	L	SiO_2	1	101.03	600
3	H	Nb_2O_5	1	64.3	600
4	L	SiO_2	1	101.03	600
5	H	Nb_2O_5	1	64.3	600
6	L	SiO_2	1	101.03	600
7	H	Nb_2O_5	1	64.3	600
8	L	SiO_2	1	101.03	600
9	H	Nb_2O_5	1	64.3	600
10	L	SiO_2	1	101.03	600
11	H	Nb_2O_5	1	64.3	600
12	L	SiO_2	1	101.03	600
13	H	Nb_2O_5	1	64.3	600
14	L	SiO_2	1	101.03	600
15	H	Nb_2O_5	1	64.3	600

16	L	SiO_2	1	101.03	600
17	H	Nb_2O_5	1	64.3	600

1.4 Silver mirror coating

Layer	Index	Material	Optical thickness	Physical thickness	Reference wavelength
1	A	Ag	0.044	100	500

1.5 Beam splitter

Layer	Index	Material	Optical thickness	Physical thickness	Reference wavelength
1	H	Nb_2O_5	0.386	20.149	500
2	L	SiO_2	0.808	67.874	500
3	H	Nb_2O_5	0.848	44.252	500
4	L	SiO_2	1.094	91.877	500
5	H	Nb_2O_5	1.074	56.032	500
6	L	SiO_2	1.616	135.716	500
7	H	Nb_2O_5	1.17	61.047	500
8	L	SiO_2	0.887	74.472	500

1.6 Notch filter

Layer	Index	Material	optical thickness	Physical thickness	Reference wavelength
1	H	Nb_2O_5_B	0.369	20.812	537
2	L	SiO_2_B	0.21	18.875	537
3	H	Nb_2O_5_B	1.186	66.904	537
4	L	SiO_2_B	0.058	5.185	537
5	H	Nb_2O_5_B	1.296	73.107	537
6	L	SiO_2_B	0.082	7.422	537
7	H	Nb_2O_5_B	2.396	135.194	537
8	L	SiO_2_B	0.122	10.971	537
9	H	Nb_2O_5_B	2.224	125.492	537
10	L	SiO_2_B	0.056	5.085	537
11	H	Nb_2O_5_B	3.535	199.486	537
12	L	SiO_2_B	0.1	8.981	537
13	H	Nb_2O_5_B	2.271	128.129	537
14	L	SiO_2_B	0.147	13.207	537
15	H	Nb_2O_5_B	2.626	148.187	537
16	L	SiO_2_B	0.124	11.158	537
17	H	Nb_2O_5_B	0.804	45.368	537

18	L	SiO_2_B	0.225	20.264	537
19	H	Nb_2O_5_B	2.258	127.397	537
20	L	SiO_2_B	0.141	12.723	537
21	H	Nb_2O_5_B	3.697	208.625	537
22	L	SiO_2_B	0.084	7.602	537
23	H	Nb_2O_5_B	2.02	113.985	537
24	L	SiO_2_B	0.103	9.314	537
25	H	Nb_2O_5_B	2.102	118.598	537
26	L	SiO_2_B	0.117	10.527	537
27	H	Nb_2O_5_B	3.716	209.68	537
28	L	SiO_2_B	0.14	12.584	537
29	H	Nb_2O_5_B	2.165	122.165	537
30	L	SiO_2_B	0.143	12.888	537
31	H	Nb_2O_5_B	3.716	209.7	537
32	L	SiO_2_B	0.15	13.552	537
33	H	Nb_2O_5_B	2.217	125.094	537
34	L	SiO_2_B	0.113	10.206	537
35	H	Nb_2O_5_B	1.499	84.575	537
36	L	SiO_2_B	0.075	6.795	537
37	H	Nb_2O_5_B	2.25	126.937	537
38	L	SiO_2_B	0.167	15.037	537
39	H	Nb_2O_5_B	3.766	212.482	537
40	L	SiO_2_B	0.166	14.991	537
41	H	Nb_2O_5_B	2.137	120.604	537
42	L	SiO_2_B	0.141	12.731	537
43	H	Nb_2O_5_B	3.644	205.629	537
44	L	SiO_2_B	0.165	14.845	537
45	H	Nb_2O_5_B	2.168	122.317	537
46	L	SiO_2_B	0.176	15.825	537
47	H	Nb_2O_5_B	3.33	187.902	537
48	L	SiO_2_B	0.056	5.085	537
49	H	Nb_2O_5_B	0.452	25.532	537
50	L	SiO_2_B	0.146	13.152	537
51	H	Nb_2O_5_B	1.848	104.287	537
52	L	SiO_2_B	0.092	8.323	537
53	H	Nb_2O_5_B	2.049	115.638	537
54	L	SiO_2_B	0.146	13.162	537
55	H	Nb_2O_5_B	3.719	209.848	537
56	L	SiO_2_B	0.169	15.217	537
57	H	Nb_2O_5_B	2.148	121.201	537
58	L	SiO_2_B	0.164	14.77	537
59	H	Nb_2O_5_B	3.694	208.441	537
60	L	SiO_2_B	0.14	12.58	537
61	H	Nb_2O_5_B	2.059	116.161	537

62	L	SiO_2_B	0.116	10.426	537
63	H	Nb_2O_5_B	1.995	112.555	537
64	L	SiO_2_B	0.121	10.922	537
65	H	Nb_2O_5_B	3.724	210.152	537
66	L	SiO_2_B	0.171	15.396	537
67	H	Nb_2O_5_B	2.177	122.862	537
68	L	SiO_2_B	0.153	13.804	537
69	H	Nb_2O_5_B	3.644	205.61	537
70	L	SiO_2_B	0.116	10.405	537
71	H	Nb_2O_5_B	2.102	118.589	537
72	L	SiO_2_B	0.139	12.558	537
73	H	Nb_2O_5_B	2.076	117.168	537
74	L	SiO_2_B	0.09	8.118	537
75	H	Nb_2O_5_B	3.6	203.151	537
76	L	SiO_2_B	0.151	13.611	537
77	H	Nb_2O_5_B	2.228	125.713	537
78	L	SiO_2_B	0.207	18.604	537
79	H	Nb_2O_5_B	2.519	142.134	537
80	L	SiO_2_B	0.282	25.393	537
81	H	Nb_2O_5_B	0.576	32.515	537
82	L	SiO_2_B	0.438	39.458	537
83	H	Nb_2O_5_B	2.212	124.829	537
84	L	SiO_2_B	0.218	19.609	537
85	H	Nb_2O_5_B	2.538	143.183	537
86	L	SiO_2_B	0.259	23.312	537
87	H	Nb_2O_5_B	0.578	32.59	537
88	L	SiO_2_B	0.357	32.153	537
89	H	Nb_2O_5_B	2.202	124.25	537
90	L	SiO_2_B	0.136	12.295	537
91	H	Nb_2O_5_B	5.361	302.503	537
92	L	SiO_2_B	0.238	21.446	537
93	H	Nb_2O_5_B	0.552	31.143	537
94	L	SiO_2_B	0.204	18.332	537
95	H	Nb_2O_5_B	3.518	198.518	537
96	L	SiO_2_B	0.136	12.256	537
97	H	Nb_2O_5_B	0.52	29.356	537
98	L	SiO_2_B	0.984	88.608	537

1.7 Fabry Perot filter

Layer	Index	Material	Optical thickness	Physical thickness	Reference wavelength
1	H	HfO_2	1	41.507	355
2	L	SiO_2	1	59.233	355

3	H	HfO_2	1	41.507	355
4	L	SiO_2	1	59.233	355
5	H	HfO_2	1	41.507	355
6	L	SiO_2	1	59.233	355
7	H	HfO_2	1	41.507	355
8	L	SiO_2	1	59.233	355
9	H	HfO_2	1	41.507	355
10	L	SiO_2	1	59.233	355
11	H	HfO_2	1	41.507	355
12	L	SiO_2	10	592.326	355
13	H	HfO_2	1	41.507	355
14	L	SiO_2	1	59.233	355
15	H	HfO_2	1	41.507	355
16	L	SiO_2	1	59.233	355
17	H	HfO_2	1	41.507	355
18	L	SiO_2	1	59.233	355
19	H	HfO_2	1	41.507	355
20	L	SiO_2	1	59.233	355
21	H	HfO_2	1	41.507	355
22	L	SiO_2	1	59.233	355
23	H	HfO_2	1	41.507	355
24	L	SiO_2	1	59.233	355
25	H	HfO_2	1	41.507	355
26	L	SiO_2	1	59.233	355
27	H	HfO_2	1	41.507	355
28	L	SiO_2	1	59.233	355
29	H	HfO_2	1	41.507	355
30	L	SiO_2	1	59.233	355
31	H	HfO_2	1	41.507	355
32	L	SiO_2	1	59.233	355
33	H	HfO_2	1	41.507	355
34	L	SiO_2	1	59.233	355
35	H	HfO_2	1	41.507	355
36	L	SiO_2	10	592.326	355
37	H	HfO_2	1	41.507	355
38	L	SiO_2	1	59.233	355
39	H	HfO_2	1	41.507	355
40	L	SiO_2	1	59.233	355
41	H	HfO_2	1	41.507	355
42	L	SiO_2	1	59.233	355
43	H	HfO_2	1	41.507	355
44	L	SiO_2	1	59.233	355
45	H	HfO_2	1	41.507	355
46	L	SiO_2	1	59.233	355

47	H	HfO_2	1	41.507	355

1.8 Bonne Mère

Layer	Index	Material	Optical thickness	Physical thickness	Reference wavelength
1	H	Nb_2O_5	0.422	22.855	516
2	L	SiO_2	0.329	28.57	516
3	H	Nb_2O_5	0.947	51.31	516
4	L	SiO_2	0.263	22.787	516
5	H	Nb_2O_5	2.475	134.061	516
6	L	SiO_2	0.264	22.865	516
7	H	Nb_2O_5	2.431	131.65	516
8	L	SiO_2	2.046	177.399	516
9	H	Nb_2O_5	1.082	58.616	516
10	L	SiO_2	0.309	26.785	516
11	H	Nb_2O_5	0.369	20	516
12	L	SiO_2	2.817	244.297	516
13	H	Nb_2O_5	0.639	34.587	516
14	L	SiO_2	0.231	20	516
15	H	Nb_2O_5	0.921	49.86	516
16	L	SiO_2	0.775	67.217	516
17	H	Nb_2O_5	0.369	20	516
18	L	SiO_2	0.636	55.156	516
19	H	Nb_2O_5	2.393	129.625	516
20	L	SiO_2	0.359	31.156	516
21	H	Nb_2O_5	2.248	121.733	516
22	L	SiO_2	2.064	178.941	516
23	H	Nb_2O_5	2.251	121.905	516
24	L	SiO_2	0.298	25.875	516
25	H	Nb_2O_5	2.634	142.674	516
26	L	SiO_2	0.269	23.283	516
27	H	Nb_2O_5	2.51	135.937	516
28	L	SiO_2	0.325	28.224	516
29	H	Nb_2O_5	2.198	119.025	516
30	L	SiO_2	0.355	30.793	516
31	H	Nb_2O_5	2.528	136.921	516
32	L	SiO_2	2.297	199.149	516
33	H	Nb_2O_5	0.502	27.212	516
34	L	SiO_2	2.088	181.022	516
35	H	Nb_2O_5	5.076	274.907	516
36	L	SiO_2	4.035	349.882	516
37	H	Nb_2O_5	3.815	206.612	516
38	L	SiO_2	0.342	29.68	516

39	H	Nb_2O_5	2.247	121.669	516
40	L	SiO_2	1.909	165.51	516
41	H	Nb_2O_5	1.884	102.023	516
42	L	SiO_2	3.479	301.64	516
43	H	Nb_2O_5	1.659	89.871	516
44	L	SiO_2	0.709	61.447	516
45	H	Nb_2O_5	2.144	116.122	516
46	L	SiO_2	1.685	146.136	516
47	H	Nb_2O_5	2.33	126.216	516
48	L	SiO_2	0.419	36.338	516
49	H	Nb_2O_5	2.317	125.47	516
50	L	SiO_2	0.438	37.97	516
51	H	Nb_2O_5	6.34	343.391	516
52	L	SiO_2	1.194	103.567	516
53	H	Nb_2O_5	1.898	102.798	516
54	L	SiO_2	1.266	109.747	516
55	H	Nb_2O_5	1.816	98.332	516
56	L	SiO_2	0.303	26.301	516
57	H	Nb_2O_5	1.875	101.566	516
58	L	SiO_2	1.582	137.217	516
59	H	Nb_2O_5	0.883	47.829	516
60	L	SiO_2	1.793	155.507	516
61	H	Nb_2O_5	1.184	64.146	516
62	L	SiO_2	1.567	135.898	516
63	H	Nb_2O_5	2.573	139.372	516
64	L	SiO_2	0.234	20.291	516
65	H	Nb_2O_5	2.227	120.616	516
66	L	SiO_2	0.282	24.442	516
67	H	Nb_2O_5	5.266	285.218	516
68	L	SiO_2	0.28	24.294	516
69	H	Nb_2O_5	2.282	123.576	516
70	L	SiO_2	0.322	27.915	516
71	H	Nb_2O_5	3.256	176.333	516
72	L	SiO_2	0.272	23.563	516
73	H	Nb_2O_5	3.966	214.816	516
74	L	SiO_2	0.231	20	516
75	H	Nb_2O_5	0.513	27.774	516
76	L	SiO_2	0.231	20	516
77	H	Nb_2O_5	3.015	163.277	516
78	L	SiO_2	0.231	20	516
79	H	Nb_2O_5	2.326	125.986	516
80	L	SiO_2	0.292	25.326	516
81	H	Nb_2O_5	2.549	138.045	516
82	L	SiO_2	0.554	48.075	516
83	H	Nb_2O_5	2.39	129.438	516

84	L	SiO_2	0.445	38.579	516
85	H	Nb_2O_5	2.512	136.03	516
86	L	SiO_2	0.327	28.35	516
87	H	Nb_2O_5	2.534	137.221	516
88	L	SiO_2	0.231	20	516
89	H	Nb_2O_5	2.058	111.475	516
90	L	SiO_2	1.785	154.746	516
91	H	Nb_2O_5	8.956	485.041	516
92	L	SiO_2	0.512	44.391	516
93	H	Nb_2O_5	0.389	21.077	516
94	L	SiO_2	0.491	42.588	516
95	H	Nb_2O_5	4.625	250.46	516
96	L	SiO_2	0.231	20	516
97	H	Nb_2O_5	2.216	120.004	516
98	L	SiO_2	1.926	167.044	516
99	H	Nb_2O_5	1.601	86.734	516
100	L	SiO_2	0.785	68.068	516

1.9 OIC contest design

Layer	Index	Material	optical thickness	Physical thickness	Reference wavelength
1	H	Nb_2O_5_B	8.758	455.367	500
2	L	SiO_2_B	0.378	31.876	500
3	H	Nb_2O_5_B	0.608	31.624	500
4	L	SiO_2_B	0.468	39.436	500
5	H	Nb_2O_5_B	0.71	36.896	500
6	L	SiO_2_B	0.302	25.46	500
7	H	Nb_2O_5_B	3.115	161.965	500
8	L	SiO_2_B	0.237	20	500
9	H	Nb_2O_5_B	3.604	187.41	500
10	L	SiO_2_B	3.452	290.83	500
11	H	Nb_2O_5_B	0.385	20	500
12	L	SiO_2_B	3.085	259.957	500
13	H	Nb_2O_5_B	2.673	138.957	500
14	L	SiO_2_B	1.726	145.395	500
15	H	Nb_2O_5_B	0.593	30.849	500
16	L	SiO_2_B	0.237	20	500
17	H	Nb_2O_5_B	2.143	111.414	500
18	L	SiO_2_B	6.22	524.072	500
19	H	Nb_2O_5_B	1.549	80.551	500
20	L	SiO_2_B	0.237	20	500
21	H	Nb_2O_5_B	0.889	46.215	500
22	L	SiO_2_B	0.335	28.184	500

23	H	Nb_2O_5_B	3.339	173.619	500
24	L	SiO_2_B	0.992	83.574	500
25	H	Nb_2O_5_B	0.549	28.563	500
26	L	SiO_2_B	3.806	320.669	500
27	H	Nb_2O_5_B	3.037	157.901	500
28	L	SiO_2_B	2.197	185.124	500
29	H	Nb_2O_5_B	1.479	76.908	500
30	L	SiO_2_B	0.237	20	500
31	H	Nb_2O_5_B	1.231	63.997	500
32	L	SiO_2_B	1.17	98.581	500
33	H	Nb_2O_5_B	2.431	126.408	500
34	L	SiO_2_B	2.91	245.208	500
35	H	Nb_2O_5_B	0.956	49.71	500
36	L	SiO_2_B	1.174	98.945	500
37	H	Nb_2O_5_B	0.385	20	500
38	L	SiO_2_B	0.961	80.944	500
39	H	Nb_2O_5_B	2.504	130.2	500
40	L	SiO_2_B	4.829	406.891	500
41	H	Nb_2O_5_B	3.215	167.17	500
42	L	SiO_2_B	1.153	97.182	500
43	H	Nb_2O_5_B	3.719	193.34	500
44	L	SiO_2_B	0.864	72.831	500
45	H	Nb_2O_5_B	1.163	60.453	500
46	L	SiO_2_B	0.312	26.295	500
47	H	Nb_2O_5_B	7.927	412.158	500
48	L	SiO_2_B	0.312	26.268	500
49	H	Nb_2O_5_B	0.606	31.528	500
50	L	SiO_2_B	0.578	48.733	500
51	H	Nb_2O_5_B	1.256	65.293	500
52	L	SiO_2_B	0.654	55.107	500
53	H	Nb_2O_5_B	0.55	28.572	500
54	L	SiO_2_B	2.195	184.927	500
55	H	Nb_2O_5_B	9.199	478.279	500
56	L	SiO_2_B	2.417	203.609	500
57	H	Nb_2O_5_B	0.41	21.33	500
58	L	SiO_2_B	0.391	32.943	500
59	H	Nb_2O_5_B	2.307	119.974	500
60	L	SiO_2_B	0.329	27.7	500
61	H	Nb_2O_5_B	6.329	329.082	500
62	L	SiO_2_B	0.24	20.197	500
63	H	Nb_2O_5_B	1.005	52.275	500
64	L	SiO_2_B	0.237	20	500
65	H	Nb_2O_5_B	2.595	134.925	500
66	L	SiO_2_B	0.253	21.351	500

67	H	Nb_2O_5_B	3.332	173.222	500
68	L	SiO_2_B	1.051	88.512	500

1.10 D65 compensator filter

Layer	Index	Material	optical thickness	Physical thickness	Reference wavelength
1	L	SiO_2	1.661	205.419	733
2	H	Nb_2O_5	0.124	9.939	733
3	L	SiO_2	0.321	39.652	733
4	H	Nb_2O_5	0.475	38.026	733
5	L	SiO_2	0.162	19.973	733
6	H	Nb_2O_5	0.408	32.624	733
7	L	SiO_2	1.393	172.218	733
8	H	Nb_2O_5	1.285	102.764	733
9	L	SiO_2	1.328	164.22	733
10	H	Nb_2O_5	1.295	103.6	733
11	L	SiO_2	1.295	160.141	733
12	H	Nb_2O_5	1.189	95.094	733
13	L	SiO_2	1.248	154.293	733
14	H	Nb_2O_5	1.169	93.465	733
15	L	SiO_2	1.34	165.758	733
16	H	Nb_2O_5	1.224	97.918	733
17	L	SiO_2	1.305	161.415	733
18	H	Nb_2O_5	1.175	93.975	733
19	L	SiO_2	1.163	143.786	733
20	H	Nb_2O_5	1.254	100.3	733
21	L	SiO_2	1.122	138.772	733
22	H	Nb_2O_5	3.724	297.857	733
23	L	SiO_2	0.162	20.041	733
24	H	Nb_2O_5	0.328	26.25	733
25	L	SiO2	1.208	149.412	733
26	H	Nb2O5	0.525	41.965	733
27	L	SiO_2	0.576	71.179	733
28	H	Nb_2O_5	0.746	59.703	733
29	L	SiO_2	4.106	507.766	733
30	H	Nb_2O_5	0.29	23.165	733
31	L	SiO_2	0.252	31.183	733
32	H	Nb_2O_5	0.253	20.205	733
33	L	SiO_2	2.214	273.755	733
34	H	Nb_2O_5	0.263	21.003	733
35	L	SiO_2	0.271	33.574	733
36	H	Nb_2O_5	1.212	96.906	733
37	L	SiO_2	0.654	80.82	733

Appendix 2 – Details about the refractive indices

In this appendix we have gathered the data about the refractive index dispersion used during this thesis. The _B marked indexes are from experiments conducted at Bühler in Alzenau.

Nb_2O_5			SiO_2			HfO_2		
Wavelength	n	k	Wavelength	n	k	Wavelength	n	k
350	2.759	0.018263	350	1.499	0.00	350	2.142	0.00010
372	2.629	0.002958	372	1.497	0.00	370	2.127	0.00009
398	2.546	0.000342	398	1.495	0.00	398	2.110	0.000083
418	2.502	0.000084	418	1.493	0.00	418	2.100	0.000062
444	2.458	0.000016	444	1.491	0.00	444	2.089	0.000043
492	2.402	1.00E-06	492	1.489	0.00	492	2.074	0.000025
540	2.365	0.00	540	1.487	0.00	540	2.063	0.000016
586	2.339	0.00	586	1.485	0.00	586	2.055	0.000012
666	2.309	0.00	666	1.483	0.00	668	2.045	0.000007
754	2.287	0.00	754	1.481	0.00	754	2.037	0.000005
836	2.273	0.00	836	1.480	0.00	836	2.032	0.000004
910	2.264	0.00	910	1.480	0.00	910	2.029	0.000003
1038	2.252	0.00	1038	1.479	0.00	1038	2.025	0.000002
1104	2.248	0.00	1104	1.478	0.00	1104	2.024	0.000002
1250	2.241	0.00	1250	1.478	0.00	1250	2.021	0.000002
1510	2.233	0.00	1510	1.477	0.00	1510	2.018	0.000001

Nb_2O_5_B			SiO_2_B		
Wavelength	n	k	Wavelength	n	k
351	2.712	0.021355	351	1.562	0.00
373	2.629	0.002595	373	1.555	0.00
397	2.561	0.000352	397	1.549	0.00
421	2.509	0.000060	421	1.544	0.00
445	2.469	0.000012	445	1.540	0.00
469	2.437	0.000003	469	1.536	0.00
492	2.411	0.000001	492	1.533	0.00
540	2.374	0.000000	540	1.528	0.00
585	2.349	0.000000	585	1.525	0.00
666	2.320	0.000000	666	1.520	0.00
710	2.309	0.000000	710	1.518	0.00
801	2.294	0.000000	801	1.515	0.00
1040	2.274	0.000000	1004	1.511	0.00
1102	2.272	0.000000	1040	1.510	0.00
1350	2.265	0.000000	1102	1.509	0.00
1503	2.262	0.000000	1200	1.508	0.00

D263 glass			Fused silica glass		
Wavelength	n	k	Wavelength	n	k
351	1.561860	0.00	350	1.476891	0.00
373	1.555179	0.00	373	1.473411	0.00
397	1.549120	0.00	397	1.470447	0.00
421	1.544068	0.00	422	1.467908	0.00
445	1.539810	0.00	445	1.465951	0.00
469	1.536190	0.00	469	1.464213	0.00
492	1.533205	0.00	492	1.46278	0.00
540	1.528160	0.00	540	1.460344	0.00
585	1.524512	0.00	586	1.458519	0.00
666	1.519713	0.00	666	1.456113	0.00
710	1.517766	0.00	710	1.455068	0.00
801	1.514710	0.00	801	1.4533	0.00
1004	1.510637	0.00	1005	1.450354	0.00
1040	1.510152	0.00	1044	1.449873	0.00
1102	1.509425	0.00	1105	1.449145	0.00
1200	1.508497	0.00	1200	1.44805	0.00

Appendix 3 – Designs of Fabry-Perot filters

In this appendix, we will examine different Fabry-Perot designs that could be used as a basis for producing the narrow bandpass filter specified in chapter 3.

In the case of Fabry-Perot filters, the width of the filter can be modified by the reflectivity of the mirrors (number of layers in the mirrors), or by the interference order (the optical thickness of the cavity). We can therefore show that it is possible to define several filter designs with similar performance and with very different total thickness and number of layers.

Since only the high index layers are associated with transmittance losses due to absorption, it is in our interest to minimize this effect, even if it means compensating by a higher interference order to maintain a similar bandwidth (for a low index cavity). However, we cannot reduce the reflectivity of the mirrors too much to maintain the low transmittance required for the filter blocking band. Thus, we proposed different formulae with equivalent bandwidth that have a very different response when considering absorption. The increase in the interference order of the cavity, in addition to the significantly larger total thickness, can also lead to the appearance of new transmission bands associated with harmonic peaks in the rejection band. Since the wavelength range of the specifications is wide, additional blocking mirrors on both sides of the filter will be required to ensure the low transmittance outside the transmittance band. This means that the additional transmittance bands for designs with thick cavities are not an issue because they will be blocked by the extra mirrors.

The width of the filter is the starting point for the designs. It determines the edge stiffness and therefore the number of cavities. We started the study of Fabry-Perot filters with 5-cavity designs, and analyzed which designs meet the specifications.

$$Silica\ \text{M13 2L M13 L M15 4L M15 L M15 6L M15 L M15 4L M15 L M13 2L M13}\ Silica \quad (A3.1)$$

$$Silica\ \text{M11 10L M11 L M13 12L M13 L M13 16L M13 L M13 12L M13 L M11 10L M11}\ Silica \quad (A3.2)$$

$$Silica\ \text{M9 20L M9 L M11 30L M11 L M11 40L M11 L M11 30L M11 L M9 20L M9}\ Silica \quad (A3.3)$$

The first designs considered are represented in Eq.A3.1-3. Although the cavities are not equal, there is a symmetry toward the center of the design to secure a flat transmission in the bandpass region. Moving from the first to the last design, we start with cavities with thickness of 2L, 4L,

6L, to cavities with thickness of 10L, 12L, 16L and finally to 20L, 30L, 40L. By reducing the number of mirror layers and increasing the thickness of the cavities, we reduce the number of layers from 151 to 131 and then to 111. On the other hand, this apparent simplification of the stack is accompanied by an increase in the total thickness from 8.4 to 9.8, then to 13.5 μm, an overall increase in thickness of 40%.

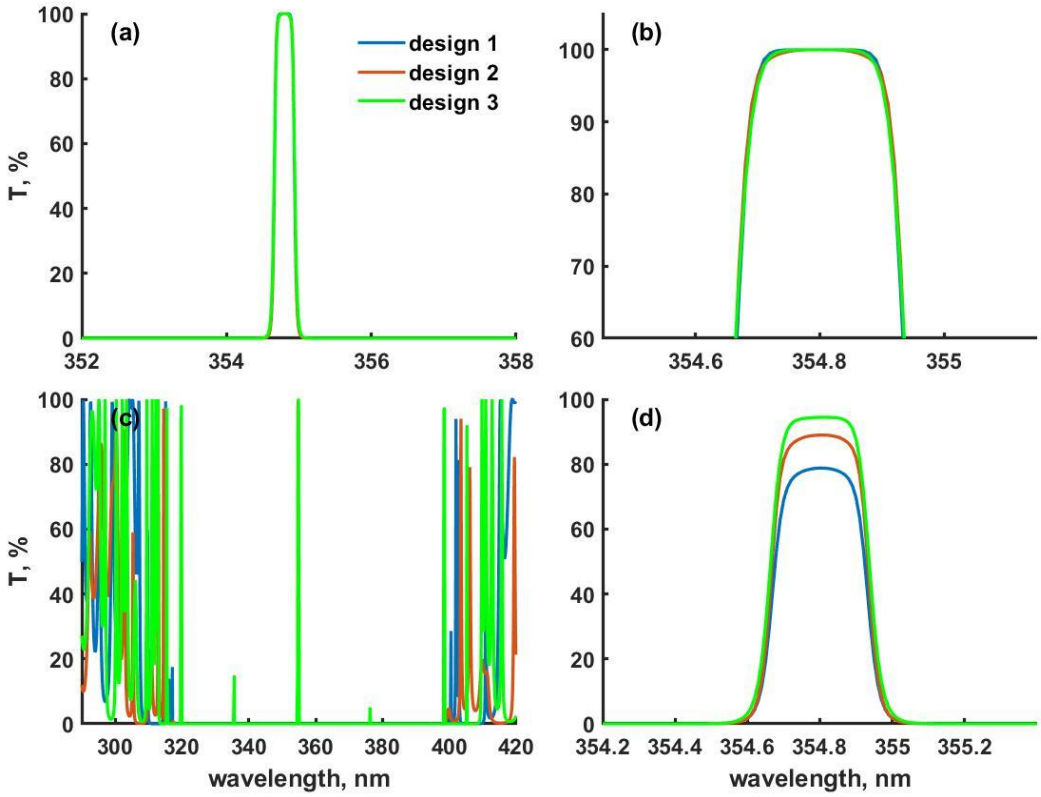

Figure A3-1 Transmittance of the 3 different 5-cavity designs (a), (b) and (c) if absorption is not considered, (d) – assuming absorption only in high index layers.

We have plotted the spectral performance of the three designs in Fig.A3-1. They are very similar although the number of layers and the total thickness vary significantly. In Fig.A3-1 (b) we can see that there is negligible difference in the response at the top of filter and that the FWHM is identical for all three formulae. As can be seen in Fig.A3-1 (c), with the design formula from Eq.A3.3, the additional blocking mirrors must be spectrally wider than those in the first two formulas to meet the specified blocking range. The difference between the designs becomes prominent when the actual value of k is considered. We have plotted in Fig.A3-1 (d) the effect of

the extinction coefficient for the different Fabry-Perot formulae. If absorption is taken into account, the first design no longer meets the specification because the maximum transmittance is too low, while other two designs are less affected.

5-cavity designs allow for filters with steep sides and a nearly rectangular shape, but with a wider bandwidth. It is also possible to meet the specification with more triangular shape filters, i.e. with a smaller number of cavities, which can lead to a reduction in the total number of layers and the total thickness. However, in this case, the full width at half maximum must be decreased. Once again, 3 designs with 3 cavities were considered. All of them have almost equivalent spectral performance, again with increasing interference orders corresponding to the decrease of the number of layers in the mirrors.

$$Silica\ \text{M17 2L M17 L M17 4L M17 L M17 2L M17}\ Silica \qquad (A3.4)$$

$$Silica\ \text{M15 8L M15 L M15 12L M15 L M15 8L M15}\ \ Silica \qquad (A3.5)$$

$$Silica\ \text{M13 20L M13 L M13 30L M13 L M13 20L M13}\ \ Silica \qquad (A3.6)$$

The designs in Eq.A3.4-6 are symmetrical, the mirrors are the same for the 3 cavities, only the interference orders vary. As for the thickness of the cavities, we must increase the thickness from 4L to 12L to 30L to maintain the performance while reducing the number of layers in the mirrors. The total number of layers can be reduced from 107 to 95 then to 83, but the thickness of the stack is again increased from 5.7 to 6.2 then to 8.1 μm. Although the sides of the filters are now less steep, they still meet the specifications for maximum width and for transmittance levels outside the transmittance band. From a production point of view, we would prefer a design with fewer cavities, as optical monitoring of the cavity layers is difficult (as discussed in chapter 3).

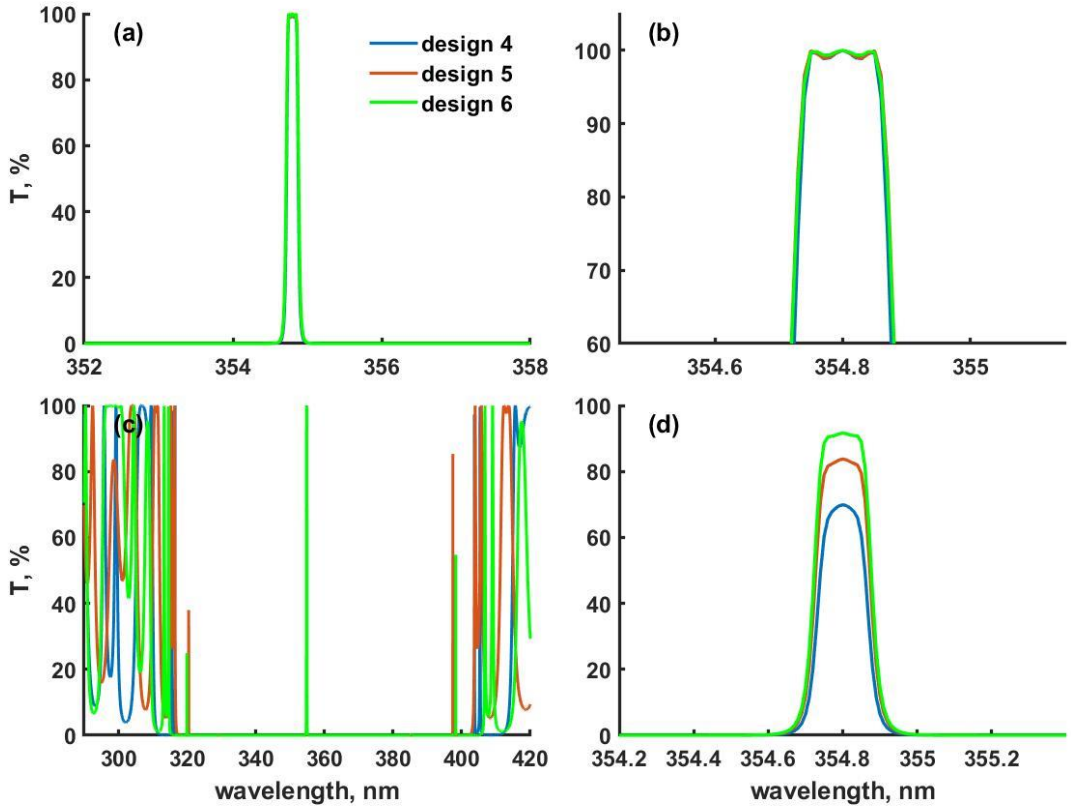

Figure A3-2 Spectral performances of the 3 different 3-cavity designs (a), (b) and (c) if absorption is not considered, (d) – assuming absorption in high index layers.

We have plotted in Fig.A3-2 (a-c) the spectral transmittance for the 3 designs. They are all similar and as can be seen in Fig.A3-3 (b), the top of the filter bandpass region has small oscillations for these designs. The filters with these designs are twice as narrow compared to the 5-cavity designs. In Fig.A3-2 (b) we cannot see the additional transmittance bands without significant magnification, but they should appear as the number of mirror layers decreases. The width of the additional blocking mirrors must be defined using the dispersion data, because the transmittance bands outside the reflective region depend on the dispersion of the refractive index. Again, we want to see how these designs compare to each other when absorption in the high index layers is present, and a similar change in performance to the 5-cavity designs can be observed in Fig.A3-2 (d). As with the 5-cavity designs, the number of layers in the mirrors strongly influences the total transmittance when absorption is taken into account. In addition to

the loss of maximum transmittance, the shape of the top of the filter is also changed. The top of the filter seems to be ‘rounded’.

To conclude the theoretical study, an intermediate 4-cavity filter design is also considered. Once again, three formulas with increased cavity thickness and reduced number of layers in the mirrors are constructed.

$$Silica\ \text{M13 6L M13 L M17 2L M17 L M17 2L M17 L M13 6L M13}\ Silica \qquad (A3.7)$$

$$Silica\ \text{M13 6L M13 L M15 8L M15 L M15 8L M15 L M13 6L M13}\ Silica \qquad (A3.8)$$

$$Silica\ \text{M11 16L M11 L M13 22L M13 L M13 22L M13 L M11 16L M11}\ Silica \qquad (A3.9)$$

Compared to the 3-cavity designs, the mirrors no longer have the same number of layers in the formulas (Eq.A3.7-9). However, the symmetry towards the center is preserved. The thicknesses of the cavity pair increases from 6L and 2L to 6L and 8L and to 16L and 22L. The number of layers decreases from 127 to 119 to 103, but the thickness of the stack increases again from 7.1 to 7.4 to 9.4 μm.

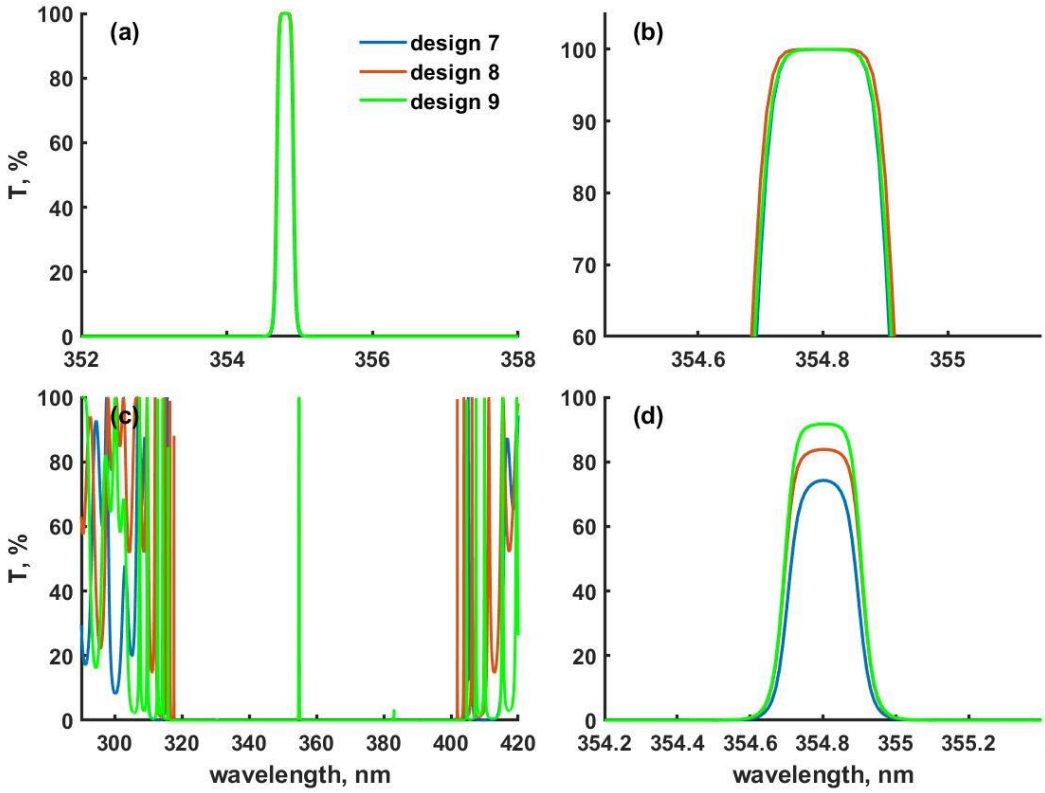

Figure A3-3 Spectral performances of the 3 different 4-cavity designs (a), (b) and (c) if absorption is not considered, (d) – assuming absorption in high index layers.

The four-cavity filter lies between the 3 and 5-cavity designs, also with respect to spectral performance. The spectral performance of the three four cavity designs is again comparable to each other Fig.A3-3 (a-c), additional transmittance bands are again expected for the 9th design with thicker cavities. Compared to the 3-cavity design, the top of the transmittance band is flatter. In Fig.A3-3 (c), we see that the rejection band is similar to that of the 3 and 5-cavity designs. The influence of the absorption in the high index layers are similar to that of the 3 and 5 cavities designs. The designs with a lower reflectivity in the mirrors and a higher interference order are less affected by potential losses due to the extinction coefficient.

As can be seen in Fig.A3-3 (d), the shape of the top of filter is less affected compared to the 3-cavity design, but absorption will *round* the top of the filter in all cases.

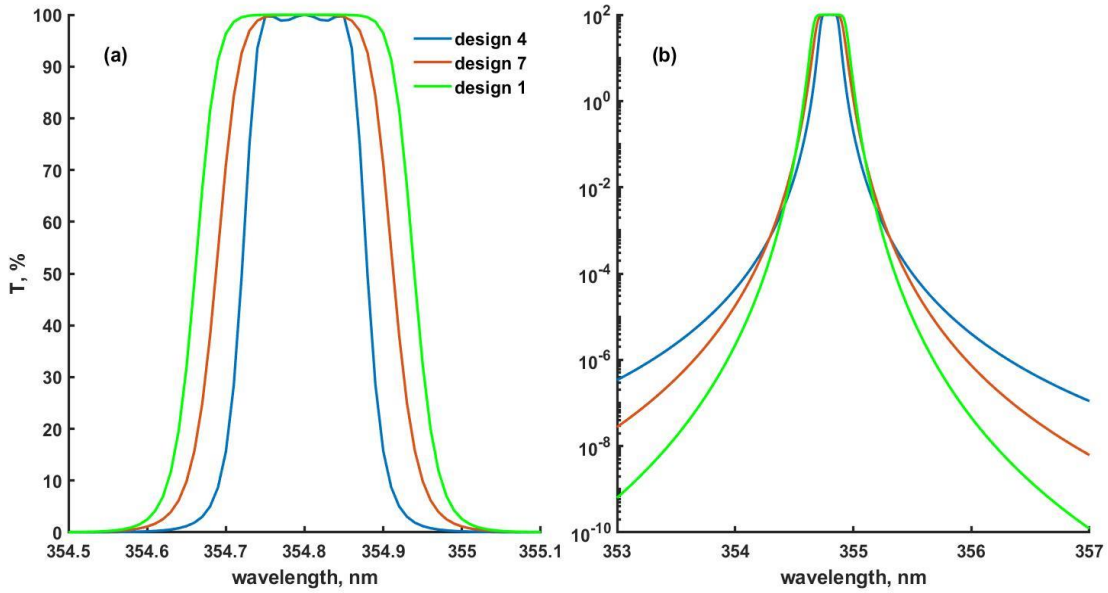

Figure A3-4 Comparison of spectral performance of designs with different numbers of cavities, (a) linear scale, (b) in log scale.

Comparing similar designs with different number of cavities, it can be seen that the by increasing the number of cavities, the sides of the filter become steeper. This is highlighted in Fig.A3-4 (b) where the filters are plotted in logarithmic scale. For all designs, the transmittance outside the transmittance band is low enough to meet the specifications.

In table A3-1, we have grouped all the main parameters regarding the designs.

number of cavities	design	number of layers	total thickness, μm
3	A3.4	107	5.7
	A3.5	95	6.2
	A3.6	83	8.1
4	A3.7	127	7.1
	A3.8	119	7.4
	A3.9	103	9.4
5	A3.1	151	8.4
	A3.2	131	9.8
	A3.3	111	13.5

Table A3-2 Comparison of designs from theoretical study.

The final choice of the design should be made taking into account the monitoring possibilities.

Appendix 4 – Details about monitoring strategies

In this appendix, detailed information about the monitoring strategies that were used for the filters demonstrated in this thesis are gathered. The _B marked indexes are from experiments conducted at Bühler in Alzenau.

4.1 Beamsplitter

				Polychromatic strategies			
Layer	Material	thickness	Monitoring method	Standard strategy	MF2	MF3	MF4
				Wavelengths			
1	Nb_2O_5	20.149	Monochromatic	595	603	603	603
2	SiO_2	67.874	Monochromatic	595	571	552	561
3	Nb_2O_5	44.252	Monochromatic	595	567	575	575
4	SiO_2	91.877	Monochromatic	595	569	562	566
5	Nb_2O_5	56.032	Monochromatic	595	626	745	694
6	SiO_2	135.716	Monochromatic	595	555	792	550
7	Nb_2O_5	61.047	Monochromatic	595	484	487	485
8	SiO_2	74.472	Monochromatic	595	628	677	628

			Broadband strategies					
Layer	Material	Thickness	Monitoring method	Wavelength range		Monitoring method	Wavelength range	
1	Nb_2O_5	20.149	Merit	400	900	Wideband	400	900
2	SiO_2	67.874	Merit	400	900	Wideband	400	900
3	Nb_2O_5	44.252	Merit	400	900	Wideband	400	900
4	SiO_2	91.877	Merit	400	900	Wideband	400	900
5	Nb_2O_5	56.032	Merit	400	900	Wideband	400	900
6	SiO_2	135.716	Merit	400	900	Wideband	400	900
7	Nb_2O_5	61.047	Merit	400	900	Wideband	400	900
8	SiO_2	74.472	Merit	400	900	Wideband	400	900

4.2 D65 filter

		Polychromatic strategy			Mixed merit strategy		
Layer	Material	Thickness	Monitoring Method	Wavelength	Monitoring method	Wavelength range	
1	SiO_2	205.388	Rate	733	Rate	--	
2	Nb_2O_5	9.952	Rate	585	Monochromatic	585	
3	SiO_2	39.626	Rate	435	Monochromatic	435	
4	Nb_2O_5	38.034	Monochromatic	422	Monochromatic	422	
5	SiO_2	20	Rate	422	Rate	--	
6	Nb_2O_5	32.603	Monochromatic	400	Merit	400	900
7	SiO_2	172.197	Monochromatic	724	Merit	400	900
8	Nb_2O_5	102.782	Monochromatic	701	Merit	400	900
9	SiO_2	164.172	Monochromatic	796	Merit	400	900
10	Nb_2O_5	103.622	Monochromatic	750	Merit	400	900
11	SiO_2	160.187	Monochromatic	812	Merit	400	900
12	Nb_2O_5	95.069	Monochromatic	765	Merit	400	900
13	SiO_2	154.331	Monochromatic	689	Merit	400	900
14	Nb_2O_5	93.479	Monochromatic	680	Merit	400	900
15	SiO_2	165.721	Monochromatic	723	Merit	400	900
16	Nb_2O_5	97.953	Monochromatic	711	Merit	400	900
17	SiO_2	161.413	Monochromatic	745	Merit	400	900
18	Nb_2O_5	93.989	Monochromatic	733	Merit	400	900
19	SiO_2	143.837	Monochromatic	670	Merit	400	900
20	Nb_2O_5	100.324	Monochromatic	673	Merit	400	900
21	SiO_2	138.73	Monochromatic	695	Merit	400	900
22	Nb_2O_5	297.882	Monochromatic	692	Merit	400	900
23	SiO_2	20	Rate	699	Merit	400	900
24	Nb_2O_5	26.231	Monochromatic	513	Merit	400	900
25	SiO_2	149.429	Monochromatic	677	Merit	400	900
26	Nb_2O_5	41.991	Monochromatic	750	Merit	400	900
27	SiO_2	71.251	Monochromatic	794	Merit	400	900
28	Nb_2O_5	59.742	Monochromatic	697	Merit	400	900
29	SiO_2	507.768	Monochromatic	708	Merit	400	900
30	Nb_2O_5	23.166	Monochromatic	608	Merit	400	900
31	SiO_2	31.129	Monochromatic	490	Merit	400	900
32	Nb_2O_5	20.268	Monochromatic	662	Merit	400	900
33	SiO_2	273.691	Monochromatic	593	Merit	400	900
34	Nb_2O_5	20.996	Monochromatic	585	Merit	400	900
35	SiO_2	33.498	Monochromatic	619	Merit	400	900
36	Nb_2O_5	96.901	Monochromatic	604	Merit	400	900
37	SiO_2	80.759	Monochromatic	609	Merit	400	900

Mixed Wideband strategy

layer	Material	Thickness	Monitoring Method	Wavelength range	
1	SiO_2	205.388	Rate	--	
2	Nb_2O_5	9.952	Monochromatic	585	
3	SiO_2	39.626	Monochromatic	435	
4	Nb_2O_5	38.034	Monochromatic	422	
5	SiO_2	20	Rate	--	
6	Nb_2O_5	32.603	Wideband	400	900
7	SiO_2	172.197	Wideband	400	900
8	Nb_2O_5	102.782	Wideband	400	900
9	SiO_2	164.172	Wideband	400	900
10	Nb_2O_5	103.622	Wideband	400	900
11	SiO_2	160.187	Wideband	400	900
12	Nb_2O_5	95.069	Wideband	400	900
13	SiO_2	154.331	Wideband	400	900
14	Nb_2O_5	93.479	Wideband	400	900
15	SiO_2	165.721	Wideband	400	900
16	Nb_2O_5	97.953	Wideband	400	900
17	SiO_2	161.413	Wideband	400	900
18	Nb_2O_5	93.989	Wideband	400	900
19	SiO_2	143.837	Wideband	400	900
20	Nb_2O_5	100.324	Wideband	400	900
21	SiO_2	138.73	Wideband	400	900
22	Nb_2O_5	297.882	Wideband	400	900
23	SiO_2	20	Wideband	400	900
24	Nb_2O_5	26.231	Wideband	400	900
25	SiO_2	149.429	Wideband	400	900
26	Nb_2O_5	41.991	Wideband	400	900
27	SiO_2	71.251	Wideband	400	900
28	Nb_2O_5	59.742	Wideband	400	900
29	SiO_2	507.768	Wideband	400	900
30	Nb_2O_5	23.166	Wideband	400	900
31	SiO_2	31.129	Wideband	400	900
32	Nb_2O_5	20.268	Wideband	400	900
33	SiO_2	273.691	Wideband	400	900
34	Nb_2O_5	20.996	Wideband	400	900
35	SiO_2	33.498	Wideband	400	900
36	Nb_2O_5	96.901	Wideband	400	900
37	SiO_2	80.759	Wideband	400	900

Full wideband strategy

layer	Material	Thickness	Monitoring Method	wavelength range	
1	SiO_2	205.388	Rate	--	
2	Nb_2O_5	9.952	Wideband	400	700
3	SiO_2	39.626	Wideband	400	700
4	Nb_2O_5	38.034	Wideband	400	700
5	SiO_2	20	Rate	--	
6	Nb_2O_5	32.603	Wideband	400	900
7	SiO_2	172.197	Wideband	400	900
8	Nb_2O_5	102.782	Wideband	400	900
9	SiO_2	164.172	Wideband	400	900
10	Nb_2O_5	103.622	Wideband	400	900
11	SiO_2	160.187	Wideband	400	900
12	Nb_2O_5	95.069	Wideband	400	900
13	SiO_2	154.331	Wideband	400	900
14	Nb_2O_5	93.479	Wideband	400	900
15	SiO_2	165.721	Wideband	400	900
16	Nb_2O_5	97.953	Wideband	400	900
17	SiO_2	161.413	Wideband	400	900
18	Nb_2O_5	93.989	Wideband	400	900
19	SiO_2	143.837	Wideband	400	900
20	Nb_2O_5	100.324	Wideband	400	900
21	SiO_2	138.73	Wideband	400	900
22	Nb_2O_5	297.882	Wideband	400	900
23	SiO_2	20	Wideband	400	900
24	Nb_2O_5	26.231	Wideband	400	900
25	SiO_2	149.429	Wideband	400	900
26	Nb_2O_5	41.991	Wideband	400	900
27	SiO_2	71.251	Wideband	400	900
28	Nb_2O_5	59.742	Wideband	400	900
29	SiO_2	507.768	Wideband	400	900
30	Nb_2O_5	23.166	Wideband	400	900
31	SiO_2	31.129	Wideband	400	900
32	Nb_2O_5	20.268	Wideband	400	900
33	SiO_2	273.691	Wideband	400	900
34	Nb_2O_5	20.996	Wideband	400	900
35	SiO_2	33.498	Wideband	400	900
36	Nb_2O_5	96.901	Wideband	400	900

37	SiO_2	80.759	Wideband		400	900

4.3 Notch filter

layer	Material	Thickness	Witness glass	Monitoring method	Wavelength
1	Nb_2O_5_B	20.812		Monochromatic	603
2	SiO_2_B	18.875		Monochromatic	655
3	Nb_2O_5_B	66.904		Monochromatic	606
4	SiO_2_B	5.185		Rate	610
5	Nb_2O_5_B	73.107		Monochromatic	650
6	SiO_2_B	7.422		Rate	664
7	Nb_2O_5_B	135.194		Monochromatic	545
8	SiO_2_B	10.971		Monochromatic	557
9	Nb_2O_5_B	125.492		Monochromatic	566
10	SiO_2_B	5.085		Rate	571
11	Nb_2O_5_B	199.486	Witness glass 1	Monochromatic	532
12	SiO_2_B	8.981		Rate	537
13	Nb_2O_5_B	128.129		Monochromatic	548
14	SiO_2_B	13.207		Monochromatic	555
15	Nb_2O_5_B	148.187		Monochromatic	548
16	SiO_2_B	11.158		Monochromatic	585
17	Nb_2O_5_B	45.368		Monochromatic	586
18	SiO_2_B	20.264		Monochromatic	541
19	Nb_2O_5_B	127.397		Monochromatic	549
20	SiO_2_B	12.723		Monochromatic	555
21	Nb_2O_5_B	208.625		Monochromatic	539
22	SiO_2_B	7.602		Rate	542
23	Nb_2O_5_B	113.985		Monochromatic	541
24	SiO_2_B	9.314		Rate	544
25	Nb_2O_5_B	118.598		Monochromatic	657
26	SiO_2_B	10.527		Monochromatic	667
27	Nb_2O_5_B	209.68		Monochromatic	697
28	SiO_2_B	12.584	Witness glass 2	Monochromatic	570
29	Nb_2O_5_B	122.165		Monochromatic	570
30	SiO_2_B	12.888		Monochromatic	580
31	Nb_2O_5_B	209.7		Monochromatic	547
32	SiO_2_B	13.552		Monochromatic	553
33	Nb_2O_5_B	125.094		Monochromatic	559
34	SiO_2_B	10.206		Monochromatic	564

35	Nb_2O_5_B	84.575		Monochromatic	538
36	SiO_2_B	6.795		Rate	540
37	Nb_2O_5_B	126.937		Monochromatic	548
38	SiO_2_B	15.037		Monochromatic	554
39	Nb_2O_5_B	212.482		Monochromatic	540
40	SiO_2_B	14.991		Monochromatic	545
41	Nb_2O_5_B	120.604		Monochromatic	548
42	SiO_2_B	12.731		Monochromatic	552
43	Nb_2O_5_B	205.629		Monochromatic	537
44	SiO_2_B	14.845		Monochromatic	540
45	Nb_2O_5_B	122.317	Witness glass 3	Monochromatic	671
46	SiO_2_B	15.825		Monochromatic	686
47	Nb_2O_5_B	187.902		Monochromatic	662
48	SiO_2_B	5.085		Rate	671
49	Nb_2O_5_B	25.532		Monochromatic	719
50	SiO_2_B	13.152		Monochromatic	588
51	Nb_2O_5_B	104.287		Monochromatic	562
52	SiO_2_B	8.323		Rate	569
53	Nb_2O_5_B	115.638		Monochromatic	561
54	SiO_2_B	13.162		Monochromatic	569
55	Nb_2O_5_B	209.848		Monochromatic	613
56	SiO_2_B	15.217		Monochromatic	549
57	Nb_2O_5_B	121.201		Monochromatic	552
58	SiO_2_B	14.77		Monochromatic	559
59	Nb_2O_5_B	208.441		Monochromatic	538
60	SiO_2_B	12.58		Monochromatic	542
61	Nb_2O_5_B	116.161		Monochromatic	543
62	SiO_2_B	10.426		Monochromatic	547
63	Nb_2O_5_B	112.555		Monochromatic	545
64	SiO_2_B	10.922		Monochromatic	549
65	Nb_2O_5_B	210.152	Witness glass 4	Monochromatic	561
66	SiO_2_B	15.396		Monochromatic	583
67	Nb_2O_5_B	122.862		Monochromatic	578
68	SiO_2_B	13.804		Monochromatic	594
69	Nb_2O_5_B	205.61		Monochromatic	636
70	SiO_2_B	10.405		Monochromatic	549
71	Nb_2O_5_B	118.589		Monochromatic	549
72	SiO_2_B	12.558		Monochromatic	557
73	Nb_2O_5_B	117.168		Monochromatic	555
74	SiO_2_B	8.118		Rate	560

75	Nb_2O_5_B	203.151		Monochromatic	664
76	SiO_2_B	13.611		Monochromatic	541
77	Nb_2O_5_B	125.713		Monochromatic	548
78	SiO_2_B	18.604		Monochromatic	556
79	Nb_2O_5_B	142.134		Monochromatic	572
80	SiO_2_B	25.393		Monochromatic	581
81	Nb_2O_5_B	32.515		Monochromatic	626
82	SiO_2_B	39.458		Monochromatic	546
83	Nb_2O_5_B	124.829		Monochromatic	552
84	SiO_2_B	19.609		Monochromatic	558
85	Nb_2O_5_B	143.183	Witness glass 5	Monochromatic	575
86	SiO_2_B	23.312		Monochromatic	789
87	Nb_2O_5_B	32.59		Monochromatic	679
88	SiO_2_B	32.153		Monochromatic	577
89	Nb_2O_5_B	124.25		Monochromatic	581
90	SiO_2_B	12.295		Monochromatic	591
91	Nb_2O_5_B	302.503		Monochromatic	598
92	SiO_2_B	21.446		Monochromatic	540
93	Nb_2O_5_B	31.143		Monochromatic	533
94	SiO_2_B	18.332		Monochromatic	580
95	Nb_2O_5_B	198.518		Monochromatic	546
96	SiO_2_B	12.256		Monochromatic	552
97	Nb_2O_5_B	29.356		Monochromatic	574
98	SiO_2_B	88.608		Monochromatic	578

4.4 Bonne Mère

			3 witness glass strategy			4 witness glass strategy		
layer	Material	Thickness	Witness glass	Monitoring Method	Wavelength	Witness glass	Monitoring Method	Wavelength
1	Nb_2O_5	22.855		Rate	606		Rate	606
2	SiO_2	28.57		Rate	729		Rate	729
3	Nb_2O_5	51.31		Monochromatic	466		Monochromatic	466
4	SiO_2	22.787		Rate	620		Rate	620
5	Nb_2O_5	134.061		Monochromatic	623		Monochromatic	623
6	SiO_2	22.865	Witness glass 1	Rate	646	Witness glass 1	Rate	646
7	Nb_2O_5	131.65		Monochromatic	632		Monochromatic	632
8	SiO_2	177.399		Monochromatic	727		Monochromatic	727
9	Nb_2O_5	58.616		Monochromatic	664		Monochromatic	664
10	SiO_2	26.785		Rate	677		Rate	677
11	Nb_2O_5	20		Monochromatic	402		Monochromatic	402

12	SiO_2	244.297		Monochromatic	714	Monochromatic	714
13	Nb_2O_5	34.587		Monochromatic	695	Monochromatic	695
14	SiO_2	20		Rate	713	Rate	713
15	Nb_2O_5	49.86		Monochromatic	590	Monochromatic	590
16	SiO_2	67.217		Monochromatic	572	Monochromatic	572
17	Nb_2O_5	20		Monochromatic	606	Monochromatic	606
18	SiO_2	55.156		Monochromatic	722	Monochromatic	722
19	Nb_2O_5	129.625		Monochromatic	684	Monochromatic	684
20	SiO_2	31.156		Rate	699	Rate	715
21	Nb_2O_5	121.733		Monochromatic	578	Monochromatic	578
22	SiO_2	178.941		Monochromatic	571	Monochromatic	571
23	Nb_2O_5	121.905		Monochromatic	725	Monochromatic	725
24	SiO_2	25.875		Rate	734	Rate	734
25	Nb_2O_5	142.674		Monochromatic	571	Monochromatic	571
26	SiO_2	23.283		Rate	598	Rate	598
27	Nb_2O_5	135.937		Monochromatic	582	Monochromatic	582
28	SiO_2	28.224		Rate	691	Rate	598
29	Nb_2O_5	119.025		Monochromatic	605	Monochromatic	605
30	SiO_2	30.793		Rate	613	Rate	599
31	Nb_2O_5	136.921		Monochromatic	596	Monochromatic	596
32	SiO_2	199.149		Monochromatic	596	Monochromatic	596
33	Nb_2O_5	27.212		Monochromatic	610	Monochromatic	610
34	SiO_2	181.022		Monochromatic	602	Monochromatic	602
35	Nb_2O_5	274.907		Monochromatic	588	Monochromatic	588
36	SiO_2	349.882		Monochromatic	804	Monochromatic	804
37	Nb_2O_5	206.612		Monochromatic	571	Monochromatic	571
38	SiO_2	29.68		Rate	587	Rate	484
39	Nb_2O_5	121.669		Monochromatic	585	Monochromatic	585
40	SiO_2	165.51		Monochromatic	685	Monochromatic	685
41	Nb_2O_5	102.023		Monochromatic	676	Monochromatic	676
42	SiO_2	301.64	Witness glass 2	Monochromatic	602	Monochromatic	602
43	Nb_2O_5	89.871		Monochromatic	572	Monochromatic	572
44	SiO_2	61.447		Monochromatic	567	Monochromatic	567
45	Nb_2O_5	116.122		Monochromatic	593	Monochromatic	593
46	SiO_2	146.136		Monochromatic	540	Monochromatic	540
47	Nb_2O_5	126.216		Monochromatic	669	Monochromatic	669
48	SiO_2	36.338		Monochromatic	568	Rate	568
49	Nb_2O_5	125.47		Monochromatic	567	Monochromatic	567
50	SiO_2	37.97		Monochromatic	579	Monochromatic	579
51	Nb_2O_5	343.391		Monochromatic	530	Monochromatic	530
52	SiO_2	103.567		Monochromatic	535	Monochromatic	535

53	Nb_2O_5	102.798		Monochromatic	590		Monochromatic	603
54	SiO_2	109.747		Monochromatic	624		Monochromatic	618
55	Nb_2O_5	98.332		Monochromatic	626		Monochromatic	610
56	SiO_2	26.301		Rate	627		Rate	424
57	Nb_2O_5	101.566		Monochromatic	598		Monochromatic	601
58	SiO_2	137.217		Monochromatic	658		Monochromatic	647
59	Nb_2O_5	47.829		Monochromatic	445		Monochromatic	804
60	SiO_2	155.507		Monochromatic	626		Monochromatic	637
61	Nb_2O_5	64.146		Monochromatic	579		Monochromatic	586
62	SiO_2	135.898		Monochromatic	660		Monochromatic	628
63	Nb_2O_5	139.372		Monochromatic	659		Monochromatic	644
64	SiO_2	20.291		Rate	660		Rate	664
65	Nb_2O_5	120.616		Monochromatic	645	Witness glass 3	Monochromatic	640
66	SiO_2	24.442		Rate	530		Rate	473
67	Nb_2O_5	285.218		Monochromatic	587		Monochromatic	600
68	SiO_2	24.294		Rate	604		Rate	459
69	Nb_2O_5	123.576		Monochromatic	671		Monochromatic	521
70	SiO_2	27.915		Rate	705		Rate	514
71	Nb_2O_5	176.333		Monochromatic	661		Monochromatic	634
72	SiO_2	23.563		Rate	550		Rate	509
73	Nb_2O_5	214.816		Monochromatic	776		Monochromatic	509
74	SiO_2	20		Rate	540		Rate	610
75	Nb_2O_5	27.774		Monochromatic	526		Monochromatic	518
76	SiO_2	20		Rate	586		Rate	536
77	Nb_2O_5	163.277		Monochromatic	583		Monochromatic	592
78	SiO_2	20		Rate	732		Rate	596
79	Nb_2O_5	125.986	Witness glass 3	Monochromatic	537		Monochromatic	525
80	SiO_2	25.326		Rate	551		Rate	522
81	Nb_2O_5	138.045		Monochromatic	566		Monochromatic	560
82	SiO_2	48.075		Monochromatic	562		Rate	485
83	Nb_2O_5	129.438		Monochromatic	640		Monochromatic	659
84	SiO_2	38.579		Rate	652		Rate	457
85	Nb_2O_5	136.03		Monochromatic	650	Witness glass 4	Monochromatic	694
86	SiO_2	28.35		Rate	630		Rate	443
87	Nb_2O_5	137.221		Monochromatic	630		Monochromatic	685
88	SiO_2	20		Rate	636		Rate	703
89	Nb_2O_5	111.475		Monochromatic	645		Monochromatic	652
90	SiO_2	154.746		Monochromatic	674		Monochromatic	704
91	Nb_2O_5	485.041		Monochromatic	580		Monochromatic	732
92	SiO_2	44.391		Monochromatic	575		Rate	762

93	Nb_2O_5	21.077	Monochromatic	652	Monochromatic	504
94	SiO_2	42.588	Monochromatic	677	Rate	676
95	Nb_2O_5	250.46	Monochromatic	662	Monochromatic	555
96	SiO_2	20	Rate	584	Rate	671
97	Nb_2O_5	120.004	Monochromatic	583	Monochromatic	576
98	SiO_2	167.044	Monochromatic	579	Monochromatic	732
99	Nb_2O_5	86.734	Monochromatic	674	Monochromatic	559
100	SiO_2	68.068	Monochromatic	669	Monochromatic	670

4.5 OIC contest design

Layer	Material	Thickness	Witness glass	Monitoring method	Wavelength range	
1	Nb_2O_5_B	455.367		Merit	400	900
2	SiO_2_B	31.876		Merit	400	900
3	Nb_2O_5_B	31.624		Merit	400	900
4	SiO_2_B	39.436		Merit	400	900
5	Nb_2O_5_B	36.896		Merit	400	900
6	SiO_2_B	25.46		Merit	400	900
7	Nb_2O_5_B	161.965		Merit	400	900
8	SiO_2_B	20		Merit	400	900
9	Nb_2O_5_B	187.41		Merit	400	900
10	SiO_2_B	290.83		Merit	400	900
11	Nb_2O_5_B	20		Merit	400	900
12	SiO_2_B	259.957	Witness glass 1	Merit	450	900
13	Nb_2O_5_B	138.957		Merit	450	900
14	SiO_2_B	145.395		Merit	450	900
15	Nb_2O_5_B	30.849		Merit	450	900
16	SiO_2_B	20		Rate	450	900
17	Nb_2O_5_B	111.414		Merit	450	900
18	SiO_2_B	524.072		Merit	450	900
19	Nb_2O_5_B	80.551		Merit	450	900
20	SiO_2_B	20		Rate	450	900
21	Nb_2O_5_B	46.215		Merit	450	900
22	SiO_2_B	28.184		Rate	450	900
23	Nb_2O_5_B	173.619		Merit	500	900
24	SiO_2_B	83.574		Merit	500	900
25	Nb_2O_5_B	28.563		Merit	500	900
26	SiO_2_B	320.669		Merit	520	900
27	Nb_2O_5_B	157.901		Merit	520	900

28	SiO_2_B	185.124	Merit	520	900
29	Nb_2O_5_B	76.908	Merit	520	900
30	SiO_2_B	20	Rate	520	900
31	Nb_2O_5_B	63.997	Merit	600	900
32	SiO_2_B	98.581	Merit	600	900
33	Nb_2O_5_B	126.408	Merit	600	900
34	SiO_2_B	245.208	Merit	600	900
35	Nb_2O_5_B	49.71	Merit	400	900
36	SiO_2_B	98.945	Merit	400	900
37	Nb_2O_5_B	20	Merit	400	900
38	SiO_2_B	80.944	Merit	400	900
39	Nb_2O_5_B	130.2	Merit	400	900
40	SiO_2_B	406.891	Merit	410	900
41	Nb_2O_5_B	167.17	Merit	410	900
42	SiO_2_B	97.182	Merit	410	900
43	Nb_2O_5_B	193.34	Merit	410	900
44	SiO_2_B	72.831	Merit	410	900
45	Nb_2O_5_B	60.453	Merit	410	900
46	SiO_2_B	26.295	Rate	500	900
47	Nb_2O_5_B	412.158	Merit	500	900
48	SiO_2_B	26.268	Rate	500	900
49	Nb_2O_5_B	31.528	Merit	500	900
50	SiO_2_B	48.733	Merit	500	900
51	Nb_2O_5_B	65.293	Merit	530	900
52	SiO_2_B	55.107	Merit	530	900
53	Nb_2O_5_B	28.572	Merit	530	900
54	SiO_2_B	184.927	Merit	530	900
55	Nb_2O_5_B	478.279	Merit	530	900
56	SiO_2_B	203.609	Merit	530	900
57	Nb_2O_5_B	21.33	Merit	530	900
58	SiO_2_B	32.943	Merit	530	900
59	Nb_2O_5_B	119.974	Merit	550	900
60	SiO_2_B	27.7	Rate	550	900
61	Nb_2O_5_B	329.082	Merit	550	900
62	SiO_2_B	20.197	rate	550	900
63	Nb_2O_5_B	52.275	Merit	550	900
64	SiO_2_B	20	rate	550	900
65	Nb_2O_5_B	134.925	Merit	550	900
66	SiO_2_B	21.351	rate	550	900
67	Nb_2O_5_B	173.222	Merit	610	900
68	SiO_2_B	88.512	Merit	610	900

Witness glass 2

Appendix 5 – GREAT project

This thesis is a part of the GREAT (Grating Reflectors Enabled laser Application and Training) project.

As the name of the project suggests the project deals with lasers systems where the building blocks are grating reflectors. The reason why one would like to replace the conventional mirrors with the grating reflectors (or grating waveguide structures -GWS) is that it is a powerful solution for the high-power laser beam tailoring (spectral, special beam shaping and polarization control). The GWS are combination of sub-wavelength gratings into a planar waveguide. Because the laser systems are complex, and in order to have complete control over all the included elements, 15 early-stage researchers (ESR's) are employed as Ph.D students to cover all the elements from design to manufacturing to implementation to characterization of the GWS for custom-build laser systems.

There are 8 universities and 7 industrial partners in the project (located in France, Finland, Germany, and United Kingdom). More information about the partners and the project can be found at http://itn-great.eu/.

My part in this project is to provide improved control over one part of the fabrication process of the GWS – the thickness control of the dielectric thin film coatings for the planar waveguides.

There are five applications for the GWS within the GREAT project:

- A1-A2 (application 1 and 2) Pulse compression for 1000 and 2000 nm wavelength ranges
- A3-A4 Spectral stabilization and wavelength multiplexing of high-power solid-state and diode lasers.
- A5 Radial and azimuthal polarization control (intra-cavity and extra-cavity application)

We will look in this appendix only at the dielectric designs that were deposited during this thesis. In this project, there are also designs with crystalline materials, fabricated by other ESR. The materials for the dielectric coatings were HfO_2 and Nb_2O_5 for the high index layers and SiO_2 for low index layers, substrates were fused silica and YAG depending on the design and application. Details about the designs are provided in the table A5-1. The coating designs are the property of the IFSW (University of Stuttgart).

	Design	High index material	Reference wavelength, nm	AOI, degrees	Number of layers	Substrate	Additional information
1	A1D3	HfO_2	1030	51.4	41	Silica	Thickness of last two layers SiO_2=110nm, HfO_2=256nm
2	A2D2	HfO_2	2050	55	41	Silica	Thickness of last two layers SiO_2=237nm, HfO_2=498nm
3	A3D1	Nb_2O_5	976	51.4	29	Silica	
4	A3D3	Nb_2O_5	976	61.74	28	Silica	
5	A4D1	Nb_2O_5	1030	56.3	27	Silica	Thickness of last two layers SiO_2=79nm, Nb_2O_5=88nm
6	A5D1	Nb_2O_5	1030	0	29	YAG	Thickness of last two layers SiO_2=40nm, Nb_2O_5=120nm
7	A5D3	Nb_2O_5	1030	0	12	Silica	Grating in substrate, 2-layer AR coating on backside
8	A5D5	Nb_2O_5	1030	0	29	Silica	Top Nb_2O_5 layer 570nm thick

Table A5-1 designs of the waveguides deposited for GREAT project.

The designs are mostly quarter-wave structures, meaning that the layers are quarter-wave thick at the reference wavelength for corresponding angle of incidence. The last layers are the ones facing the air, and the first is the one directly on substrate. In several designs the thicknesses of the last layers are altered (no longer quarter-wave), the gratings are then fabricated in these layers.

For each of the designs, a monitoring strategy was created. As already shown in chapter 5, broadband and monochromatic strategies were used to coat these mirrors. Therefore, several strategies for these designs were used. The strategies are listed below (Tab.A5-2 to Tab.A5-9) are not in the order of deposition runs but in order of the designs. For the monochromatic strategies, the wavelengths were selected manually. Initially one wavelength strategy was considered for all of the designs, however since the number of layers exceeds 20, it was not possible to find one satisfactory monitoring wavelength. Therefore, two wavelengths were selected, and in one case, monitoring by deposition rate for the last layers was performed. For the designs monitored by broadband methods, the wavelength range was reduced as the number of layers increased to avoid spectral resolution limits.

We have showed two examples of the performances of these designs in chapter 5. The spectral measurements of the coatings provided to the project partners who will later implement the gratings are in good agreement with theory.

One component (grating and coating) that has been manufactured at the moment of completing this thesis is the A5D3 design. The spectral performance is plotted in Fig.A5-1.

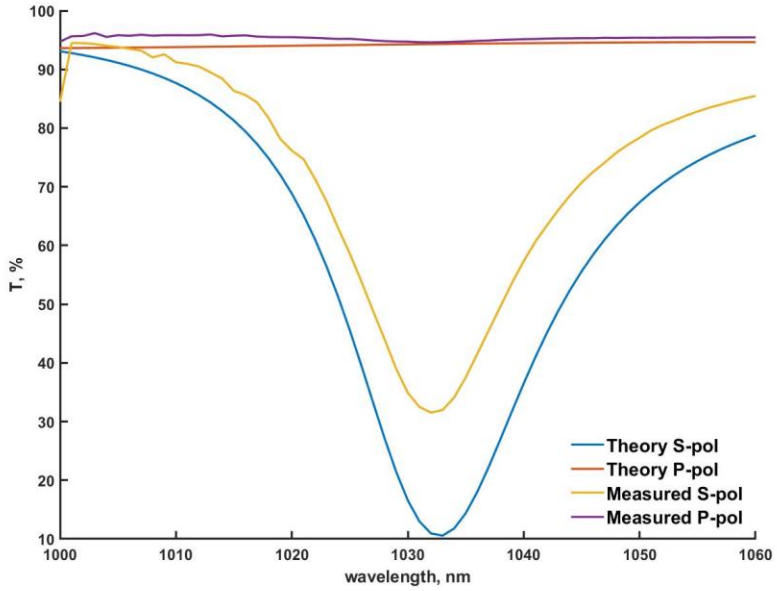

Figure A5-1 Measured and theoretical performance of the D5D3 component

As can be seen the match between theory and experiment is not perfect, there is slight shift in centering wavelength and the measured transmittance for the S polarized light is higher than the theoretical one. For this application the most important parameter is the transmittance difference between both polarizations, and first estimations show that it is sufficient.

Design	A1D3		
Layer	Material	Monitoring method	Monitoring wavelength
1	HfO_2	Monochromatic	1054
…	…	…	…
24	SiO_2	Monochromatic	1054
25	HfO_2	Monochromatic	1031
…	…	…	…
41	HfO_2	Monochromatic	1031

Table A5-2 Monitoring strategy for the A1D3 design

Design	A2D2		
Layer	Material	Monitoring method	Monitoring wavelength
1	HfO_2	Monochromatic	700
2	SiO_2	Monochromatic	700

3	HfO_2	Monochromatic	700
4	SiO_2	Monochromatic	1185
…	…	…	
41	HfO_2	Monochromatic	1185

Table A5-3 Monitoring strategy for the A2D2 design

Design	A3D1		
Layer	Material	Monitoring method	Monitoring wavelength
1	Nb_2O_5	Monochromatic	987
…	…	…	…
21	Nb_2O_5	Monochromatic	987
22	SiO_2	Rate	--
…	…	…	…
28	SiO_2	Rate	--

Table A5-4 Monitoring strategy for the A3D1 design

Design	A3D3			
layer	material	Monitoring method	Monitoring wavelength range	
1	Nb_2O_5	Broadband (Merit)	400	900
2	SiO_2	Broadband (Merit)	400	900
3	Nb_2O_5	Broadband (Merit)	500	900
…	…	…	…	…
26	SiO_2	Broadband (Merit)	500	900
27	Nb_2O_5	Broadband (Merit)	600	900
28	SiO_2	Broadband (Merit)	600	900
29	Nb_2O_5	Broadband (Merit)	600	900

Table A5-5 Monitoring strategy for the A3D3 design

Design	A4D1		
Layer	Material	Monitoring method	Monitoring wavelength
1	Nb_2O_5	Monochromatic	1025
…	…	…	…
15	Nb_2O_5	Monochromatic	1025
16	SiO_2	Monochromatic	992
…	…	…	…
29	Nb_2O_5	Monochromatic	992

Table A5-6 Monitoring strategy for the A4D1 design

Design	A5D1			
layer	material	Monitoring method	Monitoring wavelength range	
1	Nb_2O_5	Broadband (Merit)	400	900
…	…	…	…	…
7	Nb_2O_5	Broadband (Merit)	400	900
8	SiO_2	Broadband (Merit)	500	900
…	…	…	…	…
21	Nb_2O_5	Broadband (Merit)	500	900
22	SiO_2	Broadband (Merit)	530	870
…	…	…	…	…
29	Nb_2O_5	Broadband (Merit)	530	870

Table A5-7 Monitoring strategy for the A5D1 design

Design	A5D3			
layer	material	Monitoring method	Monitoring wavelength range	
1	Nb_2O_5	Broadband (Wideband)	400	900
…	…	…	…	…
4	SiO_2	Broadband (Wideband)	400	900
5	Nb_2O_5	Broadband (Wideband)	500	900
…	…	…	…	…
12	SiO_2	Broadband (Wideband)	500	900

Table A5-8 Monitoring strategy for the A5D3 design

Design	A5D5			
layer	material	Monitoring method	Monitoring wavelength range	
1	Nb_2O_5	Broadband (Merit)	400	900
…	…	…	…	…
5	Nb_2O_5	Broadband (Merit)	400	900
6	SiO_2	Broadband (Merit)	500	870
…	…	…	…	…
22	SiO_2	Broadband (Merit)	500	870
23	Nb_2O_5	Broadband (Merit)	530	870
…	…	…	…	…
29	Nb_2O_5	Broadband (Merit)	530	870

Table A5-9 Monitoring strategy for the A15D5 design